



HAL
open science

Robust observer designs for singular linear parameter-varying systems

Manh-Hung Do

► **To cite this version:**

Manh-Hung Do. Robust observer designs for singular linear parameter-varying systems. Automatic. Université Grenoble Alpes [2020-..], 2020. English. NNT : 2020GRALT053 . tel-03155716

HAL Id: tel-03155716

<https://theses.hal.science/tel-03155716v1>

Submitted on 2 Mar 2021

HAL is a multi-disciplinary open access archive for the deposit and dissemination of scientific research documents, whether they are published or not. The documents may come from teaching and research institutions in France or abroad, or from public or private research centers.

L'archive ouverte pluridisciplinaire **HAL**, est destinée au dépôt et à la diffusion de documents scientifiques de niveau recherche, publiés ou non, émanant des établissements d'enseignement et de recherche français ou étrangers, des laboratoires publics ou privés.

THÈSE

pour obtenir le grade de

DOCTEUR DE L'UNIVERSITÉ DE GRENOBLE ALPES

Spécialité : **AUTOMATIQUE - PRODUCTIQUE**

Arrêté ministériel : 25 mai 2016

Présentée par

Manh Hung DO

Thèse dirigée par **Damien KOENIG**, MCF - HDR, Université Grenoble Alpes et

codirigée par **Didier THEILLIOL**, Professeur, Université de Lorraine

préparée au sein du **Laboratoire Grenoble Images Parole Signal Automatique (GIPSA-lab)**

dans l'**École Doctorale Electronique, Electrotechnique, Automatique, Traitement du Signal (EEATS)**

Synthèse robuste d'observateurs pour systèmes singuliers linéaires à paramètres variants

Robust observer designs for singular linear parameter-varying systems

Thèse soutenue publiquement le **5 Novembre 2020**,
devant le jury composé de:

M. Olivier SENAME

Professeur, Grenoble INP, Président

M. David HENRY

Professeur, Université de Bordeaux, Examineur

M. Vincent COCQUEMPOT

Professeur, Université de Lille, Rapporteur

M. Saïd MAMMAR

Professeur, Université d'Évry-Val-d'Essonne, Rapporteur

M. Damien KOENIG

Maître de Conférences - HDR, Grenoble INP, Directeur de thèse

M. Didier THEILLIOL

Professeur, Université de Lorraine, Co-directeur de thèse



Contents

Acknowledgements	ix
Table of Notations and Acronyms	xvii
List of Publications	xix
Résumé en français	1
Thesis Framework	9
1 Theoretical background	15
1.1 Different classes of dynamical systems	15
1.1.1 Nonlinear system	16
1.1.2 Singular/Descriptor Linear Time-Invariant (S-LTI) systems	16
1.1.3 Singular Linear Parameter-Varying (S-LPV) systems	17
1.2 Stability Conditions	19
1.2.1 Stability for LTI systems	19
1.2.2 Stability for LPV systems	20
1.2.3 Stability for time-delay LPV systemz	21
1.3 Finite LMI solution for LPV systems	23
1.3.1 Polytopic Approach	23
1.3.2 Gridding Approach	25
1.3.2.1 Number of gridding points $n_g^{\rho_i}$	25
1.3.2.2 Choice of basis functions	26
1.3.2.3 General Algorithm	26
1.4 Observability	27

1.4.1	Observability of S-LTI systems	27
1.4.2	Observability of S-LPV systems	28
1.5	Useful Lemmas, Norms and Reformulations	30
1.5.1	Useful Lemmas	30
1.5.1.1	Schur's Complement	30
1.5.1.2	Majorization Lemma	30
1.5.1.3	Projection Lemma	31
1.5.1.4	Young relation	31
1.5.1.5	Jensen's inequality	31
1.5.1.6	Partial differential Matrix	31
1.5.2	\mathcal{H}_∞ (or \mathcal{L}_2 to \mathcal{L}_2) performance	32
1.5.2.1	LTI system	32
1.5.2.2	LPV system	32
1.5.3	System Reformulations	33
1.5.3.1	Output-Input filters	33
1.5.3.2	Output decomposition	34
1.6	Conclusion	35
I FDD and FTC in Non-singular systems		37
2 Robust observer-controller co-design for FDD of drift faults		39
2.1	Introduction	40
2.1.1	Related works	40
2.1.2	Chapter Contributions	40
2.2	Problem Formulation	41
2.2.1	LPV system representation	41
2.2.2	Design objectives	42

2.3	Main results	43
2.3.1	Robust Co-Design of \mathcal{H}_∞ PI Observer and State-feedback Controller	43
2.3.2	Discussion on Active FTC design	50
2.4	FDD Application to sensor fault in Suspension system	51
2.4.1	Platform INOVE	51
2.4.2	LPV Modeling for faulty suspension system	53
2.4.3	System uncertainty	54
2.4.4	Experimental conditions	54
2.4.4.1	Road profile z_r	54
2.4.4.2	Test Scenario	55
2.4.4.3	Varying parameter	56
2.4.5	Observer design for semi-active suspension	56
2.4.6	Frequency Analysis	60
2.4.7	Validation result	63
2.4.7.1	Scenario 1	63
2.4.7.2	Scenario 2	64
2.4.7.3	Time Convergence Tuning	66
2.5	Conclusion	66
3	Robust-stochastic integrated designs for FDD-FTC of actuator degradation	69
3.1	Introduction	70
3.1.1	State of the art	70
3.1.2	Chapter Contributions	72
3.2	Problem formulation	73
3.2.1	Degradation modeling	73
3.2.2	Stochastic LPV System representation	75
3.2.3	Design objectives	77

3.2.4	UI-Matching conditions and Proposed design solutions	78
3.3	Robust-stochastic integrated design for Matched UI	79
3.3.1	Methodology of Frequency-Shaping filter	79
3.3.2	Observer design for Matched UI	81
3.3.3	Fault accommodation Controller design	83
3.3.4	Observer-Controller synthesis for Matched UI	84
3.4	Robust-stochastic integrated design for Unmatched UI	91
3.4.1	Observer Design for Unmatched UI	92
3.4.2	Observer-Controller synthesis for Unmatched UI	93
3.4.3	Discussion on Theorem 3.4.1	95
3.5	Anti-windup solution	96
3.5.1	LPV-Saturation problem	96
3.5.2	Observer design with input saturation for matched UI	97
3.5.3	Anti-windup controller design for matched UI	98
3.5.4	Anti-windup observer-based fault compensator synthesis under degradation occurrence for matched UI	99
3.6	Method illustration	102
3.6.1	Mathematical example	102
3.6.2	Frequency analysis	105
3.6.3	Simulation condition	108
3.6.4	Simulation result	108
3.7	Conclusion	111
II	Observer Designs for Singular Systems	113
4	Fault estimation for S-LTI System with partially decoupled UI	115
4.1	Introduction	116
4.1.1	Related Works	116

4.1.2	Chapter Contributions	117
4.2	Problem Formulation	117
4.2.1	System presentation	117
4.2.2	Design Objectives	119
4.3	Observer design	120
4.3.1	Approach 1: Global \mathcal{H}_∞ attenuation	120
4.3.2	Approach 2: Combination of the frequency-shaping filter and \mathcal{H}_∞ at- tenuation	123
4.3.3	Discussions on Frequency-shaping filter and \mathcal{H}_∞ synthesis	125
4.4	Numerical Example	127
4.4.1	Model Example	127
4.4.2	Frequency Analysis	128
4.4.3	Test Conditions	129
4.4.4	Simulation results	130
4.5	Conclusion	132
5	\mathcal{H}_2 UI Observer for Singular Nonlinear Parameter-Varying System	133
5.1	Introduction	134
5.1.1	State of the art	134
5.1.2	Chapter Contributions	136
5.2	Problem formulation	136
5.2.1	Case (a): $T_a = T$ and $N_a = N$ are parameter-independent matrices and $TD_{1(\rho)} = 0$	138
5.2.2	Case (b): $T_b = T_{(\rho)}$ and $N_b = N_{(\rho)}$ such that $T_{(\rho)}D_{1(\rho)} = 0$	139
5.2.3	Case (c) - Proposed method: $T_c = T_{(Z)}$ and $N_c = N_{(Z)}$ such that $T_{(Z)}D_{1(\rho)} \rightarrow 0$	140
5.3	Main Results - Observer design of Case (c)	142
5.4	Analytical Existence Condition for observer design	145

5.4.1	Impulse-free condition	146
5.4.2	R-detectability condition	146
5.5	Observer Implementation	146
5.5.1	Finite reformulation for Cost objective in Theorem 5.3.1	147
5.5.2	Algorithm for the grid-based solution	147
5.6	Illustration Example	148
5.6.1	Model Parameters	148
5.6.2	Frequency Analysis	150
5.6.3	Time-domain Simulation	151
5.7	Conclusion	153
6	\mathcal{H}_∞ Observer Design for Singular Time-delay Nonlinear Parameter-Varying System	155
6.1	Introduction	156
6.1.1	Related works	156
6.1.2	Chapter Contributions	157
6.2	Problem formulation	158
6.2.1	SD-NLPV representation	158
6.2.2	Design objectives for time-delay NLPV \mathcal{H}_∞ observer	159
6.3	Main results	161
6.3.1	\mathcal{H}_∞ full-order NLPV Observer design with exact memory (known $h(t)$) .	161
6.3.2	\mathcal{H}_∞ full-order NLPV Observer design for S-NLPV systems	168
6.4	General Discussion	170
6.4.1	Analytical Existence Condition for \mathcal{H}_∞ observer designs	170
6.4.1.1	Impulse-free Condition	171
6.4.1.2	R-detectability condition when $h(t) = 0$	171
6.4.2	Implementation Algorithm	171

6.5	Numerical Examples	173
6.5.1	Model Parameters	173
6.5.2	Frequency Analysis	174
6.5.3	Simulation result	176
6.6	Conclusion	177
Conclusions and Perspectives		179
A Suspension/Quarter-car LPV Modeling		185
A.1	Linear Model of Damper	186
A.2	Nonlinear Model of Damper	186
Appendix		184
B R-detectability of singular systems		189
B.1	R-detectability condition for UI observer in S-LTI systems	189
B.2	R-detectability condition for UI observer in S-NLPV systems	191
Bibliography		201

Acknowledgements

I can only say that I have been blessed to have been surrounded by friendly, supportive and dynamic colleagues from GIPSA-lab Automatic Control Department. These three years have been the most meaningful and enjoyable moments.

I would like to give the very first thank-you to my supervisors, Assoc.Prof. Damien Koenig and Prof. Didier Theilliol, who have inspired and supported me in making my PhD possible. You are the ones who have brought me into the world of advanced Automatic Control and never refused to offer great mentoring advice. Three years of studying PhD with you has been a great pleasure for me. Again, a sincere thanks to you.

I would like to give the second thanks to the rapporteurs and examiners of this thesis, Prof. Vincent Cocquempot, Prof. Saïd Mammar, Prof. David Henry and Prof. Olivier Sename. The COVID-19 pandemic has again caused national lockdown and thus hardships for you to attend my PhD defense. Still, none of you were absent, and all were very concentrated on my presentation. I'm extremely grateful for your time, co-operation and especially, constructive feedback which help perfect my Thesis to a great extent.

Thank you to my earliest teachers at ESISAR – Prof. Eduardo Mendes and Damien Koenig – who stoked the flame of Automatic Control within me, and without whom I might never continue my higher education.

More than anyone else, my family is the ones that I am indebted to the most. They have always been there beside me through ups and downs. To say I'm incredibly grateful would be an understatement. Especially you Mom, I'm eternally indebted to you. A special thanks to my little sister, who has always been my best sounding board and who was able to make all my research papers readable and understandable. Truly appreciate your "magical aura", Heo.

Thank you to the administrative team, particularly Virginie, Marielle and Patricia who released me from all the burdensome bureaucratic procedures and to the technical team, particularly Gabriel, Suzanne and Rattena who assisted me with experiments on the INOVE platform.

For the last words, I would like to advise you, future PhDs. Youth is like a cup of tea, right at the moment you finish your tea, BAM! you are now a PhD and at least 27 years have passed (VERY FAST). Do not stick your head to research all the time and end up experiencing no romantic relationships. Play hard and get wasted along the way or you will suffer. I am the living evidence, so believe me, I know.

List of Figures

1	Thesis Reading Layout (*: Essential support)	14
1.1	Grid of parameter space.	25
2.1	Robust Co-design - Robust FDD scheme	43
2.2	Integrated design for Active FTC	50
2.3	Schematic of INOVE experimental platform	51
2.4	SOBEN car of platform INOVE ANR 2010	52
2.5	Dynamics of uncertain system	55
2.6	Road profile z_r (d): highway with gravel	55
2.7	Varying parameter ρ	57
2.8	LPV observer on a linear grid.	58
2.9	Implementation Scheme.	58
2.10	Sensitivity function $ e_{f_{z_{def}}} / d $	61
2.11	Sensitivity function $ e_{f_{z_{def}}} / f_a $	61
2.12	Complementary sensitivity function $ \hat{f}_{z_{def}} / f_{z_{us}} $	62
2.13	Complementary sensitivity function $ \hat{f}_{z_{def}} / f_{z_{def}} $	62
2.14	Comparison between model and experimental sensitivity function $ \hat{f}_{z_{def}} / f_{z_{def}} $	63
2.15	Fault estimation result in Scenario 1.	64
2.16	Fault estimation result in Scenario 2.	65
2.17	State-feedback controller in Scenario 2.	65
2.18	Fault estimation result with α modification.	66
3.1	Relation between degradation d and frequency f_w	75
3.2	Scheme of robust-stochastic integrated design	78

3.3	General scheme for estimation process	80
3.4	Robust-stochastic integrated design for matched UI	92
3.5	Robust-stochastic integrated design for unmatched UI	95
3.6	Anti-windup integrated design for matched UI	101
3.7	Anti-windup integrated design for unmatched UI	101
3.8	Process noise v_1	103
3.9	Measurement noise v_2	103
3.10	Actuator behavior	103
3.11	Sensitivity e_d/w	106
3.12	Sensitivity \hat{d}/d	106
3.13	Frequency responses of e_d to process and measurement noises	107
3.14	Frequency responses of e_x to process and measurement noises	107
3.15	Actuator degradation estimation \hat{d}	109
3.16	Actuator degradation estimation error e_d	109
3.17	Saturation indicator	110
3.18	Fault tolerant control u	110
3.19	System output y affected by noise	111
4.1	General scheme of UI observer	120
4.2	Frequency-shaping filter implementation for UI observer	124
4.3	Weighting function implementation in \mathcal{H}_∞ synthesis.	126
4.4	Output filter	128
4.5	Actuator fault f	128
4.6	Sensitivity $ e_f/w_2 $	129
4.7	Sensitivity $ e_f/w_3 $	130
4.8	Fault estimation under influence of w_1	130
4.9	Estimation error under influence of w_1	131

4.10	Estimation error under influence of w_1 and w_2	131
4.11	Fault error under influence of all UIs (w_1, w_2, w_3)	132
5.1	Implementation scheme of \mathcal{H}_2 UI NLPV observer	141
5.2	Sensitivity function $ S_{e_{x_1}w} = e_{x_1}/w $	150
5.3	Sensitivity function $ S_{e_{x_2}w} = e_{x_2}/w $	150
5.4	Sensitivity function $ S_{e_{x_3}w} = e_{x_3}/w $	151
5.5	x_1 estimation	152
5.6	x_2 estimation	152
5.7	x_3 estimation	152
6.1	Implementation scheme of \mathcal{H}_∞ time-delay observer	160
6.2	Sensitivity function $e_z(t)/w(t)$	175
6.3	Sensitivity function $e_z(t)/\tilde{\phi}(t)$	175
6.4	Sensitivity function $e_z(t)/\tilde{\phi}_d(t-h(t))$	176
6.5	z_1 estimation	177
6.6	z_2 estimation	177
A.1	The quarter-car scheme	185

List of Tables

2.1	Quarter-car parameters	53
2.2	Fault estimation and UI attenuation table for the $f_{z_{def}}$ PI observer.	64
3.1	RMS value of estimation error with sampling time $T = 0.001 s$	110
4.1	UI attenuation Comparison	129
4.2	RMS of estimation error	132
5.1	RMS Evaluation of estimation error	153
6.1	RMS Evaluation of estimation error	177

Table of Notations and Acronyms

Notations

\mathbb{R}	Set of real numbers
\mathbb{C}	Set of complex numbers
\mathbb{R}^n	n-dimensional Euclidean space
$\mathbb{R}^{m \times n}$	Set of all $m \times n$ real matrices
$\mathbb{R}_{\geq 0}$	Set of non-negative real numbers
\mathbb{S}^n	Set of $n \times n$ symmetric matrices
0	Zero matrix with appropriate dimensions
I	Identity matrix with appropriate dimensions
$(*)$	Transposed block in the symmetric position
X^T	Transpose of the matrix X ;
X^\dagger	Moore-Penrose inverse of X
$Tr(X)$	Trace of matrix X
$eig(X)$	Eigenvalues of matrix X
$\sigma(X)$	Singular values of matrix X
\bar{x}	Largest bound of variable x
\underline{x}	Smallest bound of variable x
$i = 1 : N$	$i \in \{1, 2, \dots, N - 1, N\}$
$[a, b]$	Set of all values from a to b
$\mathcal{R}(x)$	Real part of the complex number x
$\exp(x)$	Exponential of x
$\mathbb{E}\{.\}$	Expected value operator
p	Laplace variable
$\mathcal{H}\{A\}$	$A + A^T$
N_g	Number of time-frozen points in Gridding approach

Acronyms

DAE	Differential Algebraic Equation
ODE	Ordinary Differential Equation
LTI	Linear Time-Invariant
LPV	Linear Parameter-Varying
LTV	Linear Time-Varying
NLPV	NonLinear Parameter-Varying
S-LTI	Singular Linear Time-Invariant
S-LPV	Singular Linear Parameter-Varying
S-LTV	Singular Linear Time-Varying
S-NLPV	Singular NonLinear Parameter-Varying
LMI	Linear Matrix Inequality
LME	Linear Matrix Equality
FDD	Fault Detection and Diagnosis
FDI	Fault Detection and Isolation
FE	Fault Estimation
FA	Fault Accommodation
FTC	Fault Tolerant Control
PI	Proportional Integral
UI	Unknown Input
TVP	Time-Varying Parameter
RMS	Root-Mean-Square

List of Publications

Journal papers

- (J.1) Manh-Hung Do, Damien Koenig, and Didier Theilliol (2020). Robust observer-based controller for uncertain stochastic LPV system under actuator degradation. *International Journal of Robust and Nonlinear Control*. DOI: 10.1002/rnc.5302
- (J.2) Manh-Hung Do, Damien Koenig, and Didier Theilliol (2020). Robust \mathcal{H}_∞ proportional-integral observer-based controller for uncertain LPV system. *Journal of the Franklin Institute*. Vol. 357 (4), 2099-2130. [Do, Koenig, and Theilliol 2020c]

International conference papers with proceedings

- (C.1) Manh-Hung Do, Damien Koenig, and Didier Theilliol (2020). \mathcal{H}_∞ observer design for Singular Nonlinear Parameter-varying System. In *2020 59th IEEE Conference on Decision and Control (CDC)*. IEEE. [Do, Koenig, and Theilliol 2020b]
- (C.2) Manh-Hung Do, Damien Koenig, Didier Theilliol, and Peter Gáspár (2020). Frequency-shaping observer-based controller design for actuator degradation : Application to suspension system. In *2020 28th Mediterranean Conference on Control and Automation (MED)*. IEEE. [Do et al. 2020]
- (C.3) Manh-Hung Do, Damien Koenig, and Didier Theilliol (2020). Fault estimation methods in descriptor system with partially decoupled disturbances. In *2020 21st IFAC World Congress*. IFAC. [Do, Koenig, and Theilliol 2020a]
- (C.4) Manh-Hung Do, Damien Koenig, and Didier Theilliol (2019). Robust \mathcal{H}_2 observer design for actuator degradation: Application to suspension system. In *2019 4th Conference on Control and Fault Tolerant Systems (SysTol)*. IEEE. DOI:10.1109/SYSTOL.2019.8864738. [Do, Koenig, and Theilliol 2019]
- (C.5) Manh-Hung Do, Damien Koenig, and Didier Theilliol (2018). An integrated design for robust actuator fault accommodation based on \mathcal{H}_∞ proportional-integral observer. In *2018 57th IEEE Conference on Decision and Control (CDC)*, 6346–6352. IEEE. [Do, Koenig, and Theilliol 2018a]
- (C.6) Manh-Hung Do, Damien Koenig, and Didier Theilliol (2018). Robust \mathcal{H}_∞ proportional integral observer design for actuator fault estimation. In *2018 16th International Mini Conference on Vehicle System Dynamics, Identification and Anomalies (VSDIA), Budapest, Hungary*. [Do, Koenig, and Theilliol 2018b]
- (C.7) Manh-Hung Do, Damien Koenig, and Didier Theilliol (2018). Robust \mathcal{H}_∞ proportional-integral observer for fault diagnosis: Application to vehicle suspension. In *2018 10th*

IFAC Symposium on Fault Detection, Supervision and Safety for Technical Processes (SAFEPROCESS), IFAC-PapersOnLine, 51(24), 536–543. [Do, Koenig, and Theilliol 2018c]

National conferences without proceedings

- (C.8) Manh-Hung Do, Damien Koenig, and Didier Theilliol (2020). \mathcal{H}_∞ observer design for Singular Nonlinear Parameter-varying System. *In Journée du Groupe de Travail "Sûreté - Surveillance - Supervision" (GTS3), France.*
- (C.9) Manh-Hung Do, Damien Koenig, and Didier Theilliol (2020). Robust \mathcal{H}_∞ Proportional-Integral Observer-based Controller for Uncertain LPV system : Application to suspension system. *In Journée du Groupe de Travail "Automatique et Transports Terrestres" (GTATT), France.*
- (C.10) Manh-Hung Do, Damien Koenig, and Didier Theilliol (2019). An Integrated Design for Robust Actuator Fault Accommodation based on \mathcal{H}_∞ PI Observer. *In Journée du Groupe de Travail "Automatique et Transports Terrestres" (GTATT), France.*

Résumé (in French)

Introduction générale

Au cours des dernières années, la modélisation linéaire à paramètres variants (LPV) a été largement appliquée dans les véhicules et les systèmes aérospatiaux [Wu 2001; Senname, Gaspar, and Bokor 2013] car elle permet la représentation linéaire de systèmes non linéaires avec des matrices de distribution à paramètres variants. Pour estimer l'état/le paramètre des systèmes LPV perturbés par des perturbations, de nombreux chercheurs ont largement développé la synthèse d'observateurs, en particulier dans les processus FDD (Détection et diagnostic des défaillances) et FTC (Commande tolérante aux fautes) [Chen and Patton 2012; Ding 2008]. En particulier, l'observateur en FDD est responsable de la détection des défauts et de l'estimation de ses magnitudes. En même temps, les méthodes FTC sont classées en deux groupes selon le contexte de la conception des contrôleurs : active et passive [Zhang and Jiang 2007; Jiang and Yu 2012]. Pour la FTC active, le contrôleur est reconfiguré par des mécanismes de configuration, tels que la compensation des défauts, en utilisant les informations de défaut obtenues du FDD. D'autre part, le contrôleur en FTC passive peut être synthétisé sans l'aide du FDD pour rendre le système en boucle fermée aussi insensible que possible à l'ensemble des défauts de base. C'est pourquoi cette thèse focalise principalement sur les conceptions des observateurs pour les systèmes LPV (non) singuliers (S-LPV), ainsi que sur leurs modèles linéaires invariants (S-LTI).

Cependant, de nombreux problèmes doivent encore être résolus dans les systèmes (S-)LPV. Des discussions plus approfondies sur les problèmes existants, ainsi que des suggestions de solutions, sont présentées ci-dessous:

1. Incertitude paramétrique dans les processus FDD et FTC

Comme mentionnée dans [Jabbari and Benson 1992], l'incertitude paramétrique peut avoir un impact négatif sur les synthèses d'observateurs. En raison de la présence de l'état du système x dans la dynamique de l'erreur d'estimation e , c'est-à-dire dans \dot{e} , elle peut entraîner une instabilité de l'observateur et invalider l'important principe de séparation dans le contrôleur basé sur l'observateur où la relation entre x et \dot{e} doit être nulle. Par conséquent, de nombreuses mesures ont été prises pour minimiser son influence, en particulier dans les processus FDD et FTC où la qualité de l'estimation des défauts (FE) et la communication observateur-contrôleur définissent la performance et la stabilité des systèmes en boucle fermée. [Zhang and Jiang 2007]

Concernant le processus FDD, la problématique de l'incertitude a été récemment intégrée dans la conception des observateurs par la mise en œuvre d'observateurs proportionnels (multiples) intégraux (P(M)I) et l'optimisation des LMI. Dans [Hassanabadi, Shafiee, and Puig

2017], la conception des observateurs P(M)I \mathcal{H}_∞ pour les systèmes LPV présente une complication dans la synthèse car son modèle polytopique à double couche exige non seulement que les matrices et les incertitudes du système soient présentées sous forme polytopique, mais aussi que la matrice de sortie soit indépendante du paramètre variant. Par conséquent, il est nécessaire de trouver une solution généralisée et efficace pour assurer une synthèse robuste des observateurs PI dans les systèmes LPV incertains, quelle que soit leur représentation.

Concernant la conception FTC active, [Lan and Patton 2016] a récemment introduit la notion de conception intégrée. Dans ce cas, les défauts estimés du FDD sont utilisés directement pour le contrôleur afin de compenser les effets des défauts (intégration) et les deux gains observateur-contrôleur sont obtenus simultanément par une solution unique d'LMI (co-conception). Sur la base de l'observateur adaptatif et du compensateur de défauts à retour d'état, une conception intégrée pour les systèmes LPV a été proposée dans [Rodrigues et al. 2014]. Cependant, ses solutions d'optimisation de l'LMI sont probablement irréalisables car la matrice positive définie P de la fonction de Lyapunov nécessite une méthode algébrique restrictive conditions pour favoriser le découplage de la conception des observateurs et des contrôleurs. En outre, les impacts de l'incertitude et des perturbations sur la conception intégrée des LPV ne sont pas encore complètement compris. Par conséquent, une nouvelle conception intégrée observateur-contrôleur est encore nécessaire pour les systèmes LPV où le contrôleur basé sur l'observateur est mis en œuvre.

Pour répondre aux problèmes mentionnés ci-dessus concernant l'impact de l'incertitude paramétrique sur la FDD et la FTC, la thèse mène les études suivantes sur les systèmes LPV incertains. Pour la FDD, **Chapitre 2** développe un nouveau co-design robuste de contrôleur-observateur pour les défauts de dérive. Dans laquelle, parmi les approches pour l'analyse de la stabilité robuste (polytopique, lemme de majorisation, et lemme de projection), le lemme de majorisation est choisi pour s'attaquer à la forme générique du terme incertain et réduire la quantité d'LMI à résoudre indépendamment de la formulation LPV du système initial. En outre, l'observateur est construit sur la base de la synthèse en boucle fermée de l'observateur PI et du contrôleur de retour d'état et peut donc être mis en œuvre sans contrôleur (sauf dans la synthèse de conception). Ensuite, sur la base de la méthodologie de co-conception de la FDD dans le **Chapitre 2**, le **Chapitre 3** introduit une conception intégrée stochastique robuste pour la FTC active afin de traiter la dégradation de l'actionneur en présence simultanée de perturbations.

2. Problème multi-objectif dans l'atténuation des perturbations

Pendant le fonctionnement du système, il existe toujours des perturbations qui interfèrent négativement avec les performances du système global. En fonction du contexte, les perturbations peuvent être classées comme des incertitudes paramétriques, des UIs (des entrées inconnues) et des bruits stochastiques. À la connaissance de l'auteur, seules deux au maximum des trois questions ci-dessus doivent être examinées en même temps. Même cela, le problème multi-objectif peut toujours se produire dans le processus d'atténuation des perturbations et conduire à un réglage coûteux pour une performance compromise. Un exemple typique est

l'optimisation de $\mathcal{H}_\infty / \mathcal{H}_2$ pour l'entrée inconnue de \mathcal{L}_2 -norme et le bruit à énergie unitaire [Khosrowjerdi, Nikoukhah, and Safari-Shad 2004], qui est un problème non convexe et qui est généralement résolu en choisissant des performances fixes γ_∞ pour la performance \mathcal{H}_∞ et en minimisant γ_2 pour la synthèse de \mathcal{H}_2 -noise. Par conséquent, pour éviter les problèmes d'optimisation multi-objectifs, une solution alternative atténuant les perturbations est exigée.

En conséquence, la thèse a proposé un filtre de sortie adapté à la fréquence des perturbations. Ensuite, une conception intégrée observateur-contrôleur basée sur Kalman filtre, qui permet non seulement d'atténuer les impacts simultanés des perturbations mais aussi d'éviter le problème de l'optimisation multi-objectifs, est présentée dans **Chapitre 3**.

3. Non-linéarité du paramètre variant ρ dans les systèmes LPV

Dans certaines circonstances, telles que les systèmes quasi-LPV, le paramètre variant ρ est choisi comme formulation non linéaire des états et paramètres du système. Cependant, il peut induire l'inexactitude dans la conception des observateurs en raison de l'estimation inexacte des états/paramètres. Ainsi, pour éviter ce problème, l'observateur polytopique pour les systèmes non singuliers a été proposé [López-Estrada et al. 2015b]. Malheureusement, la représentation polytopique requise et la synthèse complexe avec le système en boucle fermée limitent sa mise en œuvre. D'autre part, même si le problème de la non-linéarité puisse être directement résolu par la condition de Lipschitz [Us Saqib et al. 2017; Pham, Sename, Dugard, et al. 2019], cette approche ne fonctionne que dans les systèmes LPV non singuliers. Par conséquent, le développement d'un observateur LPV non linéaire Il est essentiel que les conceptions qui fonctionnent à la fois pour les systèmes LPV et S-LPV soient conformes à la non-linéarité de Lipschitz.

Dans cette thèse, une nouvelle classe de système singulier et non linéaires à paramètres variant et en retard (SD-NLPV) est introduite pour unifier tous les systèmes LPV existants jusqu'à présent. De plus, les conceptions des observateurs correspondants seront présentées dans **chapitres 5 et 6**.

4. Contrainte de découplage des entrées inconnue dans l'observateur à l'entrée inconnue (UI)

Afin de contrer l'impact négatif des entrées inconnues sur les systèmes dynamiques, les observateurs à l'entrée inconnue ont été largement étudiés. Le principe principal de ce type d'observateur est d'éliminer la présence d'entrées inconnues dans la dynamique des erreurs d'estimation en utilisant la condition algébrique structurelle. En d'autres termes, il doit trouver une matrice conçue de telle sorte que sa multiplication avec la matrice de l'entrée inconnue soit nulle [Darouach, Zasadzinski, and Xu 1994]. Pour atténuer cette contrainte restrictive de découplage des entrées inconnues, certains travaux récents ont été réalisés comme suit :

Pour les systèmes LTI, la notation de l'entrée inconnue partiellement découplée a été introduite dans [Xu et al. 2016; Gao, Liu, and Chen 2016] où les entrées inconnues sont

divisées en deux groupes : l'un satisfait aux contraintes de découplage de l'entrée inconnue, et l'autre non. Néanmoins, ces travaux ne sont applicables qu'aux systèmes non singuliers. Il est donc nécessaire de développer une plus grande extension pour les systèmes S-LTI. Pour les systèmes LPV, ce découplage de l'interface utilisateur devient plus problématique puisque la matrice d'entrée inconnue dépend du paramètre variant dans le temps (TVP) ; par conséquent, la synthèse d'une matrice conçue de manière unique n'est plus efficace. Récemment, [Marx et al. 2019] a reformulé le système et formulé des hypothèses supplémentaires pour concevoir une matrice conçue variant en garantissant les contraintes algébriques de découplage de l'entrée inconnues. Malheureusement, la synthèse de conception est complexe et ne s'applique qu'aux systèmes LPV non singuliers. Il est donc nécessaire de concevoir un observateur d'interface utilisateur LPV plus simple qui fonctionne même pour les systèmes S-LPV.

Dans cette thèse, les solutions suivantes sont proposées pour surmonter les problèmes ci-dessus. Pour les systèmes S-LTI, un résultat étendu du travail de [Gao, Liu, and Chen 2016] et une nouvelle conception basée sur des filtres de mise en forme de fréquence sont développés dans **Chapitre 4** pour l'entrée inconnue partiellement découplée. Pour les systèmes S-LPV, afin de contourner la condition de découplage des entrées inconnues dépendantes des paramètres, une nouvelle méthodologie d'observateur d'entrée inconnue basée sur les critères de \mathcal{H}_2 sera introduite dans **Chapitre 5**, tandis que l'approche \mathcal{H}_∞ est développée dans **Chapitre 6**. Il convient de noter que ces observateurs sont applicables non seulement aux systèmes S-LPV, mais aussi à une classe plus complète qui comprend la non-linéarité Lipschitz et le problème des délais.

Structure de la thèse et contributions

Sur la base des problèmes abordés, le manuscrit et ses contributions sont organisés comme suit :

- **Chapitre 1** rappelle le contexte théorique des systèmes dynamiques, leur stabilité et leur observabilité. Enfin, quelques lemmes, normes et reformulations de systèmes utiles sont démontrées pour faciliter l'exposé de la thèse.

Ensuite, les cinq chapitres suivants sont divisés en deux parties correspondant aux systèmes non singuliers et singuliers :

- **Part I** : FDD et FTC dans les systèmes non singuliers.

Cette première partie présente les contributions des conceptions robustes d'observateurs-contrôleurs dans les processus FDD et FTC. En particulier,

- **Chapitre 2** propose une solution FDD robuste pour les défauts à variation lente dans les systèmes LPV incertains en utilisant la co-conception de \mathcal{H}_∞ observateur proportionnel intégral (PI) et contrôleur de retour d'état. De plus, une formulation

générique des termes incertains est introduite pour simplifier le processus de conception. Les résultats expérimentaux pour la FDD des défauts des capteurs sont réalisés pour le système de suspension dans la plate-forme INOVE.

- **Chapitre 3** fournit la modélisation de la dégradation non linéaire du système sous la formulation de défaut polynomial. Ensuite, la méthodologie d'un filtre de mise en forme de fréquence est présentée comme une méthode alternative d'atténuation de l'entrée inconnue. En outre, sur la base de la fréquence de travail de l'UI, une stratégie générique de conceptions intégrées robust-stochastiques est proposée pour les systèmes LPV polytopiques afin d'estimer en ligne la dégradation de l'actionneur et de compenser son impact sous les contraintes de saturation et l'influence simultanée des incertitudes paramétriques, des entrées inconnues, et des bruits stochastiques.

- **Part II** : Conceptions d'observateurs pour les systèmes singuliers.

La deuxième partie de la thèse présente une diversité de conceptions d'observateurs qui non seulement permettent de surmonter les problèmes existants dans les S-LTI mais aussi de promouvoir l'estimation de l'état dans une nouvelle classe de systèmes LPV, appelés systèmes à paramètres non linéaires singuliers (S-NLPV). Les détails sont donnés ci-après :

- **Chapitre 4** développe une approche générique pour l'estimation des défauts d'actionneurs dans S-LTI systèmes perturbés par l'entrée inconnue partiellement découplée. Dans cette approche, le défaut de l'actionneur est exprimé sous une forme générale tandis que les entrées inconnues partiellement découplées sont divisées en entrées inconnues découplées et non découplées en fonction de la satisfaction de la condition de découplage des entrées inconnues. Sur la base de la connaissance de la fréquence de l'entrée inconnue, deux approches sont proposées pour la conception de l'observateur de l'entrée inconnue.
- **Chapitre 5** introduit une nouvelle classe de systèmes S-LPV avec la non-linéarité Lipschitzienne (S-NLPV), qui unifie tous les systèmes LPV existants jusqu'à présent. En outre, une conception générique d'un observateur à l'entrée inconnue a été introduite afin d'atténuer le problème du découplage de l'entrée inconnue en fonction des paramètres et elle peut être mise en œuvre indépendamment de la représentation du système LPV.
- **Chapitre 6** présente un processus de conception générique pour les observateurs NLPV qui est applicable aux systèmes SD-NLPV, ainsi qu'aux systèmes S-NLPV, quelle que soit leur représentation LPV. La solution proposée est basée sur la forme générique d'observateur d'ordre entier, qui intègre les retards d'entrée d'état et la non-linéarité Lipschitzienne et aborde l'impact des entrées inconnues par synthèse \mathcal{H}_∞ . En outre, la stabilité des erreurs d'estimation dépendante des paramètres et des retards est étudiée.

- **Annexe:**

Il y a deux annexes dans cette thèse. L'annexe A fournit des informations complémentaires sur la modélisation de la suspension dans les systèmes LPV et NLPV. L'appendice B est consacré aux preuves des conditions de détectabilité R dans les systèmes singuliers utilisés pour les chapitres 4 à 6.

Dans cette thèse, la matrice singulière E des systèmes S-LPV, ainsi que leurs systèmes étendus, serait maintenue constante. En fait, la forme $E_{(\rho)}$ dépendant des paramètres pose de nombreuses difficultés dans l'analyse de la régularité et de la stabilité des systèmes singuliers, et n'est donc pas encore étudiée de manière approfondie et considérée comme un développement à long terme de la thèse. En fait, la forme $E_{(\rho)}$ dépendant des paramètres pose de nombreuses difficultés dans l'analyse de la régularité et de la stabilité des systèmes singuliers, et n'est donc pas encore étudiée de manière approfondie et considérée comme un développement à long terme de la thèse.

Perspectives

Malgré les performances effectives des modèles proposés, il existe encore des problèmes de validation expérimentale et des hypothèses de conception qui doivent être assouplies ou levées si possible. Vous trouverez ci-dessous les suggestions pour le développement à court et à long terme, classées en fonction de la complexité des problèmes et de la disponibilité des références.

Développement à court terme

- **Estimation de dégradation**

Dans le chapitre 2, seuls des exemples numériques sont utilisés pour démontrer la capacité du contrôleur proposé basé sur l'observation à estimer la dégradation et l'accommodation. À l'avenir, il est nécessaire de vérifier la méthode avec une plate-forme réelle où son actionneur est étiré jusqu'à son point de dégradation. En fait, l'auteur prévoit de coopérer avec le laboratoire CRAN à Nancy pour le test expérimental.

- **Mesure/Estimation inexacte du paramètre variable dans le temps ρ**

Comme mentionné au chapitre 3, la fréquence de l'entrée inconnue, qui agit comme un paramètre variant dans les conceptions intégrées, étant estimée/identifiée, il existe une incertitude dans la dynamique du filtre adapté à la fréquence de l'entrée inconnue. Il convient donc de réaliser une étude sur son impact sur les performances du système en boucle fermée. En outre, la synthèse des observateurs des chapitres 5 et 6 pour les systèmes S-NLPV devrait également tenir compte de l'incertitude du paramètre variable dans le temps ρ et de la condition de Lipschitz sur la non-linéarité, comme dans la recherche robuste de [López-Estrada et al. 2015a].

- **Mesure stochastique dans les observateurs d'ordre entier**

Dans les chapitres 4 à 6, les observateurs de plein droit ne s'appliquent qu'à l'entrée inconnue déterministe w . En outre, le bruit stochastique de la mesure peut intervenir dans la dynamique de l'erreur d'estimation, affectant ainsi la qualité et la précision générales de l'estimation. Par conséquent, un observateur d'ordre entier intégrant le filtrage de Kalman devrait être envisagé à l'avenir comme dans [Darouach et al. 1995] pour les systèmes S-LTI.

- **Problème d'estimation des défauts dans les systèmes S-NLPV**

Bien que les modèles d'observateurs développés dans les chapitres 5-6 soient capables d'estimer l'état dans les systèmes S-NLPV et SD-NLPV, leur application à l'estimation des défauts n'a pas encore été étudiée. Une solution possible est de réécrire les défauts en tant qu'états augmentés du système S-NLPV, similaire à [Shi and Patton 2015a] dans les systèmes S-LPV.

- **Non-linéarité dans les systèmes S-NLPV**

Dans cette thèse, la contrainte Lipschitzienne est supposée afin de traiter la non-linéarité dans le système S-NLPV. Cependant, sa constante Lipschitzienne γ doit être fixée, c'est-à-dire la limite maximale de la non-linéarité, ce qui signifie que la solution LMI ne donne pas réellement la valeur optimale. Par conséquent, l'étude sur la variation des paramètres $\gamma(\rho)$ et son impact sur la synthèse de la stabilité devrait être menée pour obtenir de meilleures valeurs des gains des observateurs. Une étude notable sur ce sujet est [Yang, Rotondo, and Puig 2019] où la stabilité quadratique avec une contrainte Lipschitzienne paramétrique est étudiée pour la synthèse du contrôleur.

En outre, comme la condition Lipschitzienne n'est pas toujours réalisable dans la pratique, des solutions pour une propriété plus générale de non-linéarité, telle que la condition Hö plus ancienne [Kress, Maz'ya, and Kozlov 1989], sont nécessaires dans les travaux futurs.

Développement à long terme

- **Stabilité dépendant du paramètre variant pour la conception intégrée stochastique**

Pour incorporer le problème stochastique dans la conception intégrée, une matrice constante \mathcal{X} a été utilisée au chapitre 3, assurant ainsi la stabilité indépendante des paramètres (stabilité quadratique) de la synthèse en boucle fermée. Étant donné que \mathcal{X} est conservatrice, il est nécessaire de trouver un paramètre variant $\mathcal{X}(\rho)$ afin d'élargir la zone de faisabilité de la solution LMI. Malheureusement, jusqu'à présent, seules les recherches concernant la constante d'utilisation \mathcal{X} pour le bruit stochastique, telles que [Wu et al. 1996] et [Tuan, Apkarian, and Nguyen 2001], ont été menées.

- **Conception intégrée pour les systèmes S-NLPV**

Dans les chapitres 2 et 3, la conception intégrée des systèmes LPV classiques a été abordée. Cependant, en raison de la non-linéarité du système S-NLPV, le contrôleur linéaire basé sur l'observateur avec compensation des défauts n'est plus applicable.

Par conséquent, il est nécessaire d'adopter une nouvelle conception intégrée basée sur l'accommodation des défauts non linéaires, à savoir la combinaison d'un contrôle de mode glissant [Tanelli et al. 2016] et d'une compensation des défauts. En outre, une co-conception robuste pour la FDD et une conception intégrée pour la FTC peuvent être déduites pour les systèmes S-NLPV incertains.

- **Matrice singulière dépendant du paramètre variant $E_{(\rho)}$ pour la famille des systèmes S-LPV**

À la connaissance de l'auteur, l'utilisation de E constants est le cas d'étude le plus appliqué pour les systèmes S-LPV afin de profiter de l'analyse et de la synthèse des observateurs dans les systèmes S-LTI. En attendant, le cas où $E_{(\rho(t))}$ dépend du paramètre variant $\rho(t)$ n'a pas encore été largement étudié en raison de difficultés dans l'analyse de la régularité dépendant du paramètre, de l'état sans impulsion et de la stabilité.

En revanche, dans les systèmes singulière variant dans le temps (S-LTV), l'observabilité [Hernández et al. 2019] et l'analyse des impulsions [Yan and Duan 2006] ont été réalisées pour $E(t)$. Cependant, l'application de ces travaux aux systèmes VLT doit être examinée avec soin car les systèmes VLT sont considérés comme une généralisation de la classe générale des systèmes LTV [Briat 2008]. De plus, $E_{(\rho(t))}$ des systèmes LTV dépend de $\rho(t)$ mesuré en temps réel au lieu d'être connu au préalable comme $E(t)$ des systèmes LTV. Par conséquent, $E_{(\rho(t))}$ est un sujet d'étude intéressant pour élargir la modélisation et l'application des systèmes S-LPV.

- **Résultats de l'extension pour les systèmes multi-agents**

Bien que l'observateur \mathcal{H}_∞ développé dans cette thèse soit appliqué aux systèmes S-NPV à retardement, il peut être modifié pour les systèmes multi-agents. En fait, les systèmes multi-agents [Dorri, Kanhere, and Jurdak 2018] partagent de nombreuses caractéristiques communes avec les systèmes SD-NPLV, ayant également des retards de communication et nécessitant des contraintes algébriques dans la relation entrée-sortie comme les systèmes S-NLPV. [Chadli, Davoodi, and Meskin 2016] et [Chen et al. 2016] sont deux articles typiques sur \mathcal{H}_∞ observer pour les systèmes LPV multi-agents. Cependant, ces travaux n'ont pas encore pris en compte les délais de propagation dans l'état/entrée/sortie.

Thesis Framework

General Introduction

Over the last few years, the linear parameter-varying (LPV) modeling has been widely applied in vehicle and aerospace systems [Wu 2001; Sename, Gaspar, and Bokor 2013] as it allows the linear representation of non-linear systems with time-varying distribution matrices. To estimate the system state/parameter in LPV systems perturbed by disturbances, many researchers have extensively developed observer design, particularly in FDD and FTC processes [Chen and Patton 2012; Ding 2008]. In specific, the observer in FDD is responsible for fault detection and magnitude estimation. Meanwhile, FTC methods are classified into two groups depending on the context of controller designs: active and passive [Zhang and Jiang 2007; Jiang and Yu 2012]. For active FTC, the controller is reconfigured by configuration mechanisms, such as fault compensation, by using the fault information obtained from FDD. On the other hand, the controller in passive FTC can be synthesized without the help of FDD to make the closed-loop system as insensitive as possible to the set of basic faults. Therefore, the main focus of this Thesis is on the observer designs for (non-)singular LPV (S-LPV) systems, as well as their local time-frozen Singular Linear Time-Invariant (S-LTI) models.

However, there are still many issues needed to be overcome in (S-)LPV systems. More discussions on the existing problems, along with suggestions for solutions, are presented below:

1. Parametric Uncertainty in FDD and FTC processes

As mentioned in [Jabbari and Benson 1992], parametric uncertainty can have a negative impact on observer-based designs. Due to the presence of system state x in the dynamics of estimation error e , i.e. in \dot{e} , it may lead to observer instability and invalidate the important separation principle in the observer-based controller where the relation between x and \dot{e} is required to be null. Consequently, many attempts have been made to minimize its influence, especially in FDD and FTC processes where the quality of fault estimation (FE) and the observer-controller communication define the performance and stability of closed-loop systems. [Zhang and Jiang 2007]

Regarding the FDD process, the uncertainty issue has been recently integrated into observer design through the implementation of \mathcal{H}_∞ Proportional-(Multiple) Integral (P(M)I) observers [Koenig 2005] and LMI optimization. In [Hassanabadi, Shafiee, and Puig 2017], the \mathcal{H}_∞ PI observer design for LPV systems experiences a complication in synthesis because its double-layer polytopic model requires not only system matrices and uncertainties to be expressed in polytopic form, but also output matrix to be independent of the time-varying scheduling parameter. Consequently, there is a need for an efficient generalized solution to robust \mathcal{H}_∞ PI observer synthesis in uncertain LPV systems regardless of their representation.

Regarding the active FTC designs, [Lan and Patton 2016] has recently introduced the notion of Integrated Design. Herein, the estimated faults from FDD are used directly for the controller to compensate for the effects of the faults (integration) and both observer-controller gains are simultaneously obtained by a unique LMI solution (co-design). Based on the adaptive observer and state-feedback fault compensator, an integrated design for LPV systems has been proposed in [Rodrigues et al. 2014]. However, its LMI optimization solutions are likely unattainable because the positive definite matrix P of Lyapunov function requires restrictive algebraic conditions to promote the decoupling of observer and controller design. Furthermore, the impacts of uncertainty and disturbance on LPV integrated design are not completely yet understood. Therefore, a novel observer-controller integrated design is still in need for LPV systems where the observer-based controller is implemented.

To address the above concerns over the impact of parametric uncertainty on FDD and FTC, the Thesis conducts the following studies on uncertain LPV systems. For FDD, **Chapter 2** develops a new robust observer-controller co-design for drift faults. In which, among the approaches for the analysis of robust stability (polytopic, majorization lemma, and projection lemma), the majorization lemma is chosen to tackle the generic form of uncertain term and reduce the amount of LMIs to be solved regardless of LPV formulation of the initial system. Also, the observer is built based on the closed-loop synthesis of \mathcal{H}_∞ PI observer and state-feedback controller and thus can be implemented without controller (except in the design synthesis). Then based on the methodology of FDD co-design in **Chapter 2**, **Chapter 3** introduces a robust stochastic integrated design for active FTC to deal with the actuator degradation under the simultaneous presence of disturbances.

2. Multi-objective problem in Disturbances Attenuation

During the system operation, there always exist disturbances that interfere adversely with the performance of the global system. Depending on the context, the disturbances can be categorized as parametric uncertainties, UIs, and stochastic noises. To the best of author's knowledge, only two maximum out of the above three issues are to be examined at the same time. Even that, the multi-objective problem can still happen in the disturbance attenuation process and lead to a time-costly tuning for a compromised performance. A typical instance is the $\mathcal{H}_\infty / \mathcal{H}_2$ optimization for \mathcal{L}_2 -norm UI and noise with unity energy [Khosrowjerdi, Nikoukhah, and Safari-Shad 2004], which is a non-convex problem and commonly solved by choosing fixed γ_∞ for \mathcal{H}_∞ -performance and minimizing γ_2 for \mathcal{H}_2 -noise synthesis. Hence, to avoid the multi-objective optimization issues, a disturbance-attenuating alternative solution is demanded.

As a result, the Thesis has proposed an output frequency-shaping filter that works based on the knowledge of disturbance frequency. Then, a Kalman-based observer-controller integrated design, which not only allows the attenuation of simultaneous disturbance impacts but also avoids the multi-objective optimization issue, is presented in **Chapter 3**.

3. Nonlinearity of scheduling parameter ρ in LPV systems

In some circumstances such as quasi-LPV systems, the scheduling parameter ρ is chosen as the nonlinear formulation of system states and parameters. However, it can induce the inaccuracy in observer design due to the inexact estimation of states/parameters. Thus, to avoid this problem, the polytopic observer for non-singular systems has been suggested [López-Estrada et al. 2015b]. Unfortunately, the required polytopic representation and the complex synthesis with the closed-loop system limit its implementation. On the other hand, although the nonlinearity problem can be directly tackled by Lipschitz condition [Us Saqib et al. 2017; Pham, Sename, Dugard, et al. 2019], this approach only works in non-singular LPV systems. Hence, the development of nonlinear LPV observer designs that work for both LPV and S-LPV systems under the existence of Lipschitz nonlinearity is essential.

In this thesis, a new class of Singular time-delay NonLinear Parameter Varying (S-NLPV) system is introduced to unify all the so far existing LPV systems. Also, the corresponding UI observer designs will be presented in **Chapters 5 and 6**.

4. UI-decoupling constraint in UI Observers

To handle the negative impact of UI on the dynamical systems, UI observers have been widely studied. The main principle of this kind of observer is to eliminate the UI presence in the dynamics of estimation errors by using structurally algebraic condition. In other words, it has to find a designed matrix such that its multiplication with the UI matrix should be null [Darouach, Zasadzinski, and Xu 1994]. To relax this restrictive UI-decoupling constraint, some recent works have been realized as follows:

For LTI systems, the notation of partially decoupled UI has been introduced in [Xu et al. 2016; Gao, Liu, and Chen 2016] where UIs are divided into two groups: one satisfies the UI-decoupling constraints, and the other does not. Nonetheless, these works are only applicable to non-singular systems. Therefore, the development of a greater extension for S-LTI systems is required.

For LPV systems, this UI-decoupling becomes more problematic since the UI matrix depends on the time-varying parameter (TVP); hence, the synthesis of a unique designed matrix is no longer effective. Recently, [Marx et al. 2019] has made system reformulations and additional assumptions to design a time-varying designed matrix while still ensuring the restrictively parameter-dependent UI-decoupling algebraic constraints. Unfortunately, the design synthesis is complex and only applicable to non-singular LPV systems. Thus, there is an exigence for a simpler LPV UI-observer design that works even for S-LPV systems.

In this Thesis, the following solutions are proposed to overcome the above problems. For S-LTI systems, an extended result from the work of [Gao, Liu, and Chen 2016] and a novel design based on frequency-shaping filters are developed in **Chapter 4** for partially decoupled UI. For S-LPV systems, to bypass the parameter-dependent UI-decoupling condition, a new

methodology of UI observer based on \mathcal{H}_2 criteria will be introduced in **Chapter 5**, while \mathcal{H}_∞ approach is developed in **Chapter 6**. It should be noted that these observers are applicable to not only S-LPV systems but also for a more comprehensive class which includes Lipschitz nonlinearity and time-delay problem.

Thesis Structure and Contributions

Based on the discussed problems, the manuscript with its contributions is organized as below:

- **Chapter 1** recalls the theoretical background on dynamical systems, their stability and observability. Also, the modeling of suspension systems is provided. Finally, some useful lemmas, norms, and systems reformulations are demonstrated for the ease of the Thesis's exposition.

Then, the next five chapters are divided into two parts corresponding to non-singular and singular systems:

- **Part I:** FDD and FTC in Non-Singular Systems.

This first part presents contributions of robust observer-controller designs in the FDD and FTC processes. In specific,

- **Chapter 2** proposes a robust FDD solution for slowly time-varying faults in uncertain LPV systems by using the co-design of \mathcal{H}_∞ Proportional-Integral (PI) observer and state-feedback controller. Also, a generic formulation of uncertain terms is introduced to simplify the design process. The experimental results for FDD of sensor faults are realized for the suspension system in the platform INOVE.
- **Chapter 3** provides the modeling of nonlinear system degradation under the formulation of polynomial fault. Next, the methodology of a frequency-shaping filter is presented as an alternative method of UI attenuation. Also, based on the working frequency of UI, a generic strategy of robust-stochastic integrated designs is proposed for polytopic LPV systems to estimate on-line the actuator degradation and compensate its impact under saturation constraints and the simultaneous influence of parametric uncertainties, unknown inputs, and stochastic noises.

- **Part II:** Observer Designs for Singular Systems.

The second part of the Thesis provides a diversity of observer designs which not only overcome the existing problems in S-LTI but also promote the state estimation in a new class of LPV system, called Singular NonLinear Parameter-Varying (S-NLPV) systems. Details are given as follows:

- **Chapter 4** develops a generic approach for actuator fault estimation in S-LTI systems perturbed by the partially decoupled Unknown Input (UI). In which, the

actuator fault is expressed in a general form while partially decoupled UIs are divided into decoupled and non-decoupled UI depending on the satisfaction of UI-decoupling condition. Based on the knowledge of UI frequency, two approaches in UI observer design are proposed.

- **Chapter 5** introduces a new class of S-LPV systems with Lipschitz nonlinearity (S-NLPV), which unifies all the so far existing LPV systems. Also, a generic design for an \mathcal{H}_2 UI observer design has been introduced to relax the parameter-dependent UI-decoupling problem and it can be implemented regardless of LPV system representation.
- **Chapter 6** demonstrates a generic design process for \mathcal{H}_∞ NLPV observers that is applicable to SD-NLPV systems, as well as S-NLPV systems, regardless of their LPV representation. This proposed solution is based on the generic form of full-order observer, which integrates the state-input delays and Lipschitz nonlinearity and tackles the impact of UIs by \mathcal{H}_∞ synthesis. Additionally, the parameter-(in)dependent and the delay-dependent stability of estimation errors are studied.





- **Appendix:**

There are two appendices in this Thesis. Appendix A provides complementary information about suspension modeling in LPV and NLPV systems. Meanwhile, Appendix B is devoted to the proofs for R-detectability conditions in singular systems used for Chapters 4-6.

In this dissertation, the singular matrix E of S-LPV systems, as well as their extended systems, would be kept constant. In fact, the parameter-dependent form $E_{(\rho)}$ causes many difficulties in the analysis of regularity, impulse-free condition, and stability in singular systems, thus not being broadly studied yet and considered as long-term development of the Thesis.

How to read the Thesis

Although each chapter can be separately read without loss of overall understanding, Chapter 1 "Theoretical Background" is highly recommended for the readers to familiarize themselves with the basic concepts used in this Thesis.

It should be noted that all Chapters/Sections/Equations in the Thesis can be easily accessed with interactive hyperlinks (where the mouse pointer  is presented as ). Additionally, in the pdf viewer, such as Acrobat reader, the readers can use the keyboard shortcut  +  to quickly go back to the previous reading position after clicking on a hyperlink.

The reading layout can be summarized in the following figure.

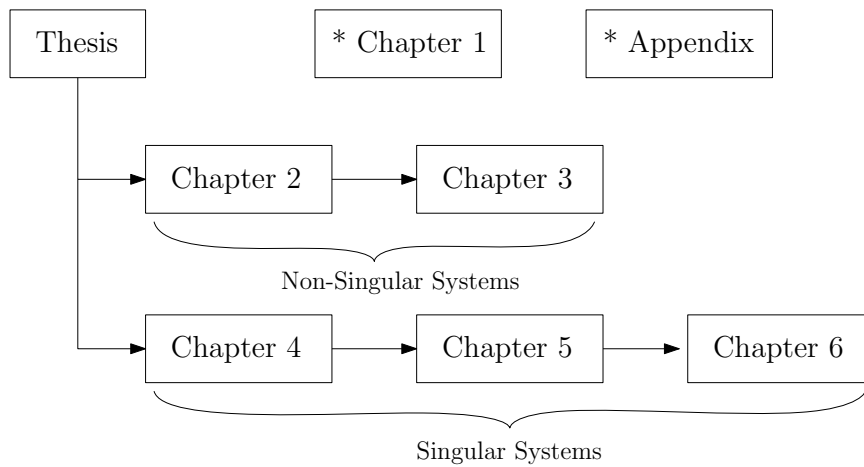


Figure 1: Thesis Reading Layout (*: Essential support)

Conclusions

In this Chapter, current issues in observer designs for (S-)LTI and (S-)LPV systems have been addressed together with the proposed solutions. Then, the research structure is introduced, serving as an orientation foundation for the next six chapters. In detail, a general background on the theory of these dynamical systems, as well as useful tools and lemmas, will be presented in Chapter 1. Meanwhile, in Chapters 2-6, the dissertation demonstrates the developed solutions for the existing problems in observer designs.

Theoretical background

Abstract: This chapter recalls theoretical backgrounds on the control theory and optimization which are used in the next chapters. It should be noted that these frameworks serve as a comprehensive review to provide unfamiliar readers with better understanding of LMI and LPV approaches. Thus, the definitions of dynamical systems, their stability and observability are introduced. Finally, some useful lemmas, norms, and system reformulations are demonstrated.

Contents

1.1	Different classes of dynamical systems	15
1.1.1	Nonlinear system	16
1.1.2	Singular/Descriptor Linear Time-Invariant (S-LTI) systems	16
1.1.3	Singular Linear Parameter-Varying (S-LPV) systems	17
1.2	Stability Conditions	19
1.2.1	Stability for LTI systems	19
1.2.2	Stability for LPV systems	20
1.2.3	Stability for time-delay LPV systems	21
1.3	Finite LMI solution for LPV systems	23
1.3.1	Polytopic Approach	23
1.3.2	Gridding Approach	25
1.4	Observability	27
1.4.1	Observability of S-LTI systems	27
1.4.2	Observability of S-LPV systems	28
1.5	Useful Lemmas, Norms and Reformulations	30
1.5.1	Useful Lemmas	30
1.5.2	\mathcal{H}_∞ (or \mathcal{L}_2 to \mathcal{L}_2) performance	32
1.5.3	System Reformulations	33
1.6	Conclusion	35

1.1 Different classes of dynamical systems

In this section, different classes of system dynamics used in the thesis are described. Particularly, the LPV system and its derivatives will be discussed in detail.

1.1.1 Nonlinear system

The nonlinear dynamical systems, which can be presented by nonlinear Differential Algebraic Equations (DAE), are of great interest in this Thesis. In fact, the DAEs representation demonstrates not only the classical nonlinear ODEs but also the algebraic constraints for input-state relation in the nonlinear system.

Definition 1.1.1 (*Nonlinear system*)

For given nonlinear functions f and h , a nonlinear dynamical system is expressed as:

$$\begin{cases} E\dot{x}(t) &= f(x(t), u(t)), \\ y(t) &= h(x(t), u(t)), \end{cases} \quad (1.1)$$

where $x(t) \in \mathbb{R}^{n_x}$ is the system state vector, $u(t) \in \mathbb{R}^{n_u}$ is the input vector, and $y(t) \in \mathbb{R}^{n_y}$ is the output/measurement vector of the system. The matrix $E \in \mathbb{R}^{n_q \times n_x}$ ($n_q \leq n_x$) is singular with $\text{rank}(E) < n_x$. When E is a non-singular matrix, i.e. $n_q = n_x$ and $\text{rank}(E) = n_x$ the DAEs representation can always be rewritten in the form of Ordinary Differential Equations (ODE).

1.1.2 Singular/Descriptor Linear Time-Invariant (S-LTI) systems

A singular/descriptor LTI (S-LTI) modeling displays the physical system through linear DAEs as presented below.

Definition 1.1.2 (*S-LTI dynamical system*)

Given constant matrices $A \in \mathbb{R}^{n_q \times n_x}$, $B \in \mathbb{R}^{n_q \times n_u}$, $C \in \mathbb{R}^{n_y \times n_x}$ and $D \in \mathbb{R}^{n_y \times n_u}$, a Singular Linear Time Invariant (S-LTI) system is described as:

$$\begin{cases} E\dot{x}(t) &= Ax(t) + Bu(t), \\ y(t) &= Cx(t) + Du(t), \end{cases} \quad (1.2)$$

where $x(t) \in \mathbb{R}^{n_x}$ is the system state vector, $u(t) \in \mathbb{R}^{n_u}$ is the input vector, and $y(t) \in \mathbb{R}^{n_y}$ is the output/measurement vector of the system. The matrix $E \in \mathbb{R}^{n_q \times n_x}$ ($n_q \leq n_x$) is singular with $\text{rank}(E) < n_x$.

When E is a non-singular matrix, i.e. $n_q = n_x$ and $\text{rank}(E) = n_x$, the S-LTI systems become the well-known LTI systems.

$$\begin{cases} \dot{x}(t) &= E^{-1}Ax(t) + E^{-1}Bu(t), \\ y(t) &= Cx(t) + Du(t), \end{cases} \quad (1.3)$$

Compared with nonlinear dynamical system (1.1), the S-LTI system (1.2) is considered as the local approximation of the nonlinear behaviors around operation/equilibrium points.

In essence, a S-LTI system can be decomposed into two subsystems as mentioned in [Dai 1989]:

Definition 1.1.3 (Slow and fast subsystems)

For any singular system (1.2), there exist two non-singular matrices Q and P such that (1.2) is restricted system equivalent to:

$$\text{Slow subsystem} \quad \begin{cases} \dot{x}_1 = A_1 x_1 + B_1 u \\ y_1 = C_1 x_1 + D_1 u \end{cases}, \quad (1.4)$$

$$\text{Fast subsystem} \quad \begin{cases} N\dot{x}_2 = x_2 + B_2 u \\ y_2 = C_2 x_2 + D_2 u \end{cases}, \quad (1.5)$$

$$y = y_1 + y_2, \quad (1.6)$$

with the coordinate transformation:

$$\begin{bmatrix} x_1 \\ x_2 \end{bmatrix} = P^{-1}x, \quad x_1 \in \mathbb{R}^{n_1 \times n_2}, \quad x_2 \in \mathbb{R}^{n_2 \times n_2}, \quad QEP = \text{diag}\{I_{n_1}, N\}, \quad (1.7)$$

$$QAP = \text{diag}\{A_1, I_{n_2}\}, \quad QB = \begin{bmatrix} B_1 \\ B_2 \end{bmatrix}, \quad CP = [C_1 \ C_2], \quad D = [D_1 \ D_2], \quad (1.8)$$

where $n_1 + n_2 = n$, $N \in \mathbb{R}^{n_2 \times n_2}$ is nilpotent.

The slow subsystem presents the dynamics of ODEs in the form of a LTI system, whereas the fast subsystem illustrates the impulse component or algebraic equations.

1.1.3 Singular Linear Parameter-Varying (S-LPV) systems

As previously mentioned, a major limitation of a S-LTI model is that it can only describe the system locally, thus not being able to express completely the nonlinear behavior and provide global stabilization. To deal with this drawback, Singular Linear Parameter-Varying (S-LPV) systems are considered, whose representation can be either linear for state and input or nonlinear for the parameter. Therefore, this special class of nonlinear systems is able to maintain the characteristic of nonlinearity while still implementing the analysis and design tools for S-LTI systems. In specific, a S-LPV system can be defined as follows:

Definition 1.1.4 (S-LPV dynamical system)

Considering $\rho(t)$ as a measurable time-varying parameter vector that takes values in the parameter space \mathcal{P}_ρ (a convex set) such that:

$$\mathcal{P}_\rho := \{\rho := [\rho_1 \ \dots \ \rho_m]^T \in \mathbb{R}^m, \ \underline{\rho}_i \leq \rho_i \leq \bar{\rho}_i, \ \forall i = 1 : m\} \quad (1.9)$$

where m is the number of varying parameters.

For given time-varying matrices $A(\rho) \in \mathbb{R}^{n_q \times n_x}$, $B(\rho) \in \mathbb{R}^{n_q \times n_u}$, $C(\rho) \in \mathbb{R}^{n_y \times n_x}$, and $D(\rho) \in \mathbb{R}^{n_y \times n_u}$, a Singular Linear Parameter-Varying (S-LPV) dynamical system can be

described as:

$$\begin{cases} E\dot{x}(t) &= A_{(\rho)}x(t) + B_{(\rho)}u(t), \\ y(t) &= C_{(\rho)}x(t) + D_{(\rho)}u(t), \end{cases} \quad (1.10)$$

where $x(t) \in \mathbb{R}^{n_x}$ is the system state vector, $u(t) \in \mathbb{R}^{n_u}$ is the input vector, and $y(t) \in \mathbb{R}^{n_y}$ is the output/measurement vector of the system. The matrix $E \in \mathbb{R}^{n_q \times n_x}$ ($n_q \leq n_x$) is singular with $\text{rank}(E) < n_x$.

Remark 1.1.1

In this dissertation, E is considered as a constant singular matrix for S-LPV systems. However, the case of parameter-dependent $E_{(\rho)}$ has not been broadly studied yet due to its difficulties in analyzing parameter-dependent regularity, impulse-free characteristic, and stability. Therefore, singular systems with $E_{(\rho)}$ will be examined in the future works.

Without loss of generality, the case where E is a singular square matrix, i.e. $n_q = n_x$ and $\text{rank}(E) < n_x$, is studied in Numerical Examples of this Thesis to illustrate the proposed observer designs.

When E is a non-singular matrix, i.e. $n_q = n_x$ and $\text{rank}(E) = n_x$, the S-LPV system implies the classical LPV system, as below:

$$\begin{cases} \dot{x}(t) &= E^{-1}A_{(\rho)}x(t) + E^{-1}B_{(\rho)}u(t), \\ y(t) &= C_{(\rho)}x(t) + D_{(\rho)}u(t), \end{cases} \quad (1.11)$$

Remark 1.1.2

- $\rho(\cdot) = \rho$ is a constant value, (1.11) is a LTI system.
- $\rho(\cdot) = \rho(t)$ is an externally measurable/estimated parameter vector, (1.11) is a LPV system.
- $\rho(\cdot) = \rho(x(t))$, (1.11) is a quasi-Linear Parameter Varying (qLPV) system.

In the presence of dead-zone in the mechanical system or the long-distant transmission in network systems, loss/delay is inevitable in the input/output/state data, adversely affecting system stability. Therefore, the impact of time-varying delay is focused in the Thesis. Hereunder is the extended version of Definition 1.10 adapting to Time-delay S-LPV system.

Definition 1.1.5 (*Time-delay S-LPV dynamical system*)

For given time-varying matrices $A_{(\rho)} \in \mathbb{R}^{n_q \times n_x}$, $A_{d(\rho)} \in \mathbb{R}^{n_q \times n_x}$, $B_{(\rho)} \in \mathbb{R}^{n_q \times n_u}$, $B_{d(\rho)} \in \mathbb{R}^{n_q \times n_u}$, $C_{(\rho)} \in \mathbb{R}^{n_y \times n_x}$, $C_{d(\rho)} \in \mathbb{R}^{n_y \times n_x}$, $D_{(\rho)} \in \mathbb{R}^{n_y \times n_u}$, and $D_{d(\rho)} \in \mathbb{R}^{n_y \times n_u}$, a Time-delay

Singular Linear Parameter-Varying (S-LPV) dynamical system can be described as:

$$\begin{cases} E\dot{x}(t) &= A_{(\rho)}x(t) + A_{d(\rho)}x(t - h(t)) + B_{(\rho)}u(t), \\ y(t) &= C_{(\rho)}x(t) + C_{d(\rho)}x(t - h(t)) + D_{(\rho)}u(t), \\ x(\lambda) &= \varpi_x(\lambda), \lambda \in [-\bar{h}, 0], \end{cases} \quad (1.12)$$

where $x(t) \in \mathbb{R}^{n_x}$ is the system state vector, $u(t) \in \mathbb{R}^{n_u}$ is the input vector, and $y(t) \in \mathbb{R}^{n_y}$ is the output/measurement vector of the system, $\varpi_x(t)$ is the functional initial condition for state x , and $h(t)$ is time-varying delay. The matrix $E \in \mathbb{R}^{n_q \times n_x}$ ($n_q \leq n_x$) is singular with $\text{rank}(E) < n_x$.

When E is a non-singular matrix, i.e. $n_q = n_x$ and $\text{rank}(E) = n_x$, the classical time-delay LPV system is re-obtained.

$$\begin{cases} \dot{x}(t) &= E^{-1}A_{(\rho)}x(t) + E^{-1}A_{d(\rho)}x(t - h(t)) + E^{-1}B_{(\rho)}u(t), \\ y(t) &= C_{(\rho)}x(t) + C_{d(\rho)}x(t - h(t)) + D_{(\rho)}u(t), \\ x(\lambda) &= \varpi_x(\lambda), \lambda \in [-\bar{h}, 0], \end{cases} \quad (1.13)$$

In this Thesis, the time-varying delay $h(t)$ is assumed to be known and belongs to the set \mathcal{H}_d :

$$\mathcal{H}_d = \{h : \mathbb{R}_{\geq 0} \rightarrow [0, \bar{h}], \dot{h}(t) \leq \mu < 1, t \geq 0\}, \quad (1.14)$$

In fact, the constraint on the derivative of delay $\dot{h}(t)$, which guarantees that state signal direction will never reverse, has been widely chosen in the study of time-delay phenomena [Tan, Grigoriadis, and Wu 2003; Briat 2015].

1.2 Stability Conditions

In the observer designs of this Thesis, the dynamics of estimation error are to be displayed in the non-singular form of dynamical systems. Therefore, regarding the simplicity of stability conditions, Section 1.2 will emphasize on LMI-based method to justify the stability of non-singular systems.

1.2.1 Stability for LTI systems

Consider an autonomous LTI system:

$$\dot{x}(t) = Ax(t) \quad (1.15)$$

Thanks to the Lyapunov theory and the Linear Matrix Inequality (LMI) optimization, the stability of the system (1.15) is defined as follows:

Definition 1.2.1 (Stability of LTI system)

The system (1.15) is quadratically stable if there exists a Lyapunov function $V(x) = x^T P x$ where $P = P^T > 0$ satisfying that:

$$A^T P + P A < 0 \quad (1.16)$$

The satisfaction of (1.16) leads to the convergence of states. Also, to modify their convergence dynamics, the following definition, which can be later applied to observer design to change the converging time of the estimated signals, is concerted:

Definition 1.2.2 (α -Stability/Pole placement)

Given the Lyapunov function $V(x) = x^T P x$ and a known scalar $\alpha > 0$, the decay rate of the system (1.15) is guaranteed if there exists $P = P^T > 0$ such that:

$$A^T P + P A + 2\alpha P < 0 \quad (1.17)$$

Compared with the classical condition for Lyapunov function $\dot{V} < 0$, the above LMI for α -stability ensures faster convergence dynamics, i.e. $\dot{V} < -2\alpha V$. Also, the poles of the system (1.15) are placed in the half-left plane of $-\alpha$.

1.2.2 Stability for LPV systems

Due to time-varying distribution matrices, LPV systems have more complex stability analysis than LTI systems. Although a LPV system can be stable for all time-frozen parameter values, it becomes (increasingly) unstable in case of varying parameters as a result of switches among subsystems. Hence, in this section, the stability of LPV systems, which is ensured thanks to the quadratic Lyapunov function, is recalled.

Consider the following autonomous LPV system:

$$\dot{x}(t) = A_{(\rho)} x(t). \quad (1.18)$$

Hereunder are the two definitions of stability for LPV systems: [Barmish 1985; Lu and Doyle 1993; Wu 1995]

Definition 1.2.3 (Quadratic Stability / Parameter-independent Stability)

The system (1.18) is quadratically stable if there exists a quadratic Lyapunov function $V(x(t)) = x(t)^T P x(t) > 0$ with the constant matrix $P = P^T > 0$ satisfying: $\forall \rho$

$$A_{(\rho)}^T P + P A_{(\rho)} < 0 \quad (1.19)$$

Remark 1.2.1

When $A_{(\rho)} = A$ is constant matrix, the LMI-based stability for LTI system in Definition 1.2.1 is re-obtained.

Since only parameter-independent P is required $\forall \rho$, the quadratic stability is considered highly conservative, thus possibly leading to an unfeasible solution. To avoid this issue, the following definition is proposed:

Definition 1.2.4 (Robust Stability / Parameter-dependent Stability)

The system (1.18) is parametrically-dependent stable if there exists a quadratic Lyapunov function $V(x(t)) = x(t)^T P_{(\rho)} x(t) > 0$ with the parameter-dependent matrix $P_{(\rho)} = P_{(\rho)}^T > 0$ satisfying: $\forall \rho$

$$A_{(\rho)}^T P_{(\rho)} + P_{(\rho)} A_{(\rho)} + \sum_{i=1}^m \dot{\rho}_i \frac{\partial P_{(\rho)}}{\partial \rho_i} < 0 \quad (1.20)$$

The parameter variation rates are assumed to be bounded, i.e. $|\dot{\rho}_i| \leq \vartheta_i \forall i = 1 : m$. As a result, the above condition can be verified by solving the following inequality: [Wu 1995]

$$A_{(\rho)}^T P_{(\rho)} + P_{(\rho)} A_{(\rho)} + \sum_{i=1}^m \pm \vartheta_i \frac{\partial P_{(\rho)}}{\partial \rho_i} < 0 \quad (1.21)$$

Remark 1.2.2

Since $P_{(\rho)}$ depends on its time-varying parameter $\rho(t)$, its derivative is also taken into account for system stability. Some calculation on $P_{(\rho)}$ can be found in Section 1.5.1.6. Besides, as the notion $\sum_i^m \pm(\cdot)$ expresses all combinations of $+(\cdot)$ and $-(\cdot)$, the inequality (1.21) actually represents 2^m different inequalities that correspond to the 2^m different combinations in the summation [Wu 1995].

Remark 1.2.3

If $P_{(\rho)} = P$, LMI (1.19) is the LMI (1.20), i.e. the quadratic stability is a particular case of parameter-dependent stability. Also, quadratic stability is a sufficient condition to stability. [Briat 2008]

1.2.3 Stability for time-delay LPV systemz

Consider the following autonomous time-delay LPV system:

$$\dot{x}(t) = A_{(\rho)} x(t) + A_{d(\rho)} x(t - h(t)). \quad (1.22)$$

where time-varying delay $h(t)$ is known and satisfies $\dot{h}(t) \leq \mu < 1$.

In term of time-delay systems, there are two fundamental definitions:[Kamen, Khargonekar, and Tannenbaum 1985; Abdallah et al. 1993; Olgac and Sipahi 2002; Abdallah et al. 2011; Briat 2015]

Definition 1.2.5 (*Delay-Independent Stability*)

The time-delay system (1.22) is stable independently of the delay or delay-independent stable if stability does not depend on the delay value, that is, if the system is stable for any delay value in $[0, \infty)$.

Definition 1.2.6 (*Delay-Dependent Stability*)

The time-delay system (1.22) is delay-dependent stable if there exists an (bounded) interval $\mathbb{I} \in \mathbb{R}_{\geq 0}$ such that the system is stable for any delay in \mathbb{I} , and unstable otherwise.

In practice, the stability of a real physical system is frequently impacted by the value of delays. Therefore, the delay-dependent definition, which is built on the changes of delay and its limitation, reflects the reality better than the delay-independent one, which ensures the stability for all value of $h(t)$.

The LMI-based stability of time-delay system is obtained by using Lyapunov-Krasovskii functionals, which are chosen as follows: [Xu and Lam 2007; Briat 2008]

- **Delay-Independent Stability:** $h(t) \in [0, +\infty)$

$$V_{(\rho)} = x^T(t)P_{(\rho)}x(t) + \int_{t-h(t)}^t x(\theta)Qx(\theta)d\theta. \quad (1.23)$$

- **Delay-Dependent Stability:** $h(t) \in [0, \bar{h}]$, $\bar{h} < +\infty$

$$V_{(\rho)} = x^T(t)P_{(\rho)}x(t) + \int_{t-h(t)}^t x(\theta)Qx(\theta)d\theta + \bar{h} \int_{-\bar{h}}^0 \int_{t+\theta}^t \dot{x}^T(s)R\dot{x}(s) ds d\theta. \quad (1.24)$$

where $P_{(\rho)}$, Q , and R are symmetric positive definite matrices.

Therefore, the two following definitions can be obtained: [Wu and Grigoriadis 2001; Tan, Grigoriadis, and Wu 2003; Gouaisbaut and Peaucelle 2006; Briat 2015]

Definition 1.2.7 (*Delay-Independent Stability for time-varying delay*)

The system (1.22) with time-varying delay $h(t)$ satisfying $\dot{h}(t) \leq \mu < 1$ is stable independently of the delay if there exist symmetric positive definite matrices $P_{(\rho)}$ and Q such that:

$$\begin{bmatrix} A_{(\rho)}^T P_{(\rho)} + P_{(\rho)} A_{(\rho)} + \sum_{i=1}^m \dot{\rho}_i \frac{\partial P_{(\rho)}}{\partial \rho_i} + Q & P_{(\rho)} A_{d(\rho)} \\ (*) & -(1 - \mu)Q \end{bmatrix} < 0 \quad (1.25)$$

Definition 1.2.8 (*Delay-dependent Stability using Jensen's Inequality*)

The system (1.22) is delay-dependent stable for all time-varying delays $h(t) \in [0, \bar{h}]$ satisfying $\dot{h}(t) \leq \mu < 1$ if there exist symmetric positive definite matrices $P_{(\rho)}$, Q and R such that:

$$\begin{bmatrix} A_{(\rho)}^T P_{(\rho)} + P_{(\rho)} A_{(\rho)} + \sum_{i=1}^m \dot{\rho}_i \frac{\partial P_{(\rho)}}{\partial \rho_i} + Q - R & P_{(\rho)} A_{d(\rho)} + R & \bar{h} A_{(\rho)}^T R \\ (*) & -(1 - \mu)Q - R & \bar{h} A_{d(\rho)}^T R \\ (*) & (*) & -R \end{bmatrix} < 0 \quad (1.26)$$

Remark 1.2.4

- When $P_{(\rho)} = P$ a constant matrix, i.e. $\frac{\partial P_{(\rho)}}{\partial t} = \sum_{i=1}^m \dot{\rho}_i \frac{\partial P_{(\rho)}}{\partial \rho_i} = 0$, the quadratic stability of LPV systems in Definition 1.2.3 is ensured. Otherwise, the parameter-dependent stability in Definition 1.2.4 is applied.
- The LMI conditions for constant delay $h(t) = h$ are also those for time-varying delay with $\mu = 0$.

1.3 Finite LMI solution for LPV systems

Although the Definitions (1.20)–(1.21) and (1.25)–(1.26) in Section 1.2 have presented the LMI-based stability for (time-delay) LPV systems, their LMI conditions present an infinitive-dimension problem due to the infinite values of ρ . Thus, one challenge of the LPV framework is to reformulate the infinite set of LMIs into a finite one that can be solved via semi-definite programming. Regarding the simplicity in methodology and synthesis, the two following approaches, as mentioned in [Hoffmann and Werner 2015], are proposed in this Thesis:

- Polytopic approach,
- Gridding approach,

which are widely used for Quadratic Stability and Robust Stability. Meanwhile, LMI optimization problem or semi-definite programming is solved by the implementation of [Lofberg 2004; Toh, Todd, and Tütüncü 1999].

1.3.1 Polytopic Approach

To implement this approach, the LPV system must be presented in the polytopic formulation. The following definition is recalled:

Definition 1.3.1 (Polytopic LPV system)

A LPV system is said to be polytopic if the parameter dependence of its state-space matrices $A_{(\rho)}$, $B_{(\rho)}$, $C_{(\rho)}$, $D_{(\rho)}$ on ρ is affine and ρ varies inside a polytope $\Theta = Co\{\omega_1, \dots, \omega_{2^N}\}$ where ω_i are the vertices of the polytope formed by the boundness of each element in time-varying vector ρ . In that case, its state-space matrices also range over each corner of the polytope as follows:

$$\left[\begin{array}{c|c} A_{(\rho)} & B_{(\rho)} \\ \hline C_{(\rho)} & D_{(\rho)} \end{array} \right] = \sum_{i=1}^{2^m} \delta_{i(\rho)} \left[\begin{array}{c|c} A_i & B_i \\ \hline C_i & D_i \end{array} \right] = \sum_{i=1}^{2^m} \delta_{i(\rho)} \left[\begin{array}{c|c} A_{(\omega_i)} & B_{(\omega_i)} \\ \hline C_{(\omega_i)} & D_{(\omega_i)} \end{array} \right] \quad (1.27)$$

where the coefficients of polytopic decomposition $\delta_{i(\rho)} \geq 0$ and $\sum_{i=1}^{N=2^m} \delta_{i(\rho)} = 1$.

To calculate the coefficients, the following formulation is proposed as its systematic procedure can be easily applied to any number m of parameters: [Biannic 1996; Bruzelius 2004; Poussot-Vassal et al. 2008]

$$\delta_{i(\rho_1)} = \frac{\prod_{j=1}^m |\rho_j - \mathcal{C}_{(\omega_i)j}^\delta|}{\prod_{j=1}^m (\bar{\rho}_j - \underline{\rho}_j)} \quad (1.28)$$

where $\mathcal{C}_{(\omega_i)j}^\delta$ is the j^{th} component of the vector $\mathcal{C}_{(\omega_i)}^\delta$ defined as:

$$\mathcal{C}_{(\omega_i)j}^\delta = \{\rho_{1j} | \rho_j = \bar{\rho}_j \text{ if } (\omega_i)_j = \underline{\rho}_j \text{ or } \rho_j = \underline{\rho}_j \text{ otherwise}\}. \quad (1.29)$$

Due to the polytopic representation, only the polytopic quadratic stability of the LPV system can be implied from the Definition 1.2.3.

Proposition 1.3.1 (Polytopic Quadratic Stability)

If LPV system (1.15) can be presented in the polytopic formulation, i.e.

$$\dot{x}(t) = A_{(\rho)}x(t) = \sum_{i=1}^{2^m} \delta_{i(\rho)} A_i x(t), \quad (1.30)$$

then it is quadratically stable if there exists a matrix $P = P^T > 0$ such that:

$$A_i^T P + P A_i < 0, \quad (1.31)$$

holds for all $i = 1, \dots, 2^m$.

Similar to Definition 1.2.3, Definition 1.3.1 also uses a unique matrix P to ensure the finite set of LMI corresponding to all local values A_i that present the parameter-dependent matrix $A_{(\rho)}$. Therefore, polytopic quadratic stability is considered conservative. To avoid this issue, the gridding approach is introduced in the next section and can be applied regardless of system representations.

1.3.2 Gridding Approach

In this approach, the parameter space is divided in the form of a grid that is defined by the number of gridding points $n_g^{\rho_i}$, i.e. the number of gridding points for element ρ_i of vector ρ ($i = 1 : m$). For instance, Fig. 1.1 demonstrates the grid representation of parameter space when the number of TVPss $m = 2$. Also, it should be noted that if $n_g^{\rho_1} = n_g^{\rho_2} = \dots = n_g^{\rho_m} = n_g$ then the number of time-frozen points is $N_g = n_g^m$. Furthermore, at each time-frozen point ρ^j ($j = 1 : N_g$, $N_g = n_g^{\rho_1} \times n_g^{\rho_2} \times \dots \times n_g^{\rho_m}$), i.e. the coordinates in the grid, the (singular) LPV system is considered as (singular) linear time-invariant system [Apkarian, Gahinet, and Becker 1995]. Consequently, the grid-based approach is applicable to not only (non) convex set but also both kinds of stability (quadratic and robust), regardless of system representation.

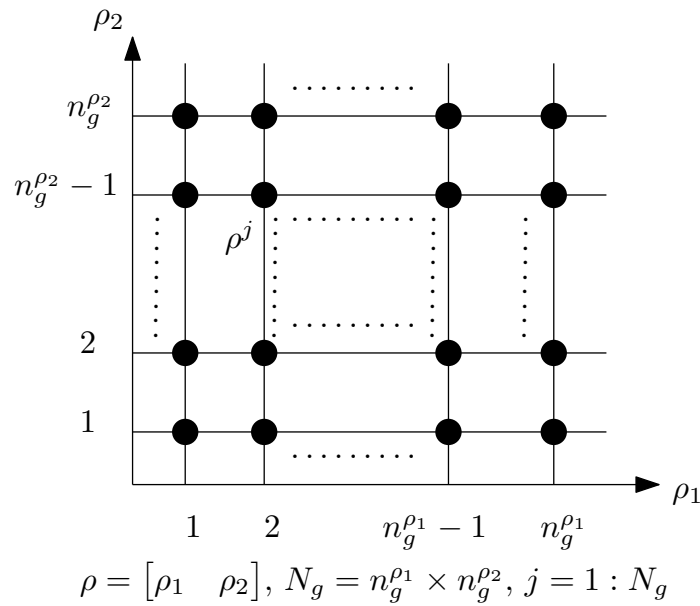


Figure 1.1: Grid of parameter space.

To successfully apply the gridding approach/method, the two following aspects are to be carefully examined.

1.3.2.1 Number of gridding points $n_g^{\rho_i}$

Since the inequalities (1.20)–(1.21) and (1.25)–(1.26) are rewritten as a set of LMIs defined at each time-frozen point ρ^j , the grid density will determine the cost of LMI computation and its complexity. To the best of author's knowledge, no accurate method of choosing $n_g^{\rho_i}$ has been developed. In general, the appropriate number $n_g^{\rho_i}$ of points must be neither too small to assure the performance and stability of the observer-controller design, nor too large to avoid the numerical problem and computation complexity. Meanwhile, the gridding approach does not rigorously guarantee the stability and performance of the proposed observer. Hence, a

post-analysis on a much denser grid for the parameter-dependent LMIs must be performed to ensure the correctness of the solution [Hoffmann and Werner 2015]. If this check fails, the grid density is then increased until local guarantees are established on a sufficiently dense grid. Unfortunately, an unavoidable drawback of this method is that the number of LMIs to be solved increases exponentially with the number of time-varying parameters. Also, the grid-based solution is always an approximate approach regardless of how dense the grid can be.

1.3.2.2 Choice of basis functions

The basis functions are chosen for the parameter-dependent matrices to be found in the LMI, for instance, $P_{(\rho)}$ in the LMI (1.21). By approximating the matrix $P_{(\rho)}$ with a finite basis function of ρ , a solution for the infinite parameter-dependent LMI can be achieved through a finite dimensional set. Unfortunately, to the best of author's knowledge, the choice depends heavily on practice. Concerning simplicity, $P_{(\rho)}$ can be either affine or polynomial, i.e.

$$P_{(\rho)} = P_0 + \sum_{i=1}^{N_1} P_i \rho_i, \quad P_{(\rho)} = P_0 + \sum_{i=1}^{N_2} P_i \rho^i, \quad (1.32)$$

where P_i are constant matrices satisfying $P_{(\rho)} > 0$ and the set of LMIs that presents the inequality (1.21) at each point ρ^j .

Other practical choices are presented in [Wu 1995; Apkarian and Adams 2000; Abbas et al. 2014]. More discussions about the gridding solution, particularly its effectiveness and drawbacks, are given in [Wu 1995; Apkarian and Adams 2000; Hoffmann and Werner 2015].

1.3.2.3 General Algorithm

In general, the grid-based algorithm consists of two steps:

- **Offline Computation**

Firstly, the number of gridding points and the basis functions are chosen. Then, the parameter-dependent LMI presenting the stability of the studied system is rewritten as a set of LMIs which corresponds to all time-frozen points ρ^j in the grid of parameter space. The solution is a posteriori checked on a much denser grid to verify its correctness. At the end of this process, all time-invariant matrices that partly define the time-varying components are computed. For instance, the matrices P_i , along with ρ , define the time-varying matrix $P_{(\rho)}$ in (1.32).

- **Online Implementation**

For each instant t , update the value of parameter-varying vector $\rho(t)$. Next, calculate the time-varying parameter-dependent matrices based on the value of $\rho(t)$ and the constant time-invariant matrices.

More details on the implementation will be presented later in Experimental Applications and Numerical Examples of the Thesis. It should be noted that although the above grid-based algorithm is computationally inexpensive, it may require large amounts of memory to store the local parameters.

1.4 Observability

Since the Thesis is focused on the observer designs for the dynamical systems mentioned in Section 1.1, the observability conditions for S-LTI and S-LPV systems are recalled in this part. In addition to the observability, the detectability - its slightly weaker notion - is also discussed as it is implied from observability. Indeed, a system is detectable if all the unobservable states are stable.

1.4.1 Observability of S-LTI systems

As indicated in [Dai 1989], the observability of S-LTI systems, which reflects the ability to reconstruct the whole system state (impulse terms are included) from output measurements and control input, is built based on that of each subsystem (slow and fast).

Definition 1.4.1 (*Observability of Singular Systems (S-LTI)*)

The singular system (1.2) is observable if both of the following conditions are satisfied:

- Its slow subsystem is observable, i.e.

$$\text{rank} \begin{bmatrix} pE - A \\ C \end{bmatrix} = n, \quad \forall p \in \mathbb{C}, \quad p \text{ is finite.} \quad (1.33)$$

- Its fast subsystem is observable (Impulse-free condition), i.e.

$$\text{rank} \begin{bmatrix} E \\ C \end{bmatrix} = n. \quad (1.34)$$

Furthermore, the observability also has two important derivatives, Impulse-Observability and Reachable-Observability, as defined in the following definitions:

Definition 1.4.2 (*Reachable-observability/R-observability*)

The singular system (1.2) is R-observable if it is observable in reachable set - in other words, any state in the reachable set may be uniquely determined by $y(t)$ and $u(\tau)$, $0 \leq \tau \leq t$. Also, the singular system (1.2) is R-observable if and only if its slow subsystem is

observable, i.e.

$$\text{rank} \begin{bmatrix} pE - A \\ C \end{bmatrix} = n, \forall p \in \mathbb{C}, p \text{ is finite.} \quad (1.35)$$

Unlike the classical observability, R-observability characterizes the ability to reconstruct only the reachable state (impulse components are not included). Its weaker notion, R-detectability, can be expressed as:

$$\text{rank} \begin{bmatrix} pE - A \\ C \end{bmatrix} = n, \forall \mathcal{R}(p) \geq 0. \quad (1.36)$$

In addition, it yields the detectability condition for LTI systems without the impulse components:

$$\text{rank} \begin{bmatrix} pI - A \\ C \end{bmatrix} = n, \forall \mathcal{R}(p) \geq 0. \quad (1.37)$$

Definition 1.4.3 (*Impulse-Observability/I-observability*)

The singular system (1.2) is impulse observable if $x(t)$ may be uniquely determined by $y(t)$ and $u(t)$ for any $t \geq 0$. System (1.2) is impulse observable if its fast subsystem is impulse observable, i.e.

$$\text{rank} \begin{bmatrix} E & A \\ 0 & E \\ 0 & C \end{bmatrix} = n + \text{rank}(E). \quad (1.38)$$

In essence, I-observability guarantees the ability to uniquely determine the impulse behavior in $x(t)$ caused by the jump behavior in the input. Compared with the classical observability and R-observability which all consist of the finite-value terms in state response, I-observability focuses on the impulse terms. Another significant difference between the classical observability and its derivatives is that their relationship is solely one-way. In other words, a system is I/R-observable if it is observable, whereas the reverse is not true.

1.4.2 Observability of S-LPV systems

Due to the time-varying parameter, the observability of (time-delay) S-LPV systems cannot be verified by generally structural conditions as in the case of S-LTI systems. Instead, only the analytical results, which justify the local conditions of time-invariant systems at each time-frozen point in the grid-based approach or each corner in the polytopic approach, can be obtained. Therefore, even if the analytical conditions are well checked, the observability/detectability of (S-)LPV systems cannot be completely ensured.

By using the polytopic system presentation, the implied results for S-LPV systems are presented as follows: [Hamdi et al. 2012; López-Estrada 2014]

Proposition 1.4.1 (Polytopic R-observability)

The triplets (E, A_i, C) of S-LPV system (1.10) are called observable on the reachable set (R-observable) if

$$\text{rank} \begin{bmatrix} pE - A_i \\ C \end{bmatrix} = n, \quad \forall p \in \mathbb{C}, \quad p \text{ is finite}, \quad i = 1 : 2^m. \quad (1.39)$$

Also, it yields the detectability condition for polytopic LPV systems:

$$\text{rank} \begin{bmatrix} pI - A_i \\ C \end{bmatrix} = n, \quad \forall \mathcal{R}(p) \geq 0, \quad i = 1 : 2^m. \quad (1.40)$$

Proposition 1.4.2 (Polytopic I-detectability)

The triplets (E, A_i, C) of S-LPV system (1.10) are called impulse observable (I-observable) if

$$\text{rank} \begin{bmatrix} E & A_i \\ 0 & E \\ 0 & C \end{bmatrix} = n + \text{rank}(E), \quad i = 1 : 2^m. \quad (1.41)$$

Remark 1.4.1

To be consistent with the LMI solution for polytopic systems [Apkarian and Gahinet 1995], the output matrix $C_{(\rho)} = C$ is required to be independent of the time-varying parameter vector $\rho(t)$.

Besides the above polytopic condition, classical LPV systems also have the following LMI-based constraints to examine the detectability regardless of system representation: [Wu 1995]

Definition 1.4.4 (Quadratic Detectability)

The pair of matrix $(A_{(\rho)}, C_{(\rho)})$ is quadratically detectable if there exist a symmetric positive matrix P and a matrix L such that:

$$\mathcal{H}\{P(A_{(\rho)} + L_{(\rho)}C_{(\rho)})\} < 0 \quad (1.42)$$

Definition 1.4.5 (Parameter-dependent Detectability)

The pair of matrix $(A_{(\rho)}, C_{(\rho)})$ is parametrically-dependent detectable if there exist a symmetric positive matrix $P_{L(\rho)}$ and a matrix $L_{(\rho, \dot{\rho})}$ such that:

$$\mathcal{H}\{P_{(\rho)}(A_{(\rho)} + L_{(\rho, \dot{\rho})}C_{(\rho)})\} + \sum_{i=1}^m (\dot{\rho}_i \frac{\partial P_{(\rho)}}{\partial \rho}) < 0 \quad (1.43)$$

holds for all $\rho \in \mathcal{P}_\rho$ and $|\dot{\rho}_i| \leq \vartheta_i$.

In fact, the above LMIs in Definitions 1.4.4-1.4.5 are inferred from the implementation of Definitions 1.2.3 (Quadratic Stability)-1.2.4 (Parameter-dependent Stability) in the dynamics of estimation error $e = x - \hat{x}$, which is expressed as follows:

$$\dot{e} = (A_{(\rho)} + L_{(\rho, \dot{\rho})}C_{(\rho)})e, \quad (1.44)$$

by considering the following LPV system and observer:

$$\text{System} : \begin{cases} \dot{x} = A_{(\rho)}x, \\ y = C_{(\rho)}x \end{cases}, \quad (1.45)$$

$$\text{Observer} : \dot{\hat{x}} = A_{(\rho)}\hat{x} - L_{(\rho, \dot{\rho})}(y - C_{(\rho)}\hat{x}). \quad (1.46)$$

It should be noted that those conditions are verified only by solving LMIs through approximation methods such as the grid-based approach. Consequently, they cannot be as quickly verified as the above rank conditions in the polytopic approach.

1.5 Useful Lemmas, Norms and Reformulations

1.5.1 Useful Lemmas

The following lemmas, which are applied later in the Theorems' proofs, are recalled.

1.5.1.1 Schur's Complement

Suppose Q and S are symmetric matrices, the following statements are equivalent:[Boyd et al. 1994]

$$\circ \begin{bmatrix} Q & R \\ R^T & S \end{bmatrix} < 0; \quad (1.47)$$

$$\circ S < 0, \quad Q - RS^{-1}R^T < 0; \quad \text{and} \quad (1.48)$$

$$\circ Q < 0, \quad S - R^TQ^{-1}R < 0. \quad (1.49)$$

1.5.1.2 Majorization Lemma

For given matrices X and Y with appropriate dimensions, if there exists $F^T F \leq I$, the following inequality is always true with an arbitrary scalar $\sigma > 0$: [Wang, Xie, and Souza 1992]

$$XFY + Y^T F^T X^T \leq \sigma XX^T + \sigma^{-1}Y^T Y. \quad (1.50)$$

1.5.1.3 Projection Lemma

Given matrices $U \in \mathbb{R}^{p \times n}$, $V \in \mathbb{R}^{m \times n}$ and a symmetric matrix $\Psi \in \mathbb{S}^n$. Then, the following statements are equivalent: [Gahinet and Apkarian 1994]

1. There exists a matrix $\Omega \in \mathbb{R}^{m \times p}$ such that

$$\Psi + U^T \Omega^T V + V^T \Omega U < 0. \quad (1.51)$$

2. The following LMIs hold

$$U_{\perp}^T \Psi U_{\perp} < 0, \quad (1.52)$$

$$V_{\perp}^T \Psi V_{\perp} < 0, \quad (1.53)$$

where U_{\perp} and V_{\perp} are bases of the null-space of U and V , respectively.

1.5.1.4 Young relation

Given matrices X and Y with appropriate dimensions, for any invertible matrix F and scalar $\varepsilon > 0$, we have: [Boyd et al. 1994]

$$X^T Y + Y^T X \leq \varepsilon X^T F X + \varepsilon^{-1} Y^T F^{-1} Y. \quad (1.54)$$

1.5.1.5 Jensen's inequality

Let ϕ be a convex integrable function and $z : [a, b] \rightarrow \mathbb{R}$, ($a < b$), be integrable over its domain of definition. Then, the following inequality holds: [Jensen et al. 1906]

$$\phi \left(\int_a^b z(s) ds \right) \leq (b - a) \int_a^b \phi(z(s)) ds \quad (1.55)$$

1.5.1.6 Partial differential Matrix

Let $P_{(\rho)}$ be a differentiable and invertible matrix function of ρ , where the time-varying vector $\rho = [\rho_1(t) \ \rho_2(t) \ \dots \ \rho_m(t)]^T$, the following statements are always true $\forall i = 1 : m$: [Wu 1995]

$$\bullet \quad \frac{dP_{(\rho)}}{dt} = \sum_i^m \dot{\rho}_i \frac{\partial P_{(\rho)}}{\partial \rho_i}, \quad (1.56)$$

$$\bullet \quad \dot{\rho}_i \frac{\partial P_{(\rho)}}{\partial \rho_i} = -\dot{\rho}_i P_{(\rho)} \frac{\partial P_{(\rho)}^{-1}}{\partial \rho_i} P_{(\rho)}. \quad (1.57)$$

1.5.2 \mathcal{H}_∞ (or \mathcal{L}_2 to \mathcal{L}_2) performance

\mathcal{H}_∞ synthesis aims to bound the energy gain that is obtained from the \mathcal{L}_2 norm of input and output, i.e. $\|u\|_2$ and $\|y\|_2$, by a given/minimized attenuation level γ_∞ [Gahinet and Apkarian 1994; Scherer and Weiland 2001]. As a result, this approach is widely applied in practice to observer/controller designs to attenuate the impact of unavoidable negative input, i.e. disturbance, on the desired output.

1.5.2.1 LTI system

Definition 1.5.1 (\mathcal{H}_∞ norm)

The \mathcal{H}_∞ norm of a proper LTI system (1.3) ($E = I$) from input $u(t)$ to output $y(t)$ is the induced energy-to-energy gain (\mathcal{L}_2 to \mathcal{L}_2 norm) defined as,

$$\|G(s)\|_\infty = \sup_{\omega \in \mathbb{R}} \bar{\sigma}(G(s)) = \sup_{u(s) \in \mathcal{L}_2} \frac{\|y(s)\|_2}{\|u(s)\|_2} = \max_{u(t) \in \mathcal{L}_2} \frac{\|y\|_2}{\|u\|_2}, \quad (1.58)$$

where $G(s) = C(sI - A)^{-1}B + D$.

As the \mathcal{H}_∞ -norm represents the maximal gain for the frequency response of the system, it also demonstrates the worst-case attenuation level. For SISO systems, it reflects the maximal peak value on the Bode magnitude.

To ensure both the \mathcal{H}_∞ -norm performance and the system stability, the following lemma is given:[Gahinet and Apkarian 1994]

Lemma 1.5.1 (*Bounded Real Lemma*)

The LTI system is asymptotically stable and $\|G\|_\infty < \gamma_\infty$, if there exists a symmetric positive definite matrix P such that the following LMI holds:

$$\begin{bmatrix} A^T P + PA & PB & C^T \\ B^T P & -\gamma_\infty I & D^T \\ C & D & -\gamma_\infty I \end{bmatrix} < 0 \quad (1.59)$$

1.5.2.2 LPV system

Due to the time-varying characteristic of scheduling parameters, the \mathcal{H}_∞ norm in LTI system has to be re-defined as the induced \mathcal{L}_2 -norm in LPV system:

Definition 1.5.2 (*Induced \mathcal{L}_2 -norm for LPV system* –[Wu 1995])

Consider LPV system (1.11), let us define the operator Σ_{LPV_ρ} such that $y(t) = (\Sigma_{LPV_\rho} u)(t)$ for some parameter trajectory ρ . For zeros initial state condition, i.e. $x(0) =$

0, the induced \mathcal{L}_2 norm is defined as:

$$\|\Sigma_{LPV_\rho}\|_{i,2} = \sup_{\rho(t) \in \mathcal{P}_\rho, \|u\|_2 \neq 0, u \in \mathcal{L}_2} \frac{\|y\|_2}{\|u\|_2}, \quad (1.60)$$

which is often referred as the \mathcal{H}_∞ gain of the LPV system from input $u(t)$ to output $y(t)$.

Considering the impact of time-varying parameter $\rho(t)$ on LPV system stability, Lemma 1.5.1 is extended to Generalized Bounded Real Lemma, demonstrated as follows: [Wu 1995]

Lemma 1.5.2 (Generalized Bounded Real Lemma)

The LPV system (1.11) ($E = I$) is parametrically-dependent stable and ensures the induced \mathcal{L}_2 -norm performance $\|\Sigma_{LPV_\rho}\|_{i,2} < \gamma_\infty$ if there exists a symmetric positive-definite matrix $P(\rho)$ such that:

$$\begin{bmatrix} A(\rho)^T P(\rho) + P(\rho) A(\rho) + \sum_{i=1}^m \pm \vartheta_i \frac{\partial P}{\partial \rho_i} & P(\rho) B(\rho) & C(\rho)^T \\ B(\rho)^T P(\rho) & -\gamma_\infty I & D(\rho)^T \\ C(\rho) & D(\rho) & -\gamma_\infty I \end{bmatrix} < 0 \quad (1.61)$$

holds for all $\rho \in \mathcal{P}_\rho$ and $|\dot{\rho}_i| \leq \vartheta_i$.

1.5.3 System Reformulations

1.5.3.1 Output-Input filters

Consider the following S-LPV system:

$$\begin{cases} E\dot{x}_a & = A_{(\rho)}x_a + B_{(\rho)}u, \\ y & = C_{(\rho)}x_a + D_{(\rho)}u \end{cases}, \quad (1.62)$$

To synthesize the controller and observer, the input-output matrices B and C are sometimes required to be independent of the time-varying parameter vector ρ , like in case of polytopic approach [Apkarian and Gahinet 1995]. Therefore, the following reformulations for LPV systems are listed.

• Input Filter

To obtain a parameter-independent input matrix, the following stable filter W_u [Apkarian, Gahinet, and Becker 1995] is implemented to the input u :

$$W_u : \begin{bmatrix} \dot{x}_F \\ u \end{bmatrix} = \begin{bmatrix} A_F & B_F \\ C_F & 0 \end{bmatrix} \begin{bmatrix} x_F \\ u^* \end{bmatrix}. \quad (1.63)$$

By using (1.63), the following augmented state-space representation which has parameter-

independent input matrix \bar{B} is given:

$$\begin{cases} \bar{E}\dot{x}_a &= \bar{A}_{(\rho)}x_a + \bar{B}u^* \\ y &= \bar{C}_{(\rho)}x_a \end{cases}, \quad (1.64)$$

In which, $x_a = \begin{bmatrix} x \\ x_F \end{bmatrix}$ is the augmented state vector, u^* is the new input vector, $\bar{E} = \begin{bmatrix} E & 0 \\ 0 & I \end{bmatrix}$, $\bar{A}_{(\rho)} = \begin{bmatrix} A_{(\rho)} & B_{(\rho)}C_F \\ 0 & A_u \end{bmatrix}$, $\bar{C}_{(\rho)} = [C_{(\rho)} \quad D_{(\rho)}C_F]$, and $\bar{B} = \begin{bmatrix} 0 \\ B_F \end{bmatrix}$.

• Output Filter

To obtain a parameter-independent output, the following stable filter W_y [Apkarian, Gahinet, and Becker 1995] is implemented to the output y :

$$W_y : \begin{bmatrix} \dot{x}_F \\ y^* \end{bmatrix} = \begin{bmatrix} A_F & B_F \\ C_F & 0 \end{bmatrix} \begin{bmatrix} x_F \\ y \end{bmatrix}. \quad (1.65)$$

By using (1.63), the following augmented state-space representation which has parameter-independent output is given:

$$\begin{cases} \bar{E}\dot{x}_a &= \bar{A}_{(\rho)}x_a + \bar{B}_{(\rho)}u \\ y^* &= \bar{C}x_a \end{cases}, \quad (1.66)$$

In which, $x_a = \begin{bmatrix} x \\ x_u \end{bmatrix}$ is the augmented state vector, y^* is the new input vector, $\bar{E} = \begin{bmatrix} E & 0 \\ 0 & I \end{bmatrix}$, $\bar{A}_{(\rho)} = \begin{bmatrix} A_{(\rho)} & 0 \\ B_FC_{(\rho)} & A_F \end{bmatrix}$, $\bar{C} = [0 \quad C_F]$, and $\bar{B}_{(\rho)} = \begin{bmatrix} B_{(\rho)} \\ B_FD_{(\rho)} \end{bmatrix}$.

1.5.3.2 Output decomposition

The following S-LPV system is considered:

$$\begin{cases} E\dot{x} &= A_{(\rho)}x + B_{(\rho)}u + D_{1(\rho)}w \\ y &= Cx + D_2w \end{cases} \quad (1.67)$$

where $\text{rank } C > \text{rank } D_2$ and w is a vector of unknown inputs/disturbances.

The assumption that the output y depends only on system state x , i.e. $y = Cx$, is essential in some observer designs, such as the those in Chapters 4-6. Therefore, to achieve this representation, under the condition $\text{rank } C > \text{rank } D$, the output y in (1.67) can always be decomposed into y_1 , which is dependent on the UI w , and y_2 , which is independent of w .

$$y = C_yx + D_2w \implies \begin{cases} y_1 = C_1x + D_{21}w, \\ y_2 = C_2x, \end{cases} \quad (1.68)$$

where C_{y1} and C_{y2} are the combination of rows in C_y . Then, the system (1.67) can be rewritten as:

$$\begin{cases} \begin{bmatrix} E \\ 0 \end{bmatrix} \dot{x} &= \begin{bmatrix} A_{(\rho)} \\ C_1 \end{bmatrix} x + \begin{bmatrix} B_{(\rho)} & 0 \\ 0 & I \end{bmatrix} \begin{bmatrix} u^T & y_1^T \end{bmatrix}^T + \begin{bmatrix} D_{1(\rho)} \\ D_{21} \end{bmatrix} w, \\ y_2 &= C_2 x, \end{cases} \quad (1.69)$$

which has the UI-free output y_2 .

Then, the reformulated system (1.69) with the new input $u^* = [u^T \ y_1^T]^T$ and the new output y_2 will be used for the observer synthesis instead of the system (1.67).

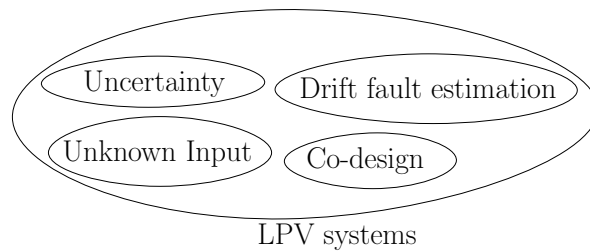
1.6 Conclusion

In this section, the theoretical backgrounds on the stability and observability for diversity classes of dynamical systems have been recalled. Also, useful lemmas, norms, and systems reformulations are mentioned for the ease of the Thesis's exposition.

Part I
FDD and FTC in Non-singular
systems

Robust observer-controller co-design for FDD of drift faults

Abstract: The main contribution of Chapter 2 is a robust observer-controller co-design for FDD in uncertain LPV systems with drift faults. In which, the parametric uncertainties are presented in a generic form and then handled by Majorization lemma, thus reducing the amount of LMIs and complexity of stability solution. Concerning the co-design, the \mathcal{H}_∞ PI observer for FDD is robustly synthesized through the closed-loop system, which is built on \mathcal{H}_∞ PI observer and state-feedback controller. Accordingly, both observer and controller gains are simultaneously obtained by a unique linear matrix inequality (LMI). Finally, its application to a vehicle suspension platform is presented to highlight the importance of robust synthesis in observer-based designs and the FDD process.



Contents

2.1 Introduction	40
2.1.1 Related works	40
2.1.2 Chapter Contributions	40
2.2 Problem Formulation	41
2.2.1 LPV system representation	41
2.2.2 Design objectives	42
2.3 Main results	43
2.3.1 Robust Co-Design of \mathcal{H}_∞ PI Observer and State-feedback Controller . . .	43
2.3.2 Discussion on Active FTC design	50
2.4 FDD Application to sensor fault in Suspension system	51
2.4.1 Platform INOVE	51
2.4.2 LPV Modeling for faulty suspension system	53
2.4.3 System uncertainty	54

2.4.4	Experimental conditions	54
2.4.5	Observer design for semi-active suspension	56
2.4.6	Frequency Analysis	60
2.4.7	Validation result	63
2.5	Conclusion	66

2.1 Introduction

2.1.1 Related works

As mentioned in [Isermann 2006; Alwi, Edwards, and Tan 2011], some faults like an actuator jam, a hardover and offsets in sensor outputs are slow varying, i.e. $\dot{f} \approx 0$ (drift faults). Thus, their estimation methods are of great interest in the research and industry community. Since the drift fault f can be considered as an augmented state, the proportional-integral (PI) observer [Wojciechowski 1978] has been widely implemented to estimate both system states and faults. In [Marx, Koenig, and Georges 2003], \mathcal{H}_∞ PI observer is proposed to handle the disturbances/UIs. Then, [Hamdi et al. 2012] presented a more comprehensive design for LPV systems by combining UI and PI observers. Unfortunately, its restrictive constraint on the UI-decoupling condition cannot be always satisfied. Hence, to tackle this issue, [Hassanabadi, Shafiee, and Puig 2015] has developed a \mathcal{H}_∞ proportional-integral (PI) observer so that the UI effect on estimation error is also attenuated by \mathcal{H}_∞ synthesis. Meanwhile, [Zhang, Zhang, and Wang 2015] have built a \mathcal{H}_∞ high-order PI observer to estimate the actuator faults and attenuate the perturbation impact. On the other hand, too few studies are mentioned for the impact of parametric uncertainty [Jabbari and Benson 1992] on PI observer, which causes observer instability by generating state x in the dynamics of estimation error \dot{e} . A notable LPV research on this topic belongs to [Hassanabadi, Shafiee, and Puig 2017], addressing the uncertainty influence on PI observer for descriptor LPV systems. However, the polytopic expression of system uncertainty presents a complicated solution to observer design as a result of the double-layer polytopic model. Moreover, not only are system data required to be expressed in polytopic form, but the output matrix must also be independent of TVP. Hence, there is a need for an efficient solution to robust \mathcal{H}_∞ PI observer synthesis regardless of system representation.

2.1.2 Chapter Contributions

In this Chapter, to tackle the above obstacles concerning uncertainty, the following contributions have been made for the LPV framework:

- An approach for uncertainty representation in LPV system, which overcomes the limitation of polytopic expression. By using the Majorization lemma, the proposed generic

form of uncertainty promotes a simple integration of the robust problem in the stability analysis without generating the supplementary conditions as in the case of Projection lemma;

- A generic approach of robust LPV observer-controller co-design for FDD purpose, in which the observer is implied from the stability of the closed-loop system while both observer-controller gains are simultaneously synthesized by a unique LMI solution. In fact, this co-design serves as the foundation for developing an integrated design for active FTC in Chapter 3.

In addition, during FDD application to the suspension system, the comparison among different design approaches proves the importance of the robust solution in coping with system uncertainty. Hence, the performance of the proposed co-design is highlighted.

The Chapter is organized as follows. Firstly, the uncertain faulty LPV model, along with design objectives, is introduced in Section 2.2. Next, Section 2.3 presents the robust observer-controller co-design against system uncertainties and a discussion on active FTC. Then in Section 2.4, the experimental validation is realized in platform INOVE with the existence of actuator and sensor faults. Finally, a conclusion with remarks is made in Section 2.5.

2.2 Problem Formulation

2.2.1 LPV system representation

Consider the following class of faulty and uncertain LPV system:

$$\begin{cases} \dot{x} &= (A_{(\rho)} + \Delta A_{(\rho)})x + B_{(\rho)}u + E_{d(\rho)}d + E_{f(\rho)}f \\ y &= (C_{(\rho)} + \Delta C_{(\rho)})x + D_{(\rho)}u + F_{d(\rho)}d + F_{f(\rho)}f \end{cases} \quad (2.1)$$

where:

- $x \in \mathbb{R}^{n_x}$ is the state vector; $y \in \mathbb{R}^{n_y}$ is the measurement output vector; $u \in \mathbb{R}^{n_u}$ is the input vector; $d \in \mathbb{R}^{n_d}$ is the UI vector with bounded energy (\mathcal{L}_2 -norm); $f \in \mathbb{R}^{n_f}$ is the fault vector to be estimated.
- Matrices $A_{(\rho)}$, $B_{(\rho)}$, $C_{(\rho)}$, $D_{(\rho)}$, $E_{d(\rho)}$, $E_{f(\rho)}$, $F_{d(\rho)}$, and $F_{f(\rho)}$ are parameter-varying matrices in the nominal system. Their value depends on the parameter-varying vector $\rho(t)$, which belongs to the parameter space \mathcal{P}_ρ :

$$\mathcal{P}_\rho = \{\rho = [\rho_1(t) \quad \rho_2(t) \quad \dots \quad \rho_m(t)]^T \mid \underline{\rho}_i(t) \leq \rho_i \leq \bar{\rho}_i(t), \forall i = 1 : m, t \geq 0.\}$$

- Terms $\Delta A_{(\rho)}$ and $\Delta C_{(\rho)}$ are time-varying parameter matrices corresponding to the uncertainties of nominal system, which can be expressed as:

$$\begin{cases} \Delta A_{(\rho)} = M_{a(\rho)} \Delta_a N_{a(\rho)}, \\ \Delta C_{(\rho)} = M_{c(\rho)} \Delta_c N_{c(\rho)}. \end{cases} \quad (2.2)$$

In which, $M_{a(\rho)}$, $N_{a(\rho)}$, $M_{c(\rho)}$, and $N_{c(\rho)}$ with appropriate dimensions are measurable parameter-varying matrices. The terms Δ_a and Δ_c are matrices satisfying $\Delta_a^T \Delta_a \leq I$ and $\Delta_c^T \Delta_c \leq I$.

Remark 2.2.1

The formulation (2.2) enables the generic representation of parametric uncertainties without the need to approximate them by the polytopic representation. Thus, no requirement for the polytopic form of system (2.1) is needed, and consequently, the double-layer polytopic problem which exceeds the amount of LMIs in stability synthesis is avoided.

Remark 2.2.2

In case of uncertainties in input matrices ($\Delta B_{(\rho)}$ and $\Delta D_{(\rho)}$) and fault matrices ($\Delta E_{f(\rho)}$ and $\Delta F_{f(\rho)}$), the representation (2.1) can always be obtained by using the input filters proposed in Section 1.5.3.1 with singular matrix $E = I$.

The following assumptions are required for FDD co-design of the above LPV system (2.1):

- (A.1) Faults are \mathcal{L}_2 -bounded and in low frequency domain, i.e., $\dot{f} \simeq 0$ [Marx, Koenig, and Georges 2003; Hamdi et al. 2012].
- (A.2) Parameter variations are bounded. In other words, $|\rho_i| \leq \vartheta_i$ where ϑ_i is non-negative constant boundness corresponding to each element of parameter-varying vector $\rho(t)$ [Wu et al. 1996].

2.2.2 Design objectives

Under Assumptions (A.1)-(A.2), the aim of this Chapter is to find a robust co-design, which is also a \mathcal{H}_∞ PI observer-based controller, for FDD in the faulty-uncertain LPV system (2.1).

$$\begin{cases} \dot{\hat{x}} &= A_{(\rho)}\hat{x} + B_{(\rho)}u + L_{P(\rho)}(y - \hat{y}) + E_{f(\rho)}\hat{f} \\ \dot{\hat{f}} &= L_{I(\rho)}(y - \hat{y}) \\ \hat{y} &= C_{(\rho)}\hat{x} + D_{(\rho)}u + F_{f(\rho)}\hat{f} \\ u &= -K_{(\rho)}\hat{x} \end{cases} \quad (2.3)$$

where $L_{P(\rho)}$, $L_{I(\rho)}$, and $K_{(\rho)}$ are the proportional-integral (PI) gains of PI observer and the feedback gain of controller, respectively. In specific, these gains have to satisfy the following objectives:

- For $w = [d^T \quad f^T]^T = 0$, the closed-loop system, demonstrated later in (2.10), is asymptotically stable and robust against parametric uncertainty.
- For $w \neq 0$, the effects of exogenous input w on the fault estimation error e_f are attenuated by minimizing γ such that: [Wu et al. 1996]

$$\sup_{\rho \in \mathcal{P}_\rho, \|w\|_2 \neq 0, w \in \mathcal{L}_2} \frac{\|e_f\|_2}{\|w\|_2} \leq \gamma, \quad (2.4)$$

The interaction among uncertain LPV system (2.1), \mathcal{H}_∞ PI observer and controller u in (2.3) is presented in Fig. 2.1. In which, the observer inputs are composed of the system command u and the system output y , whereas vectors f and d are considered as exogenous input $w = \begin{bmatrix} d \\ f \end{bmatrix}$.

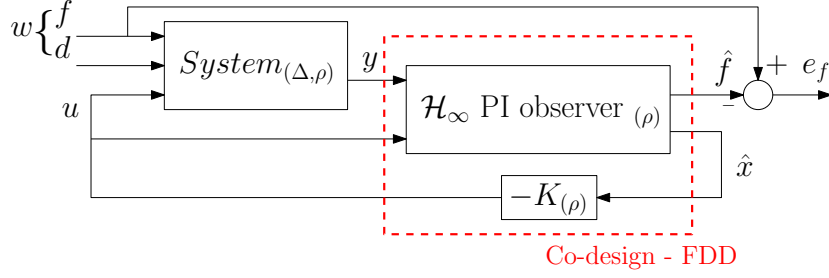


Figure 2.1: Robust Co-design - Robust FDD scheme

The robust \mathcal{H}_∞ PI observer-based controller, i.e. robust co-design for FDD, of uncertain LPV system (2.1) is designed in the next section. Also, the reason for the synthesis of \mathcal{H}_∞ PI observer through an observer-based controller will be explained.

2.3 Main results

2.3.1 Robust Co-Design of \mathcal{H}_∞ PI Observer and State-feedback Controller

In this section, details on the design process for the robust observer-controller co-design are presented.

The state estimation error e_x and fault estimation error e_f are defined as:

$$\begin{cases} e_x = x - \hat{x} \\ e_f = f - \hat{f} \end{cases} \quad (2.5)$$

Using the observer-based controller (2.3), system (2.1) becomes:

$$\dot{x} = (A(\rho) + \Delta A(\rho) - B(\rho)K(\rho))x + B(\rho)K(\rho)e_x + E_{d(\rho)}d + E_{f(\rho)}f \quad (2.6)$$

Combining (2.1) and (2.3), the dynamics of estimation errors is given by:

$$\begin{aligned} \dot{e}_x &= (A(\rho) - L_{P(\rho)}C(\rho))e_x + (E_{f(\rho)} - L_{P(\rho)}F_{f(\rho)})e_f \\ &\quad + (E_{d(\rho)} - L_{P(\rho)}F_{d(\rho)})d + (\Delta A(\rho) - L_{P(\rho)}\Delta C(\rho))x. \end{aligned} \quad (2.7)$$

$$\dot{e}_f = -L_{I(\rho)}C(\rho)e_x - L_{I(\rho)}F_{f(\rho)}e_f - L_{I(\rho)}F_{d(\rho)}d - L_{I(\rho)}\Delta C(\rho)x. \quad (2.8)$$

The closed-loop system can be expressed as:

$$\begin{cases} \dot{x} &= (A_{(\rho)} + \Delta A_{(\rho)} - B_{(\rho)}K_{(\rho)})x + B_{(\rho)}K_{(\rho)}C_{ax}e + E_{d(\rho)}d + E_{f(\rho)}f, \\ \dot{e} &= (A_{a(\rho)} - L_{a(\rho)}C_{a(\rho)})e + (E_{da(\rho)} - L_{a(\rho)}F_{d(\rho)})d + (\Delta A_{a(\rho)} - L_{a(\rho)}\Delta C_{(\rho)})x. \end{cases} \quad (2.9)$$

In which, $e = \begin{bmatrix} e_x \\ e_f \end{bmatrix}$, $e_x = C_{ax}e$, $C_{ax} = [I_{n_x} \quad 0_{n_x \times n_f}]$, $A_{a(\rho)} = \begin{bmatrix} A_{(\rho)} & E_{f(\rho)} \\ 0 & 0 \end{bmatrix}$, $L_{a(\rho)} = \begin{bmatrix} L_{P(\rho)} \\ L_{I(\rho)} \end{bmatrix}$, $C_{a(\rho)} = [C_{(\rho)} \quad F_{f(\rho)}]$, $E_{da(\rho)} = \begin{bmatrix} E_{d(\rho)} \\ 0 \end{bmatrix}$, and $\Delta A_{a(\rho)} = \begin{bmatrix} \Delta A_{(\rho)} \\ 0 \end{bmatrix}$.

From (2.10), the closed-loop system can be expressed as:

$$\begin{aligned} \begin{bmatrix} \dot{x} \\ \dot{e} \end{bmatrix} &= \begin{bmatrix} A_{(\rho)} + \Delta A_{(\rho)} - B_{(\rho)}K_{(\rho)} & B_{(\rho)}K_{(\rho)}C_{ax} \\ \Delta A_{a(\rho)} - L_{a(\rho)}\Delta C_{(\rho)} & A_{a(\rho)} - L_{a(\rho)}C_{a(\rho)} \end{bmatrix} \begin{bmatrix} x \\ e \end{bmatrix} \\ &+ \begin{bmatrix} E_{d(\rho)} \\ E_{da(\rho)} - L_{a(\rho)}F_{d(\rho)} \end{bmatrix} d + \begin{bmatrix} E_{f(\rho)} \\ 0 \end{bmatrix} f \end{aligned} \quad (2.10)$$

Due to the uncertainty, the term $(\Delta A_{a(\rho)} - L_{a(\rho)}\Delta C_{(\rho)})$ in observer dynamics of (2.10), which reflects the relationship between \dot{e} and x , is not null, thereby causing instability in both observer and closed-loop system. To overcome this issue, [Do, Koenig, and Theilliol 2018c] has developed a robust \mathcal{H}_∞ PI observer for the open-loop system. Unfortunately, the zero-element in the diagonal of the LMI solution can generate numerical problems. Thus, another approach is proposed - a co-design in a closed-loop system, which prevents the coupling issue in \dot{e} and x by simultaneously calculating the gains of observer and controller. In fact, this method implicitly offers two solutions:

- A robust \mathcal{H}_∞ PI observer for the FDD process, which allows the state-fault estimation in the presence of parametric uncertainties and can be applied without controller (except in synthesis).
- A robust observer-based controller that stabilizes the closed-loop systems. For active FTC, this controller requires a fault compensator in order to become an integrated design. More details are provided later in Section 2.3.2.

The controller gain $K_{(\rho)}$ and observer gain $L_{a(\rho)}$ will be simultaneously synthesized by the following Theorem.

Theorem 2.3.1

Under Assumptions (A.1)-(A.2), for given positive scalars $\varepsilon, \sigma_1, \sigma_2, \sigma_3$, and σ_4 , if there exist symmetric positive definite matrices $P_{k(\rho)}$ and matrices $Q_{k(\rho)}$ ($k = 1, 2, 3$) which minimize $\gamma > 0$ such that:

$$\begin{bmatrix} \Omega_{11} & \Omega_{12} & \Omega_{13} \\ (*) & \Omega_{22} & 0 \\ (*) & (*) & \Omega_{33} \end{bmatrix} < 0, \quad (2.11)$$

where

$$\Omega_{11} = \begin{bmatrix} \Gamma_{11} & 0 & 0 & E_{d(\rho)} & E_{f(\rho)} \\ (*) & \Gamma_{22} & \Gamma_{23} & \Gamma_{24} & 0 \\ (*) & (*) & \Gamma_{33} & \Gamma_{34} & 0 \\ (*) & (*) & (*) & \Gamma_{44} & 0 \\ (*) & (*) & (*) & (*) & \Gamma_{55} \end{bmatrix}, \quad (2.12)$$

$$\Gamma_{11} = \mathcal{H}\{A_{(\rho)}P_{1(\rho)} - B_{(\rho)}Q_{1(\rho)}\} - \sum_i^m \pm \vartheta_i \frac{\partial P_{1(\rho)}}{\partial \rho_i}, \quad (2.13)$$

$$\Gamma_{22} = \mathcal{H}\{P_{2(\rho)}A_{(\rho)} + Q_{2(\rho)}C_{(\rho)}\} + \sum_i^m \pm \vartheta_i \frac{\partial P_{2(\rho)}}{\partial \rho_i}, \quad (2.14)$$

$$\Gamma_{33} = \mathcal{H}\{Q_{3(\rho)}F_{f(\rho)}\} + I + \sum_i^m \pm \vartheta_i \frac{\partial P_{3(\rho)}}{\partial \rho_i}, \quad (2.15)$$

$$\Gamma_{23} = P_{2(\rho)}E_{f(\rho)} + Q_{2(\rho)}F_{f(\rho)} + C_{(\rho)}^T Q_{3(\rho)}^T, \quad (2.16)$$

$$\Gamma_{24} = P_{2(\rho)}E_{d(\rho)} + Q_{2(\rho)}F_{d(\rho)}, \quad (2.17)$$

$$\Gamma_{34} = Q_{3(\rho)}F_{d(\rho)}, \quad (2.18)$$

$$\Gamma_{44} = -\gamma^2 I_{n_d}, \quad \Gamma_{55} = -\gamma^2 I_{n_f}, \quad (2.19)$$

$$\Omega_{12} = \begin{bmatrix} B_{(\rho)}Q_{1(\rho)} & 0 & P_{1(\rho)}N_{a(\rho)}^T & P_{1(\rho)}N_{c(\rho)}^T \\ 0 & I & 0 & 0 \\ 0 & 0 & 0 & 0 \\ 0 & 0 & 0 & 0 \\ 0 & 0 & 0 & 0 \end{bmatrix}, \quad (2.20)$$

$$\Omega_{13} = \begin{bmatrix} M_{a(\rho)} & 0 & 0 & 0 \\ 0 & P_{2(\rho)}M_{a(\rho)} & Q_{2(\rho)}M_{c(\rho)} & \\ 0 & 0 & 0 & Q_{3(\rho)}M_{c(\rho)} \\ 0 & 0 & 0 & 0 \\ 0 & 0 & 0 & 0 \end{bmatrix}, \quad (2.21)$$

$$\Omega_{22} = -\text{diag}\{\varepsilon^{-1}P_{1(\rho)}, \varepsilon P_{1(\rho)}, \frac{\sigma_1\sigma_2}{\sigma_1 + \sigma_2}I, \frac{\sigma_3\sigma_4}{\sigma_3 + \sigma_4}I\}, \quad (2.22)$$

$$\Omega_{33} = -\text{diag}\{\sigma_1^{-1}I, \sigma_2^{-1}I, \sigma_3^{-1}I, \sigma_4^{-1}I\}, \quad (2.23)$$

then the gains of robust feedback controller $K_{(\rho)}$ and robust \mathcal{H}_∞ PI observer $L_{(\rho)} = \begin{bmatrix} L_{P(\rho)}^T & L_{I(\rho)}^T \end{bmatrix}^T$, which solve the above design problems of LPV system (2.10), can be calculated by using: $K_{(\rho)} = Q_{1(\rho)}P_{1(\rho)}^{-1}$, $L_{P(\rho)} = -P_{2(\rho)}^{-1}Q_{2(\rho)}$, and $L_{I(\rho)} = -P_{3(\rho)}^{-1}Q_{3(\rho)}$.

Remark 2.3.1

The notion $\sum_i^m \pm(\cdot)$ in (2.13), (2.14), and (2.15) expresses all combinations of $+(\cdot)$ and $-(\cdot)$ that are included in the inequality (2.11). [Wu et al. 1996; Wu 1995]. The infinite LMI (2.11) of Theorem 2.3.1 can be solved by using the Gridding approach, which is mentioned in Section 1.3.2.

Proof: The sufficient stability for the PI observer-based controller (2.3) and the objective of attenuating exogenous inputs (2.4) can be achieved by minimizing $\gamma > 0$ such that: [Scherer, Gahinet, and Chilali 1997; Darouach, Boutat-Baddas, and Zerrougui 2011]

$$J = \dot{V}_{(\rho)} + e_f^T e_f - \gamma^2 w^T w < 0, \quad (2.24)$$

where the LPV-Lyapunov candidate function $V_{(\rho)} > 0$ (and $\dot{V}_{(\rho)} < 0$) is chosen as: [Gahinet, Apkarian, and Chilali 1996]

$$V_{(\rho)} = \begin{bmatrix} x^T & e_x^T & e_f^T \end{bmatrix} P_{(\rho)} \begin{bmatrix} x \\ e_x \\ e_f \end{bmatrix}. \quad (2.25)$$

Assume that $P_{(\rho)} > 0$ in (2.25) has the form:

$$P_{(\rho)} = \text{diag}\{P_{1(\rho)}^{-1}, P_{2(\rho)}, P_{3(\rho)}\}, \quad (2.26)$$

in which $P_{1(\rho)}^{-1}$, $P_{2(\rho)}$, and $P_{3(\rho)}$ are symmetric positive definite matrices. Therefore, (2.25) can be displayed as follows:

$$V = x^T P_{1(\rho)}^{-1} x + e_x^T P_{2(\rho)} e_x + e_f^T P_{3(\rho)} e_f. \quad (2.27)$$

Remark 2.3.2

In spite of the zero-diagonal block presented in (2.26), LPV-Lyapunov function (2.27) is still widely applied to tackle the robustness problem, notably in [Lien 2004; Kheloufi et al. 2013].

Using (2.6), (2.7), and (2.8), the left-hand side of (2.24) can be expressed as:

$$J = \begin{bmatrix} x^T & e_x^T & e_f^T & d^T & f^T \end{bmatrix} \Gamma^{(1)} \begin{bmatrix} x \\ e_x \\ e_f \\ d \\ f \end{bmatrix}, \quad (2.28)$$

where

$$\Gamma^{(1)} = \begin{bmatrix} \Gamma_{11}^{(1)} & \Gamma_{12} & 0 & \Gamma_{14} & \Gamma_{15} \\ (*) & \Gamma_{22}^{(1)} & \Gamma_{23} & \Gamma_{24} & 0 \\ (*) & (*) & \Gamma_{33}^{(1)} & \Gamma_{34} & 0 \\ (*) & (*) & (*) & \Gamma_{44} & 0 \\ (*) & (*) & (*) & (*) & \Gamma_{55} \end{bmatrix} + X_{1(\rho)} F_1 Y_{1(\rho)} + Y_{1(\rho)}^T F_1^T X_{1(\rho)}^T, \quad (2.29)$$

$$\Gamma_{11}^{(1)} = \mathcal{H}\{P_{1(\rho)}^{-1} A(\rho) - P_{1(\rho)}^{-1} B(\rho) K(\rho)\} + \sum_i^m \dot{\rho}_i \frac{\partial P_{1(\rho)}^{-1}}{\partial \rho_i}, \quad (2.30)$$

$$\Gamma_{12} = P_{1(\rho)}^{-1} B(\rho) K(\rho), \quad (2.31)$$

$$\Gamma_{14} = P_{1(\rho)}^{-1} E_d(\rho), \quad (2.32)$$

$$\Gamma_{15} = P_{1(\rho)}^{-1} E_f(\rho), \quad (2.33)$$

$$\Gamma_{22}^{(1)} = \mathcal{H}\{P_{2(\rho)}A_{(\rho)} + Q_{2(\rho)}C_{(\rho)}\} + \sum_i^m \dot{\rho}_i \frac{\partial P_{2(\rho)}}{\partial \rho_i}, \quad (2.34)$$

$$\Gamma_{33}^{(1)} = \mathcal{H}\{Q_{3(\rho)}F_{f(\rho)}\} + I + \sum_i^m \dot{\rho}_i \frac{\partial P_{3(\rho)}}{\partial \rho_i}, \quad (2.35)$$

$$Y_{1(\rho)}^T = \begin{bmatrix} N_{a(\rho)}^T & N_{a(\rho)}^T & N_{c(\rho)}^T & N_{c(\rho)}^T \\ 0 & 0 & 0 & 0 \\ 0 & 0 & 0 & 0 \\ 0 & 0 & 0 & 0 \end{bmatrix}, \quad (2.36)$$

$$F_1^T = \begin{bmatrix} \Delta_a^T & 0 & 0 & 0 \\ 0 & \Delta_a^T & 0 & 0 \\ 0 & 0 & \Delta_c^T & 0 \\ 0 & 0 & 0 & \Delta_c^T \end{bmatrix}, \quad (2.37)$$

$$X_{1(\rho)}^T = \begin{bmatrix} M_{a(\rho)}^T P_{1(\rho)}^{-1} & 0 & 0 & 0 & 0 \\ 0 & M_{a(\rho)}^T P_{2(\rho)} & 0 & 0 & 0 \\ 0 & M_{c(\rho)}^T Q_{2(\rho)}^T & 0 & 0 & 0 \\ 0 & 0 & M_{c(\rho)}^T Q_{3(\rho)}^T & 0 & 0 \end{bmatrix}. \quad (2.38)$$

By applying Majorization lemma (1.5.1.2) to $\Gamma^{(1)}$, $\forall \sigma_1, \sigma_2, \sigma_3, \sigma_4 > 0$, (2.29) implies:

$$\Gamma^{(1)} \leq \Gamma^{(2)}, \quad (2.39)$$

where

$$\Gamma^{(2)} = \begin{bmatrix} \Gamma_{11}^{(2)} & \Gamma_{12} & 0 & \Gamma_{14} & \Gamma_{15} \\ (*) & \Gamma_{22}^{(2)} & \Gamma_{23} & \Gamma_{24} & 0 \\ (*) & (*) & \Gamma_{33}^{(2)} & \Gamma_{34} & 0 \\ (*) & (*) & (*) & \Gamma_{44} & 0 \\ (*) & (*) & (*) & (*) & \Gamma_{55} \end{bmatrix}, \quad (2.40)$$

$$\begin{aligned} \Gamma_{11}^{(2)} &= \mathcal{H}\{P_{1(\rho)}^{-1}A_{(\rho)} - P_{1(\rho)}^{-1}B_{(\rho)}K_{(\rho)}\} + \sigma_1 P_{1(\rho)}^{-1}M_{a(\rho)}M_{a(\rho)}^T P_{1(\rho)}^{-1} \\ &\quad + (\sigma_1^{-1} + \sigma_2^{-1})N_{a(\rho)}^T N_{a(\rho)} + (\sigma_3^{-1} + \sigma_4^{-1})N_{c(\rho)}^T N_{c(\rho)} + \sum_i^m \dot{\rho}_i \frac{\partial P_{1(\rho)}^{-1}}{\partial \rho_i}, \end{aligned} \quad (2.41)$$

$$\begin{aligned} \Gamma_{22}^{(2)} &= \mathcal{H}\{P_{2(\rho)}A_{(\rho)} + Q_{2(\rho)}C_{(\rho)}\} + \sum_i^m \dot{\rho}_i \frac{\partial P_{2(\rho)}}{\partial \rho_i} \\ &\quad + \sigma_2 P_{2(\rho)}M_{a(\rho)}M_{a(\rho)}^T P_{2(\rho)} + \sigma_3 Q_{2(\rho)}M_{c(\rho)}M_{c(\rho)}^T Q_{2(\rho)}^T, \end{aligned} \quad (2.42)$$

$$\Gamma_{33}^{(2)} = \mathcal{H}\{Q_{3(\rho)}F_{f(\rho)}\} + \sum_i^m \dot{\rho}_i \frac{\partial P_{3(\rho)}}{\partial \rho_i} + \sigma_4 Q_{3(\rho)}M_{c(\rho)}M_{c(\rho)}^T Q_{3(\rho)}^T + I. \quad (2.43)$$

Remark 2.3.3

In fact, the Projection lemma in Section 1.5.1.3 may be applied to handle the uncertainty in inequality $\Gamma^{(1)} < 0$, but there will exist the difficulties in finding the parameter-dependent $X_{1\perp(\rho)}$ and $Y_{1\perp(\rho)}$, which are bases of the null-space of $X_{1(\rho)}$ and $Y_{1(\rho)}$ $\forall \rho$, especially if $X_{1(\rho)}$ has com-

plicated representation. Also, this usage will generate the complimentary LMIs, i.e. additional constraints corresponding to $X_{1(\rho)}$ and $Y_{1(\rho)}$. For such reasons, the majorization lemma is chosen to tackle the uncertainty term and to handle minimum amount of LMI.

For the property (2.24) to hold, i.e. $J < 0$, (2.39) follows that $\forall [x^T \ e_x^T \ e_f^T \ d^T \ f^T]^T \neq 0$:

$$\Gamma^{(2)} < 0. \quad (2.44)$$

Pre-multiplying and post-multiplying the above inequality by $\text{diag}\{P_{1(\rho)}, I, I, I, I\}$. Then, by using Differential Lemma (1.5.1.6), (2.44) becomes:

$$\Gamma^{(3)} = \begin{bmatrix} \Gamma_{11}^{(3)} & B_{(\rho)}K_{(\rho)} & 0 & E_{d(\rho)} & E_{f(\rho)} \\ (*) & \Gamma_{22}^{(2)} & \Gamma_{23} & \Gamma_{24} & 0 \\ (*) & (*) & \Gamma_{33}^{(2)} & \Gamma_{34} & 0 \\ (*) & (*) & (*) & \Gamma_{44} & 0 \\ (*) & (*) & (*) & (*) & \Gamma_{55} \end{bmatrix} < 0, \quad (2.45)$$

where

$$\begin{aligned} \Gamma_{11}^{(3)} &= \mathcal{H}\{A_{(\rho)}P_{1(\rho)} - B_{(\rho)}Q_{1(\rho)}\} + \sigma_1 M_{a(\rho)} M_{a(\rho)}^T - \sum_i^m \dot{\rho}_i \frac{\partial P_{1(\rho)}}{\partial \rho_i} \\ &+ (\sigma_1^{-1} + \sigma_2^{-1})P_{1(\rho)}N_{a(\rho)}^T N_{a(\rho)}P_{1(\rho)} + (\sigma_3^{-1} + \sigma_4^{-1})P_{1(\rho)}N_{c(\rho)}^T N_{c(\rho)}P_{1(\rho)}. \end{aligned} \quad (2.46)$$

The term $\Gamma^{(3)}$ can be rewritten as:

$$\Gamma^{(3)} = \Omega_{11}^{(1)} + X_2^T Y_2 + Y_2^T X_2, \quad (2.47)$$

where

$$\Omega_{11}^{(1)} = \begin{bmatrix} \Gamma_{11}^{(3)} & 0 & 0 & E_{d(\rho)} & E_{f(\rho)} \\ (*) & \Gamma_{22}^{(2)} & \Gamma_{23} & \Gamma_{24} & 0 \\ (*) & (*) & \Gamma_{33}^{(2)} & \Gamma_{34} & 0 \\ (*) & (*) & (*) & \Gamma_{44} & 0 \\ (*) & (*) & (*) & (*) & \Gamma_{55} \end{bmatrix}, \quad (2.48)$$

$$X_2 = [(B_{(\rho)}K_{(\rho)})^T \ 0 \ 0 \ 0 \ 0], \quad (2.49)$$

$$Y_2 = [0 \ I \ 0 \ 0 \ 0]. \quad (2.50)$$

Using Young relation (1.5.1.4) with $F = P_{1(\rho)}$, it follows that:

$$\Gamma^{(3)} \leq \Gamma^{(4)}, \quad (2.51)$$

where

$$\Gamma^{(4)} = \Omega_{11}^{(1)} + \varepsilon X_2^T P_{1(\rho)} X_2 + \varepsilon^{-1} Y_2^T P_{1(\rho)}^{-1} Y_2 = \Omega_{11}^{(1)} - \Omega_{12} \Omega_{22}^{-1} \Omega_{12}^T, \quad (2.52)$$

$$\Omega_{12} = [X_2^T P_{1(\rho)} \ Y_2^T] = \begin{bmatrix} B_{(\rho)}Q_{1(\rho)} & 0 \\ 0 & I \\ 0 & 0 \\ 0 & 0 \\ 0 & 0 \end{bmatrix}, \quad (2.53)$$

$$\Omega_{22}^{-1} = \begin{bmatrix} -\varepsilon P_{1(\rho)}^{-1} & 0 \\ 0 & -\varepsilon^{-1} P_{1(\rho)}^{-1} \end{bmatrix}. \quad (2.54)$$

The condition (2.45) holds if:

$$\Gamma^{(4)} < 0. \quad (2.55)$$

Applying the Schur complement (1.5.1.1) to $\Gamma^{(4)}$, it yields that:

$$\begin{bmatrix} \Omega_{11}^{(1)} & \Omega_{12} \\ (*) & \Omega_{22} \end{bmatrix} < 0. \quad (2.56)$$

Based on Assumptions (A.2), the inequality (2.56) only holds if the following simplified condition is verified: [Wu et al. 1996]

$$\begin{bmatrix} \Omega_{11}^{(2)} & \Omega_{12} \\ (*) & \Omega_{22} \end{bmatrix} < 0. \quad (2.57)$$

In which,

$$\Omega_{11}^{(2)} = \begin{bmatrix} \Gamma_{11}^{(4)} & 0 & 0 & E_{d(\rho)} & E_{f(\rho)} \\ (*) & \Gamma_{22}^{(3)} & \Gamma_{23} & \Gamma_{24} & 0 \\ (*) & (*) & \Gamma_{33}^{(3)} & \Gamma_{34} & 0 \\ (*) & (*) & (*) & \Gamma_{44} & 0 \\ (*) & (*) & (*) & (*) & \Gamma_{55} \end{bmatrix}, \quad (2.58)$$

$$\begin{aligned} \Gamma_{11}^{(4)} &= \mathcal{H}\{A_{(\rho)}P_{1(\rho)} - B_{(\rho)}Q_{1(\rho)}\} + \sigma_1 M_{a(\rho)}M_{a(\rho)}^T - \sum_i^m \pm\vartheta_i \frac{\partial P_{1(\rho)}}{\partial \rho_i} \\ &+ (\sigma_1^{-1} + \sigma_2^{-1})P_{1(\rho)}N_{a(\rho)}^T N_{a(\rho)}P_{1(\rho)} + (\sigma_3^{-1} + \sigma_4^{-1})P_{1(\rho)}N_{c(\rho)}^T N_{c(\rho)}P_{1(\rho)}, \end{aligned} \quad (2.59)$$

$$\begin{aligned} \Gamma_{22}^{(3)} &= \mathcal{H}\{P_{2(\rho)}A_{(\rho)} + Q_{2(\rho)}C_{(\rho)}\} + \sum_i^m \pm\vartheta_i \frac{\partial P_{2(\rho)}}{\partial \rho_i} \\ &+ \sigma_2 P_{2(\rho)}M_{a(\rho)}M_{a(\rho)}^T P_{2(\rho)} + \sigma_3 Q_{2(\rho)}M_{c(\rho)}M_{c(\rho)}^T Q_{2(\rho)}^T, \end{aligned} \quad (2.60)$$

$$\Gamma_{33}^{(3)} = \mathcal{H}\{Q_{3(\rho)}F_{f(\rho)}\} + \sum_i^m \pm\vartheta_i \frac{\partial P_{3(\rho)}}{\partial \rho_i} + \sigma_4 Q_{3(\rho)}M_{c(\rho)}M_{c(\rho)}^T Q_{3(\rho)}^T + I. \quad (2.61)$$

By applying Schur complement (1.5.1.1) many times to $\Gamma_{11}^{(4)}$, $\Gamma_{22}^{(3)}$, and $\Gamma_{33}^{(3)}$ in the above inequality, the LMI (2.11) is obtained, which completes the proof. \blacksquare

Remark 2.3.4

Although the Majorization lemma (1.5.1.2) and Young relation (1.5.1.4) seem conservative, they give more freedom in LMI solution through the choice of priority factors σ and ϵ . The effectiveness of this kind of solution is discussed in [Kheloufi et al. 2013].

In summary, Theorem 2.3.1 has displayed the generic solution for observer-controller co-design. In which, the \mathcal{H}_∞ PI observer gain $L_{(\rho)}$ can serve for fault estimation in FDD without the implementation of controller gain $K_{(\rho)}$.

2.3.2 Discussion on Active FTC design

Although the state-feedback controller in Section 2.3.1 is able to stabilize states of the closed-loop system, it cannot take advantage of fault estimation in FDD to eliminate the negative impact of faults. Thus, in order to obtain the integrated design [Lan and Patton 2016] in active FTC, the initial co-design is to be modified as follows:

- For actuator fault f_a , by assuming $B_{(\rho)}^\dagger$ exists for all ρ , the actuator fault accommodation (FA) controller is displayed as:

$$u = -K_{(\rho)}\hat{x} - B_{(\rho)}^\dagger B_{(\rho)}\hat{f}_a, \quad (2.62)$$

where $-K_{(\rho)}\hat{x}$ is the nominal state-feedback controller and $-B_{(\rho)}^\dagger B_{(\rho)}\hat{f}_a$ is the actuator fault compensation.

Remark 2.3.5

The input filter in Section 1.5.3.1 can be applied to obtain a parameter-dependent input matrix B , thus ensuring the existence of B^\dagger .

- For sensor fault f_s , the non-faulty output y_c can be easily derived from the faulty output y and estimated sensor fault \hat{f}_s , as illustrated below:

$$y_c = y - \hat{f}_s. \quad (2.63)$$

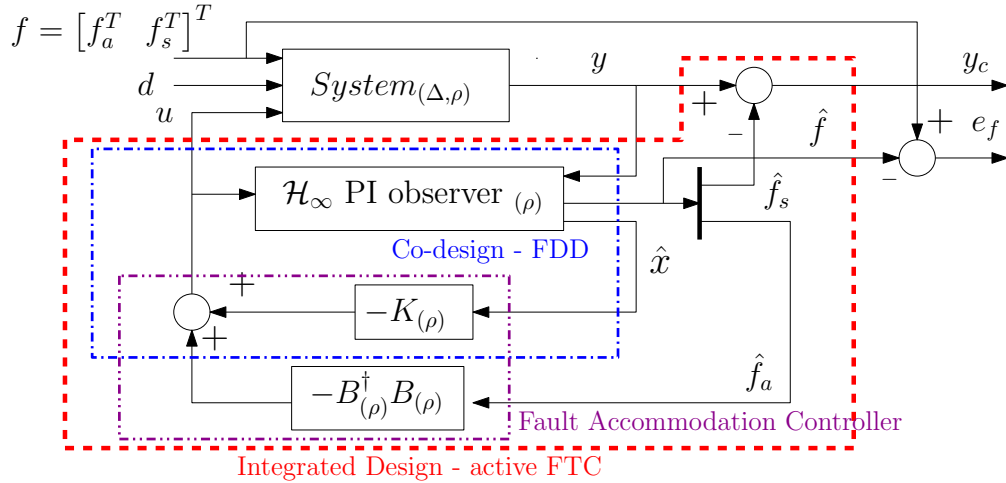


Figure 2.2: Integrated design for Active FTC

Fig. 2.2 illustrates the integrated design scheme for active FTC, which is based on co-design and fault compensation. In which, the robust observer in co-design gives the FDD information on actuator and sensor faults, then the FA controller compensates the actuator fault while stabilizing the closed-loop system. Meanwhile, the correct output is recovered thanks to the compensation of the sensor fault.

The synthesis for active FTC can be similarly derived from the proof of Theorem 2.3.1. However, this result will not be presented in this Chapter, but later in Chapter 3. In specific, in the experiments conducted for Chapter 2, the fault mimic process and fault accommodation cannot be realized at the same time for a healthy suspension, thus preventing the usage of active FTC. Also, the nonlinearity of the damper mentioned in Section A.2 can generate the inaccuracy in the implementation of the calculated controller.

2.4 FDD Application to sensor fault in Suspension system

To highlight the performance of the robust observer-controller co-design in the FDD process for uncertain LPV system, the semi-active suspension system in platform INOVE at the GIPSA laboratory will be used to obtain the experimental results.

2.4.1 Platform INOVE

Platform INOVE enables the behavioral study on a vehicle subjected to the dynamics of the roll, pitch angles and particularly the vertical movement of the car. This experimental testbed is composed of three main parts as illustrated in Fig.2.3: [Tudón-Martínez et al. 2015; Nguyen 2016]

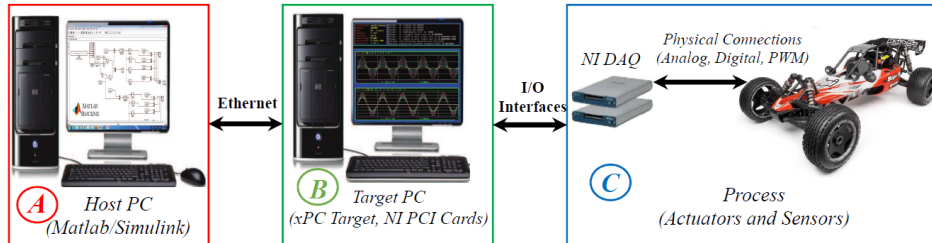


Figure 2.3: Schematic of INOVE experimental platform

- **Host PC:** The *Matlab/SimulinkTM* interface allows the user to initialize the system parameters, configure the desired road profile, implement the observer/controller algorithms for ER suspension and record the acquired data.
- **Target PC:** The RT system (*xPC TargetTM*) operated on this computer permits the execution of algorithms in Host PC and recording of the sensor data at the sampling time of 200 Hz (or 5 ms), thanks to National Instruments Data Acquisition Cards (NI DAQs).
- **Mechanical System:** A 1 : 5-scaled racing car (see Fig. 2.4) modeling a full vehicle includes wheels, engine, steering, braking system, and most importantly a semi-active suspension system (which is the key element).

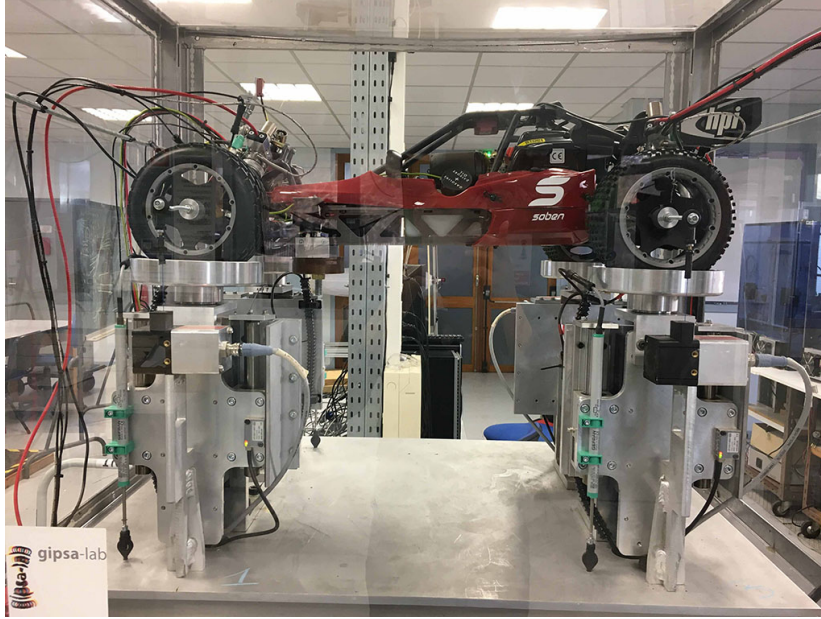


Figure 2.4: SOBEN car of platform INOVE ANR 2010

The Semi-Active suspension system includes four ER dampers whose force range is 50 N and input voltages are controlled by PWM signals at 25 kHz. Meanwhile, the desired road profile is modeled by the linear DC motors which are located below each wheel with the maximum velocity of 1.5 m/s and a working bandwidth of 0 – 20 Hz with.

To capture the vertical dynamics of the vehicle, a variety of sensors are needed. For instance, accelerometers to measure the vertical accelerations of the unsprung masses \ddot{z}_{us} ; displacement sensors to obtain the excitation of the terrain, i.e. road profile z_r , and the deflection of the suspensions z_{def} ; draw-wire sensors to measure the unsprung masses displacements z_{us} ; force sensors to record the change of dampers' force. Moreover, thanks to Kalman filtering, the inertial sensor computes not only three angular velocities (pitch rate - $\dot{\phi}$, roll rate - $\dot{\theta}$, and yaw rate - $\dot{\psi}$) but also the accelerations of the sprung mass including longitudinal (\ddot{x}), lateral (\ddot{y}) and vertical (\ddot{z}).

Remark 2.4.1

Certain operational considerations must be taken into account for the experimental platform INOVE:

- *PWM signals controlling ER dampers can vary in the range [0.1, 0.8]. However, the experiment reveals that when the PWM signal is higher than 0.35, the damper forces display the same behaviors.*
- *Only the vertical dynamics, pitch, roll, and vertical bounce are inferred from the system operation. Other dynamics (longitudinal or lateral) should be neglected.*

The parameters for the SOBEN quarter-car are presented in Table 2.1.

Table 2.1: Quarter-car parameters

Parameters	Unit	Value	Description
m_s	kg	2.64	A quarter-car chassis mass
m_{us}	kg	0.485	Rear tire mass
k_s	N/m	1396	Suspension stiffness
c_{min}	$N.s/m$	17.59	Minimum damping coefficient
c_{max}	$N.s/m$	1028	Maximum damping coefficient
k_t	N/m	12270	Tire stiffness

In the next section, the faulty-uncertain LPV model of the suspension system will be studied.

2.4.2 LPV Modeling for faulty suspension system

Two available outputs are used in platform INOVE: z_{def} is the displacement between z_s and z_{us} , and \ddot{z}_{us} is the tire acceleration. Consequently, in the semi-active suspension models, there may exist the following faults: $f_{z_{def}}$ in the displacement sensor z_{def} , $f_{\ddot{z}_{us}}$ in the tire acceleration sensor \ddot{z}_{us} and f_a in the damper actuator (control input u). Also, as defined in [Savaresi et al. 2010], the faults f_a and $f_{\ddot{z}_{us}}$ are supposed to exist in low frequency, given the domain from 0 to 2 Hz, and the working frequency of the road profile d is from 0 to 20 Hz. Such practical dynamics are directly linked to Assumptions (A.1).

From the initial LPV model in Appendix A.1 where deflection speed \dot{z}_{def} is chosen as the time-varying parameter ρ , the following faulty LPV suspension system is introduced:

$$\begin{cases} \dot{x} &= A_{(c)}x + B_{(\rho)}u + E_d d + E_{f(\rho)}f \\ y &= C_{(c)}x + D_{(\rho)}u + F_d d + F_{f(\rho)}f \end{cases}, \quad (2.64)$$

$$\text{where } x = [z_{def} \quad \dot{z}_s \quad z_{us} \quad \dot{z}_{us}]^T, y = [z_{def} \quad \ddot{z}_{us}]^T, d = z_r, A_{(c)} = \begin{bmatrix} 0 & 1 & 0 & -1 \\ -\frac{k_s}{m_s} & -\frac{c}{m_s} & 0 & \frac{c}{m_s} \\ 0 & 0 & 0 & 1 \\ \frac{k_s}{m_{us}} & \frac{c}{m_{us}} & -\frac{kt}{m_{us}} & -\frac{c}{m_{us}} \end{bmatrix},$$

$$C_{(c)} = \begin{bmatrix} 1 & 0 & 0 & 0 \\ \frac{k_s}{m_{us}} & \frac{c}{m_{us}} & -\frac{kt}{m_{us}} & -\frac{c}{m_{us}} \end{bmatrix}, B_{(\rho)} = \begin{bmatrix} 0 \\ -\frac{\rho}{m_s} \\ 0 \\ \frac{\rho}{m_{us}} \end{bmatrix}, D_{(\rho)} = \begin{bmatrix} 0 \\ \frac{\rho}{m_{us}} \end{bmatrix}, E_d = \begin{bmatrix} 0 \\ 0 \\ 0 \\ \frac{kt}{m_{us}} \end{bmatrix}, F_d = \begin{bmatrix} 0 \\ \frac{kt}{m_{us}} \end{bmatrix},$$

$$\begin{bmatrix} 0 \\ \frac{kt}{m_{us}} \end{bmatrix}, f = [f_a^T \quad f_{z_{def}}^T \quad f_{\ddot{z}_{us}}^T]^T, E_{f(\rho)} = [B_{(\rho)} \quad 0_{nx \times ny}], \text{ and } F_{f(\rho)} = [D_{(\rho)} \quad I_{ny}].$$

According to [Do et al. 2011; Zin et al. 2008], $c_0 = (c_{min} + c_{max})/2$ is chosen as the nominal damping value. Since the damping coefficient c varies from c_{min} to c_{max} , there exists

the uncertainty range of $\Delta c_0 = (c_{max} - c_{min})/2$ comparing to the nominal value c_0 , i.e. $c = c_0 \pm \Delta c_0$. That leads to the definition for uncertainty term ΔA as below:

- When $\Delta A = 0$, $A_{(c)} = A_{(c_0)}$.
- When $\Delta A \neq 0$, $A_{(c)} = A_{(c_0)} + \Delta A$ where $|\Delta A| = |M_a \Delta_a N_a| \leq \Delta \bar{A} = M_a \cdot I \cdot N_a$, $N_a = [0 \ 1 \ 0 \ -1]$, and $M_a = \begin{bmatrix} 0 & -\frac{\Delta c_0}{m_s} & 0 & \frac{\Delta c_0}{m_{us}} \end{bmatrix}^T$. Therefore, $A_{(c_{max})} = A_{(c_0)} + \Delta \bar{A}$ and $A_{(c_{min})} = A_{(c_0)} - \Delta \bar{A}$.

Similar interpretations are applied to uncertainty term ΔC with $M_c = \begin{bmatrix} 0 & \frac{\Delta c_0}{m_{us}} \end{bmatrix}^T$ and $N_c = N_a$.

To demonstrate the performance of the proposed method, the solution for $f_{z_{def}}$ PI observer, whose UI vector includes the road profile d and the non-estimated faults f_a and $f_{z_{us}}$, is presented in this study. Hence, the faulty-uncertain LPV system (2.64) can be rewritten as:

$$\begin{cases} \dot{x} &= (A_{(c_0)} + \Delta A)x + B_{(\rho)}u + E_{\bar{d}(\rho)}\bar{d} + E_{f_{z_{def}}}f_{z_{def}} \\ y &= (C_{(c_0)} + \Delta C)x + D_{(\rho)}u + F_{\bar{d}(\rho)}\bar{d} + F_{f_{z_{def}}}f_{z_{def}} \end{cases}, \quad (2.65)$$

where $\bar{d} = [d^T \ f_a^T \ f_{z_{us}}^T]^T$, $E_{\bar{d}(\rho)} = [E_d \ B_{(\rho)} \ 0_{n \times 1}]$, $E_{f_{z_{def}}} = 0_{n \times 1}$,

$$F_{\bar{d}(\rho)} = [F_d \ D_{(\rho)} \ [0 \ 1]^T], \text{ and } F_{f_{z_{def}}} = [1 \ 0]^T.$$

The impact of uncertainty term ΔA on the dynamics of suspension will be examined in the next section.

2.4.3 System uncertainty

Fig. 2.5 illustrates three important cases of the uncertainty impact, i.e.e $c = c_0$, $c = c_{min}$ and $c = c_{max}$, on system dynamics, which is expressed by the eigenvalues of $(A + \Delta A)$. The results show that the variation in damping coefficient has modified the system dynamics. Therefore, a robust observer is needed to deal with this problem.

2.4.4 Experimental conditions

2.4.4.1 Road profile z_r

The road profile (see Fig. 2.6) is modeled as a highway with gravel (road profile type C), according to International Organization for Standardization (ISO) 8608 classification [Tudón-Martínez et al. 2015; ISO 1995]. This profile represents one of the worst cases that a suspension has to deal with, thus allowing the evaluation of the greatest impact of z_r on fault estimation results.

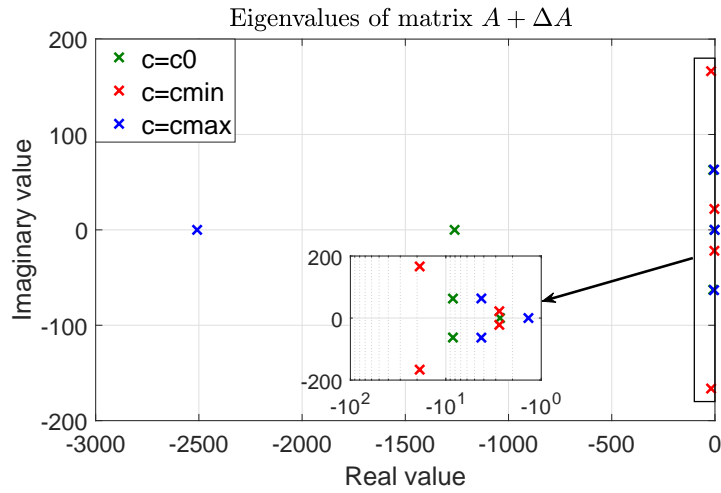
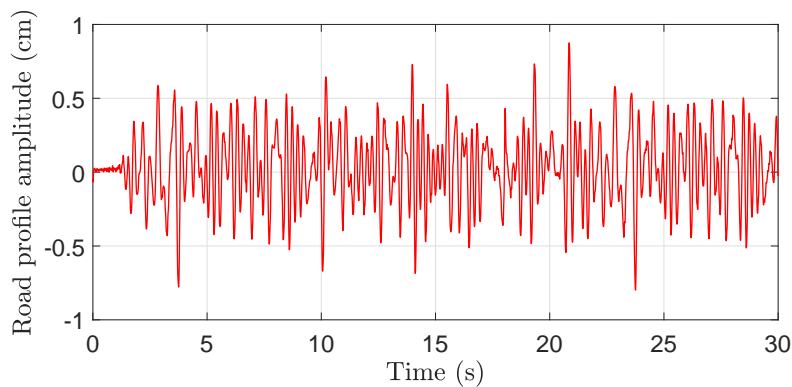


Figure 2.5: Dynamics of uncertain system

Figure 2.6: Road profile z_r (d): highway with gravel

2.4.4.2 Test Scenario

As the \mathcal{H}_∞ PI observer can be implemented independently without the feedback controller in Theorem 2.3.1, two scenarios are studied to prove its performance.

- Scenario 1: Open-loop validation, which justifies the capability of \mathcal{H}_∞ PI observer to attenuate the UI and estimate the fault.

In this case, $f_{z_{def}}$ is the fault to estimate, whereas the faults $f_{z_{us}}$, f_a and road profile z_r are considered as UIs. Also, abrupt faults (stepwise) are included in the test to simulate the

slow-varying faults:

$$f_{z_{def}} = \begin{cases} 0.03 & \text{if } (1s \leq t \leq 7s) \\ 0 & \text{otherwise} \end{cases} \quad (m), \quad (2.66)$$

$$f_{\ddot{z}_{us}} = \begin{cases} 2 & \text{if } (11s \leq t \leq 17s) \\ 0 & \text{otherwise} \end{cases} \quad (ms^{-2}), \quad (2.67)$$

$$f_a = \begin{cases} -20 & \text{if } (21s \leq t \leq 27s) \\ 0 & \text{otherwise} \end{cases} \quad (Ns/m). \quad (2.68)$$

The estimation result of the proposed method is then compared with that of [Mendoza et al. 2016], which also considers parameter variation in the gridding - \mathcal{H}_∞ PI observer design. Here, the two methods are examined with the same order of basic functions, the number of gridding points N_g for ρ , and level of attenuation $\gamma_{z_{def}}$. However, the latter does not take into account the robust perspective on the uncertainty - it neglects the uncertainty term in the relation \dot{e} and x during the design process. Therefore, the comparison between the two approaches highlights the advancement in the performance of the proposed observer, especially in terms of robust synthesis.

Remark 2.4.2

Faults do not happen simultaneously. In this study, only the result of the displacement sensor z_{def} is presented. Other observers can be designed similarly.

- Scenario 2: Closed-loop validation allows the performance comparison of its \mathcal{H}_∞ PI observer with that of open-loop system. Also, this scenario demonstrates the control input's behavior in the presence of a fault.

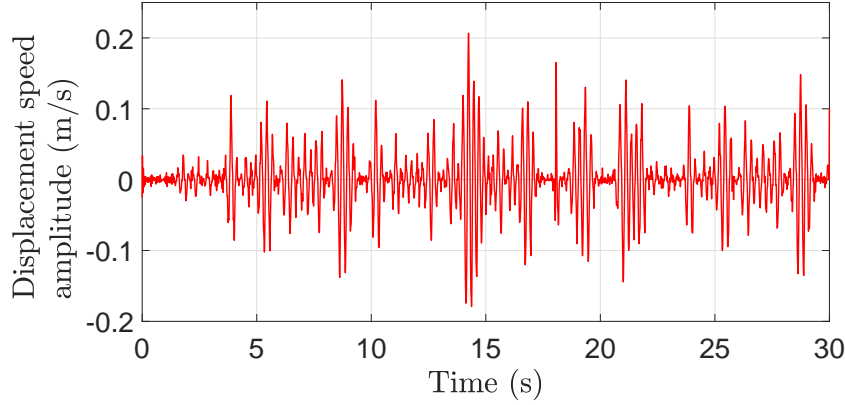
Only the displacement sensor fault $f_{z_{def}}$ is considered, which is also studied in Scenario 1, and the state-feedback controller is applied. The gains of \mathcal{H}_∞ PI observer and controller are inferred from Theorem 2.3.1.

2.4.4.3 Varying parameter

The TVP is chosen as defection speed, i.e. $\rho = \dot{z}_{def}$. Its behavior is presented in Fig. 2.7.

2.4.5 Observer design for semi-active suspension

In order to solve the LMI (2.11), the gridding approach mentioned in Section 1.3.2 is applied. In which, the matrices $P_{k(\rho)}$ and $Q_{k(\rho)}$ are chosen as polynomial functions of ρ . The order of these functions is practically identified in accordance with the application and numerical

Figure 2.7: Varying parameter ρ .

calculation problem ($k = 1, 2, 3$).

$$P_{k(\rho)} = P_{k0} + \rho P_{k1} + \rho^2 P_{k2} \implies \frac{\partial P_{k(\rho)}}{\partial \rho} = P'_{k(\rho)} = P_{k1} + 2(\rho)P_{k2}, \quad (2.69)$$

$$Q_{k(\rho)} = Q_{k0} + \rho Q_{k1} + \rho^2 Q_{k2}, \quad (2.70)$$

where parameter matrices P_{k0} , P_{k1} , P_{k2} , Q_{k0} , Q_{k1} , and Q_{k2} are constant matrices and can be found by solving the LMI (2.11).

Remark 2.4.3

In essence, the solution for symmetric matrices P_{k0} , P_{k1} , and P_{k2} is supposed to ensure $P_{k(\rho)} > 0$ for the whole varying set of $\rho = z_{def}$. The choices for the functions $P_{k(\rho)}$ and $Q_{k(\rho)}$, defining the feasible set of LMI solution, are discussed in [Wu 1995; Apkarian and Adams 2000; Abbas et al. 2014]. Also, the priority factors ε , σ_1 , σ_2 , σ_3 , and σ_4 are given according to the study of [Kheloufi et al. 2013].

Algorithms for the gridding-based solution are summarized into 2 steps:

Step 1: Offline Synthesis

- Defining n_g gridding points of varying parameter $\rho = z_{def}$ ($m = 1$), so $N_g = n_g$ time-frozen values ρ^j ($j = 1 : n_g$) can be obtained.
- Defining the boundness ϑ of $\dot{\rho} = \ddot{z}_{def}$.
- The gridding-based synthesis: for $j = 1$ to N_g (see Fig. 2.8)
 - Defining distribution matrices corresponding to ρ^j .
 - Defining $P_{k(\rho^j)}$, $\frac{\partial P_{k(\rho^j)}}{\partial \rho^j}$, and $Q_{k(\rho^j)}$.
 - Defining the finite set of LMIs which represent the LMI (2.11).

- From all the above set of LMIs, finding the constant time-invariant matrices P_{k0} , P_{k1} , P_{k2} , Q_{k0} , Q_{k1} , and Q_{k2} .

$$\begin{cases} \dot{\hat{x}} = A\hat{x} + B_{(\rho^j)}u + L_{P(\rho^j)}(y - \hat{y}) + E_{f_{z_{def}}} \hat{f}_{z_{def}} \\ \dot{\hat{f}}_{z_{def}} = L_{I(\rho^j)}(y - \hat{y}) \\ \hat{y} = C\hat{x} + D_{(\rho^j)}u + F_{f_{z_{def}}} \hat{f}_{z_{def}} \end{cases}$$

$\rho^1 = \dot{z}_{def}^{min} \quad \circ \circ \circ \circ \circ \circ \quad \rho^j \quad \circ \circ \circ \circ \circ \circ \quad \rho^{N_g} = \dot{z}_{def}^{max}$

Figure 2.8: LPV observer on a linear grid.

Step 2: Online Implementation

- For instant t , update the value of TVP vector $\rho(t)$.
- Compute the time-varying matrices $P_{k(\rho(t))}$ and $Q_{k(\rho(t))}$ defined by $\rho(t)$ and the offline-calculated matrices P_{k0} , P_{k1} , P_{k2} , Q_{k0} , Q_{k1} , and Q_{k2} .
- Calculate the time-varying matrices $L_{P(\rho)}$, $L_{I(\rho)}$, and $K(\rho)$ through $P_{k(\rho)}$ and $Q_{k(\rho)}$ definitions in Theorem 2.3.1.

That completes the implementation process with the gridding approach, whose implementation scheme process is summarized in Fig. 2.9.

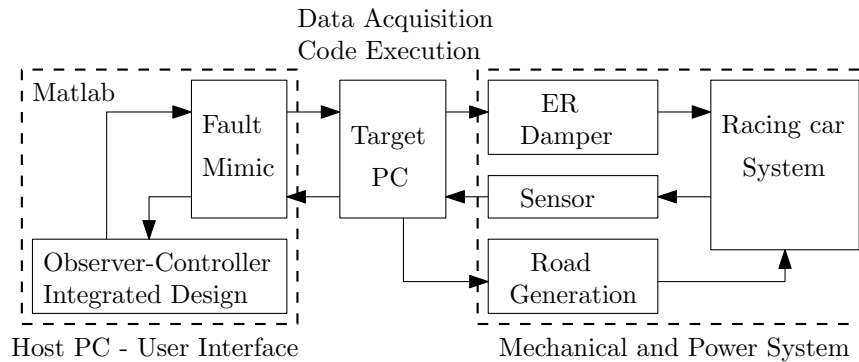


Figure 2.9: Implementation Scheme.

In the LPV suspension model, the varying parameter ρ is defined as the displacement variation \dot{z}_{def} , whose boundness depends on the characteristics of the road profile (such as the frequency spectrum and the amplitude) and the controlled duty cycle/current that is applied to semi-active suspension. For validation process, the testing condition described in Section 2.4.4 results in the following boundness: $-0.18 \leq \rho \leq 0.21$ (m/s) (see Fig. 2.7) and $|\dot{\rho}| \leq 9.46$ (m/s^2).

The gridding point number n_g is chosen equal to 30, based on the estimation performance and capacity of computation. By using Matlab, toolbox Yalmip [Lofberg 2004] and solver *sdpt3* [Toh, Todd, and Tütüncü 1999], the LMI optimization problem is solved thanks to the optimal \mathcal{H}_∞ performance of the PI observer $\gamma_{z_{def}} = 0.01$.

The parameters of $P_{k(\rho)}$ and $Q_{k(\rho)}$ ($k = 1, 2, 3$) are presented as following:

$$P_{10} = \begin{bmatrix} 3.562 & 9.480 & 0.009 & 6.460 \\ (*) & 1.936e3 & -0.157 & 29.709 \\ (*) & (*) & 0.399 & 4.995 \\ (*) & (*) & (*) & 1.001e4, \end{bmatrix}, \quad (2.71)$$

$$P_{11} = \begin{bmatrix} 0.014 & -0.136 & -0.004 & -0.1777 \\ (*) & -0.618 & -0.016 & -6.896 \\ (*) & (*) & 0.004 & 0.087 \\ (*) & (*) & (*) & 105.484 \end{bmatrix}, \quad (2.72)$$

$$P_{12} = \begin{bmatrix} -0.027 & -0.030 & 0.005 & 0.346 \\ (*) & 37,536 & -0,140 & 192.121 \\ (*) & (*) & 0.008 & -0.049 \\ (*) & (*) & (*) & -921.484 \end{bmatrix}, \quad (2.73)$$

$$Q_{10} = [11.147 \quad -8.761 \quad -1.887 \quad 17.158] \quad (2.74)$$

$$Q_{11} = [618.890 \quad -201.530 \quad -1.112e3 \quad 437.972], \quad (2.75)$$

$$Q_{12} = [-1.010e3 \quad 509.440 \quad 1.570e3 \quad -1.006e3], \quad (2.76)$$

$$P_{20} = \begin{bmatrix} 4.555e7 & -1.670e3 & -59.596 & 1.678e3 \\ (*) & 0.1208 & -0.062 & -0.068 \\ (*) & (*) & 4.313 & -0.005 \\ (*) & (*) & (*) & 0.066 \end{bmatrix}, \quad (2.77)$$

$$P_{21} = \begin{bmatrix} -1.736e6 & 139.568 & -6.353 & -140.017 \\ (*) & -0.002 & -0.001 & 0.006 \\ (*) & (*) & 0.010 & -2.672e-4 \\ (*) & (*) & (*) & -0.010 \end{bmatrix}, \quad (2.78)$$

$$P_{22} = \begin{bmatrix} 6.957e7 & -5.749e3 & 391.339 & 5.765e3 \\ (*) & -0.011 & -0.110 & -0.208 \\ (*) & (*) & 0.161 & 0.048 \\ (*) & (*) & (*) & 0.428 \end{bmatrix}, \quad (2.79)$$

$$Q_{20} = \begin{bmatrix} -6.925e11 & -1.6765e3 \\ -2.519e7 & 0.066 \\ 4.166e4 & 0.007 \\ 2.5217e7 & -0.064 \end{bmatrix}, \quad (2.80)$$

$$Q_{21} = \begin{bmatrix} 4.642e10 & 139.079 \\ -5.956e5 & -0.006 \\ 9.983e3 & 7.5743e-5 \\ 6.135e5 & 0.010 \end{bmatrix}, \quad (2.81)$$

$$Q_{22} = \begin{bmatrix} -1.780e12 & -5.677e3 \\ 1.949e7 & 0.213 \\ 4.643e4 & 0.005 \\ -2.036e7 & -0.434 \end{bmatrix}, \quad (2.82)$$

$$P_{30} = 1.266e6, \quad (2.83)$$

$$P_{31} = -3.217e4, \quad (2.84)$$

$$P_{32} = 1.233e6, \quad (2.85)$$

$$Q_{30} = [-1.038e12 \quad -7.248], \quad (2.86)$$

$$Q_{31} = [2.040e10 \quad -1.269], \quad (2.87)$$

$$Q_{32} = [-7.819e11 \quad 88.192]. \quad (2.88)$$

2.4.6 Frequency Analysis

From the suspension model (in Matlab simulation), the frequency analysis is illustrated in Fig. 2.10, Fig. 2.11, Fig. 2.12 and Fig. 2.13 to evaluate the sensitivity of the fault estimation error $e_{f_{z_{def}}}$ to UIs.

The number of gridding points n_g is defined as 30, so we obtain 30 values ρ^j , $j = 1 : 30$. As a consequence, the sensitivity ρ^j represents the frequency response at each time-frozen value ρ^j of varying parameter ρ , i.e. LPV system is treated as LTI system at each ρ^j . The value of ρ^j is varying from $\rho^1 = -0.18$ to $\rho^{30} = 0.21$ with average value $\rho^{15} = 0.0083$ (m/s) (see Fig. 2.7); thus, without loss of generality, only the sensitivities ρ^1 , ρ^{10} , and ρ^{15} are presented to evaluate the whole varying range. In general, all above sensitivities satisfy the condition (2.4).

Fig. 2.10 shows the effective impact attenuation of road profile d (cm) on fault estimation error $e_{f_{z_{def}}}$. It reveals that the attenuation reaches its maximum at 2.38 Hz, which reflects with the worst case of -65.3 dB in its frequency range.

The influence of the actuator fault f_a on fault estimation error decreases in the range of 0 to 2 Hz, with a perfect attenuation of less than -110 dB in Fig. 2.11.

With the magnitude less than -110 dB, Bode diagram in Fig. 2.12 indicates that the $f_{z_{us}}$ fault impact is perfectly attenuated. The higher the frequency, the lesser the impact of the fault on estimation error $e_{f_{z_{def}}}$.

In Fig. 2.13, $|T_{\hat{f}_{z_{def}} f_{z_{def}}}| \approx 0$ from 0 to 0.04 Hz, so the fault $f_{z_{def}}$ can be well estimated if its bandwidth is less than 0.04 Hz.

Fig. 2.14 illustrates a comparison between the experimental sensitivity and sensitivity of mathematical model for $f_{z_{def}}$ fault estimation. It points out that the experimental curve rests between sensitivities of ρ_{10} and $\rho_{15} = [-0.0590, 0.0083]$; thus, the analyzed results from the

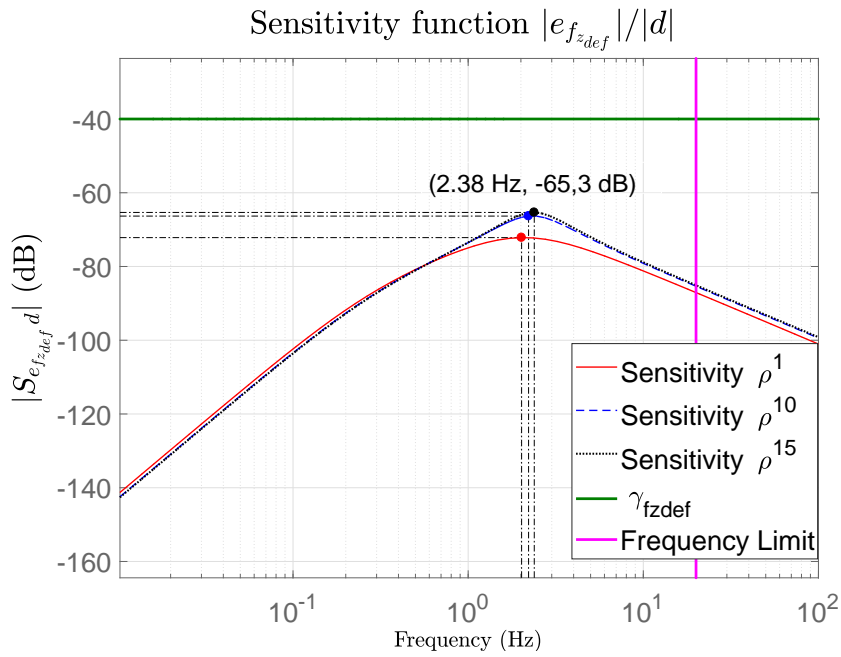


Figure 2.10: Sensitivity function $|e_{f_{z_{def}}}|/|d|$.

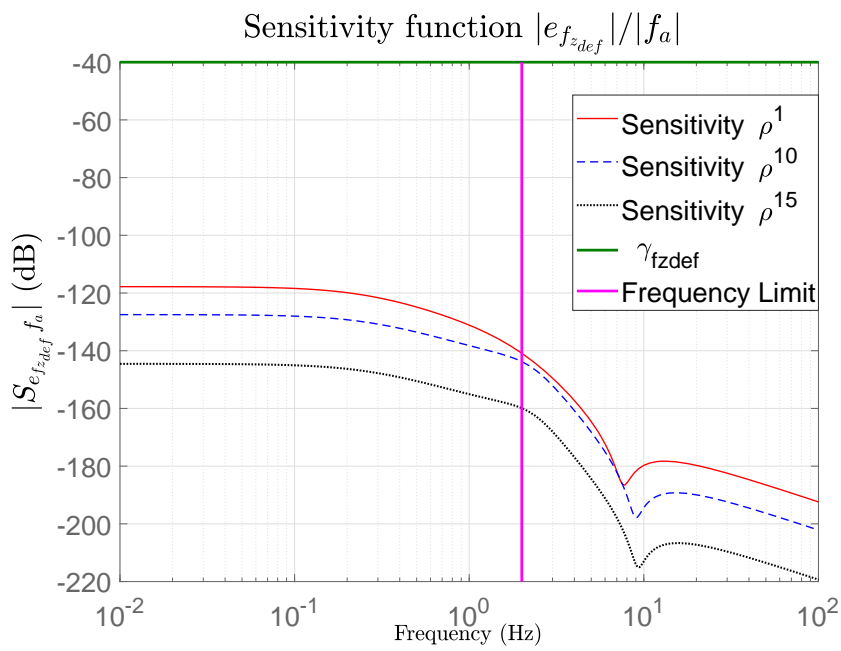
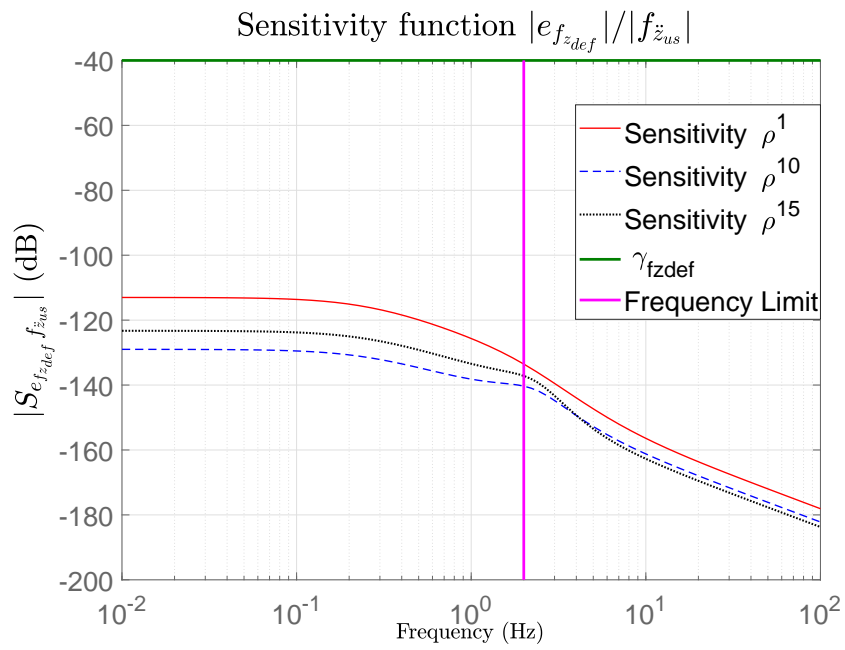
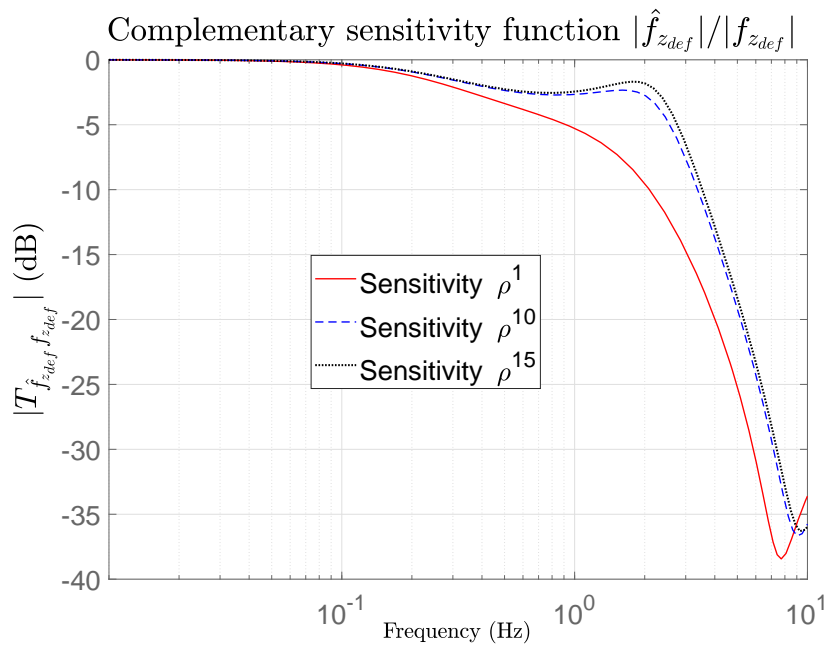


Figure 2.11: Sensitivity function $|e_{f_{z_{def}}}|/|f_a|$.

mathematical model can be applied to a real system and experimental validation.

Figure 2.12: Complementary sensitivity function $|\hat{f}_{z_{def}}|/|f_{z_{us}}|$.Figure 2.13: Complementary sensitivity function $|\hat{f}_{z_{def}}|/|f_{z_{def}}|$.

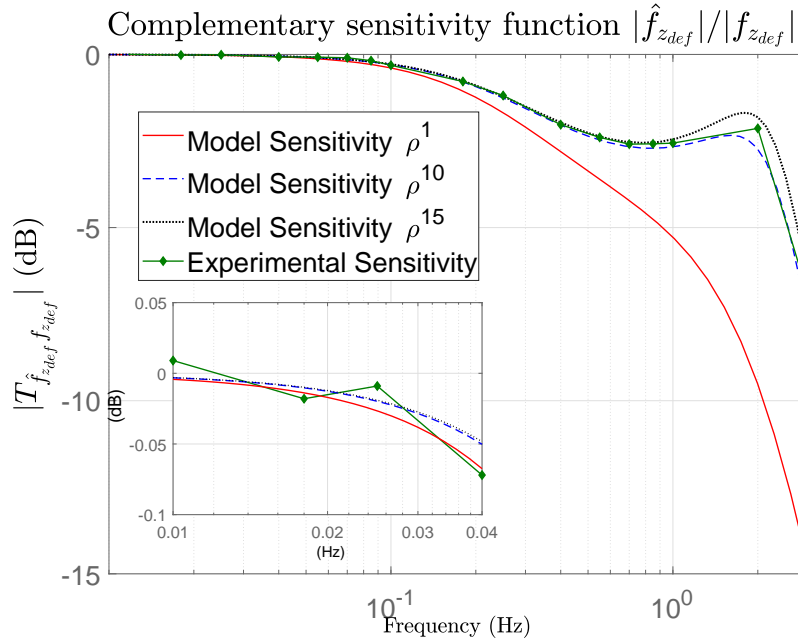


Figure 2.14: Comparison between model and experimental sensitivity function $|\hat{f}_{z_{def}}|/|f_{z_{def}}|$.

2.4.7 Validation result

The parameters of \mathcal{H}_∞ PI observer-based controller obtained from (2.71)-(2.88) are implemented for the experimental conditions and scenarios introduced in Section 2.4.4.

2.4.7.1 Scenario 1

The open-loop validation process ends after 30 seconds.

The fault estimation of $f_{z_{def}}$ is presented in Fig. 2.15. Despite the road profile disturbance, the displacement fault $f_{z_{def}}$ is well estimated with the rising time about 2.5 - 3 seconds. Also, the impact of faults f_a and $f_{\ddot{z}_{us}}$ on estimation result is greatly attenuated by the proposed method. Moreover, with the same level of attenuation $\gamma_{z_{def}}$ and rising time, the proposed method is proved to be more effective in handling the influence of parametric uncertainty's variation than the non-robust approach in [Mendoza et al. 2016], thus emphasizing the importance of the robust solution.

To assess the accuracy of the proposed method in fault estimation, the root-mean-square error (RMSE) is calculated:

$$RMSE = \sqrt{\frac{\sum_{t=t_1}^{t_2} (\hat{f}_{z_{def},t} - f_{z_{def},t})^2}{N_{data}}}, \quad (2.89)$$

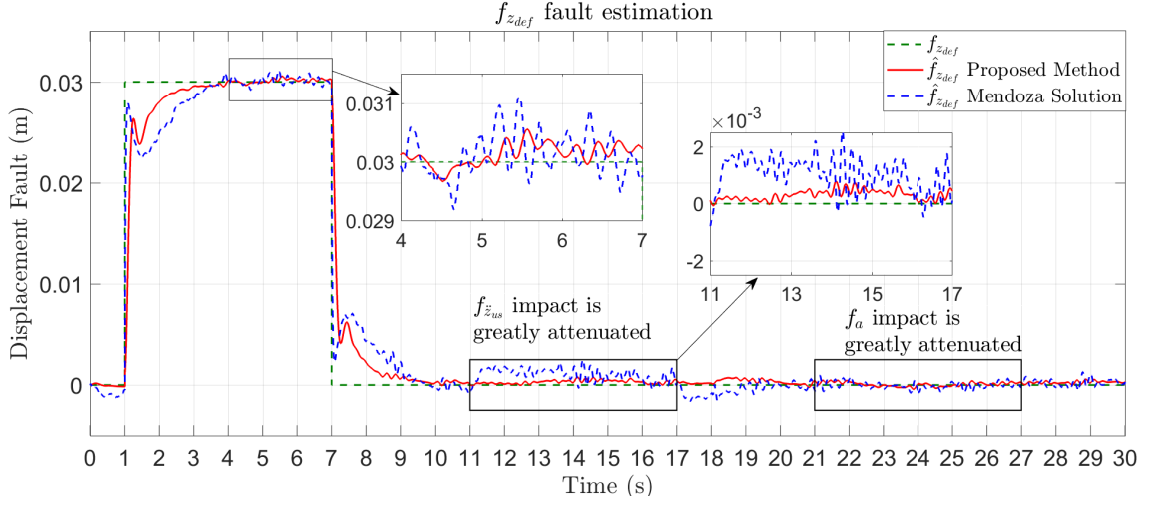


Figure 2.15: Fault estimation result in Scenario 1.

where N_{data} is the total number of $f_{z_{def}}$ data obtained from validation process in the interval time $[t_1, t_2]$.

When $[t_1, t_2] = [0s, 11s]$, which demonstrates the estimation time for the fault $f_{z_{def}}$, then $RMSE = 4.09e-3$. Indeed, there always exists a difference between the estimated and the reference values as a result of PI dynamics' impact on RMSE.

When $[t_1, t_2] = [11s, 30s]$, which represents the estimation period dealing with UI from other faults, then $RMSE = 3.53e-4$ m, below the threshold 0.001 m for fault $f_{z_{def}}$ existence. In other words, the coupling problem with other faults has negligible effects on fault estimation thanks to the \mathcal{H}_∞ application as described in table 2.2.

Table 2.2: Fault estimation and UI attenuation table for the $f_{z_{def}}$ PI observer.

Fault	$f_{z_{def}}$ PI Observer
$f_{z_{def}}$	$ \hat{f}_{z_{def}}/f_{z_{def}} _{w=0:0.04Hz} = 1$ (0 dB)
f_a	$\ e_{f_{z_{def}}}\ _2/\ f_a\ _2 \leq \gamma_{z_{def}}$
$f_{\ddot{z}_{us}}$	$\ e_{f_{z_{def}}}\ _2/\ f_{\ddot{z}_{us}}\ _2 \leq \gamma_{z_{def}}$
d	$\ e_{f_{z_{def}}}\ _2/\ d\ _2 \leq \gamma_{z_{def}}$

With reasonable RMSE, the robust \mathcal{H}_∞ PI observer has proven its performance in the fault estimation process.

2.4.7.2 Scenario 2

The closed-loop test lasts 12 seconds.

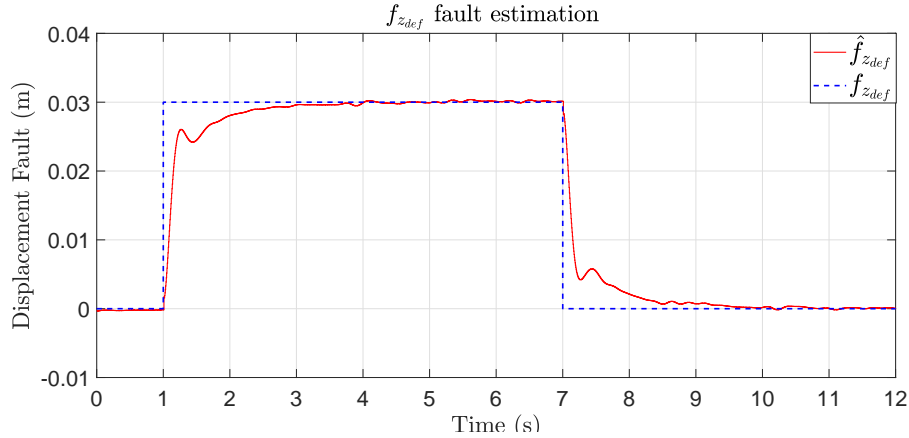


Figure 2.16: Fault estimation result in Scenario 2.

Like Fig. 2.15, Fig. 2.16 also demonstrates good estimation of the displacement fault $f_{z_{def}}$. Moreover, as the difference in estimation quality between closed-loop ($RMSE = 4.04e-3$) and open-loop systems ($RMSE = 4.09e-3$) is negligible, the \mathcal{H}_∞ PI observer derived from the synthesis of observer-based controller can still work independently for FDD process without controller.

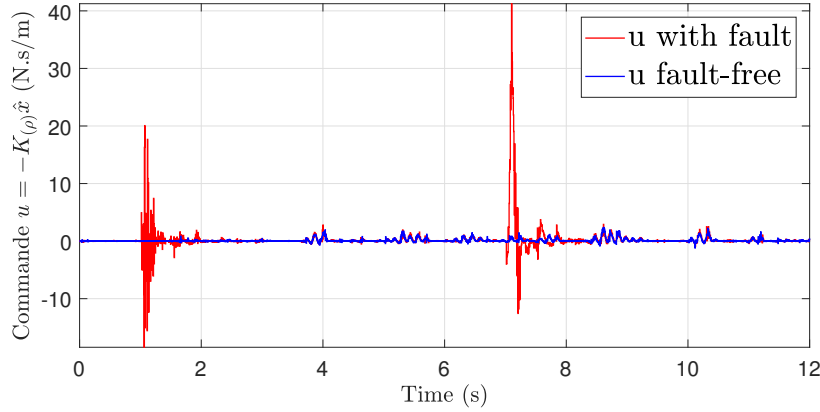


Figure 2.17: State-feedback controller in Scenario 2.

The behavior of feedback control input u in faulty-free and faulty cases is demonstrated in Fig. 2.17. At $t = 1$ (s) and $t = 7$ (s), fault $f_{z_{def}}$ generates inaccuracy in states, thus triggering some impulse responses. Meanwhile, when $t = 3$ (s) and $t = 9$ (s), i.e. $\hat{f}_{z_{def}} \rightarrow f_{z_{def}}$, the control input u , which promotes the stability of the system, is nearly the same in both cases.

2.4.7.3 Time Convergence Tuning

In order to change the response time, the pole placement method is applied in choosing the observer pole within a region of half-left plane [Wu 1995; Scherer, Gahinet, and Chilali 1996]. Thus, the dynamics of fault estimation error is also modified. This objective can be expressed as an additive LMI condition for Theorem 2.3.1 as below [Wu 1995; Scherer, Gahinet, and Chilali 1996]:

$$\mathcal{H}\{Q_{3(\rho)}F_{f(\rho)}\} + \sum_i^m \pm \vartheta_i \frac{\partial P_{3(\rho)}}{\partial \rho_i} + 2\alpha P_{3(\rho)} < 0, \quad (2.90)$$

where $\alpha > 0$, which defines the pole dynamics of e_f .

A comparison between different values of α is demonstrated in Fig. 2.18. In specific, there are 4 signals corresponding to $\alpha_1 = 3.65e5$ (as presented in tests for Scenarios 1 and 2), $\alpha_2 = 8e5$, $\alpha_3 = 20e5$, and $\alpha_4 = 25e5$.

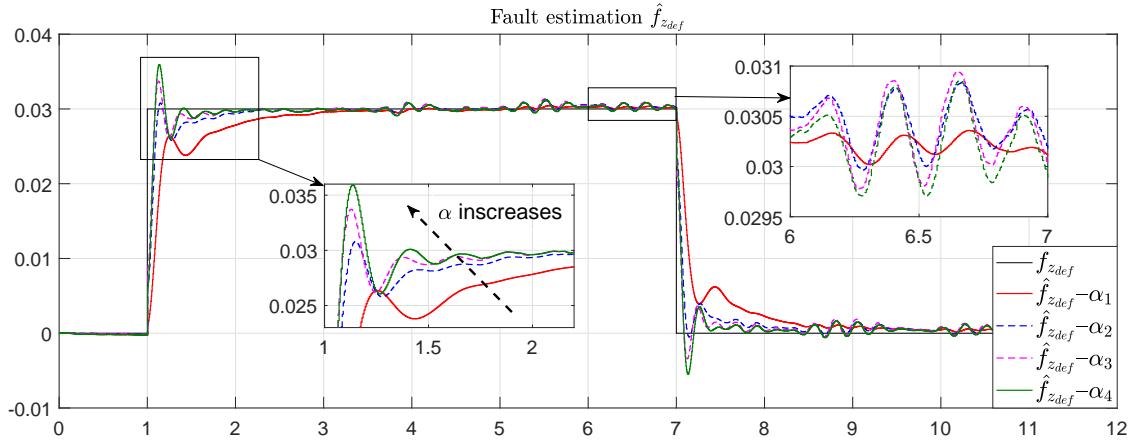


Figure 2.18: Fault estimation result with α modification.

Fig. 2.18 indicates that the estimation in cases α_2 , α_3 , and α_4 has faster convergence speed and response time (less than 1 second). The bigger α , the faster observer dynamics; however, more oscillation and overshoots are also generated. In addition, the resulting estimation error (after convergence) is more affected by the road profile (UI) at high values of α . Depending on the design requirements, different values of α are considered to achieve the compromise between the estimation dynamics and attenuation of UI impact.

2.5 Conclusion

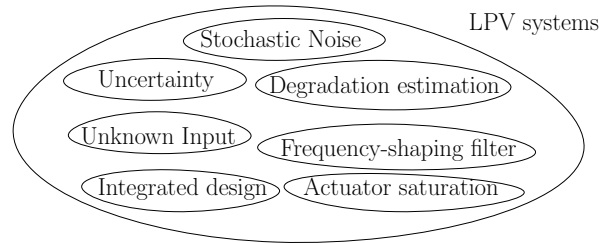
In this Chapter, the system uncertainty problem has been taken into account in the co-design of observer and controller for FDD in uncertain LPV systems. In which, both the observer and the controller are simultaneously synthesized by a unique LMI solution. Also,

compared with polytopic formulation and projection lemma, the majorization lemma used in the proposed method is able to handle the generic formulation of uncertainty term and thus, reduce the complexity in the observer design. Through its application to the semi-active suspension system, the proposed observer-based controller design for LPV systems has justified its capability for robust fault estimation in open-loop and closed-loop systems, thus promoting the usage of co-design for robust FDD designs.

On the other hand, the nonlinearity of the damper is a factor that needs to be overcome to develop and implement a FTC integrated design in the suspension system.

Robust-stochastic integrated designs for FDD-FTC of actuator degradation

Abstract: The main contribution of Chapter 3 is a generic strategy of designing polytopic observer-based fault compensators for estimation and accommodation of actuator degradation in uncertain stochastic linear parameter varying (LPV) system. In these integrated designs, robust observer-controller gains are synthesized with a unique linear matrix inequality (LMI) solution such that the impact of UIs on observer estimation is attenuated by a frequency-shaping filter or \mathcal{H}_∞ synthesis (depending on the matching condition of UI frequency), while the closed-loop stability is ensured against system uncertainties and stochastic noise. Finally, a numerical example is illustrated to highlight the performance of the proposed methods.



Contents

3.1 Introduction	70
3.1.1 State of the art	70
3.1.2 Chapter Contributions	72
3.2 Problem formulation	73
3.2.1 Degradation modeling	73
3.2.2 Stochastic LPV System representation	75
3.2.3 Design objectives	77
3.2.4 UI-Matching conditions and Proposed design solutions	78
3.3 Robust-stochastic integrated design for Matched UI	79
3.3.1 Methodology of Frequency-Shaping filter	79
3.3.2 Observer design for Matched UI	81
3.3.3 Fault accommodation Controller design	83
3.3.4 Observer-Controller synthesis for Matched UI	84
3.4 Robust-stochastic integrated design for Unmatched UI	91
3.4.1 Observer Design for Unmatched UI	92

3.4.2	Observer-Controller synthesis for Unmatched UI	93
3.4.3	Discussion on Theorem 3.4.1	95
3.5	Anti-windup solution	96
3.5.1	LPV-Saturation problem	96
3.5.2	Observer design with input saturation for matched UI	97
3.5.3	Anti-windup controller design for matched UI	98
3.5.4	Anti-windup observer-based fault compensator synthesis under degradation occurrence for matched UI	99
3.6	Method illustration	102
3.6.1	Mathematical example	102
3.6.2	Frequency analysis	105
3.6.3	Simulation condition	108
3.6.4	Simulation result	108
3.7	Conclusion	111

3.1 Introduction

3.1.1 State of the art

During system operation, mechanical components gradually degrade as a result of normal wear and tear, causing technical malfunction or even severe accidents to operators. Therefore, prediction and accommodation of degradation in health maintenance have been of great interest in research and industry [Kothamasu, Huang, and VerDuin 2006]. Thanks to [Luo et al. 2008] and [Abou Jaoude 2015], the degradation is modeled as a polynomial of the operating cycle, which evolves through its working lifetime and the frequency of exogenous disturbance. Although its coefficients can be identified, a large amount of data are required [Sobczyk and Trebicki 2000; Kim, An, and Choi 2017]. Thus, that makes the online estimation, where the degradation information needs to update at every sampling period, become difficult. Meanwhile, from another perspective, degradation can be considered as a kind of faults, which has multiple solutions of FDD (Fault Detection and Diagnosis) and FTC (Fault-Tolerant Control). One popular method is to use an observer-based controller for the LPV system. In this approach, the dynamics of a non-linear system is rewritten in LPV model. Then, the observer is used for fault and state estimation, while the controller reconfigures the control laws based on the observer data.

In terms of observer design, there are two aspects that need careful consideration: (1) - the polynomial modeling of actuator degradation and (2) - multi-objective disturbance attenuation for the impact of noise, unknown input (UI), and uncertainty.

Regarding the problem (1), a \mathcal{H}_∞ high-order proportional-integral (PI) observer [Koenig 2005; Zhang, Zhang, and Wang 2015] was developed to attenuate the impact of perturbation

on estimation, thereby accurately identifying the defect. Unfortunately, the model is unable to represent the relation between the UI frequency and the fault itself in degradation. Meanwhile, [Rodrigues et al. 2015] has developed a LPV adaptive estimation method for actuator fault. However, the degradation process could not be demonstrated because the fault derivative needs to be bounded while estimation errors converge to a non-zero-bounded region. Hence, there is a need for a more comprehensive study on fault estimation and observer design to examine the degradation modeling.

Concerning the issue (2), many attempts have been made to handle the disturbances (uncertainties, UIs, and noise). Except the state-space filter form of LPV filters proposed by [Grenaille, Henry, and Zolghadri 2008; Henry 2012; Henry et al. 2015] that possesses an important number of degrees of freedom, separately or only two maximum out of the above disturbances can be simultaneously examined. For instance, [Marx et al. 2019] has succeeded in developing a LPV UI observer to decouple the UI in dynamics of estimation error, but fail to handle uncertainty and noise. Meanwhile, [Hassanabadi, Shafiee, and Puig 2017] tackles the uncertainties in the time-varying parameter to estimate the actuator fault in the descriptor LPV system. Unfortunately, the polytopic representation of uncertainty in that research creates a complicated double-layer polytopic model. Then, to concurrently deal with impacts of UI and noise, a mixed synthesis $\mathcal{H}_\infty/\mathcal{H}_2$ has been widely implemented in observer designs, namely [Khosrowjerdi, Nikoukhah, and Safari-Shad 2004]. In which, the \mathcal{H}_∞ norm is used to attenuate the influence of UI on the estimation error or the desired output, while the \mathcal{H}_2 norm minimizes the effects of noise on observer's estimation. Nevertheless, the method entails two major drawbacks as below:

- Multi-objective optimization problem $\mathcal{H}_\infty/\mathcal{H}_2$ is a non-convex problem, which is commonly solved by fixing γ_∞ and minimizing γ_2 or vice versa [Scherer and Weiland 2001]. Another method is to imply a trade-off convex performance γ from γ_2 and γ_∞ , which is expressed as [Yamamoto et al. 2015]: $\gamma = \alpha\gamma_2 + (1 - \alpha)\gamma_\infty$ with a given $\alpha \in [0, 1]$. However, both of these approaches require lots of effort to find a compromise for the observer performance, and sometimes there is no feasible solution for this kind of problem;
- The application of \mathcal{H}_2 norm to noise cancellation is limited because the white noise v is a zero-mean signal with identity power spectrum density (PSD) matrix, i.e. $\mathbb{E}\{v(t)v(\tau)^T\} = I\delta_{(t-\tau)}$ [Boyd et al. 1994; Gahinet, Apkarian, and Chilali 1996].

Based on the well-known Kalman filtering [Kalman 1960; Lewis, Vrabie, and Syrmos 2012], a modified UI observer [Wang, Puig, and Cembrano 2018] is synthesized against noise with various PSD and UI, but its estimation result varies in a bounded interval defined by system uncertainties. Consequently, there is a great need of a robust observer, which not only deals with the simultaneous existence of uncertainty, UI, and noise with various PSD, but also avoids the multi-objective optimization for both UI attenuation and noise cancellation.

In terms of observer-based controller synthesis, the combination of feed-back controller and Kalman observer for state estimation allows the LPV Linear-Quadratic-Gaussian (LQG) design [Wu and Packard 1995] to handle the influence of Gaussian noise on process and mea-

surement. Nonetheless, UI is not taken into consideration in its observer design while the separation principle in closed-loop stability analysis, i.e. the controller and observer gains are synthesized separately in two steps (see Remark 3.3.2), can be violated due to the uncertainty existence. It is then emphasized in [Yamamoto et al. 2019] for the steering system by using the $\mathcal{H}_\infty/\mathcal{H}_2$ PI observer and LPV feedback controller. Consequently, to conquer the robust problem in this design concept and compensate for the effects of the faults, an integrated design has been developed. In the approach, the controller is incorporated in the fault compensation and both observer-controller gains can be simultaneously synthesized in one step. Notably, in [Lan and Patton 2016], the disturbance impact on fault estimation is decoupled by UI observer while \mathcal{H}_∞ sliding mode control assures the quality of controlled output against system disturbances and uncertainties. Unfortunately, despite the effective performance, the controller design demands restrictive conditions for the positive definite matrix P of Lyapunov function to decouple the observer and controller design, which may lead to an unfeasible solution for LMI optimization. The same problems, as discussed in [Kheloufi et al. 2013], are also found in the integrated design of [Rodrigues et al. 2014]. Nevertheless, these integrated designs do not take into account the impact of noise. Therefore, the development of an observer-controller co-design that is robust against not only uncertainties but also the UIs and the stochastic noise is still in need.

In brief, the existing problems can be summarized as follows:

- Polynomial modeling of degradation estimation.
- Multi-objective optimization for disturbance attenuation.
- Integration of stochastic noise problem in the classical integrated design of active FTC, which is also mentioned in Section 2.3.2.

3.1.2 Chapter Contributions

To overcome the above issues, this Chapter makes the following contributions:

- The polynomial model of actuator degradation, which depends on the disturbance frequency and operating time, is studied in the context of observer design and degradation accommodation;
- By assuming the unmeasurable UIs has unknown magnitude but known or bounded frequency, the match condition of UI frequency is chosen. Accordingly to this classification of UIs, the following methodologies are introduced:
 - Matched UI: A novel frequency-shaping filter is proposed as an alternative to the classical \mathcal{H}_∞ -norm in attenuating the impact of UI on degradation estimation, thus avoiding the multi-objective optimization which may lead to an unfeasible solution. Also, this solution takes advantage of degradation modeling;

- Unmatched UI: An extension result is obtained for the well-known $\mathcal{H}_\infty/\mathcal{H}_2$ synthesis to handle the white noise with various PSD, thus removing the limitation of \mathcal{H}_2 for unity PSD noise;
- LPV robust-stochastic integrated designs, which incorporate the methodology of Kalman filtering into the classical integrated design, are robust against the unmeasurable uncertainty under the existence of stochastic noise and UI. Moreover, by assuming the system is re-configurable, the actuator saturation can be rewritten into polytopic LPV form to develop anti-windup controllers for the integrated designs.

The Chapter is organized as follows. Firstly, Section 3.2 presents the degradation modeling, the system representation, and design objectives based on the matching condition of UI frequency. Then, Section 3.3 demonstrates in detail the new methodology of observer and controller design for the degradation estimation and accommodation to handle the matched UI. Next, an extension result for $\mathcal{H}_\infty/\mathcal{H}_2$ observer-based fault compensator is introduced in Section 3.4. The anti-windup problem is integrated into the design in Section 3.5. To prove the performance of the proposed method, a simulation example with the frequency analysis is then illustrated to consider a more realistic extension of the proposed approach in Section 3.6. Finally, conclusions with future work are presented in Section 3.7.

3.2 Problem formulation

3.2.1 Degradation modeling

In any system, disturbance causes the states/outputs to vary, i.e. "excited" by its existence, and this variation depends mainly on the frequency of exogenous input. Herein, the number of series that a system is repeatedly influenced by a fixed frequency of disturbance during its operating time is called the operating cycle, i.e. working period [Suciu and Yaguchi 2009; Giurgiutiu 2007].

According to the prognostic model [Luo et al. 2008] and Taylor series [Zill, Wright, and Cullen 2011], for a constant excitation frequency F_w , the polynomial of operating cycle $\bar{N}_c = F_w t$ can be used to describe the degradation D of an actuator:

$$D = D_{(F_w, t)} = \sum_{j=0}^m \alpha_j \left(\sum_{i=0}^s \beta_i \bar{N}_c^i \right)^j, \quad (3.1)$$

where α_j, β_i are the polynomial's coefficients.

In fact, the same experimental results are also found for suspension system. Notably, [Suciu and Yaguchi 2009] shows that the dissipated energy of damper is expressed similarly as an exponential equation of the number of working cycles for a constant road frequency F_w . Meanwhile, [Yao and Pecht 2018] identifies that damper coefficient degrades as: $c_{(\bar{N}_c)} = a(\bar{N}_c)^b + c$ with a, b, c are identified coefficients.

All the above nonlinear relations can be rewritten as follows thanks to the Taylor series:

$$D = D_{(F_w, t)} = \sum_{k=0}^s \beta_k \bar{N}_c^k = \sum_{k=0}^s \beta_k (F_w)^k t^k. \quad (3.2)$$

These assessments have not only strengthened the reliability of a theoretical model, but also promoted a general polynomial model of actuator degradation. In this Chapter, the UI vector $w = [w_1 \ w_2 \ \dots \ w_{n_w}]^T \in \mathbb{R}^{n_w}$ is the combination of all UIs w_i , while f_w is defined as a vector containing all the excitation frequency $f_{w(i)}$ corresponding to each exogenous input w_i , where $i = 1 : n_w$. For each w_i with the frequency $f_{w(i)}$ ($i = 1 : n_w$), the degradation d_{ji} ($j = 1 : n_u$), addressing the degrading influence of disturbance w_i on the actuator u_j , is expressed as:

$$d_{ji} = d_{j(f_{w(i)}, t)} = \sum_{k=0}^s \beta_{jik} (N_{c(i)})^k = \sum_{k=0}^s \beta_{jik} (f_{w(i)})^k (t)^k. \quad (3.3)$$

Then actuator degradation d_j is assumed to be presented under a polytope of its elements d_{ji} :

$$d_j = \sum_{i=1}^{n_w} \alpha_{ji} d_{ji}, \quad \sum_{i=1}^{n_w} \alpha_{ji} = 1. \quad (3.4)$$

In other words, d_j is a polynomial of time t and its unknown coefficients $\Phi(j, k, f_{w(i=1:n_w)})$ are functions that depend on the elements of frequency vector f_w and have a defined value at the moment t .

$$d_j = \sum_{k=0}^s \Phi(j, k, f_{w(i=1:n_w)})(t)^k, \quad (3.5)$$

Thereby, the degradation vector $d = [d_1 \ \dots \ d_{n_u}]^T$ can be rewritten as:

$$d = D_0 + D_1 t + \dots + D_s t^s = \sum_{k=0}^s D_k t^k, \quad (3.6)$$

where $D_k = [\Phi(1, k, f_{w(i=1:n_w)}) \ \dots \ \Phi(n_u, k, f_{w(i=1:n_w)})]^T$ for all $k = 0 : s$.

In fact, the above degradation form is a special case of classical polynomial fault [Koenig 2005] whose coefficients depend on f_w . Consequently, all solutions for polynomial fault can be applied to the estimation of actuator degradation.

From a practical point of view, the frequency $f_{w(i)}$ is supposed to be slowly varying, i.e. $\dot{f}_{w(i)} = 0$. To better interpret this assumption, the Fig. 1 illustrates the actuator degradation when $n_w = n_u = 1$, which is also the study case mentioned in works of [Suciu and Yaguchi

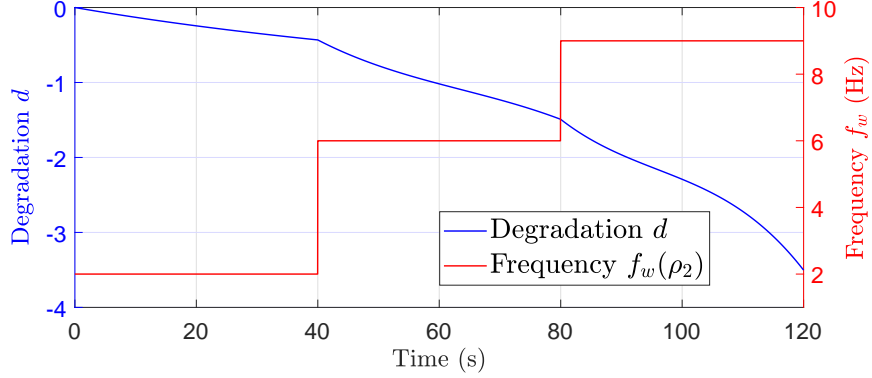


Figure 3.1: Relation between degradation d and frequency f_w

2009; Yao and Pecht 2018] or in examples of [Luo et al. 2008; Abou Jaoude 2015] where the characteristic of suspension degradation changes according to the road frequency.

Based on the above definition of degradation, a comprehensive study on the degradation estimation and accommodation will be developed in the next section.

3.2.2 Stochastic LPV System representation

Consider the following uncertain stochastic LPV system with actuator degradation:

$$\begin{cases} \dot{x} &= (A_{(\rho_1)} + \Delta A_{(\rho_1)})x + Bu + Bd + E_{(\rho_1)}w + H_{(\rho_1)}v_1, \\ y &= (C + \Delta C)x + v_2 \end{cases}, \quad (3.7)$$

where:

- $x \in \mathbb{R}^{n_x}$ is the state vector; $y \in \mathbb{R}^{n_y}$ is the measurement output vector; $u \in \mathbb{R}^{n_u}$ is the nominal input vector; $w \in \mathbb{R}^{n_w}$ is the UI disturbance vector; $d \in \mathbb{R}^{n_d}$ is the actuator degradation vector to be estimated, which can be expressed as an s -order polynomial in (3.6), i.e. $d = D_0 + D_1t + \dots + D_s t^s = \sum_{k=0}^s D_k t^k$, such that $d^{(s+1)} = 0$ and D_k ($k = 0 : s$) are unknown coefficients. As discussed in Section 3.1, the degradation is a specific study of polynomial fault whose coefficients D_k depend on the frequency vector f_w of the UI w .
- Matrices $A_{(\rho_1)}$, $E_{(\rho_1)}$, and $H_{(\rho_1)}$ are parameter-varying matrices corresponding to the nominal system whose time-varying parameter vector $\rho_1(t)$ takes values in the parameter space \mathcal{P}_{ρ_1} :

$$\mathcal{P}_{\rho_1} = \{\rho_1 = [\rho_{11}(t) \quad \rho_{12}(t) \quad \dots \quad \rho_{1m}(t)]^T \mid \underline{\rho}_{1i}(t) \leq \rho_i \leq \overline{\rho}_{1i}(t)\}, \forall i = 1 : m, t \geq 0. \quad (3.8)$$

- Terms $\Delta A_{(\rho_1)}$ and ΔC are time-varying parameter matrices corresponding to the uncertainty of the nominal system, which can be expressed as:

$$\begin{cases} \Delta A_{(\rho_1)} = M_{(\rho_1)} \Delta_a N_{(\rho_1)} \\ \Delta C = F \Delta_c G \end{cases} \quad (3.9)$$

Here $M_{(\rho_1)}$, $N_{(\rho_1)}$, F , and G with appropriate dimensions are measurable parameter-varying matrices. Meanwhile, the terms Δ_a and Δ_c are uncertain matrices satisfying $\Delta_a^T \Delta_a \leq I$ and $\Delta_c^T \Delta_c \leq I$.

Remark 3.2.1

The formulation (3.9) enables the generic representation of parametric uncertainties without the need to approximate them by the polytopic representation, thus avoiding the double-layer polytopic problem that exceeds the number of LMIs.

- $v_1 \in \mathbb{R}^{n_{v_1}}$ and $v_2 \in \mathbb{R}^{n_y}$ are zero-mean Gaussian white noise vectors, respectively, in the process and measurement that satisfy

$$\mathbb{E}\{v_1(t_1)v_1^T(t_2)\} = V_1 \delta(t_1 - t_2), \quad (3.10)$$

$$\mathbb{E}\{v_2(t_1)v_2^T(t_2)\} = V_2 \delta(t_1 - t_2), \quad (3.11)$$

$$\mathbb{E}\{v_1(t_1)v_2^T(t_2)\} = 0, \quad (3.12)$$

where t_1 and t_2 represent momentary time samplings; $V_1 \geq 0$ and $V_2 > 0$.

- Parameter-dependent distribution matrices can be expressed in the polytopic coordinates, where the coefficients of the polytopic decomposition are denoted as $\delta_{i(\rho_1)}$ and vary within the convex set \mathcal{P}_δ : [Biannic 1996; Poussot-Vassal et al. 2008]

$$\mathcal{P}_\delta = \left\{ \delta_{(\rho_1)} = [\delta_{1(\rho_1)} \quad \delta_{2(\rho_1)} \quad \dots \quad \delta_{N(\rho_1)}]^T \mid \delta_{i(\rho_1)} = \frac{\prod_{j=1}^m |\rho_{1j} - \mathcal{C}_{(\omega_i)j}^\delta|}{\prod_{j=1}^m (\bar{\rho}_{1j} - \underline{\rho}_{1j})} \geq 0, \sum_{i=1}^{N=2^m} \delta_{i(\rho_1)} = 1 \right\}, \quad (3.13)$$

where ω_i ($i = 1 : N$, $N = 2^m$) are the vertices of the polytope formed by the boundness of each TVP and $\mathcal{C}_{(\omega_i)j}^\delta$ is the j^{th} component of the vector $\mathcal{C}_{(\omega_i)}^\delta$ defined as :

$$\mathcal{C}_{(\omega_i)j}^\delta = \{\rho_{1j} \mid \rho_{1j} = \bar{\rho}_{1j} \text{ if } (\omega_i)_j = \underline{\rho}_{1j} \text{ or } \rho_{1j} = \underline{\rho}_{1j} \text{ otherwise}\}. \quad (3.14)$$

As a result, $A_{(\rho_1)} = \sum_{i=1}^N \delta_{i(\rho_1)} A_{(i)}$ where $A_{(i)} = A_{(\omega_i)}$ is the value of $A_{(\rho_1)}$ at each corner of the polytope. Similar interpretations can be applied to $E_{(\rho_1)}$, $H_{(\rho_1)}$, $M_{(\rho_1)}$, and $N_{(\rho_1)}$.

Remark 3.2.2

The input matrix B is independent of the varying parameter, which is consistent with the LMI solution for polytopic system [Apkarian and Gahinet 1995]. In case $B = B_{(\rho_1)}$,

where $B_{(\rho_1)}$ depends on the varying parameter ρ_1 , the representation (3.7) can always be obtained by using the input filter in Section 1.5.3.1 with singular matrix $E = I$.

Consider the s^{th} derivatives of d , system (3.7) becomes an equivalent augmented system:

$$\begin{cases} \dot{x}_a &= (A_{a(\rho_1)} + \Delta A_{a(\rho_1)})x_a + B_a u + E_{a(\rho_1)} w + H_{a(\rho_1)} v_1, \\ y &= (C_a + \Delta C_a)x_a + v_2 \end{cases}, \quad (3.15)$$

where $x_a = \begin{bmatrix} x \\ d \\ d^{(1)} \\ \dots \\ d^{(s-1)} \\ d^{(s)} \end{bmatrix} \in \mathbb{R}^{n_{x_a}}$, $n_{x_a} = n_x + (s+1)n_u$, $\Delta A_{a(\rho_1)} = M_{a(\rho_1)} \Delta_a N_{a(\rho_1)}$,

$$B_a = \begin{bmatrix} B \\ 0 \\ 0 \\ \dots \\ 0 \\ 0 \end{bmatrix}, E_{a(\rho_1)} = \begin{bmatrix} E_{(\rho_1)} \\ 0 \\ 0 \\ \dots \\ 0 \\ 0 \end{bmatrix}, H_{a(\rho_1)} = \begin{bmatrix} H_{(\rho_1)} \\ 0 \\ 0 \\ \dots \\ 0 \\ 0 \end{bmatrix}, A_{a(\rho_1)} = \begin{bmatrix} A_{(\rho_1)} & B & 0 & 0 & \dots & 0 \\ 0 & 0 & I & 0 & \dots & 0 \\ 0 & 0 & 0 & I & \dots & 0 \\ \dots & \dots & \dots & \dots & \dots & \dots \\ 0 & 0 & 0 & 0 & \dots & I \\ 0 & 0 & 0 & 0 & \dots & 0 \end{bmatrix},$$

$$M_{a(\rho_1)} = \begin{bmatrix} M_{(\rho_1)}^T & 0^T & 0^T & \dots & 0^T & 0^T \end{bmatrix}^T, N_{a(\rho_1)} = \begin{bmatrix} N_{(\rho_1)} & 0 & 0 & \dots & 0 & 0 \end{bmatrix},$$

$$C_a = \begin{bmatrix} C & 0 & 0 & \dots & 0 & 0 \end{bmatrix}, \Delta C_a = \begin{bmatrix} \Delta C & 0 & 0 & \dots & 0 & 0 \end{bmatrix} = F_a \Delta_c G_a, F_a = F, \text{ and } G_a = \begin{bmatrix} G & 0 & 0 & \dots & 0 & 0 \end{bmatrix}$$

To estimate the degradation d through the estimation of augmented state x_a , the system (3.15) is assumed to be observable or at least detectable. Its detectability can be later verified by condition (3.29).

3.2.3 Design objectives

The aim of this Chapter is to design robust-stochastic LPV integrated models for the augmented system (3.15), as illustrated in Fig. 3.2.

Hereunder are the objectives of these designs.

- **Observer:** The degradation d is robustly estimated under the presence of uncertainties, UI, and stochastic noise, such that:

(O.1) When UI $w = 0$, the influence of Gaussian noise $\bar{v} = [v_1^T \ v_2^T]^T$ on the estimation error $e = [e_x^T \ e_d^T]^T$ is minimized through objective $J_e = \mathbb{E}\{e^T e\}$, in which e_x is the state-estimation error and e_d is the degradation estimation error.

(O.2) When noise $\bar{v} = 0$, the impact of UI w on the estimation error e is attenuated by \mathcal{H}_∞ synthesis or frequency-shaping filter, depending on the matching condition of UI frequency.

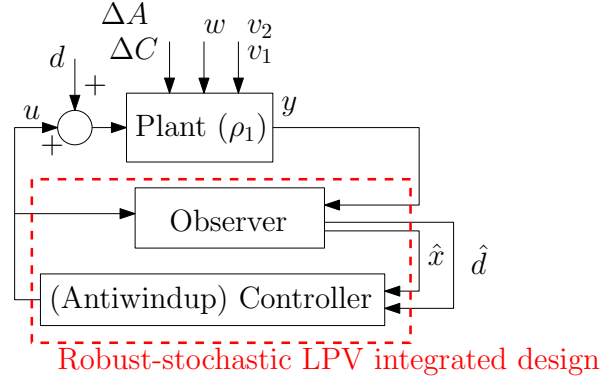


Figure 3.2: Scheme of robust-stochastic integrated design

- **Controller:** The output y is accommodated against the degradation d and $y \xrightarrow{t \rightarrow \infty} \Omega_w$, a zero-converging region whose radius R_Ω is bounded by the disturbances w and \bar{v} . The saturation problem is also formulated as a LPV problem in order to obtain an antiwindup controller.
- **Observer-controller Stability:** The gains of observer and controller in the integrated design (active FTC) are synthesized simultaneously to assure the robust stability of the closed-loop system under the influence of parametric uncertainty and fault occurrence.

The design solutions will be proposed in the next section.

3.2.4 UI-Matching conditions and Proposed design solutions

In this Thesis, UIs are classified based on their frequency because UI frequency can be estimated/identified in the degradation modeling. Thus, there are 2 cases for UI vector w :

- Matched UI: whose frequency $f_{w(i)}$ ($i = 1 : n_w$) is known or bounded.

This case is the main focus of the Chapter, where a joint design of the frequency-shaping filter and Gaussian noise cancellation is promoted as an alternative to $\mathcal{H}_\infty/\mathcal{H}_2$ synthesis, which avoids the non-convex multi-objective optimization while giving the better performance. Also, its solution can take advantage of the degradation definition, where its coefficients depend partially on the frequency vector f_w , to greatly attenuate the impact of UI. Details on the design process are presented in Section 3.3.

- Unmatched UI: whose energy (\mathcal{L}_2 -norm) is bounded and where no information on frequency $f_{w(i)}$ is available.

In this circumstance, the well-known \mathcal{H}_∞ norm can be implemented to attenuate UI influence on the estimation error e , which has to satisfy that:

$$\sup_{\rho_1 \in \mathcal{P}_{\rho_1}, \|w\|_2 \neq 0, w \in \mathcal{L}_2} \frac{\|e\|_2}{\|w\|_2} \leq \gamma_\infty \quad (3.16)$$

Lemma 1.5.2 concerning \mathcal{H}_∞ performance for UI attenuation can be applied to obtain the general solution for this case, which has been broadly studied. More information on its drawbacks when it is combined with \mathcal{H}_2 -norm noise cancellation can be found in the Introduction. Meanwhile, an extension of the mixed $\mathcal{H}_\infty/\mathcal{H}_2$ for various PSD of noise will be presented in Section 3.4.

Obviously, the solution to the unmatched UI can be applied for the matched UI but it may not result in an efficient performance due to multi-objective problems. To highlight such issue, a comparison between the matched UI solution and the well-known mixed $\mathcal{H}_\infty/\mathcal{H}_2$ will be presented in the simulation.

The actuator saturation will be re-addressed under the polytopic form while the stochastic LPV system is assumed to be re-configurable under the presence of saturation. Its solution is given in Section 3.5.

3.3 Robust-stochastic integrated design for Matched UI

In this Section, the robust-stochastic integrated design for matched UI is presented. In which, the observer is built based on PMI (Proportional Multiple-Integral) observer and the output frequency filter, while the controller is a state-feedback fault compensator.

3.3.1 Methodology of Frequency-Shaping filter

The methodology of frequency-shaping filter, which is considered as an alternative to \mathcal{H}_∞ synthesis, is based on the study on optimal control and the principle of UI observer. Details are given below:

In the synthesis for optimal control [Levine 2010], the desired performance for stochastic system can be defined through the classical cost functional over time τ :

$$\min_u J(t) = \lim_{\tau \rightarrow \infty} \mathbb{E} \left\{ \frac{1}{\tau} \int_0^\tau (y_{(t)}^T Q^T Q y_{(t)} + u_{(t)}^T R^T R u_{(t)}) dt \right\}. \quad (3.17)$$

Using the Parseval's Theorem [Kammler 2007], the above cost J can be rewritten in the frequency domain as:

$$\min_u J(\omega) = \lim_{\tau \rightarrow \infty} \mathbb{E} \left\{ \frac{1}{\tau} \frac{1}{2\pi} \int_{-\infty}^{\infty} (y_{(j\omega)}^* Q_{(j\omega)}^* Q_{(j\omega)} y_{(j\omega)} + u_{(j\omega)}^* R_{(j\omega)}^* R_{(j\omega)} u_{(j\omega)}) d\omega \right\}, \quad (3.18)$$

where $y_{(j\omega)}^* = y_{(-j\omega)}^T$ is the complex conjugate transpose of signal $y_{(j\omega)}$. In which, the control performance cost can be specified for a frequency zone by employing the appropriate frequency-weighting filter $Q_{(j\omega)}$ and $R_{(j\omega)}$.

Hence, a unitary frequency weighted functional J is obtained:

$$\min_{\bar{u}} J(\omega) = \frac{1}{2\pi} \int_{-\infty}^{\infty} (\bar{y}_{(j\omega)}^* \bar{y}_{(j\omega)} + \bar{u}_{(j\omega)}^* \bar{u}_{(j\omega)}) d\omega \quad (3.19)$$

where $\bar{y} = Q_{(j\omega)} y$ and $\bar{u} = R_{(j\omega)} u$. Also, J can be rewritten in the time domain as:

$$\min_{\bar{u}} J(t) = \int_0^{\infty} (\bar{y}_{(t)}^T \bar{y}_{(t)} + \bar{u}_{(t)}^T \bar{u}_{(t)}) dt \quad (3.20)$$

In which, the weighting filters characterize the controller and output components to achieve the desired control cost at various frequencies [Levine 2010]. Consequently, the implementation of these filters to observer design becomes an interest in this Chapter.

In addition, it should be noted that the principle of common UI observer is to generate zero transmissions from UIs to the output measurement [Chen, Patton, and Zhang 1996], i.e. the decoupling between the estimation error and UI. Thus, an output filter should be applied, which generates a fictive output \bar{y} such that the transmissions between \bar{y} and UI are nearly zeros, i.e. a similar effect of UI decoupling in UI observer.

Therefore, based on the idea of the two above methodologies, this Chapter promotes an output frequency-shaping filter for observer design procedure that can generate a similar UI-decoupling/attenuating effect in a specific frequency zone. The estimation process for actuator degradation is presented in Fig. 3.3 where a stable filter $Q_{(f_w)}$ is applied to the output y , generating the signal \bar{y} as an input to the observer. This filter specifies the attenuation of disturbance influence on the degradation estimation according to the knowledge on f_w .

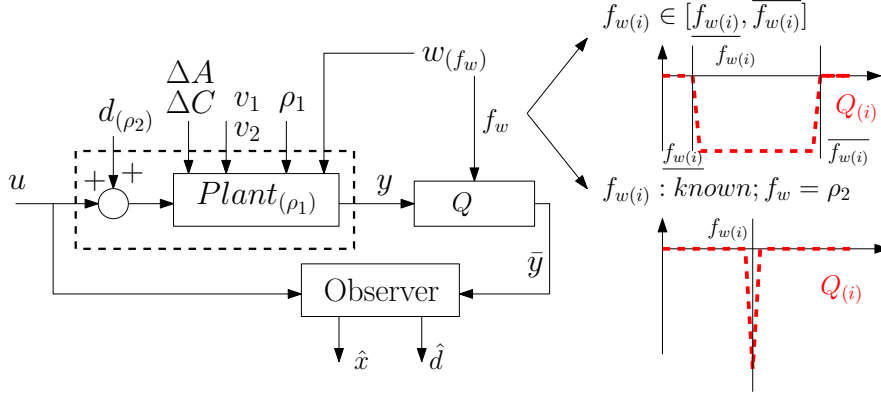


Figure 3.3: General scheme for estimation process

The two following cases are considered:

- **Case 1:** f_w is known.

f_w can be considered as a varying parameter vector ρ_2 modifying the filter $Q_{(f_w)}$, which represents a series of filters $Q_{(i)}$ attenuating the UIs at each known frequency $f_{w(i)}$. This

output filter can be displayed in a general form:

$$Q_{(f_w)} = Q_{(\rho_2)} : \begin{cases} \dot{x}_Q = A_{Q(\rho_2)}x_Q + B_Q y \\ \bar{y} = C_Q x_Q + D_Q y \end{cases}, \quad (3.21)$$

$$\Leftrightarrow \begin{cases} \dot{x}_Q = A_{Q(\rho_2)}x_Q + B_Q(C_a + \Delta C_a)x + B_Q v_2 \\ \bar{y} = C_Q x_Q + D_Q(C_a + \Delta C_a)x + D_Q v_2 \end{cases}, \quad (3.22)$$

where $x_Q \in \mathbb{R}^{n_{x_Q}}$ is the state of the frequency-shaping filter.

- **Case 2:** f_w is not exactly known but $f_{w(i)}$ is bounded by $[\underline{f_{w(i)}}, \overline{f_{w(i)}}]$ ($i = 1 : n_w$)

A series of constant notch filters is proposed to attenuate each frequency zone $[\underline{f_{w(i)}}, \overline{f_{w(i)}}]$. As the final filter formulation Q is the same, the design process for bounded frequency is similar to that for the known one.

Without loss of generality, observer design for specific f_w is focused in this Chapter while $\rho_2 = f_w$ is chosen as a time-varying parameter.

3.3.2 Observer design for Matched UI

In this section, a robust PMI observer is proposed to estimate the degradation.

Consider a new parameter-varying vector $\rho = [\rho_1^T \ \rho_2^T]^T \in \mathbb{R}^k$, which generates a new polytope convex set P_θ with the coefficients of the polytopic decomposition $\theta_{(\rho)}$:

$$\mathcal{P}_\theta = \{\theta_{(\rho)} = [\theta_{1(\rho)} \ \theta_{2(\rho)} \ \dots \ \theta_{\bar{N}(\rho)}]^T \mid \theta_{i(\rho)} = \frac{\prod_{j=1}^k |\rho_j - \underline{C}_{(\omega_i)j}^\theta|}{\prod_{j=1}^k (\bar{\rho}_j - \underline{\rho}_j)} \geq 0, \sum_{i=1}^{\bar{N}=2^k} \theta_{i(\rho)} = 1\}, \quad (3.23)$$

$$C_{(\omega_i)j}^\theta = \{\rho_j \mid \rho_j = \bar{\rho}_j \text{ if } (\omega_i)_j = \underline{\rho}_j \text{ or } \rho_j = \underline{\rho}_j \text{ otherwise}\}. \quad (3.24)$$

As a result, a new system is derived from (3.15) and (3.22):

$$\begin{cases} \dot{\bar{x}}_a = (\bar{A}_{a(\rho)} + \Delta \bar{A}_{a(\rho)})\bar{x}_a + \bar{B}_a u + \bar{E}_{a(\rho)} w + \bar{H}_{a(\rho)} \bar{v} \\ \bar{y} = (\bar{C}_a + \Delta \bar{C}_a)\bar{x}_a + \bar{D}_Q \bar{v} \end{cases}. \quad (3.25)$$

In which $\bar{x}_a = \begin{bmatrix} x_a \\ x_Q \end{bmatrix} \in \mathbb{R}^{n_{\bar{x}_a}}$, $n_{\bar{x}_a} = n_x + (s+1)n_u + n_{x_Q}$, $\bar{v} = \begin{bmatrix} v_1 \\ v_2 \end{bmatrix}$, $\bar{A}_{a(\rho)} = \begin{bmatrix} A_{a(\rho_1)} & 0 \\ B_Q C_a & A_{Q(\rho_2)} \end{bmatrix}$, $\bar{B}_a = \begin{bmatrix} B_a \\ 0 \end{bmatrix}$, $\bar{E}_{a(\rho)} = \begin{bmatrix} E_{a(\rho_1)} \\ 0 \end{bmatrix}$, $\bar{H}_{a(\rho)} = \begin{bmatrix} H_{a(\rho_1)} & 0 \\ 0 & B_Q \end{bmatrix}$, $\Delta \bar{A}_{a(\rho)} = \begin{bmatrix} \Delta A_{a(\rho_1)} & 0 \\ B_Q \Delta C_a & 0 \end{bmatrix}$, $\Delta \bar{C}_a = \begin{bmatrix} D_Q \Delta C_a & 0 \end{bmatrix}$, $\bar{C}_a = \begin{bmatrix} D_Q C_a & C_Q \end{bmatrix}$, and $\bar{D}_Q = D_Q \begin{bmatrix} 0_{n_y \times n_{v_1}} & I_{n_y} \end{bmatrix}$.

The robust PMI LPV observer for uncertain stochastic system (3.25) is designed as:

$$\begin{cases} \dot{\hat{x}}_a &= \bar{A}_{a(\rho)}\hat{x}_a + \bar{B}_a u + \bar{L}_{a(\rho)}(\bar{y} - \hat{y}) \\ \hat{y} &= \bar{C}_a \hat{x}_a \end{cases}, \quad (3.26)$$

where \hat{x}_a (or \hat{y}) is the estimated of \bar{x}_a (or \bar{y}), $\hat{x}_a = \left[\hat{x}^T \quad \hat{d}^T \quad \hat{d}^{(1)T} \quad \dots \quad \hat{d}^{(s-1)T} \quad \hat{d}^{(s)T} \quad \hat{x}_Q^T \right]^T$, and \bar{L}_a is the observer gain which is later synthesized based on the methodology of Kalman filtering.

Remark 3.3.1

The order s of the estimated fault \hat{d} chosen for observer synthesis must equal to or greater than the real order of the degradation d . In practice, the value of s is chosen as large as possible without exceeding the capability of the computer in computation.

As the designed filter $Q_{(f_w)}$ is stable, the existing conditions, i.e. the detectability in the context of polytope, for the observer (3.26) are: [Koenig 2005; Shi and Patton 2015a]

$$\text{rank} \begin{bmatrix} pI_{n_{x_a}} - \bar{A}_{a(i)} \\ \bar{C}_a \end{bmatrix} = n_{\bar{x}_a}, \quad \forall \mathcal{R}(p) \geq 0, \quad i = 1 : \bar{N}. \quad (3.27)$$

$$\Leftrightarrow \text{rank} \begin{bmatrix} pI_{n_{x_a}} - A_{a(i)} \\ C_a \end{bmatrix} = n_{x_a}, \quad \forall \mathcal{R}(p) \geq 0, \quad i = 1 : \bar{N}. \quad (3.28)$$

$$\Leftrightarrow \text{rank} \begin{bmatrix} pI_{n_x} - A_{(i)} & -B \\ 0 & pI_{n_u} \\ C & 0 \end{bmatrix} = n_x + n_u, \quad \forall \mathcal{R}(p) \geq 0, \quad i = 1 : \bar{N}. \quad (3.29)$$

It is noted that the above condition for each corner of the polytope is equivalent to the detectability condition found for proportional multi-integral observer in time-invariant system [Koenig 2005].

The variable $e_{\bar{x}_a} = \bar{x}_a - \hat{x}_a$ is chosen as estimation error whose dynamics is described as follows:

$$\dot{e}_{\bar{x}_a} = (\bar{A}_{a(\rho)} - \bar{L}_{a(\rho)}\bar{C}_a)e_{\bar{x}_a} + \bar{E}_{a(\rho)}w + (\Delta\bar{A}_{a(\rho)} - \bar{L}_{a(\rho)}\Delta\bar{C}_a)\bar{x}_a + (\bar{H}_{a(\rho)} - \bar{L}_{a(\rho)}\bar{D}_Q)\bar{v}. \quad (3.30)$$

Consider the following transformation:

$$(\Delta\bar{A}_{a(\rho)} - \bar{L}_{a(\rho)}\Delta\bar{C}_a)\bar{x}_a = \left(\left[\begin{array}{c|c|c} \Delta A_{(\rho_1)} & 0 & 0 \\ 0 & 0 & 0 \\ B_Q\Delta C & 0 & 0 \end{array} \right] - \bar{L}_{a(\rho)} [D_Q\Delta C \mid 0 \mid 0] \right) \begin{bmatrix} x \\ d \\ \dots \\ \bar{d}^{(s)} \\ x_Q \end{bmatrix} \quad (3.31)$$

$$= \left(\left[\begin{array}{c} \Delta A_{(\rho_1)} \\ 0 \\ B_Q\Delta C \end{array} \right] - \bar{L}_{a(\rho)} D_Q\Delta C \right) x \quad (3.32)$$

$$= \left(\underbrace{\begin{bmatrix} M_{(\rho_1)} & 0 \\ 0 & 0 \\ 0 & B_Q F \end{bmatrix}}_{M_{ac(\rho)}} \underbrace{\begin{bmatrix} \Delta_a & 0 \\ 0 & \Delta_c \end{bmatrix}}_{\Delta_{ac}} \underbrace{\begin{bmatrix} N_{(\rho_1)} \\ G \end{bmatrix}}_{N_{ac(\rho)}} - \bar{L}_{a(\rho)} D_Q\Delta C \right) x \quad (3.33)$$

$$= (M_{ac(\rho)}\Delta_{ac}N_{ac(\rho)} - \bar{L}_{a(\rho)}D_Q\Delta C)x. \quad (3.34)$$

Then, the dynamics of observer (3.30) can be rewritten as:

$$\begin{aligned} \dot{e}_{\bar{x}_a} &= (\bar{A}_{a(\rho)} - \bar{L}_{a(\rho)}\bar{C}_a)e_{\bar{x}_a} + \bar{E}_{a(\rho)}w + (M_{ac(\rho)}\Delta_{ac}N_{ac(\rho)} - \bar{L}_{a(\rho)}D_Q\Delta C)x \\ &\quad + (\bar{H}_{a(\rho)} - \bar{L}_{a(\rho)}\bar{D}_Q)\bar{v}. \end{aligned} \quad (3.35)$$

Eq.(3.35) shows that the dynamics of observer is affected by matched UI w , the stochastic noise \bar{v} , and especially uncertainty term corresponding to state x .

3.3.3 Fault accommodation Controller design

To handle the negative impact of actuator degradation d , the fault compensation method is applied. Accordingly, the following controller is introduced for the integrated design:

$$u = -K_{(\rho)}\hat{x} + K_d\hat{d}, \quad (3.36)$$

where state-feedback gain $K_{(\rho)}$ in $-K_{(\rho)}\hat{x}$ stabilizes state x while the compensation gain $K_d = -B^\dagger B$ allows the controller to eliminate the influence of degradation since $BK_d = -BB^\dagger B = -B$.

Hence, the system (3.7) becomes:

$$\dot{x} = (A_{(\rho)} + \Delta A_{(\rho)})x - BK_{(\rho)}\hat{x} + Bd - B\hat{d} + E_{(\rho)}w + H_{(\rho)}v_1 \quad (3.37)$$

$$\dot{x} = (A_{(\rho)} + \Delta A_{(\rho)} - BK_{(\rho)})x + [BK_{(\rho)} \quad B] \begin{bmatrix} e_x \\ e_d \end{bmatrix} + E_{(\rho)}w + H_{(\rho)}v_1, \quad (3.38)$$

where $e_x = x - \hat{x}$ is state estimation error and $e_d = d - \hat{d}$ is degradation estimation error.

$$\text{As } v_1 = \begin{bmatrix} I_{n_{V_1}} & 0_{n_{V_1} \times n_y} \end{bmatrix} \bar{v} \text{ and } \begin{bmatrix} e_x \\ e_d \end{bmatrix} = \begin{bmatrix} I_{n_x} & 0 & 0 \dots 0 & 0 \\ 0 & I_{n_u} & 0 \dots 0 & 0 \end{bmatrix} \begin{bmatrix} \frac{e_x}{e_d} \\ \frac{e_d}{e_d^{(1)}} \\ \dots \\ \frac{e_d}{e_d^{(s)}} \\ \frac{e_{x_Q}}{e_{x_Q}} \end{bmatrix} = \begin{bmatrix} T_{e1} \\ T_{e2} \end{bmatrix} e_{\bar{x}_a}, \text{ we}$$

obtain:

$$\dot{x} = (A_{(\rho)} + \Delta A_{(\rho)} - BK_{(\rho)})x + [BK_{(\rho)} \quad B] T_e e_{\bar{x}_a} + E_{(\rho)}w + \bar{H}_{(\rho)}\bar{v}, \quad (3.39)$$

$$\text{where } \bar{H}_{(\rho)} = H_{(\rho)} \begin{bmatrix} I_{n_{V_1}} & 0_{n_{V_1} \times n_y} \end{bmatrix} \text{ and } T_e = \begin{bmatrix} T_{e1} \\ T_{e2} \end{bmatrix}.$$

Like the observer, the dynamics of system state x fed by state-feedback fault compensator is also affected by matched UI w , uncertainty term $\Delta A_{(\rho)}x$, the stochastic noise \bar{v} , and the estimation error $e_{\bar{x}_a}$.

3.3.4 Observer-Controller synthesis for Matched UI

Due to uncertainty existence, state x and estimation error $e_{\bar{x}_a}$ exist in both (3.35) and (3.39), which means there is a strong coupling in observer-controller relation and a challenge to design them separately. Hence, to avoid the instability of each component, the integrated design through the stability of closed-loop systems is required.

From (3.35) and (3.39), the closed-loop dynamics is implied:

$$\begin{bmatrix} \dot{x} \\ \dot{e}_{\bar{x}_a} \end{bmatrix} = \begin{bmatrix} A_{(\rho)} + \Delta A_{(\rho)} - BK_{(\rho)} & [BK_{(\rho)} \quad B] T_e \\ M_{ac(\rho)}\Delta_{ac}N_{ac(\rho)} - \bar{L}_{a(\rho)}D_Q\Delta C & \bar{A}_{a(\rho)} - \bar{L}_{a(\rho)}\bar{C}_a \end{bmatrix} \begin{bmatrix} x \\ e_{\bar{x}_a} \end{bmatrix} + \begin{bmatrix} \bar{H}_{(\rho)} \\ \bar{H}_{a(\rho)} - \bar{L}_{a(\rho)}\bar{D}_Q \end{bmatrix} \bar{v} + \begin{bmatrix} E_{(\rho)} \\ \bar{E}_{a(\rho)} \end{bmatrix} w. \quad (3.40)$$

In other words,

$$\dot{x}_{cl} = A_{cl(\rho)}x_{cl} + B_{cl(\rho)}\bar{v} + E_{cl(\rho)}w, \quad (3.41)$$

where $x_{cl} = [x^T \quad e_{\bar{x}_a}^T]^T$ is the closed-loop state vector, $E_{cl(\rho)} = \begin{bmatrix} E_{(\rho)} \\ \bar{E}_{a(\rho)} \end{bmatrix}$, and

$$A_{cl(\rho)} = \begin{bmatrix} A_{(\rho)} + \Delta A_{(\rho)} - BK_{(\rho)} & [BK_{(\rho)} \quad B] T_e \\ M_{ac(\rho)}\Delta_{ac}N_{ac(\rho)} - \bar{L}_{a(\rho)}D_Q\Delta C & \bar{A}_{a(\rho)} - \bar{L}_{a(\rho)}\bar{C}_a \end{bmatrix}, \quad B_{cl(\rho)} = \begin{bmatrix} \bar{H}_{(\rho)} \\ \bar{H}_{a(\rho)} - \bar{L}_{a(\rho)}\bar{D}_Q \end{bmatrix}.$$

Remark 3.3.2

The closed-loop stability is adversely affected by $(M_{ac(\rho)}\Delta_{ac}N_{ac(\rho)} - \bar{L}_{a(\rho)}D_Q\Delta C)$, i.e. the term of parametric uncertainty. Normally, this term is considered null in many studies without the influence of uncertainty, so the poles of closed-loop depend on the eigenvalues of diagonal elements $(A_{(\rho)} - BK_{(\rho)})$ and $(\bar{A}_{a(\rho)} - \bar{L}_{a(\rho)}\bar{C}_a)$, which is, in fact, called the

separation principle in the basic observer-based controller design.

Since the attenuation of perturbation impact w on degradation error $e_d = d - \hat{d}$ depends on the choice of filter $Q_{(\rho_2)}$, the objective (O.2) is implicitly integrated in the closed-loop stability. Meanwhile, the objective (O.1) is tackled by considering $w = 0$. Thus, by neglecting w , the closed-loop dynamics can be rewritten as:

$$\dot{x}_{cl} = A_{cl(\rho)}x_{cl} + B_{cl(\rho)}\bar{v}. \quad (3.42)$$

where the objective of controller-observer gains is now to minimize the cost $J_e = \mathbb{E}\{e^T e\}$, which is also the main objective of Kalman filtering [Lewis, Vrabie, and Syrmos 2012] under the influence of Gaussian noise \bar{v} . In other words:

$$\begin{cases} \dot{x}_{cl} &= A_{cl(\rho)}x_{cl} + B_{cl(\rho)}\bar{v}, \\ e &= C_{cl}x_{cl} \end{cases}, \quad (3.43)$$

where

- Error of estimation $e = [e_x^T \quad e_d^T]^T = C_{cl}x_{cl}$ with $C_{cl} = [0_{(n_x+n_u) \times n_x} \quad I_e]$.
- $\mathbb{E}\{\bar{v}(t_1)\bar{v}^T(t_2)\} = \mathbb{E}\left\{ \begin{bmatrix} v_1(t_1) \\ v_2(t_1) \end{bmatrix} \begin{bmatrix} v_1^T(t_2) & v_2^T(t_2) \end{bmatrix} \right\} = \begin{bmatrix} V_1 & 0 \\ 0 & V_2 \end{bmatrix} \delta(t_1 - t_2)$,
- $\mathbb{E}\{x_{cl(0)}\} = \bar{x}_{cl0}$,
- $\mathbb{E}\{(x_{cl(0)} - \bar{x}_{cl0})(x_{cl(0)} - \bar{x}_{cl0})^T\} = \mathcal{P}_0 > 0$.

Stability of closed-loop system and objective J_e can be both achieved by satisfying Theorem 3.3.1, presented as follows:

Theorem 3.3.1

The stability of closed-loop system and the minimization objective J_e of LPV system (3.43) are achieved if there exists a symmetric positive definite matrix $\mathcal{X} < \mathcal{P}_0^{-1}$ and a symmetric matrix $\mathcal{Z} > 0$ such that $Tr(\mathcal{Z})$ is minimized and the following conditions are satisfied:

$$\begin{bmatrix} \mathcal{X}A_{cl(\rho)} + A_{cl(\rho)}^T\mathcal{X} & \mathcal{X}B_{cl(\rho)}\bar{V} \\ (*) & -I \end{bmatrix} < 0, \quad (3.44)$$

$$\begin{bmatrix} \mathcal{X} & C_{cl}^T \\ C_{cl} & \mathcal{Z} \end{bmatrix} > 0, \quad (3.45)$$

where $\bar{V} = \begin{bmatrix} V_1^{1/2} & 0 \\ 0 & V_2^{1/2} \end{bmatrix}$.

Proof: The objective J_e can be expressed as [Tuan, Apkarian, and Nguyen 2001]:

$$J_e = \mathbb{E}\{e^T e\} = \text{Tr}\mathbb{E}\{ee^T\} = \text{Tr}\mathbb{E}\{C_{cl}x_{cl}x_{cl}^T C_{cl}^T\} \quad (3.46)$$

$$= \text{Tr}(C_{cl}\mathbb{E}\{x_{cl}x_{cl}^T\}C_{cl}^T) = \text{Tr}(C_{cl}\mathcal{P}_{(t)}C_{cl}^T). \quad (3.47)$$

To minimize J_e , $\mathcal{P}_{(t)} = \mathbb{E}\{x_{cl}x_{cl}^T\}$ is the solution of Riccati equation:

$$\frac{d\mathcal{P}_{(t)}}{dt} = \dot{\mathcal{P}}_{(t)} = A_{cl(\rho)}\mathcal{P}_{(t)} + \mathcal{P}_{(t)}A_{cl(\rho)}^T + B_{cl(\rho)} \begin{bmatrix} V_1 & 0 \\ 0 & V_2 \end{bmatrix} B_{cl(\rho)}^T. \quad (3.48)$$

Applying the Schur complement [Boyd et al. 1994] to (3.44) and pre & post-multiplying by \mathcal{X}^{-1} :

$$A_{cl(\rho)}\mathcal{X}^{-1} + \mathcal{X}^{-1}A_{cl(\rho)}^T + B_{cl(\rho)} \begin{bmatrix} V_1 & 0 \\ 0 & V_2 \end{bmatrix} B_{cl(\rho)}^T < 0. \quad (3.49)$$

So there exists a $\Delta(t) > 0$ that

$$\frac{d\mathcal{X}^{-1}}{dt} = 0 = A_{cl(\rho)}\mathcal{X}^{-1} + \mathcal{X}^{-1}A_{cl(\rho)}^T + B_{cl(\rho)} \begin{bmatrix} V_1 & 0 \\ 0 & V_2 \end{bmatrix} B_{cl(\rho)}^T + \Delta(t). \quad (3.50)$$

Subtracting (3.48) from (3.50)

$$\frac{d(\mathcal{X}^{-1} - \mathcal{P}_{(t)})}{dt} = A_{cl(\rho)}(\mathcal{X}^{-1} - \mathcal{P}_{(t)}) + (\mathcal{X}^{-1} - \mathcal{P}_{(t)})A_{cl(\rho)}^T + \Delta(t). \quad (3.51)$$

The solution for (3.51) is given as [Wu 1995]:

$$\mathcal{X}^{-1} - \mathcal{P}_{(t)} = \Phi_{(\rho)}(t, 0)(\mathcal{X}^{-1} - \mathcal{P}_0)\Phi_{(\rho)}^T(t, 0) + \int_0^t \Phi_{(\rho)}(t, \tau)\Delta(\tau)\Phi_{(\rho)}^T(t, \tau)d\tau \geq 0, \quad (3.52)$$

where $\Phi_{(\rho)}(t, \tau)$ is state-transition matrix of LPV system (3.43).

Consequently, $\mathcal{X}^{-1} \geq \mathcal{P}_{(t)}$ as $\mathcal{X} < \mathcal{P}_0^{-1}$, and

$$J_e = \text{Tr}(C_{cl}\mathcal{P}_{(t)}C_{cl}^T) \leq \text{Tr}(C_{cl}\mathcal{X}^{-1}C_{cl}^T) \quad (3.53)$$

As $\mathcal{X} > 0$, (3.45) and Schur complement [Boyd et al. 1994] lead to $\mathcal{Z} > C_{cl}\mathcal{X}^{-1}C_{cl}^T$. Therefore, $J_e < \text{Tr}(\mathcal{Z})$, which completes the proof. \blacksquare

Remark 3.3.3

Theorem 3.3.1 is developed based on the methodology of Kalman filtering [Lewis, Vrabie, and Syrmos 2012], with some modifications [Wu and Packard 1995; Tuan, Apkarian, and Nguyen 2001] in the implementation of continuous LPV system. Also, it should be noted that the LMI in Theorem 3.3.1 contains the matrices V_1 and V_2 , which represent the characteristics of stochastic noise.

To solve effectively Theorem 3.3.1, its LMIs need to be interpreted as new conditions, which is expressed by observer-controller gains and distribution matrices of initial LPV system. Therefore, the following Theorem is introduced.

Theorem 3.3.2

With given positive scalars $\sigma_1, \sigma_2, \sigma_3$, and σ_4 , Theorem 3.3.1 can be solved by finding symmetric positive definite matrices $P_1 > \mathcal{P}_{01}$ and $P_2 < \mathcal{P}_{02}^{-1}$, matrices $Q_{1(i)}$ and $Q_{2(i)}$, and a symmetric matrix $\mathcal{Z} > 0$ that minimize $Tr(\mathcal{Z})$ and satisfy the following conditions:

$$\left[\begin{array}{ccc|c} \Gamma_{1,1(i)} & 0 & \bar{H}_{(i)}\bar{V} & \Theta_{1(i)} \\ (*) & \Gamma_{2,2(i)} & \Gamma_{2,3(i)} & \\ (*) & (*) & -I & \\ \hline & (*) & & \Theta_2 \end{array} \right] < 0 \quad \forall i = 1 : \bar{N}, \quad (3.54)$$

$$\begin{bmatrix} P_1 & 0 & P_1 C_{cl1}^T \\ 0 & P_2 & C_{cl2}^T \\ C_{cl1} P_1 & C_{cl2} & \mathcal{Z} \end{bmatrix} > 0, \quad (3.55)$$

where

$$\Gamma_{1,1(i)} = \mathcal{H}\{A_{(i)}P_1 + BQ_{1(i)}\}, \quad \Gamma_{2,2(i)} = \mathcal{H}\{P_2\bar{A}_{a(i)} + Q_{2(i)}\bar{C}_a\}, \quad (3.56)$$

$$\Gamma_{2,3(i)} = P_2\bar{H}_{a(i)}\bar{V} + Q_{2(i)}\bar{D}_Q\bar{V}, \quad C_{cl} = [C_{cl1} \quad C_{cl2}], \quad (3.57)$$

$$\Gamma_0 = \sigma_4 \begin{bmatrix} P_1 & 0 \\ 0 & I_{n_u} \end{bmatrix}, \quad \mathcal{P}_0 = \begin{bmatrix} \mathcal{P}_{01} & 0 \\ 0 & \mathcal{P}_{02} \end{bmatrix} > 0, \quad (3.58)$$

$$\Theta_{1(i)} = \begin{bmatrix} -BQ_{1(i)} & B & P_1 N_{ac(i)}^T & P_1 G^T & P_1 N_{(i)}^T & 0 & 0 & M_{(i)} & 0 \\ 0 & 0 & 0 & 0 & 0 & P_2 M_{ac(i)} & Q_{2(i)} D_Q F & 0 & T_e^T \\ 0 & 0 & 0 & 0 & 0 & 0 & 0 & 0 & 0 \end{bmatrix}, \quad (3.59)$$

$$\Theta_2 = -diag\{\sigma_4^{-1}P_1, \sigma_4^{-1}I, \sigma_1 I, \sigma_2 I, \sigma_3 I, \sigma_1^{-1}I, \sigma_2^{-1}I, \sigma_3^{-1}I, \Gamma_0\}, \quad (3.60)$$

then the gains of observer-controller synthesis are simultaneously calculated as below:

$$K_{(\rho)} = \sum_{i=1}^{\bar{N}} \theta_{i(\rho)} K_{(i)} = - \sum_{i=1}^{\bar{N}} \theta_{i(\rho)} Q_{1(i)} P_1^{-1}, \quad (3.61)$$

$$\bar{L}_{a(\rho)} = \sum_{i=1}^{\bar{N}} \theta_{i(\rho)} \bar{L}_{a(i)} = - \sum_{i=1}^{\bar{N}} \theta_{i(\rho)} P_2^{-1} Q_{2(i)}. \quad (3.62)$$

Proof: Supposing that

$$\mathcal{X} = \begin{bmatrix} P_1^{-1} & 0 \\ 0 & P_2 \end{bmatrix} < \mathcal{P}_0^{-1} = \begin{bmatrix} \mathcal{P}_{01}^{-1} & 0 \\ 0 & \mathcal{P}_{02}^{-1} \end{bmatrix}, \quad (3.63)$$

where $P_1 \in \mathbb{R}^{n_x \times n_x}$ and $P_2 \in \mathbb{R}^{n_{\bar{x}_a} \times n_{\bar{x}_a}}$ are symmetric positive definite matrices.

Remark 3.3.4

The purpose of the above zero-diagonal block is to reinforce the separation between the observer and the controller such that the closed-loop is stabilized under the existence of uncertainties. In fact, this method is widely chosen in literature for robustness problems [Kheloufi et al. 2013; Lien 2004].

From (3.45), it follows that:

$$\mathcal{Z} > C_{cl} \mathcal{X}^{-1} C_{cl}^T = [C_{cl1} \quad C_{cl2}] \begin{bmatrix} P_1 & 0 \\ 0 & P_2^{-1} \end{bmatrix} \begin{bmatrix} C_{cl1}^T \\ C_{cl2}^T \end{bmatrix}, \quad (3.64)$$

$$\mathcal{Z} > [C_{cl1} P_1 \quad C_{cl2}] \begin{bmatrix} P_1^{-1} & 0 \\ 0 & P_2^{-1} \end{bmatrix} \begin{bmatrix} P_1 C_{cl1}^T \\ C_{cl2}^T \end{bmatrix} = [C_{cl1} P_1 \quad C_{cl2}] \begin{bmatrix} P_1 & 0 \\ 0 & P_2 \end{bmatrix}^{-1} \begin{bmatrix} P_1 C_{cl1}^T \\ C_{cl2}^T \end{bmatrix}. \quad (3.65)$$

Applying the Schur complement [Boyd et al. 1994] to the above inequality, the LMI (3.107) is obtained:

$$\begin{bmatrix} P_1 & 0 & P_1 C_{cl1}^T \\ 0 & P_2 & C_{cl2}^T \\ C_{cl1} P_1 & C_{cl2} & \mathcal{Z} \end{bmatrix} > 0. \quad (3.66)$$

Meanwhile, the elements of (3.44) can be expressed as:

$$\mathcal{X} A_{cl(\rho)} + A_{cl(\rho)}^T \mathcal{X} = \begin{bmatrix} \Omega_{11} & \Omega_{12} \\ \Omega_{21} & \Omega_{22} \end{bmatrix}, \quad (3.67)$$

$$\mathcal{X} B_{cl(\rho)} \bar{V} = \begin{bmatrix} P_1^{-1} \bar{H}_{(\rho)} \bar{V} \\ P_2 \bar{H}_{a(\rho)} \bar{V} + Q_{2(\rho)} \bar{D}_Q \bar{V} \end{bmatrix} = \begin{bmatrix} \Omega_{13} \\ \Omega_{23} \end{bmatrix}, \quad (3.68)$$

where

$$Q_{2(\rho)} = -P_2 \bar{L}_{a(\rho)}, \quad (3.69)$$

$$\Omega_{11} = \underbrace{\mathcal{H}\{P_1^{-1} A_{(\rho)} - P_1^{-1} B K_{(\rho)}\}}_{\Omega_{111}} + \underbrace{N_{(\rho)}^T \Delta_a^T M_{(\rho)}^T P_1^{-1} + P_1^{-1} M_{(\rho)} \Delta_a N_{(\rho)}}_{\Omega_{112}} \quad (3.70)$$

$$\Omega_{12} = \underbrace{P_1^{-1} [B K_{(\rho)} \quad B] T_e}_{\Omega_{121}} + \underbrace{N_{ac(\rho)}^T \Delta_{ac}^T M_{ac(\rho)}^T P_2 + G^T \Delta_c^T F^T D_Q^T Q_{2(\rho)}^T}_{\Omega_{122}} \quad (3.71)$$

$$\Omega_{21} = \Omega_{12}^T = \Omega_{121}^T + \Omega_{122}^T, \quad (3.72)$$

$$\Omega_{22} = \mathcal{H}\{P_2 \bar{A}_{a(\rho)} + Q_{2(\rho)} \bar{C}_a\}, \quad (3.73)$$

so the left-hand of (3.44) is rewritten as:

$$\Omega = \begin{bmatrix} \Omega_{11} & \Omega_{12} & \Omega_{13} \\ (*) & \Omega_{22} & \Omega_{23} \\ (*) & (*) & -I \end{bmatrix} = \begin{bmatrix} \Omega_{111} & \Omega_{121} & \Omega_{13} \\ (*) & \Omega_{22} & \Omega_{23} \\ (*) & (*) & -I \end{bmatrix} + \begin{bmatrix} \Omega_{112} & \Omega_{122} & 0 \\ (*) & 0 & 0 \\ (*) & (*) & 0 \end{bmatrix} \quad (3.74)$$

$$\begin{aligned} \Omega &= \begin{bmatrix} \Omega_{111} & \Omega_{121} & \Omega_{13} \\ (*) & \Omega_{22} & \Omega_{23} \\ (*) & (*) & -I \end{bmatrix} \\ &+ \begin{bmatrix} N_{(\rho)}^T & N_{ac(\rho)}^T & G^T \\ 0 & 0 & 0 \\ 0 & 0 & 0 \end{bmatrix} \begin{bmatrix} \Delta_a^T & 0 & 0 \\ 0 & \Delta_{ac}^T & 0 \\ 0 & 0 & \Delta_c^T \end{bmatrix} \begin{bmatrix} M_{(\rho)}^T P_1^{-1} & 0 & 0 \\ 0 & M_{ac(\rho)}^T P_2 & 0 \\ 0 & F^T D_Q^T Q_{2(\rho)}^T & 0 \end{bmatrix} \\ &+ \begin{bmatrix} M_{(\rho)}^T P_1^{-1} & 0 & 0 \\ 0 & M_{ac(\rho)}^T P_2 & 0 \\ 0 & F^T D_Q^T Q_{2(\rho)}^T & 0 \end{bmatrix}^T \begin{bmatrix} \Delta_a^T & 0 & 0 \\ 0 & \Delta_{ac}^T & 0 \\ 0 & 0 & \Delta_c^T \end{bmatrix}^T \begin{bmatrix} N_{(\rho)}^T & N_{ac(\rho)}^T & G^T \\ 0 & 0 & 0 \\ 0 & 0 & 0 \end{bmatrix}^T. \quad (3.75) \end{aligned}$$

Applying the *Lemma 1* to Ω , it yields that:

$$\Omega \leq \begin{bmatrix} \Omega'_{11} & \Omega_{121} & \Omega_{13} \\ (*) & \Omega'_{22} & \Omega_{23} \\ (*) & (*) & -I \end{bmatrix}, \quad (3.76)$$

where

$$\Omega'_{11} = \Omega_{111} + \sigma_1^{-1} N_{ac(\rho)}^T N_{ac(\rho)} + \sigma_2^{-1} G^T G + \sigma_3 P_1^{-1} M_{(\rho)} M_{(\rho)}^T P_1^{-1} + \sigma_3^{-1} N_{(\rho)}^T N_{(\rho)}, \quad (3.77)$$

$$\Omega'_{22} = \Omega_{22} + \sigma_1 P_2 M_{ac(\rho)} M_{ac(\rho)}^T P_2 + \sigma_2 Q_{2(\rho)} D_Q F F^T D_Q^T Q_{2(\rho)}^T. \quad (3.78)$$

The property $\Omega < 0$, i.e. condition (3.44), holds if:

$$\begin{bmatrix} \Omega'_{11} & \Omega_{121} & \Omega_{13} \\ (*) & \Omega'_{22} & \Omega_{23} \\ (*) & (*) & -I \end{bmatrix} < 0. \quad (3.79)$$

Pre & Post-multiplying the above inequality by $\begin{bmatrix} P_1 & 0 & 0 \\ 0 & I & 0 \\ 0 & 0 & I \end{bmatrix}$, then (3.79) becomes:

$$\Omega' = \begin{bmatrix} \Omega''_{11} & \Omega'_{12} & \Omega'_{13} \\ (*) & \Omega'_{22} & \Omega_{23} \\ (*) & (*) & -I \end{bmatrix} < 0, \quad (3.80)$$

where

$$Q_{1(\rho)} = -K_{(\rho)} P_1, \quad (3.81)$$

$$\begin{aligned} \Omega''_{11} = & \mathcal{H}\{A_{(\rho)} P_1 + B Q_{1(\rho)}\} + \sigma_1^{-1} P_1 N_{ac(\rho)}^T N_{ac(\rho)} P_1 + \sigma_2^{-1} P_1 G^T G P_1 \\ & + \sigma_3 M_{(\rho)} M_{(\rho)}^T + \sigma_3^{-1} P_1 N_{(\rho)}^T N_{(\rho)} P_1, \end{aligned} \quad (3.82)$$

$$\Omega'_{12} = [BK_{(\rho)} \quad B] T_e, \quad (3.83)$$

$$\Omega'_{13} = \bar{H}_{(\rho)} \bar{V}. \quad (3.84)$$

The matrix Ω' in (3.80) can be decomposed as:

$$\Omega' = \begin{bmatrix} \Omega''_{11} & 0 & \Omega'_{13} \\ (*) & \Omega'_{22} & \Omega_{23} \\ (*) & (*) & -I \end{bmatrix} + \underbrace{\begin{bmatrix} [BK_{(\rho)} \quad B] \\ 0 \\ 0 \end{bmatrix} [0 \quad T_e \quad 0] + \begin{bmatrix} 0 \\ T_e^T \\ 0 \end{bmatrix} [[BK_{(\rho)} \quad B]^T \quad 0 \quad 0]}_{\Gamma}, \quad (3.85)$$

with $T_e \in \mathbb{R}^{(n_x+n_u) \times n_{\bar{x}_a}}$ and $[BK_{(\rho)} \quad B] \in \mathbb{R}^{n_x \times (n_x+n_u)}$.

Implementing *Lemma 2* to Γ in (3.85):

$$\Gamma \leq \sigma_4 \begin{bmatrix} [BK_{(\rho)} & B] \\ 0 \\ 0 \end{bmatrix} \begin{bmatrix} P_1 & 0 \\ 0 & I_{n_u} \end{bmatrix} \begin{bmatrix} [K_{(\rho)}^T B^T] & 0 & 0 \end{bmatrix} + \sigma_4^{-1} \begin{bmatrix} 0 \\ T_e^T \\ 0 \end{bmatrix} \begin{bmatrix} P_1 & 0 \\ 0 & I_{n_u} \end{bmatrix}^{-1} \begin{bmatrix} 0 & T_e & 0 \end{bmatrix}, \quad (3.86)$$

$$\Gamma \leq \sigma_4 \begin{bmatrix} [BK_{(\rho)} & B] \\ 0 \\ 0 \end{bmatrix} \begin{bmatrix} P_1 & 0 \\ 0 & I_{n_u} \end{bmatrix} \begin{bmatrix} P_1 & 0 \\ 0 & I_{n_u} \end{bmatrix}^{-1} \begin{bmatrix} P_1 & 0 \\ 0 & I_{n_u} \end{bmatrix} \begin{bmatrix} [K_{(\rho)}^T B^T] & 0 & 0 \end{bmatrix} \\ + \sigma_4^{-1} \begin{bmatrix} 0 \\ T_e^T \\ 0 \end{bmatrix} \begin{bmatrix} P_1 & 0 \\ 0 & I_{n_u} \end{bmatrix}^{-1} \begin{bmatrix} 0 & T_e & 0 \end{bmatrix}, \quad (3.87)$$

$$\leq \begin{bmatrix} -BQ_{1(\rho)} & B & 0 \\ 0 & 0 & T_e^T \\ 0 & 0 & 0 \end{bmatrix} \left[\begin{array}{cc|c} \sigma_4 P_1^{-1} & 0 & 0 \\ 0 & \sigma_4 I_{n_u} & 0 \\ \hline 0 & 0 & \sigma_4^{-1} \begin{bmatrix} P_1^{-1} & 0 \\ 0 & I_{n_u} \end{bmatrix} \end{array} \right] \begin{bmatrix} -Q_{1(\rho)}^T B^T & 0 & 0 \\ B^T & 0 & 0 \\ 0 & T_e & 0 \end{bmatrix}. \quad (3.88)$$

From (3.85), it yields that:

$$\Omega' \leq \begin{bmatrix} \Omega''_{11} & 0 & \Omega'_{13} \\ (*) & \Omega'_{22} & \Omega_{23} \\ (*) & (*) & -I \end{bmatrix} + \\ \begin{bmatrix} -BQ_{1(\rho)} & B & 0 \\ 0 & 0 & T_e^T \\ 0 & 0 & 0 \end{bmatrix} \begin{bmatrix} \sigma_4 P_1^{-1} & 0 & 0 \\ 0 & \sigma_4 I_{n_u} & 0 \\ 0 & 0 & \sigma_4^{-1} \begin{bmatrix} P_1^{-1} & 0 \\ 0 & I_{n_u} \end{bmatrix} \end{bmatrix} \begin{bmatrix} -Q_{1(\rho)}^T B^T & 0 & 0 \\ B^T & 0 & 0 \\ 0 & T_e & 0 \end{bmatrix}. \quad (3.89)$$

$\Omega < 0$ holds if the right-hand side of (3.89) < 0 , then by applying the Schur complement [Boyd et al. 1994], the following inequality is obtained:

$$\left[\begin{array}{c|c} \begin{bmatrix} \Omega''_{11} & 0 & \Omega'_{13} \\ (*) & \Omega'_{22} & \Omega_{23} \\ (*) & (*) & -I \end{bmatrix} & \begin{bmatrix} -BQ_{1(\rho)} & B & 0 \\ 0 & 0 & T_e^T \\ 0 & 0 & 0 \end{bmatrix} \\ \hline (*) & \begin{bmatrix} -\sigma_4^{-1} P_1 & 0 & 0 \\ 0 & -\sigma_4^{-1} I_{n_u} & 0 \\ 0 & 0 & \sigma_4 \begin{bmatrix} -P_1 & 0 \\ 0 & -I_{n_u} \end{bmatrix} \end{bmatrix} \end{array} \right] < 0. \quad (3.90)$$

Using Schur complement [Boyd et al. 1994] on elements Ω''_{11} and Ω'_{22} , it follows that:

$$\underbrace{\begin{bmatrix} \Gamma_{1,1(\rho)} & 0 & \bar{H}_{(\rho)} \bar{V} \\ (*) & \Gamma_{2,2(\rho)} & \Gamma_{2,3(\rho)} \\ (*) & (*) & -I \end{bmatrix}}_{\Gamma_{(\rho)}} \left| \begin{array}{c} \Theta_{1(\rho)} \\ \hline \Theta_2 \end{array} \right. < 0, \quad (3.91)$$

where

$$\Gamma_{1,1(\rho)} = \mathcal{H}\{A_{(\rho)}P_1 + BQ_{1(\rho)}\}, \quad \Gamma_{2,2(\rho)} = \mathcal{H}\{P_2\bar{A}_{a(\rho)} + Q_{2(\rho)}\bar{C}_a\}, \quad (3.92)$$

$$\Gamma_{2,3(\rho)} = P_2\bar{H}_{a(\rho)}\bar{V} + Q_{2(\rho)}\bar{D}_Q\bar{V}, \quad \Gamma_0 = \sigma_4 \begin{bmatrix} P_1 & 0 \\ 0 & I_{n_u} \end{bmatrix}, \quad (3.93)$$

$$\Theta_{1(\rho)} = \begin{bmatrix} -BQ_{1(\rho)} & B & P_1N_{ac(\rho)}^T & P_1G^T & P_1N_{(\rho)}^T & 0 & 0 & M_{(\rho)} & 0 \\ 0 & 0 & 0 & 0 & 0 & P_2M_{ac(\rho)} & Q_{2(\rho)}D_QF & 0 & T_e^T \\ 0 & 0 & 0 & 0 & 0 & 0 & 0 & 0 & 0 \end{bmatrix}, \quad (3.94)$$

$$\Theta_2 = -diag\{\sigma_4^{-1}P_1, \sigma_4^{-1}I, \sigma_1I, \sigma_2I, \sigma_3I, \sigma_1^{-1}I, \sigma_2^{-1}I, \sigma_3^{-1}I, \Gamma_0\}. \quad (3.95)$$

In the polytopic representation:

- Distribution matrices: $A_{(\rho)} = \sum_{i=1}^{\bar{N}} \theta_{i(\rho)} A_{(i)}$, $E_{(\rho)} = \sum_{i=1}^{\bar{N}} \theta_{i(\rho)} E_{(i)}$,
 $H_{(\rho)} = \sum_{i=1}^{\bar{N}} \theta_{i(\rho)} H_{(i)}$, $M_{(\rho)} = \sum_{i=1}^{\bar{N}} \theta_{i(\rho)} M_{(i)}$, and $N_{(\rho)} = \sum_{i=1}^{\bar{N}} \theta_{i(\rho)} N_{(i)}$.
- Gains of observer-controller: $K_{(\rho)} = \sum_{i=1}^{\bar{N}} \theta_{i(\rho)} K_{(i)}$, $\bar{L}_{a(\rho)} = \sum_{i=1}^{\bar{N}} \theta_{i(\rho)} \bar{L}_{a(i)}$, which leads
to: $Q_{1(\rho)} = \sum_{i=1}^{\bar{N}} \theta_{i(\rho)} Q_{1(i)}$ and $Q_{2(\rho)} = \sum_{i=1}^{\bar{N}} \theta_{i(\rho)} Q_{2(i)}$.

As a result,

$$\Gamma_{(\rho)} = \sum_{i=1}^{\bar{N}} \theta_{i(\rho)} \Gamma_{(i)} < 0, \quad (3.96)$$

where

$$\Gamma_{(i)} = \left[\begin{array}{ccc|c} \Gamma_{1,1(i)} & 0 & \bar{H}_{(i)}\bar{V} & \Theta_{1(i)} \\ (*) & \Gamma_{2,2(i)} & \Gamma_{2,3(i)} & \\ (*) & (*) & -I & \\ \hline & (*) & & \Theta_2 \end{array} \right]. \quad (3.97)$$

That yields the sufficient condition: $\Gamma_{(i)} < 0$, which completes the proof. \blacksquare

In summary, the scheme of robust-stochastic integrated design for matched UI is illustrated in Fig. 3.4. In which, ρ_2 defines the frequency-shaping filter, while the vector $\rho = [\rho_1^T \ \rho_2^T]$ decides the operating modes of both observer and controller whose gains are computed by solving Theorem 3.3.2.

3.4 Robust-stochastic integrated design for Unmatched UI

In this Section, the robust-stochastic integrated design for unmatched UI is developed. In fact, its observer is PMI with no integration of output frequency-shaping filter; thus, the parameter-varying vector ρ is reduced to ρ_1 , i.e. $\rho = \rho_1$ with m elements ρ_i ($i = 1 : m$). Meanwhile, the controller is kept unchanged as a state-feedback fault compensator. Consequently, only the modifications to the observer and integrated design are presented.

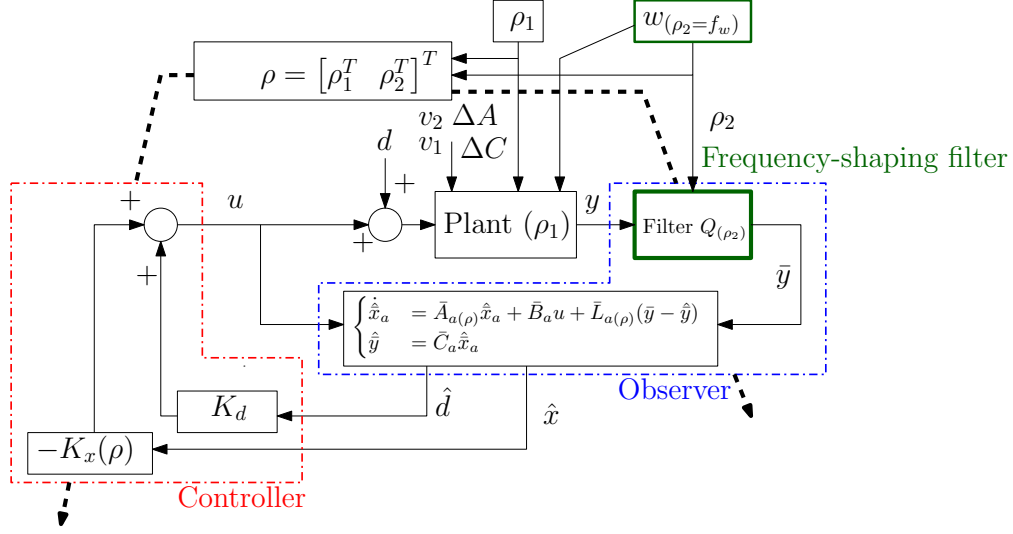


Figure 3.4: Robust-stochastic integrated design for matched UI

3.4.1 Observer Design for Unmatched UI

The robust PMI LPV observer for uncertain stochastic system (3.15) is designed as:

$$\begin{cases} \dot{\hat{x}}_a &= A_{a(\rho)}\hat{x}_a + B_a u + L_{a(\rho)}(y - \hat{y}) \\ \hat{y} &= C_a \hat{x}_a \end{cases}, \quad (3.98)$$

where \hat{x}_a (or \hat{y}) is the estimated of x_a (or y), $\hat{x}_a = [\hat{x}^T \quad \hat{d}^T \quad \hat{d}^{(1)T} \quad \dots \quad \hat{d}^{(s-1)T} \quad \hat{d}^{(s)T}]^T$, and L_a is the observer gain.

The existing condition for this observer is the same as (3.29), while the objectives (O.1)-(O.2) for the integrated design can be re-expressed as follows:

(O.1) For $w = 0$, the noise \bar{v} cancellation is achieved through the minimization of $J_e = \mathbb{E}\{e^T e\}$.

(O.2) For $\bar{v} = 0$, the impact of UI w on estimation error e is minimized by \mathcal{H}_∞ synthesis (induced- \mathcal{L}_2 norm).

The variable $e_{x_a} = x_a - \hat{x}_a$ is chosen as estimation error whose dynamics is described as follows:

$$\dot{e}_{x_a} = (A_{a(\rho)} - L_{a(\rho)}C_a)e_{x_a} + E_{a(\rho)}w + (\Delta A_{a(\rho)} - L_{a(\rho)}\Delta C_a)x_a + (\hat{H}_{a(\rho)} - L_{a(\rho)}\hat{I})\bar{v}, \quad (3.99)$$

where $\hat{H}_{a(\rho)} = [H_{a(\rho_1)} \quad 0]$ and $\hat{I} = \begin{bmatrix} 0_{n_y \times n_{v_1}} & I_{n_y} \end{bmatrix}$

Consider the following transformation:

$$(\Delta A_{a(\rho)} - L_{a(\rho)} \Delta C_a) x_a = \left(\left[\begin{array}{c|c} \Delta A_{(\rho_1)} & 0 \\ \hline 0 & 0 \end{array} \right] - L_{a(\rho)} \left[\begin{array}{c|c} \Delta C & 0 \end{array} \right] \right) \begin{bmatrix} x \\ d \\ \dots \\ d^{(s)} \end{bmatrix} \quad (3.100)$$

$$= (M_{a(\rho)} \Delta_a N_{(\rho)} - L_{a(\rho)} \Delta C) x. \quad (3.101)$$

where $M_{a(\rho)} = \begin{bmatrix} M_{(\rho_1)} \\ 0 \end{bmatrix}$ and $N_{(\rho)} = N_{(\rho_1)}$.

Then, the dynamics of observer (3.30) can be rewritten as:

$$\dot{e}_{x_a} = (A_{a(\rho)} - L_{a(\rho)} C_a) e_{x_a} + E_{a(\rho)} w + (M_{a(\rho)} \Delta_{ac} N_{(\rho)} - L_{a(\rho)} D_Q \Delta C) x + (\hat{H}_{a(\rho)} - L_{a(\rho)} \hat{I}) \bar{v}. \quad (3.102)$$

Eq.(3.102) shows that dynamics of estimation error for unmatched UI displays the same behavior as that for matched UI, in which the intervention of state x in the uncertainty term is of critical importance to observer stability.

3.4.2 Observer-Controller synthesis for Unmatched UI

Since the controller is kept unchanged, i.e the controller (3.36) is applied, the dynamics of the observer and controller for unmatched UI also affect each other through the uncertainty terms. Hence, the usage of closed-loop synthesis is necessary to obtain the robust-stochastic integrated design.

From (3.102) and (3.39), the closed-loop system can be displayed as:

$$\begin{bmatrix} \dot{x} \\ \dot{e}_{x_a} \end{bmatrix} = \begin{bmatrix} A_{(\rho)} + \Delta A_{(\rho)} - BK_{(\rho)} & [BK_{(\rho)} \ B] \hat{T}_e \\ M_{a(\rho)} \Delta_a N_{(\rho)} - L_{a(\rho)} \Delta C & A_{a(\rho)} - L_{a(\rho)} C_a \end{bmatrix} \begin{bmatrix} x \\ e_{x_a} \end{bmatrix} + \begin{bmatrix} \bar{H}(\rho) \\ \hat{H}_{a(\rho)} - L_{a(\rho)} \hat{I} \end{bmatrix} \bar{v} + \begin{bmatrix} E_{(\rho)} \\ E_{a(\rho)} \end{bmatrix} w, \quad (3.103)$$

where $e = \begin{bmatrix} e_x \\ e_d \end{bmatrix} = \begin{bmatrix} I_{n_x} & 0 & 0 \dots 0 \\ 0 & I_{n_u} & 0 \dots 0 \end{bmatrix} \begin{bmatrix} e_x \\ e_d \\ e_d^{(1)} \\ \dots \\ e_d^{(s)} \end{bmatrix} = \hat{T}_e e_{x_a}$. In other words,

$$\begin{cases} \dot{\hat{x}}_{cl} &= \hat{A}_{cl(\rho)} \hat{x}_{cl} + \hat{B}_{cl(\rho)} \bar{v} + \hat{E}_{cl(\rho)} w, \\ e &= \hat{C}_{cl} \hat{x}_{cl} \end{cases}, \quad (3.104)$$

where

- $\hat{x}_{cl} = [x^T \ e_{x_a}^T]^T$ is the closed-loop state vector,

$$\hat{A}_{cl(\rho)} = \left[\begin{array}{c|c} A_{(\rho)} + \Delta A_{(\rho)} - BK_{(\rho)} & [BK_{(\rho)} \ B] \hat{T}_e \\ \hline M_{a(\rho)} \Delta_a N_{(\rho)} - L_{a(\rho)} \Delta C & A_{a(\rho)} - L_{a(\rho)} C_a \end{array} \right], \hat{B}_{cl(\rho)} = \begin{bmatrix} \bar{H}_{(\rho)} \\ \hat{H}_{a(\rho)} - L_{a(\rho)} \hat{I} \end{bmatrix}, \hat{E}_{cl(\rho)} = \begin{bmatrix} E_{(\rho)} \\ E_{a(\rho)} \end{bmatrix},$$
 and $e = \hat{C}_{cl} \hat{x}_{cl} = \begin{bmatrix} 0 & \hat{T}_e \end{bmatrix} \hat{x}_{cl}$.
- $\mathbb{E}\{\bar{v}(t_1)\bar{v}^T(t_2)\} = \mathbb{E}\left\{ \begin{bmatrix} v_1(t_1) \\ v_2(t_1) \end{bmatrix} \begin{bmatrix} v_1^T(t_2) & v_2^T(t_2) \end{bmatrix} \right\} = \begin{bmatrix} V_1 & 0 \\ 0 & V_2 \end{bmatrix} \delta(t_1 - t_2),$
- $\mathbb{E}\{x_{cl}(0)\} = \hat{x}_{cl0},$
- $\mathbb{E}\{(x_{cl}(0) - \hat{x}_{cl0})(x_{cl}(0) - \hat{x}_{cl0})^T\} = \hat{P}_0 > 0.$
- Observer-controller gains $L_{a(\rho)}$ and $K_{(\rho)}$ for unmatched UI are synthesized by the following Theorem.

Theorem 3.4.1

With given positive scalars $\sigma_1, \sigma_2, \sigma_3,$ and $\sigma_4,$ the objectives for the unmatched-UI design can be accomplished by finding symmetric positive definite matrices $P_1 > \hat{P}_{01}$ and $P_2 < \hat{P}_{02}^{-1},$ matrices $Q_{1(i)}$ and $Q_{2(i)},$ and a symmetric matrix $Z > 0$ which minimize $Tr(\mathcal{Z})$ and γ_∞ such that:

$$\left[\begin{array}{ccc|c|c} \Gamma_{1,1(i)} & 0 & E_{(i)} & \Theta_{1(i)} & \begin{bmatrix} \hat{C}_{cl1}^T \\ \hat{C}_{cl2}^T \\ 0 \end{bmatrix} \\ (*) & \Gamma_{2,2(i)} & P_2 E_{a(i)} & & \\ (*) & (*) & -\gamma_\infty^2 I & & \\ \hline & (*) & & \Theta_2 & 0 \\ & (*) & & (*) & -I \end{array} \right] < 0 \quad \forall i = 1 : N, \quad (3.105)$$

$$\left[\begin{array}{ccc|c} \Gamma_{1,1(i)} & 0 & \bar{H}_{(i)} \bar{V} & \Theta_{1(i)} \\ (*) & \Gamma_{2,2(i)} & \Gamma_{2,3(i)} & \\ (*) & (*) & -I & \\ \hline & (*) & & \Theta_2 \end{array} \right] < 0 \quad \forall i = 1 : N, \quad (3.106)$$

$$\begin{bmatrix} P_1 & 0 & P_1 \hat{C}_{cl1}^T \\ 0 & P_2 & \hat{C}_{cl2}^T \\ \hat{C}_{cl1} P_1 & \hat{C}_{cl2} & Z \end{bmatrix} > 0, \quad (3.107)$$

where

$$\Gamma_{1,1(i)} = \mathcal{H}\{A_{(i)} P_1 + B Q_{1(i)}\}, \quad \Gamma_{2,2(i)} = \mathcal{H}\{P_2 A_{a(i)} + Q_{2(i)} C_a\}, \quad (3.108)$$

$$\Gamma_{2,3(i)} = P_2 \hat{H}_{a(i)} \bar{V} + Q_{2(i)} \hat{I} \bar{V}, \quad \hat{C}_{cl} = \begin{bmatrix} \hat{C}_{cl1} & \hat{C}_{cl2} \end{bmatrix}, \quad (3.109)$$

$$\Gamma_0 = \sigma_4 \begin{bmatrix} P_1 & 0 \\ 0 & I_{n_u} \end{bmatrix}, \quad \hat{P}_0 = \begin{bmatrix} \hat{P}_{01} & 0 \\ 0 & \hat{P}_{02} \end{bmatrix} > 0 \quad (3.110)$$

$$\Theta_{1(i)} = \begin{bmatrix} -BQ_{1(i)} & B & P_1N_{(i)}^T & P_1G^T & P_1N_{(i)}^T & 0 & 0 & M_{(i)} & 0 \\ 0 & 0 & 0 & 0 & 0 & P_2M_{a(i)} & Q_{2(i)}F & 0 & \hat{T}_e^T \\ 0 & 0 & 0 & 0 & 0 & 0 & 0 & 0 & 0 \end{bmatrix}, \quad (3.111)$$

$$\Theta_2 = -diag\{\sigma_4^{-1}P_1, \sigma_4^{-1}I, \sigma_1I, \sigma_2I, \sigma_3I, \sigma_1^{-1}I, \sigma_2^{-1}I, \sigma_3^{-1}I, \Gamma_0\}, \quad (3.112)$$

then the gains of observer-controller synthesis are simultaneously calculated by:

$$K_{(\rho)} = \sum_{i=1}^N \theta_{i(\rho)} K_{(i)} = - \sum_{i=1}^N \theta_{i(\rho)} Q_{1(i)} P_1^{-1}, \quad L_{a(\rho)} = \sum_{i=1}^N \theta_{i(\rho)} L_{a(i)} = - \sum_{i=1}^N \theta_{i(\rho)} P_2^{-1} Q_{2(i)}. \quad (3.113)$$

Proof: The proof can be easily derived from Lemma of \mathcal{H}_∞ performance in Section 1.5.2, Theorem 3.3.1, and the proof of Theorem 3.3.2. ■

In brief, the scheme of robust-stochastic integrated design for unmatched UI is demonstrated in Fig. 3.5. In which, $\rho = \rho_1$ decides the operating modes of both observer and controller whose gains are obtained from the solution of Theorem 3.4.1.

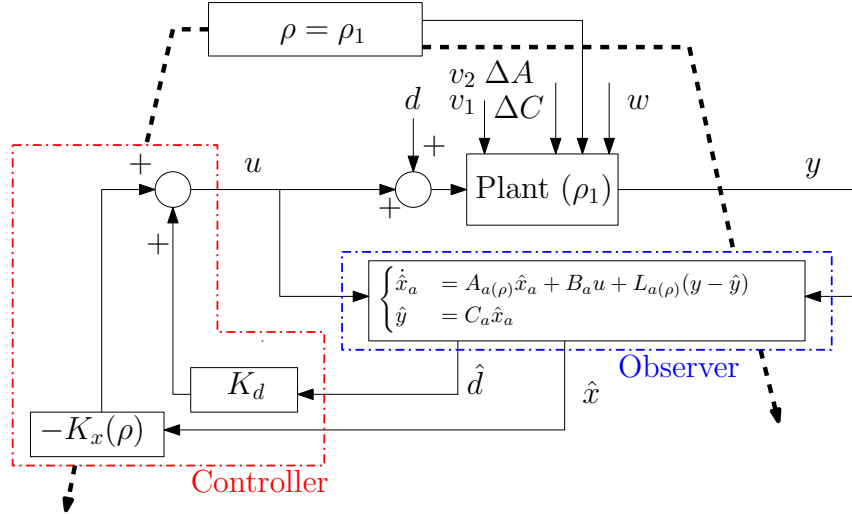


Figure 3.5: Robust-stochastic integrated design for unmatched UI

3.4.3 Discussion on Theorem 3.4.1

Compared with Theorem 3.3.2 for the matched UI, Theorem 3.4.1 for the unmatched UI requires the simultaneous optimization for both $Tr(Z)$ and the \mathcal{H}_∞ indicator γ_∞ . This is a non-convex problem whose solution is a compromise between noise cancellation and the UI attenuation objectives. In some circumstances, the smaller γ_∞ , i.e. UI better attenuation, the bigger $Tr(Z)$, i.e. the worse noise cancellation. That issue may require a lot of efforts to

determine a good combination of observer-controller designs. In addition, there might be no feasible solution to this multi-objective optimization.

On the other hand, it should be noted that if $V_1 = I$, $V_2 = I$, and there exists a scalar $\gamma_2 > 0$ such that $Tr(Z) < \gamma_2^2$, this special case of Theorem 3.4.1 becomes the common mixed $\mathcal{H}_\infty/\mathcal{H}_2$ norm through the minimization of both γ_2 and γ_∞ .

3.5 Anti-windup solution

In the industrial controlled system, actuator capacity is always saturated by the physical constraints and conditions; therefore, the input u_s calculated from the controller is likely to be different from the actual system input u . Such case is often known as "controller windup", which causes the overshoot and degradation in performance, or even system instability [Åström and Wittenmark 2013; Bernstein and Michel 1995]. To avoid this problem, one common solution is the anti-windup LPV control approach [Wu, Grigoriadis, and Packard 2000] to symmetric saturation constraint, which has recently been advanced in [Fleps-Dezasse et al. 2018] to tackle the non-symmetric problems. More details on how to integrate this procedure into the synthesis of observer-based fault compensators are presented below.

3.5.1 LPV-Saturation problem

To rewrite the actuator saturation problem in LPV formulation, suppose $u_s = [u_{s1} \ u_{s2} \ \dots \ u_{sn_u}]$ is calculated input and $u = [u_1 \ u_2 \ \dots \ u_{n_u}]$ is applied input such that $u_{j,min} \leq u_j \leq u_{j,max}$ ($j = 1 : n_u$), while the saturation $u_{j,min} < 0$ and $u_{j,max} > 0$ are not affected by the degradation d . The relation between these two inputs can be displayed by the saturation constraints as following:

$$u_j = sat(u_{s,j}) = \begin{cases} u_{j,min} & , \text{ if } u_{s,j} < u_{j,min}. \\ u_{s,j} & , \text{ if } u_{j,min} \leq u_{s,j} \leq u_{j,max}. \\ u_{j,max} & , \text{ if } u_{s,j} > u_{j,max}. \end{cases} \quad (3.114)$$

Assume that the actuator constraints are decoupled, i.e. the control signal of one actuator has no effect on the saturation of other actuators. The saturation indicator of the j^{th} actuator, which is assumed to continuously evolve over time, is defined as [Fleps-Dezasse et al. 2018]:

$$\rho_{3j} = \begin{cases} \frac{sat(u_{s,j})}{u_{s,j}} & , \text{ if } u_{s,j} \neq 0. \\ 1 & , \text{ if } u_{s,j} = 0. \end{cases} \quad (3.115)$$

Obviously, $\rho_{3j} \in [\rho_{3j}, \overline{\rho_{3j}}] = [\rho_{3j}, 1]$, where $1 > \rho_{3j} > 0$. When $\rho_{3j} = 1$, the control signal u_s can be realized by actuator, i.e. unconstrained system, whereas $\rho_{3j} = \underline{\rho_{3j}}$ expresses the degree of saturation, i.e. the delay in the activation of the anti-windup mechanism.

The saturation matrix $\Theta = \text{diag}\{\rho_3\}$ displays all the saturation indicators, where $\rho_3 = [\rho_{31} \ \rho_{32} \ \dots \ \rho_{3n_u}]^T$ allows the actuator saturation to be expressed as:

$$u = \text{sat}(u_s) = \Theta u_s. \quad (3.116)$$

Then, the faulty LPV system (3.15) is displayed as:

$$\begin{cases} \dot{x}_a &= (A_{a(\rho_1)} + \Delta A_{a(\rho_1)})x_a + B_{a(\rho_3)}u_s + E_{a(\rho_1)}w + H_{a(\rho_1)}v_1, \\ y &= (C_a + \Delta C_a)x_a + v_2 \end{cases}, \quad (3.117)$$

where $B_{a(\rho_3)} = B_a \Theta$.

Obviously, due to the usage of the scheduling parameter ρ_3 , the controlled u_s has taken into account the anti-windup problem for the system (3.7).

In the next sections, the observer-controller integrated design with an anti-windup controller for matched UI will be developed to handle the actuator saturation.

Remark 3.5.1

The anti-windup solution for the unmatched UI can be derived easily from Theorem 3.4.1 and anti-windup solution for the matched UI, so it is omitted and only the design for the matched UI will be presented in the next section.

3.5.2 Observer design with input saturation for matched UI

In this section, the PMI observer incorporating the frequency-shaping filter will be adapted to the saturation of the actuator.

By substituting (3.116) with the input u and considering the new varying-parameter vector $\rho^* = [\rho_1^T \ \rho_2^T \ \rho_3^T]^T \in \mathbb{R}^{k+n_u}$, the faulty LPV system (3.117) is displayed as:

$$\begin{cases} \dot{x}_a &= (A_{a(\rho^*)} + \Delta A_{a(\rho^*)})x_a + B_{a(\rho^*)}u_s + E_{a(\rho^*)}w + H_{a(\rho^*)}v_1, \\ y &= (C_a + \Delta C_a)x_a + v_2 \end{cases}, \quad (3.118)$$

In which, $A_{a(\rho^*)} = A_{a(\rho_1)}$, $\Delta A_{a(\rho^*)} = \Delta A_{a(\rho_1)}$, $B_{a(\rho^*)} = B_{a(\rho_3)}$, $E_{a(\rho^*)} = E_{a(\rho_1)}$, $H_{a(\rho^*)} = H_{a(\rho_1)}$, and ρ^* generates the convex set \mathcal{P}_ϕ with the coefficients of the polytopic decomposition $\phi_{(\rho^*)}$ defined as below:

$$\mathcal{P}_\phi = \left\{ \phi_{(\rho^*)} = \left[\phi_{1(\rho^*)} \ \phi_{2(\rho^*)} \ \dots \ \phi_{\hat{N}(\rho^*)} \right]^T \mid \phi_{i(\rho^*)} = \frac{\prod_{j=1}^{k+n_u} |\rho_j^* - \mathcal{C}_{(\omega_i)j}^\phi|}{\prod_{j=1}^{k+n_u} (\bar{\rho}_j^* - \underline{\rho}_j^*)} \geq 0, \sum_{i=1}^{\hat{N}=2^{k+n_u}} \phi_{i(\rho^*)} = 1 \right\}, \quad (3.119)$$

$$\mathcal{C}_{(\omega_i)j}^\phi = \{ \rho_j^* \mid \rho_j^* = \bar{\rho}_j^* \text{ if } (\omega_i)_j = \underline{\rho}_j^* \text{ or } \rho_j^* = \underline{\rho}_j^* \text{ otherwise} \}. \quad (3.120)$$

By implementing the frequency-shaping filter (3.22), a new system is derived from (3.118)

:

$$\begin{cases} \dot{\hat{x}}_a &= (\bar{A}_{a(\rho^*)} + \Delta\bar{A}_{a(\rho^*)})\hat{x}_a + \bar{B}_{a(\rho^*)}u_s + \bar{E}_{a(\rho^*)}w + \bar{H}_{a(\rho^*)}\bar{v} \\ \hat{y} &= (\bar{C}_a + \Delta\bar{C}_a)\hat{x}_a + D_Qv_2 \end{cases}. \quad (3.121)$$

In which, $\bar{A}_{a(\rho^*)} = \bar{A}_{a(\rho)}$, $\bar{B}_{a(\rho^*)} = \begin{bmatrix} B_{a(\rho^*)} \\ 0 \end{bmatrix} = \bar{B}_a\Theta$, $\bar{E}_{a(\rho^*)} = \bar{E}_{a(\rho)}$, $\bar{H}_{a(\rho^*)} = \bar{H}_{a(\rho)}$, and $\Delta\bar{A}_{a(\rho^*)} = \Delta\bar{A}_{a(\rho)}$.

The robust PMI LPV observer for uncertain stochastic system (3.121) is designed as:

$$\begin{cases} \dot{\hat{x}}_a &= \bar{A}_{a(\rho^*)}\hat{x}_a + \bar{B}_{a(\rho^*)}u_s + \bar{L}_{a(\rho^*)}(\bar{y} - \hat{y}) \\ \hat{y} &= \bar{C}_a\hat{x}_a \end{cases}. \quad (3.122)$$

In other words,

$$\begin{cases} \dot{\hat{x}}_a &= \bar{A}_{a(\rho)}\hat{x}_a + \bar{B}_a\Theta u_s + \bar{L}_{a(\rho^*)}(\bar{y} - \hat{y}) \\ \hat{y} &= \bar{C}_a\hat{x}_a \end{cases}. \quad (3.123)$$

From (3.121) and (3.123), the dynamics of the estimation error is expressed as:

$$\begin{aligned} \dot{e}_{\bar{x}_a} &= (\bar{A}_{a(\rho^*)} - \bar{L}_{a(\rho^*)}\bar{C}_a)e_{\bar{x}_a} + \bar{E}_{a(\rho^*)}w + \bar{B}_a(u - \Theta u_s) + \\ &+ (M_{ac(\rho^*)}\Delta_{ac}N_{ac(\rho^*)} - \bar{L}_{a(\rho^*)}D_Q\Delta C)x + (\bar{H}_{a(\rho^*)} - \bar{L}_{a(\rho^*)}\bar{D}_Q)\bar{v}. \end{aligned} \quad (3.124)$$

It is noted that the convergence properties of $e_{\bar{x}_a}$ are related to the difference among u , $sat(u_s) = \Theta u_s$, the disturbance w , the state x of system, and the noise \bar{v} . If the control input constraints are always satisfied, i.e. $u = sat(u_s) = \Theta u_s$, the dynamics (3.124) becomes:

$$\begin{aligned} \dot{e}_{\bar{x}_a} &= (\bar{A}_{a(\rho^*)} - \bar{L}_{a(\rho^*)}\bar{C}_a)e_{\bar{x}_a} + \bar{E}_{a(\rho^*)}w + (M_{ac(\rho^*)}\Delta_{ac}N_{ac(\rho^*)} - \bar{L}_{a(\rho^*)}D_Q\Delta C)x \\ &+ (\bar{H}_{a(\rho^*)} - \bar{L}_{a(\rho^*)}\bar{D}_Q)\bar{v}. \end{aligned} \quad (3.125)$$

3.5.3 Anti-windup controller design for matched UI

To handle the saturation problem in the actuator, an anti-windup controller is needed. Also, the system will be assumed to be re-configurable even under the existence of actuator saturation.

To avoid the existence of a varying parameter in the input matrix, the controlled u_s is proposed as below, which is inspired from stable input filter W_u in Section 1.5.3.1 and the original strategy (3.36):

$$\begin{cases} \dot{x}_f = A_u x_f + B_u(u_c) \\ u_x = C_u x_f \\ u_s = u_x + K_{d(\rho^*)}\hat{d} \end{cases}, \quad (3.126)$$

where A_u is a Hurwitz matrix and $x_f \in \mathbb{R}^{n_f}$ and $K_{d(\rho^*)} = -(B\Theta)^\dagger B$. Also, since $\Theta \neq 0$, $(B\Theta)^\dagger$ always exists.

From (3.7) and $u = \Theta u_s$, it follows that:

$$\dot{x}_s = (A_{s(\rho^*)} + \Delta A_{s(\rho^*)})x_s + B_s u_c + D_s e_d + E_{s(\rho^*)} w + H_{s(\rho^*)} v_1, \quad (3.127)$$

where $x_s = \begin{bmatrix} x^T & x_f^T \end{bmatrix}^T$, $A_{s(\rho^*)} = \begin{bmatrix} A(\rho^*) & B\Theta C_u \\ 0 & A_u \end{bmatrix}$, $\Delta A_{s(\rho^*)} = \begin{bmatrix} \Delta A(\rho^*) & 0 \\ 0 & 0 \end{bmatrix} = M_{s(\rho^*)} \Delta_a N_{s(\rho^*)}$, $M_{s(\rho^*)} = \begin{bmatrix} M(\rho) \\ 0 \end{bmatrix}$, $N_{s(\rho^*)} = \begin{bmatrix} N(\rho) & 0 \end{bmatrix}$, $B_s = \begin{bmatrix} 0 \\ B_u \end{bmatrix}$, $D_s = \begin{bmatrix} B \\ 0 \end{bmatrix}$, $E_{s(\rho^*)} = \begin{bmatrix} E(\rho^*) \\ 0 \end{bmatrix}$, and $H_{s(\rho^*)} = \begin{bmatrix} H(\rho^*) \\ 0 \end{bmatrix}$.

The new input u_c is chosen as:

$$\begin{aligned} u_c &= -K_{x(\rho^*)} \hat{x} - K_{f(\rho^*)} x_f \\ &= -K_{x(\rho^*)} x + K_{x(\rho^*)} e_x - K_{f(\rho^*)} x_f \\ &= -K_{s(\rho^*)} x_s + K_{s(\rho^*)} \begin{bmatrix} I_{n_x} \\ 0_{n_f \times n_x} \end{bmatrix} e_x \\ &= -K_{s(\rho^*)} x_s + K_{s(\rho^*)} T_1 e_{\bar{x}_a}, \end{aligned} \quad (3.128)$$

where $K_{s(\rho^*)} = \begin{bmatrix} K_{x(\rho^*)} & K_{f(\rho^*)} \end{bmatrix}$ and $T_1 = \begin{bmatrix} I_{n_x} \\ 0_{n_f \times n_x} \end{bmatrix} T_{e1}$.

From (3.127), (3.128), and $e_d = T_{e2} e_{\bar{x}_a}$, it follows that:

$$\dot{x}_s = (A_{s(\rho^*)} + \Delta A_{s(\rho^*)} - B_s K_{s(\rho^*)})x_s + \begin{bmatrix} B_s K_s & D_s \end{bmatrix} T_s e_{\bar{x}_a} + E_{s(\rho^*)} w + \bar{H}_{s(\rho^*)} \bar{v}, \quad (3.129)$$

where $T_s = \begin{bmatrix} T_1 \\ T_{e2} \end{bmatrix}$, and $\bar{H}_{s(\rho^*)} = \begin{bmatrix} H_{s(\rho^*)} & 0_{n_x \times n_y} \end{bmatrix}$.

3.5.4 Anti-windup observer-based fault compensator synthesis under degradation occurrence for matched UI

With the actuator saturation, the dynamics of estimation error (3.129) and system state (3.124) is also affected by the uncertainty, thereby making the separated design for each component difficult. Hence, the stability of the closed-loop system will be considered in order to obtain robust designs for both observer and anti-windup controller.

From (3.129) and (3.124), the closed-loop system is obtained:

$$\begin{bmatrix} \dot{x}_s \\ \dot{e}_{\bar{x}_a} \end{bmatrix} = \begin{bmatrix} A_{s(\rho^*)} + M_{s(\rho^*)} \Delta_a N_{s(\rho^*)} - B_s K_{s(\rho^*)} & \begin{bmatrix} B_s K_{s(\rho^*)} & D_s \end{bmatrix} T_s \\ M_{ac(\rho^*)} \Delta_{ac} N_{sac(\rho^*)} - \bar{L}_{a(\rho^*)} D_Q F \Delta_c G_s & \bar{A}_{a(\rho^*)} - \bar{L}_{a(\rho^*)} \bar{C}_a \end{bmatrix} \begin{bmatrix} x_s \\ e_{\bar{x}_a} \end{bmatrix} \quad (3.130)$$

$$+ \begin{bmatrix} \bar{H}_{s(\rho^*)} \\ \bar{H}_{a(\rho^*)} - \bar{L}_{a(\rho^*)} \bar{D}_Q \end{bmatrix} \bar{v} + \begin{bmatrix} E_{s(\rho^*)} \\ \bar{E}_{a(\rho^*)} \end{bmatrix} w, \quad (3.131)$$

where $N_{sac(\rho^*)} = [N_{ac(\rho^*)} \quad 0_{n_y \times n_f}]$ and $G_s = [G \quad 0_{n_y \times n_f}]$. Meanwhile, the gains of observer $\bar{L}_{a(\rho^*)}$ and anti-windup controller $\bar{K}_{s(\rho^*)}$ are given by the solution of the following Theorem.

Theorem 3.5.1

Given positive scalars $\sigma_1, \sigma_2, \sigma_3$, and σ_4 , the anti-windup problem and stability of closed-loop system (3.131) can be solved by finding symmetric positive definite matrices $P_1 > \mathcal{P}_{01}$, $P_2 < \mathcal{P}_{02}^{-1}$, matrices $Q_{1(i)}$ and $Q_{2(i)}$, and a symmetric matrix $\mathcal{Z} > 0$ that minimize $Tr(\mathcal{Z})$ and satisfy the following conditions:

$$\left[\begin{array}{ccc|c} \Gamma_{1,1(i)} & 0 & \bar{H}_{s(i)}\bar{V} & \Theta_{1(i)} \\ (*) & \Gamma_{2,2(i)} & \Gamma_{2,3(i)} & \\ (*) & (*) & -I & \\ \hline & (*) & & \Theta_2 \end{array} \right] < 0 \quad \forall i = 1 : \hat{N} \quad ; \hat{N} = 2^{(k+n_u)}, \quad (3.132)$$

$$\begin{bmatrix} P_1 & 0 & P_1 C_{cl1}^T \\ 0 & P_2 & C_{cl2}^T \\ C_{cl1} P_1 & C_{cl2} & \mathcal{Z} \end{bmatrix} > 0, \quad (3.133)$$

where

$$\Gamma_{1,1(i)} = \mathcal{H}\{A_{s(i)}P_1 + B_s Q_{1(i)}\}, \quad \Gamma_{2,2(i)} = \mathcal{H}\{P_2 \bar{A}_{a(i)} + Q_{2(i)} \bar{C}_a\}, \quad (3.134)$$

$$\Gamma_{2,3(i)} = P_2 \bar{H}_{a(i)} \bar{V} + Q_{2(i)} \bar{D}_Q \bar{V}, \quad C_{cl} = [C_{cl1} \quad C_{cl2}], \quad (3.135)$$

$$\Gamma_0 = \sigma_4 \begin{bmatrix} P_1 & 0 \\ 0 & I_{n_u} \end{bmatrix}, \quad \mathcal{P}_0 = \begin{bmatrix} \mathcal{P}_{01} & 0 \\ 0 & \mathcal{P}_{02} \end{bmatrix} > 0, \quad (3.136)$$

$$\Theta_{1(i)} = \begin{bmatrix} -B_s Q_{1(i)} & D_s & P_1 N_{sac(i)}^T & P_1 G_s^T & P_1 N_{s(i)}^T & 0 & 0 & M_{s(i)} & 0 \\ 0 & 0 & 0 & 0 & 0 & P_2 M_{ac(i)} & Q_{2(i)} D_Q F & 0 & T_e^T \\ 0 & 0 & 0 & 0 & 0 & 0 & 0 & 0 & 0 \end{bmatrix}, \quad (3.137)$$

$$\Theta_2 = -diag\{\sigma_4^{-1} P_1, \sigma_4^{-1} I, \sigma_1 I, \sigma_2 I, \sigma_3 I, \sigma_1^{-1} I, \sigma_2^{-1} I, \sigma_3^{-1} I, \Gamma_0\}, \quad (3.138)$$

then the gains of observer-controller are calculated by:

$$K_{s(\rho^*)} = [K_{x(\rho^*)} \quad K_{f(\rho^*)}] = \sum_{i=1}^{\hat{N}} \phi_{i(\rho^*)} K_{s(i)} = - \sum_{i=1}^{\hat{N}} \phi_{i(\rho^*)} Q_{1(i)} P_1^{-1}, \quad (3.139)$$

$$\bar{L}_{a(\rho^*)} = \sum_{i=1}^{\hat{N}} \phi_{i(\rho^*)} \bar{L}_{a(i)} = - \sum_{i=1}^{\hat{N}} \phi_{i(\rho^*)} P_2^{-1} Q_{2(i)}, \quad (3.140)$$

Proof: Since (3.131) has the same structure as (3.40), the stability condition is derived directly from Theorem 3.3.2. ■

Based on the observer-controller design in Sections 3.5.2 and 3.5.3, the anti-windup in-

tegrated design is summarized in Fig. 3.6 with its gains calculated from Theorem 3.5.1. In which, ρ_1 is the parameter-varying vector of initial system with actuator degradation; ρ_2 is the UI frequency which characterizes the frequency-shaping filter; ρ_3 presents the saturation of actuator; and the combination vector $\rho^* = [\rho_1^T \ \rho_2^T \ \rho_3^T]^T$ decides the operation modes of both observer and controller.

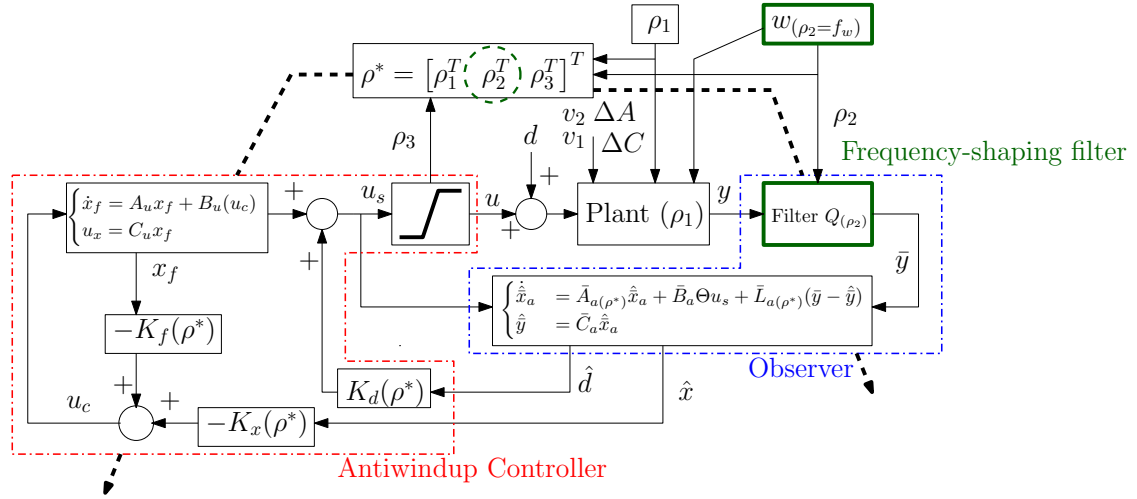


Figure 3.6: Anti-windup integrated design for matched UI

On the other hand, the design scheme of anti-windup integrated design for unmatched UI can be easily derived from Fig. 3.5 and Fig. 3.6, as illustrated in Fig. 3.7. In which, the calculated u_s and output y are the inputs of observer without the frequency-shaping filter, as well as the time-varying ρ_2 .

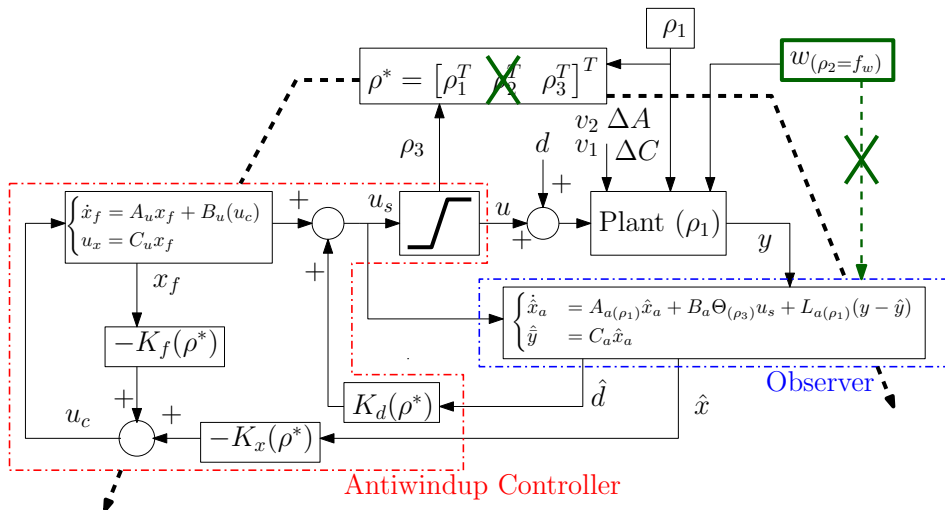


Figure 3.7: Anti-windup integrated design for unmatched UI

3.6 Method illustration

To highlight the performance of the proposed robust-stochastic integrated designs, a numerical example is examined.

3.6.1 Mathematical example

Consider the system (3.7) with the following parameters:

- State distribution matrices: $A_{(\rho_1)} = \begin{bmatrix} -1 & 1 & 0 \\ -1 & 0 & 0 \\ 0 & -1 & (-1 + \rho_1) \end{bmatrix}$, $B = \begin{bmatrix} 2 \\ 4 \\ 2 \end{bmatrix}$, $E = \begin{bmatrix} 3 \\ 0 \\ 0 \end{bmatrix}$, and

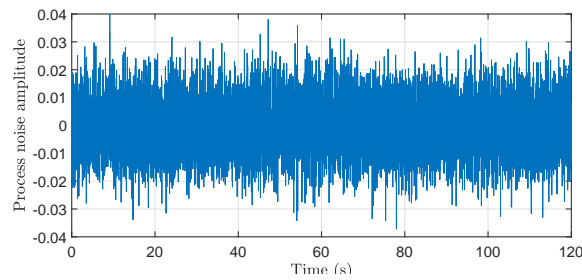
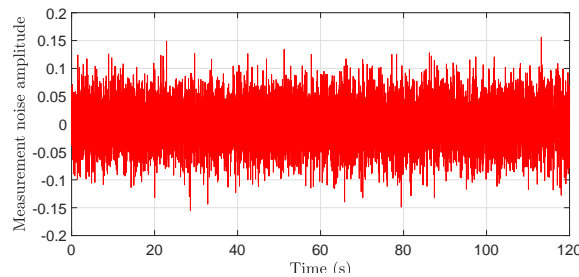
$H = \begin{bmatrix} 0.2 \\ 0 \\ 0 \end{bmatrix}$. Here, $w \in \mathbb{R}^1$ and frequency vector $f_w \in \mathbb{R}^1$ can be considered as a known frequency, i.e. the matched UI, in this example.

- Varying parameter $\rho_1 \in [\underline{\rho}_1, \bar{\rho}_1] = [-0.1, 0.1]$ is modeled as a sinus function: $\rho_1 = 0.1 \sin(2\pi 4)$.
- Uncertainty matrices (only consider ΔA for this example): $M = \begin{bmatrix} 0 \\ 0.1 \\ 0.1 \end{bmatrix}$, $N = [0 \ 1 \ 0]$.
- Output matrix: $C = [0 \ 1 \ -1]$.
- PSD of zero-mean Gaussian noises: $V_1 = 0.1^2$ for the process and $V_2 = 0.2^2$ for the measurement.
- Output filter is chosen based on practical knowledge of disturbance bandwidth in order to characterize the excitation frequency zone. In this example, the bandstop filter is used to specify a certain frequency f_w .

$$Q_{(\rho_2)} = \frac{s^2 + \omega_0^2}{s^2 + \omega_c s + \omega_0^2}, \quad (3.141)$$

where $\omega_0 = 2\pi f_w$ and ω_c are respectively the central rejected frequency and the width of the rejected band. In the state-space representation, where the frequency f_w is chosen as a varying parameter $\rho_2 \in [\underline{\rho}_2, \bar{\rho}_2]$,

$$\begin{cases} \dot{x}_Q = \begin{bmatrix} 0 & 1 \\ -(2\pi\rho_2) & -\omega_c \end{bmatrix} x_Q + \begin{bmatrix} 0 \\ 1 \end{bmatrix} y \\ \bar{y} = [0 \ -\omega_c] x_Q + y \end{cases} . \quad (3.142)$$

Figure 3.8: Process noise v_1 Figure 3.9: Measurement noise v_2

The varying parameter ρ_2 is scheduled as:

$$\rho_2 = f_w = \begin{cases} 2, & 0s \leq t \leq 40s \\ 6, & 40s \leq t \leq 80s \\ 9, & 80s \leq t \leq 150s \end{cases} \quad (3.143)$$

- Actuator behavior is then tested in 3 scenarios (see Fig. 3.10):
 - (a) With saturation and no anti-windup: $u = \text{sat}(u_s)$.
 - (b) With saturation and anti-windup synthesis integrated into the controller, there are 2 subcases to discuss:
 - * (b.1) $\rho_3 \in [0.5, 1]$.
 - * (b.2) $\rho_3 \in [0.8, 1]$.

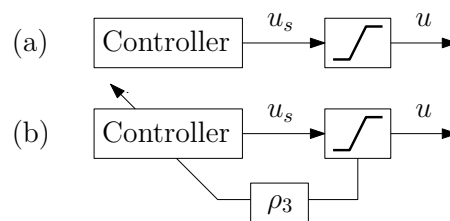


Figure 3.10: Actuator behavior

The scenario (a) uses the gains derived from Theorem 3.3.2, while those of (b) are synthesized from Theorem 3.5.1 where filter W_u is chosen as a low-pass filter with the

cut-off frequency $f_u = 50$ Hz, i.e. $A_u = -B_u = -2\pi f_u$ and $C_u = 1$. Additionally, the mixed $\mathcal{H}_\infty/\mathcal{H}_2$ norm will be implemented to the case (b.1) so that its results can be compared with those of the proposed method for the matched UI. In which, to handle the non-convex multi-objective optimization, $\gamma_\infty = 0.01$ is chosen for UI attenuation, while γ_2 is minimized for noise cancellation.

- In Theorem 3.5.1, the combination of varying-parameter vector $\rho^* = [\rho_1^T \ \rho_2^T \ \rho_3^T]^T$ leads to the $\hat{N} = 2^3 = 8$ corners in the polytope, which are defined as: (1) $\leftrightarrow \omega_1 = (\underline{\rho}_1, \underline{\rho}_2, \underline{\rho}_3)$, (2) $\leftrightarrow \omega_2 = (\bar{\rho}_1, \underline{\rho}_2, \underline{\rho}_3)$, (3) $\leftrightarrow \omega_3 = (\underline{\rho}_1, \bar{\rho}_2, \underline{\rho}_3)$, (4) $\leftrightarrow \omega_4 = (\bar{\rho}_1, \bar{\rho}_2, \underline{\rho}_3)$, (5) $\leftrightarrow \omega_5 = (\underline{\rho}_1, \underline{\rho}_2, \bar{\rho}_3)$, (6) $\leftrightarrow \omega_6 = (\bar{\rho}_1, \underline{\rho}_2, \bar{\rho}_3)$, (7) $\leftrightarrow \omega_7 = (\underline{\rho}_1, \bar{\rho}_2, \bar{\rho}_3)$, and (8) $\leftrightarrow \omega_8 = (\bar{\rho}_1, \bar{\rho}_2, \bar{\rho}_3)$. Also, the coefficients of the polytopic decomposition $\phi_{i(\rho^*)}$ are calculated as follows:

$$\phi_{1(\rho^*)} = \frac{(\bar{\rho}_1 - \rho_1)(\bar{\rho}_2 - \rho_2)(\bar{\rho}_3 - \rho_3)}{(\bar{\rho}_1 - \underline{\rho}_1)(\bar{\rho}_2 - \underline{\rho}_2)(\bar{\rho}_3 - \underline{\rho}_3)}, \quad \phi_{2(\rho^*)} = \frac{(\rho_1 - \underline{\rho}_1)(\bar{\rho}_2 - \rho_2)(\bar{\rho}_3 - \rho_3)}{(\bar{\rho}_1 - \underline{\rho}_1)(\bar{\rho}_2 - \underline{\rho}_2)(\bar{\rho}_3 - \underline{\rho}_3)}, \quad (3.144)$$

$$\phi_{3(\rho^*)} = \frac{(\bar{\rho}_1 - \rho_1)(\rho_2 - \underline{\rho}_2)(\bar{\rho}_3 - \rho_3)}{(\bar{\rho}_1 - \underline{\rho}_1)(\bar{\rho}_2 - \underline{\rho}_2)(\bar{\rho}_3 - \underline{\rho}_3)}, \quad \phi_{4(\rho^*)} = \frac{(\rho_1 - \underline{\rho}_1)(\rho_2 - \underline{\rho}_2)(\bar{\rho}_3 - \rho_3)}{(\bar{\rho}_1 - \underline{\rho}_1)(\bar{\rho}_2 - \underline{\rho}_2)(\bar{\rho}_3 - \underline{\rho}_3)}, \quad (3.145)$$

$$\phi_{5(\rho^*)} = \frac{(\bar{\rho}_1 - \rho_1)(\bar{\rho}_2 - \rho_2)(\rho_3 - \underline{\rho}_3)}{(\bar{\rho}_1 - \underline{\rho}_1)(\bar{\rho}_2 - \underline{\rho}_2)(\bar{\rho}_3 - \underline{\rho}_3)}, \quad \phi_{6(\rho^*)} = \frac{(\rho_1 - \underline{\rho}_1)(\bar{\rho}_2 - \rho_2)(\rho_3 - \underline{\rho}_3)}{(\bar{\rho}_1 - \underline{\rho}_1)(\bar{\rho}_2 - \underline{\rho}_2)(\bar{\rho}_3 - \underline{\rho}_3)}, \quad (3.146)$$

$$\phi_{7(\rho^*)} = \frac{(\bar{\rho}_1 - \rho_1)(\rho_2 - \underline{\rho}_2)(\rho_3 - \underline{\rho}_3)}{(\bar{\rho}_1 - \underline{\rho}_1)(\bar{\rho}_2 - \underline{\rho}_2)(\bar{\rho}_3 - \underline{\rho}_3)}, \quad \phi_{8(\rho^*)} = \frac{(\rho_1 - \underline{\rho}_1)(\rho_2 - \underline{\rho}_2)(\rho_3 - \underline{\rho}_3)}{(\bar{\rho}_1 - \underline{\rho}_1)(\bar{\rho}_2 - \underline{\rho}_2)(\bar{\rho}_3 - \underline{\rho}_3)}, \quad (3.147)$$

Thanks to the usage of Yalmip toolbox [Lofberg 2004] and sdpt3 solver [Toh, Todd, and Tütüncü 1999] in case (b.1), Theorem 3.5.1 is able to compute the static controller-observer gains for each corner of the polytope as given below:

– Controller gains:

$$K_{s(1)} = [-0.5793 \quad 1.3613 \quad 5.5440e-6 \quad 0.0110], \quad (3.148)$$

$$K_{s(2)} = [-0.5624 \quad 1.3200 \quad 7.4342e-6 \quad 0.0107], \quad (3.149)$$

$$K_{s(3)} = [-2.3332 \quad 5.5285 \quad 8.1293e-6 \quad 0.0498], \quad (3.150)$$

$$K_{s(4)} = [-2.3762 \quad 5.6198 \quad 9.4012e-6 \quad 0.0510], \quad (3.151)$$

$$K_{s(5)} = [-0.4322 \quad 1.0168 \quad -6.2639e-8 \quad 0.0091], \quad (3.152)$$

$$K_{s(6)} = [-0.4342 \quad 1.0215 \quad -5.6883e-8 \quad 0.0091], \quad (3.153)$$

$$K_{s(7)} = [-2.8623 \quad 6.7754 \quad 5.0679e-6 \quad 0.0626], \quad (3.154)$$

$$K_{s(8)} = [-3.3706 \quad 7.8377 \quad 1.7208e-5 \quad 0.0704]. \quad (3.155)$$

– Observer gains:

$$\bar{L}_{a(1)} = \begin{bmatrix} 462.0333 \\ 508.1081 \\ -7.5410 \\ 215.9848 \\ 146.5261 \\ 54.1090 \\ 5.4764 \\ 76.4239 \\ -180.5785 \end{bmatrix}, \quad \bar{L}_{a(2)} = \begin{bmatrix} 462.0383 \\ 508.1096 \\ -7.5446 \\ 215.9834 \\ 146.5214 \\ 54.1048 \\ 5.4747 \\ 76.4256 \\ -180.5871 \end{bmatrix}, \quad \bar{L}_{a(3)} = \begin{bmatrix} 2.2876e3 \\ 2.5158e3 \\ -37.3216 \\ 1.069e3 \\ 725.5522 \\ 267.9695 \\ 27.1408 \\ 378.3363 \\ -894.0662 \end{bmatrix}, \quad (3.156)$$

$$\bar{L}_{a(4)} = \begin{bmatrix} 2.2876e3 \\ 2.5158e3 \\ -37.3269 \\ 1.0694e3 \\ 725.5487 \\ 267.9644 \\ 27.1384 \\ 378.3411 \\ -894.0720 \end{bmatrix}, \quad \bar{L}_{a(5)} = \begin{bmatrix} 461.8504 \\ 507.9076 \\ -7.5375 \\ 215.9000 \\ 146.4690 \\ 54.0875 \\ 5.4743 \\ 76.3940 \\ -180.5080 \end{bmatrix}, \quad \bar{L}_{a(6)} = \begin{bmatrix} 461.8899 \\ 507.9438 \\ -7.5449 \\ 215.9140 \\ 146.4707 \\ 54.0831 \\ 5.4718 \\ 76.4026 \\ -180.5326 \end{bmatrix}, \quad (3.157)$$

$$\bar{L}_{a(7)} = \begin{bmatrix} 2.2876e3 \\ 2.5158e3 \\ -37.3216 \\ 1.0694e3 \\ 725.5522 \\ 267.9695 \\ 27.1408 \\ 378.3363 \\ -894.0662 \end{bmatrix}, \quad \bar{L}_{a(8)} = \begin{bmatrix} 2.2876e3 \\ 2.5158e3 \\ -37.3269 \\ 1.0694e3 \\ 725.5487 \\ 267.9644 \\ 27.1384 \\ 378.3411 \\ -894.0720 \end{bmatrix}. \quad (3.158)$$

Consequently, the online-applied gains of observer-controller are derived from the offline static gains: $K_{s(\rho^*)} = [K_{x(\rho^*)} \quad K_{f(\rho^*)}] = \sum_{i=1}^{\hat{N}} \phi_i(\rho^*) K_{s(i)}$ and $\bar{L}_{a(\rho^*)} = \sum_{i=1}^{\hat{N}} \phi_i(\rho^*) \bar{L}_{a(i)}$. Meanwhile, $K_{d(\rho^*)} = -(B\rho_3)^\dagger B$ as mentioned in (3.126).

3.6.2 Frequency analysis

The following figures demonstrate the Bode diagrams at every frozen value of parameter-varying vector ρ^* , corresponding to each corner of the polytope in the nominal system. The parameters of (b.1) derived from Theorem 3.5.1 are used to illustrate the proposed antiwindup integrated design for matched UI. As the filter $Q_{(\rho_2)}$ depends only on the excitation frequency f_w , i.e. ρ_2 , the frequency responses representing the 8 corners of the polytope (mentioned

above in section 3.6.1) are divided into 2 groups corresponding to each bound of the frequency-shaping filter. Here, group 1 (ρ_2) contains the corners (1), (2), (5), and (6); whereas the corners (3), (4), (7), (8) belong to group 2 ($\bar{\rho}_2$).

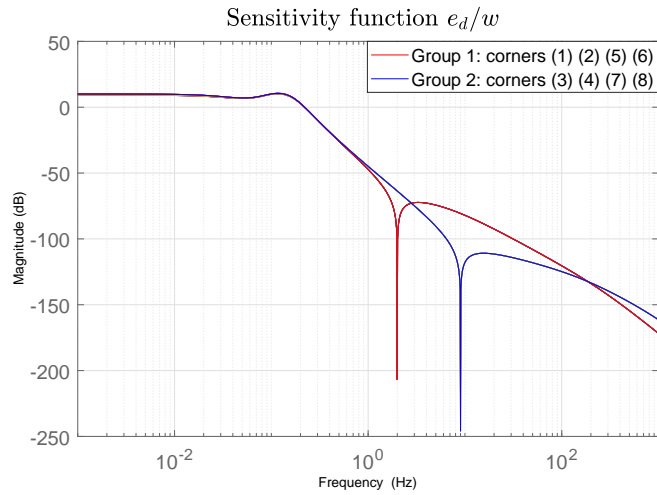


Figure 3.11: Sensitivity e_d/w

Fig. 3.11 illustrates two attenuated frequencies corresponding to the bounds of the parameter ρ_2 . The sensitivities of less than -200 dB at 2 Hz and 9 Hz assure the perfect attenuation of unknown input w to the actuator estimation error e_d .

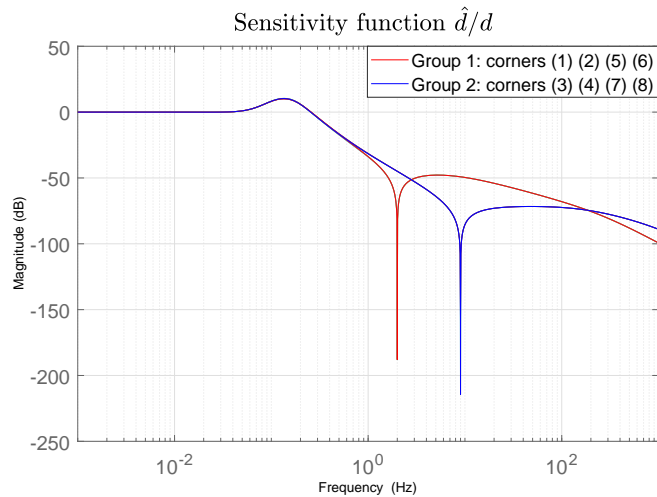


Figure 3.12: Sensitivity \hat{d}/d

In Fig. 3.12, the degradation d can be well estimated by the observer if its bandwidth is less than 0.06 Hz, which is suitable for the long-term development of component degradation.

Fig. 3.13 shows the influence of noise on the estimation error e_d of degradation. Obviously, the impact of process noise v_1 on e_d is ignorable with the attenuation less than -120 dB in high frequency domain (>40 Hz). On the other hand, although there are 2 drops of attenuation

due to the implementation of output filter $Q_{(\rho_2)}$, the measurement noise v_2 still has a great influence on the estimation result at around -17 dB. The impact on noises on the estimated state errors is illustrated in Fig. 3.14 whose results are similar to those in Fig. 3.13.

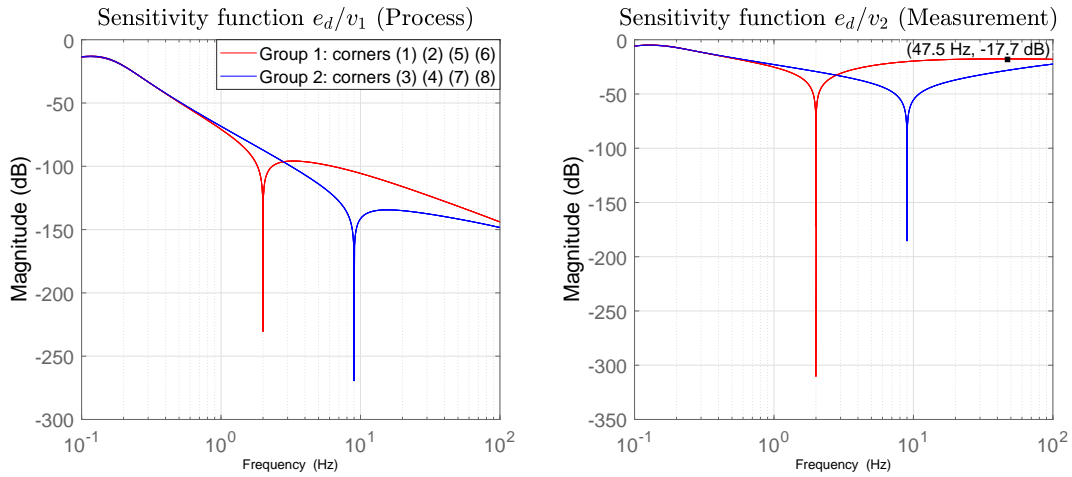


Figure 3.13: Frequency responses of e_d to process and measurement noises

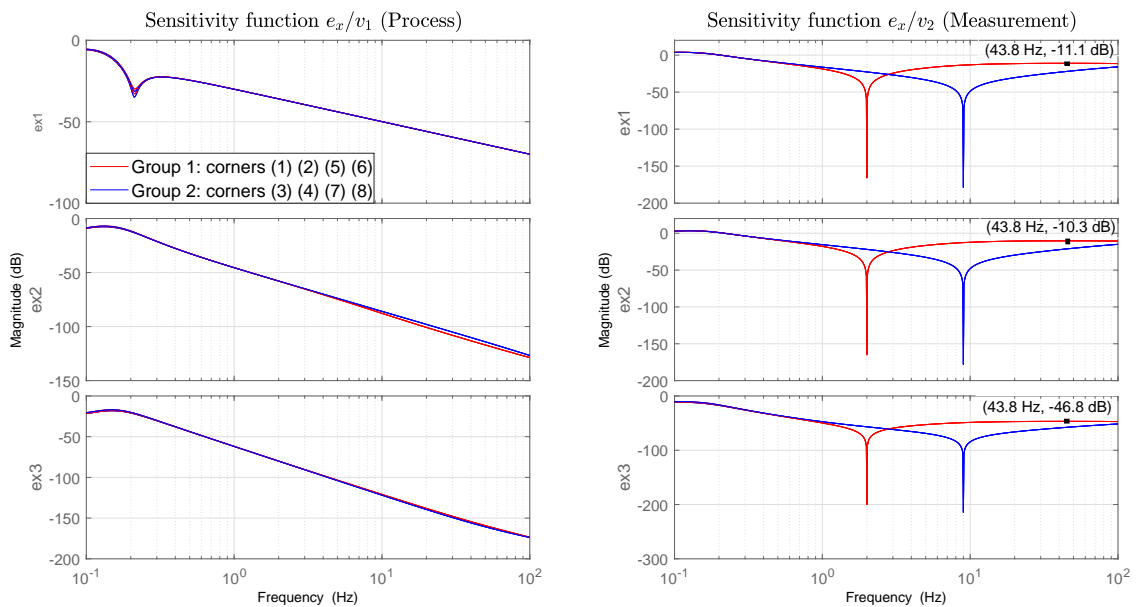


Figure 3.14: Frequency responses of e_x to process and measurement noises

3.6.3 Simulation condition

The following conditions are implemented during simulation:

- **Actuator saturation:** $-0.5 \leq u \leq 1.5$.
- **Exogenous input w :** is modeled as a sinusoidal signal with the frequency of f_w Hz.

$$w = 25\sin(2\pi f_w t) = 25\sin(2\pi\rho_2 t). \quad (3.159)$$

- **Actuator degradation d :** is illustrated in Fig. 3.15 with the following sequence.

$$d = \begin{cases} \sum_{i=0}^{s=3} \frac{(-0.07)^i (\rho_2)^i}{(10)^i i!} (t - t_0)^i - 1 & , t \leq 80 \\ -1.495 & , t > 80 \end{cases}. \quad (3.160)$$

where t_0 is the moment when the ρ_2 changes its value.

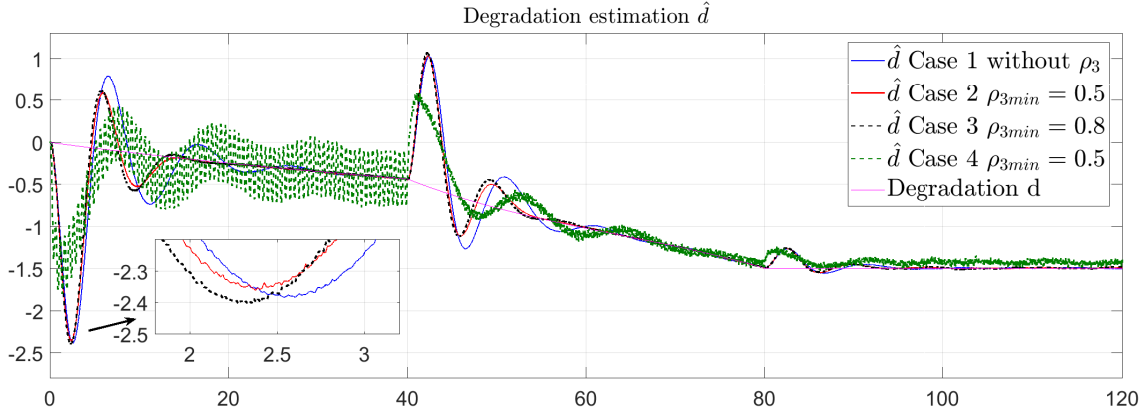
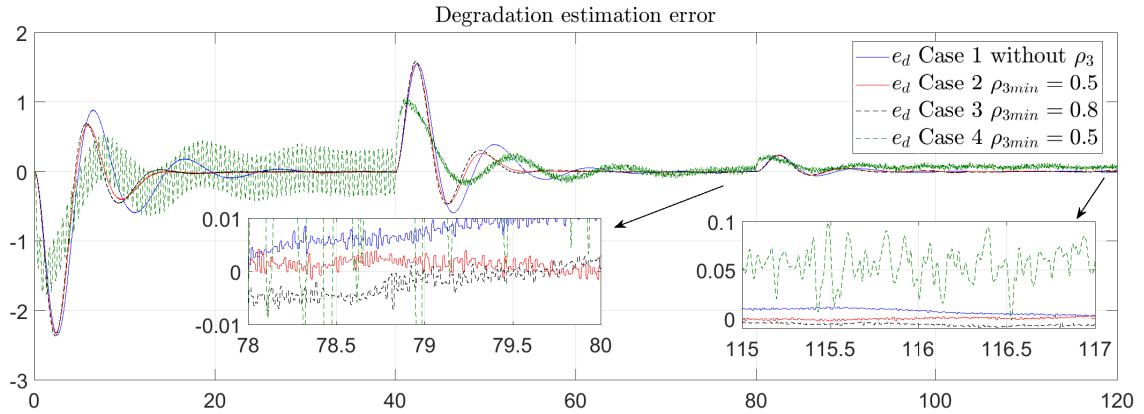
- **Initial Condition:** $x(0) = [0.1 \ 0 \ 0.1]^T$, $\hat{x}_{(0)} = [0.096 \ 0.004 \ 0.104]^T$, $\hat{x}_{Q(0)} = x_{Q(0)} = 0$, and $x_{f(0)} = 0.2$.

3.6.4 Simulation result

In the following figures, four cases (four signals) are examined to evaluate three scenarios of actuator saturation (a), (b.1), and (b.2):

- Case 1: blue signal - Theorem 3.3.2, whose implementation scheme is illustrated by Fig. 3.4, is applied to scenario (a) to obtain non-antiwindup controller.
- Case 2: red signal - The antiwindup integrated design for matched UI that integrates the frequency-shaping filter is obtained from Theorem 3.5.1 where $\rho_{3min} = 0.5$ is chosen for scenario (b.1). The implementation scheme is presented in Fig. 3.6.
- Case 3: black signal - The design for scenario (b.2) is similar to that of Case 2, but $\rho_{3min} = 0.8$ is applied.
- Case 4: green signal - The scenario (b.1) is applied through the implementation scheme in Fig. 3.7 without the need of frequency-shaping filter. Instead, \mathcal{H}_∞ synthesis is used to attenuate the UI.

It is noted that at every change of excitation frequency f_w , a different degradation is correspondingly applied, which leads to the oscillation at the beginning of each cycle in Fig. 3.15. Moreover, thanks to the saturation indicator ρ_3 , the observer in cases 3-4 is modified to improve the convergence speed under the saturation condition, thus giving better estimation results. On the other hand, the cases 1 and 4 require around 30 seconds to stabilize their estimation error, as shown in Fig. 3.16. Additionally, due to the choice in multi-objective

Figure 3.15: Actuator degradation estimation \hat{d} Figure 3.16: Actuator degradation estimation error e_d

optimization, the estimation result of case 4 - $\mathcal{H}_\infty/\mathcal{H}_2$ solution - is greatly affected by the UI and noise, which proves the performance of the proposed method integrating UI frequency-shaping filter in the case of the matched UI. Therefore, the design strategy based on UI frequency is worth to be considered.

To evaluate the estimation result, Table 3.1 is established to analyze the root-mean-square (RMS) values of estimation error when the estimation is achieved, i.e. during the last 10 seconds of each frequency sequence. Compared with noise distribution in Fig. 3.8 and Fig. 3.9, the estimation errors for cases 1-3 in Table 3.1 and Fig. 3.16 are well isolated from the impact of noise under the existence of unknown input d and the uncertainty, whereas those of case 4 - $\mathcal{H}_\infty/\mathcal{H}_2$ solution aren't.

The Fig. 3.17 displays the saturation indicator ρ_3 , which is the signal for anti-windup activation modifying the controller and the behavior of input u in Fig. 3.18. With a higher degree of saturation, the controller of case 3 is activated earlier than that of case 2, thereby resulting in faster reaction than that of non-antiwindup case 1. When the calculated input u_s is saturated, the indicator ρ_3 will inform the controller to take u_s back to the non-saturated zone, thus leading to less oscillation and smaller amplitude in the input signal u . On the other

Table 3.1: RMS value of estimation error with sampling time $T = 0.001$ s

Signal	[30, 40]	[70, 80]	[110, 120]
Case 1 without ρ_3	0.0083	0.0098	0.0060
Case 2 $\rho_{3min} = 0.5$	0.0055	0.0042	0.0065
Case 3 $\rho_{3min} = 0.8$	0.0040	0.0043	0.0069
Case 4 $\rho_{3min} = 0.5$	0.2318	0.0385	0.0707

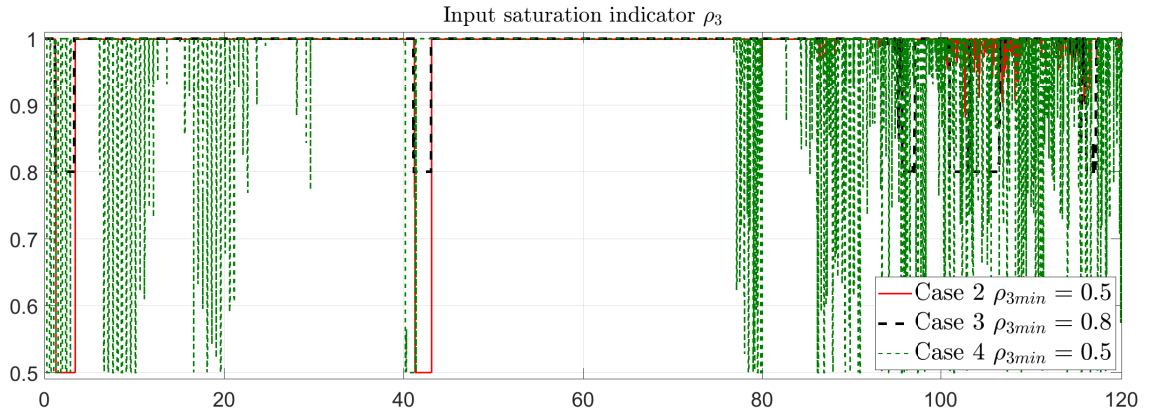


Figure 3.17: Saturation indicator

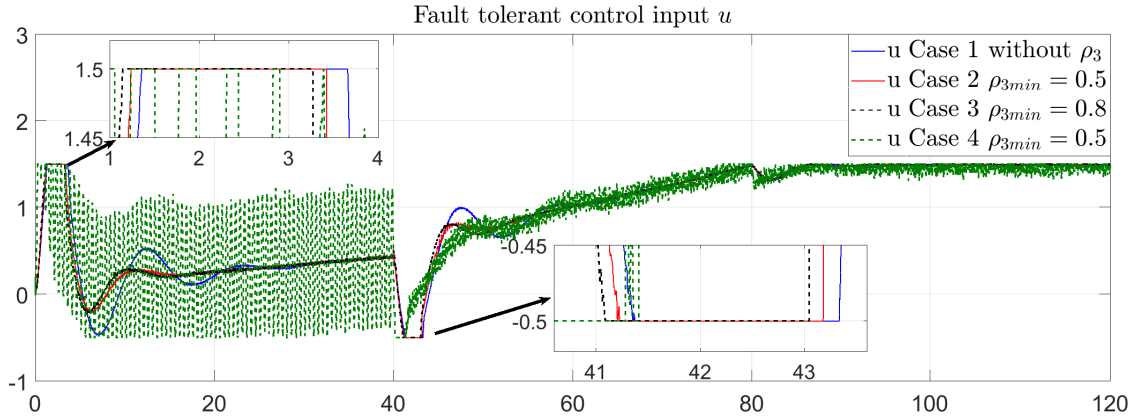
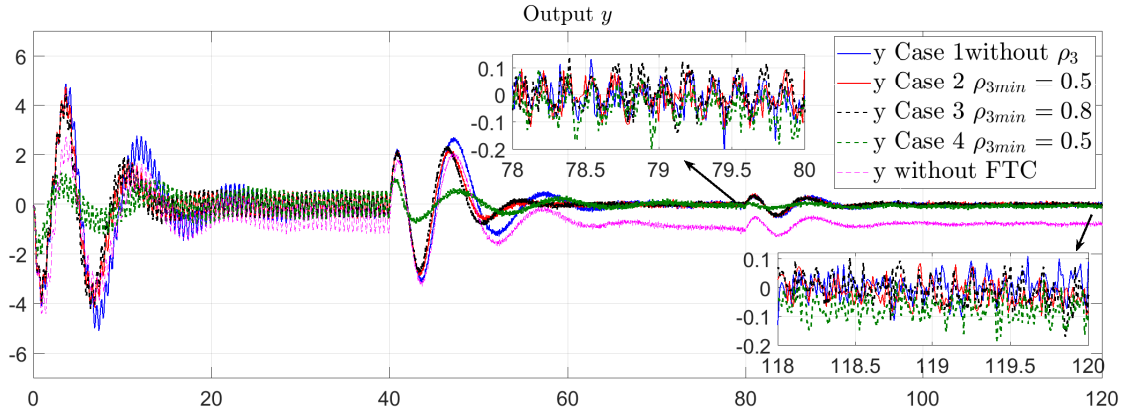


Figure 3.18: Fault tolerant control u

hand, both FTC control input and saturation indicator of case 4 - $\mathcal{H}_\infty/\mathcal{H}_2$ synthesis - are oscillated due to the infected estimation of degradation.

In Fig. 3.19, as a result of the compensation strategy, the degradation effect is successfully overcome, which enables the output to move towards 0 under the influence of noise, disturbance, and uncertainty. The output in case 3 has a little bit faster-converging speed than that of case 2 thanks to its saturation degree. Meanwhile, the output of case 4 - $\mathcal{H}_\infty/\mathcal{H}_2$ solution has the best convergence speed; however, its convergence towards 0 is affected during

Figure 3.19: System output y affected by noise

the period when the value of degradation goes near to the saturation point of the actuator ($t \geq 80$). Additionally, without the FTC strategy, the output y is easily influenced by actuator degradation.

3.7 Conclusion

In this Chapter, the actuator degradation has been modeled by a polynomial function of time and disturbance frequency. To handle this type of fault in the LPV system, robust-stochastic integrated designs are firstly classified based on the frequency-matching condition of UIs. For the matched UI, a frequency-shaping filter is integrated into the observer design to remove the impact of UI disturbance on estimation results, while the system stability is ensured thanks to a state-feedback fault compensator. This new methodology of design not only overcomes the drawbacks of the existing solutions in multi-objective disturbance attenuation but also successfully estimates the degradation in the situation where the UI, stochastic noise, and parametric uncertainties occur at the same time. For the unmatched UI, an extension result for the $\mathcal{H}_\infty/\mathcal{H}_2$ synthesis is promoted to handle the white noise with various PSD. On the other hand, by assuming the system is re-configurable, the saturation problem is reformulated as a LPV problem, thus promoting anti-windup integrated designs and rejecting the actuator saturation. Finally, the simulation example in Section 3.7 has proven the performance of the proposed method for the matched UI compared with that of the traditional method such as mixed $\mathcal{H}_\infty/\mathcal{H}_2$ -norm.

Nonetheless, the proposed designs also have some disadvantages. Firstly, although the conditions for a parameter-independent input matrix B can be bypassed by the usage of input filter in Section 1.5.3.1, the order of the augmented system will increase, thus limiting the computation for a high-order of degradation. Secondly, since the UI frequency is estimated, there exist the uncertainties in the dynamics of the frequency-shaping filter, which affect the performance of the closed-loop system. Thirdly, Theorem 3.3.1 only gives parameter-independent stability with a constant \mathcal{X} , which is conservative in some circumstances. Finally,

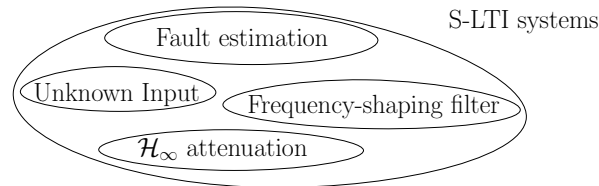
112 Robust-stochastic integrated designs for FDD-FTC of actuator degradation

the validation of the proposed method is only examined in numerical examples, which may not address correctly the behavior of real dynamical systems. Therefore, these issues are essential to be studied in the future.

Part II
Observer Designs for Singular Systems

Fault estimation for S-LTI System with partially decoupled UI

Abstract: The main contribution of Chapter 4 is a generic approach for actuator fault estimation in Singular Linear Time-Invariant (S-LTI) systems perturbed by the partially decoupled Unknown Input (UI). In which, the actuator fault is expressed in a general form (including abrupt/incipient faults, and even degradation) while partially decoupled UIs are divided into decoupled and non-decoupled UI depending on the satisfaction of UI-decoupling condition. Based on the conventional UI observer, the solution decouples the fault estimation with decoupled UIs, while the non-decoupled UIs are handled differently by \mathcal{H}_∞ synthesis or frequency-shaping filter depending on UI bandwidth. Finally, a numerical example with comparisons is illustrated to highlight the performance of proposed designs.



Contents

4.1 Introduction	116
4.1.1 Related Works	116
4.1.2 Chapter Contributions	117
4.2 Problem Formulation	117
4.2.1 System presentation	117
4.2.2 Design Objectives	119
4.3 Observer design	120
4.3.1 Approach 1: Global \mathcal{H}_∞ attenuation	120
4.3.2 Approach 2: Combination of the frequency-shaping filter and \mathcal{H}_∞ attenuation	123
4.3.3 Discussions on Frequency-shaping filter and \mathcal{H}_∞ synthesis	125
4.4 Numerical Example	127
4.4.1 Model Example	127
4.4.2 Frequency Analysis	128
4.4.3 Test Conditions	129

4.4.4	Simulation results	130
4.5	Conclusion	132

4.1 Introduction

4.1.1 Related Works

Nowadays, the S-LTI system, i.e. descriptor system, plays an important role in both theoretical and practical aspects as it can be used to model a wide range of chemical, mineral, electrical and economic systems [Dai 1989]. Thus, many studies have been conducted to analyze the system, especially in developing Fault Detection and Diagnosis (FDD) techniques. In fact, these FDD methods are built based on state estimator (observer), which is realized in [Darouach and Boutayeb 1995]. Notably, [Darouach, Zasadzinski, and Hayar 1996] introduced a reduced-order UI observer for the S-LTI system, which stabilizes the dynamics of estimation error and decouples the UIs in state estimation by choosing properly a group of parametric matrices. Hence, [Chen, Patton, and Zhang 1996] has implemented this observer to detect faults by decoupling the output residual with UIs. Meanwhile, [Koenig 2005] introduces a proportional multiple-integral UI observer to estimate faults for the S-LTI system perturbed by UI. However, one major drawback associated with the above UI observers is the satisfaction of UI-decoupling and detectability conditions [Darouach, Zasadzinski, and Hayar 1996; Koenig 2005]. Consequently, the development of UI observers with partially decoupled UIs, where only a few columns of their UI matrices are needed to satisfy the UI-decoupling condition, becomes an interesting topic in the research community.

To the best of author's knowledge, few works such as [Bezzaoucha et al. 2011] are conducted to handle partially decoupled UIs in linear systems by using the UI observer. In terms of FDD, [Xu et al. 2016] and [Gao, Liu, and Chen 2016] are the two remarkable studies. Both present a novelty in the design of UI observer, in which the UIs are divided into two groups - decoupled and non-decoupled UIs. However, the non-decoupled UIs are handled differently. In specific, for [Xu et al. 2016], the fault detection has been realized by using the set-theorem to deal with the non-decoupled UIs, whereas [Gao, Liu, and Chen 2016] applies \mathcal{H}_∞ synthesis to attenuate their impact on 2^{nd} -order polynomial fault estimation. Although these two papers have contributed meaningful findings, they are only focused on LTI systems ($E = I$) and the \mathcal{H}_∞ performance can be affected when a great amount of non-decoupled UIs are tackled. Based on their UI observer, [Liu, Wang, and Zhou 2018] introduces a solution for fault and state estimation in an augmented S-LTI system. Unfortunately, this method is implemented only if the initial system is non-singular, not to mention that its existence conditions only concern the new augmented S-LTI system instead of the original one. Hence, there is a need to promote a comprehensive design for a partially decoupled UI observer in the S-LTI framework.

4.1.2 Chapter Contributions

For such above reasons, the author is motivated to make the following contributions for the FDD process in the S-LTI system:

- Fault estimation is considered for all kinds of actuator faults, which are expressed in polynomial form;
- Based on UI bandwidth of the non-decoupled UIs, the proposed strategy consists of two approaches:
 - Approach 1: Global \mathcal{H}_∞ approach with its existence conditions for observer depending directly on the parameters of the initial S-LTI system. In fact, it is an extension result of [Gao, Liu, and Chen 2016] for S-LTI systems;
 - Approach 2: A novel method to overcome the limitation of \mathcal{H}_∞ approach in handling numerous non-decoupled UIs and to take advantage of UI bandwidth. In effect, it is the combination of frequency-shaping filter and the \mathcal{H}_∞ synthesis.

Additionally, a numerical example is presented to demonstrate the approaches. Through the frequency analysis and time simulation, the performance of methods is highlighted.

The Chapter is organized as follows. Firstly, Section 4.2 introduces the system representation. To deal with partially decoupled UIs, the observer design with the two approaches is defined in Section 4.3 whose proof of detectability condition is provided in Appendix B.1. Then, a numerical example with comparisons in Section 4.4 illustrates the performance of each solution. A general discussion on existence conditions of observer and frequency-shaping filter is mentioned in Section 4.5. Finally, Section 4.6 concludes the Chapter.

4.2 Problem Formulation

4.2.1 System presentation

Consider the following faulty S-LTI system:

$$\begin{cases} E\dot{x} &= Ax + Bu + D_w w + Bf \\ y &= Cx \end{cases}, \quad (4.1)$$

where:

- $x \in \mathbb{R}^{n_x}$ is the state vector; $y \in \mathbb{R}^{n_y}$ is the measurement output vector; $u \in \mathbb{R}^{n_u}$ is the input vector.
- Matrices $E, A, B, C, D_w = [D_{w1} \ D_{w2} \ D_{w3}]$ are constant matrices with appropriate dimension.

- $w \in \mathbb{R}^{n_w} = [w_1^T \ w_2^T \ w_3^T]^T$ is the UI vector. In which,
 - $w_1 \in \mathbb{R}^{n_{w1}}$ is the vector of UI whose matrix D_{w1} satisfies the UI-decoupling condition.
 - $w_2 \in \mathbb{R}^{n_{w2}}$ is the vector of bounded UI with known bandwidth $[\underline{f}_{w2}, \overline{f}_{w2}]$ and its matrix D_{w2} does not satisfy decoupling condition in UI observer design.
 - $w_3 \in \mathbb{R}^{n_{w3}}$ is the non-decoupled UI vector with bounded energy (\mathcal{L}_2 -norm) and unknown bandwidth.

Actually, w_1 belongs to decoupled UI group, while w_2 and w_3 are in non-decoupled UI one according to the classification in [Gao, Liu, and Chen 2016].

- $f \in \mathbb{R}^{n_u}$ is the actuator fault vector to be estimated, which can be presented as a polynomial:

$$f(t) = \alpha_0 + \alpha_1 t + \dots + \alpha_{n-1} t^{n-1} + \alpha_n t^n, \quad (4.2)$$

where the $(n+1)^{th}$ derivative of f is null (i.e, $f^{(n+1)} = 0$) and α_i ($i = 0, 1, \dots, n$) is unknown coefficient vector.

This generic formulation (4.2) addresses a wide range of faults, such as abrupt faults ($\dot{f} = 0$) and incipient faults ($\ddot{f} = 0$) [Ding 2008], or even the degradation mentioned in Chapter 3.

By considering the derivatives of f as extended states, an augmented system is obtained:

$$\begin{cases} E_a \dot{x}_a = A_a x_a + B_a u + D_{wa} w \\ y = C_a x_a \end{cases}, \quad (4.3)$$

where $x_a = [x^T \ f^T \ f^{(1)T} \ \dots \ f^{(n-1)T} \ f^{(n)T}]^T \in \mathbb{R}^{n_{x_a}}$, $n_{x_a} = n_x + (n+1)n_u$, $C_a =$

$$[C \ 0 \ 0 \ \dots \ 0 \ 0], E_a = \begin{bmatrix} E & 0 & 0 & \dots & 0 & 0 \\ 0 & I & 0 & \dots & 0 & 0 \\ 0 & 0 & I & \dots & 0 & 0 \\ \dots & \dots & \dots & \dots & \dots & \dots \\ 0 & 0 & 0 & \dots & I & 0 \\ 0 & 0 & 0 & \dots & 0 & I \end{bmatrix}, A_a = \begin{bmatrix} A & B & 0 & \dots & 0 & 0 \\ 0 & 0 & I & \dots & 0 & 0 \\ 0 & 0 & 0 & \dots & 0 & 0 \\ \dots & \dots & \dots & \dots & \dots & \dots \\ 0 & 0 & 0 & \dots & 0 & I \\ 0 & 0 & 0 & 0 & \dots & 0 \end{bmatrix},$$

$$B_a = \begin{bmatrix} B \\ 0 \\ 0 \\ \dots \\ 0 \\ 0 \end{bmatrix}, \text{ and } D_{wa} = \begin{bmatrix} D_w \\ 0 \\ 0 \\ \dots \\ 0 \\ 0 \end{bmatrix} = [D_{w1a} \ D_{w2a} \ D_{w3a}].$$

To estimate the fault f through the estimation of augmented state x_a , the augmented system (4.3) is assumed to be observable, or at least both impulse-free and R-detectable, which can be verified by conditions (C.1) and (C.2) mentioned later in Section 4.3.

4.2.2 Design Objectives

The aim of observer design is to estimate fault f in augmented system (4.3) under the existence of UI w . To fulfill this objective, a generic strategy is introduced. In which, the UI w_1 of w is decoupled from estimation process by the conventional UI observer-based design, whereas the impact of the UI $w_{23} = [w_2^T \ w_3^T]^T$ on fault estimation are tackled differently based on the bandwidth of UI w_2 . Thus, the two following approaches are proposed to tackle UI w_2 :

Approach 1: Global \mathcal{H}_∞ attenuation

The impact of non-decoupled UI w_2 , as well as w_3 , on fault estimation will be attenuated by \mathcal{H}_∞ synthesis, which explains for "Global" characteristic of this approach. In fact, this attenuation process is similar to that of [Gao, Liu, and Chen 2016] for LTI systems. Also, the existence conditions are derived from the initial S-LTI system and observer parameters must satisfy the following objectives:

- For $w_{23} = 0$, the estimation error is asymptotically stable.
- For $w_{23} \neq 0$, attenuation of exogenous input w_{23} on the fault estimation error e_f is achieved by minimizing γ_{23} such that:

$$\frac{\|e_f\|_2}{\|w_{23}\|_2} \leq \gamma_{23}, \quad (4.4)$$

where $e_f = f - \hat{f}$ is fault estimation error and \hat{f} is the estimated fault.

Approach 2: Combination of the frequency-shaping filter and \mathcal{H}_∞ attenuation.

Unlike **Approach 1**, **Approach 2** handles the UIs w_2 and w_3 separately:

- UI w_2 is attenuated by a frequency-shaping filter, corresponding to its known bandwidth.
- UI w_3 is attenuated by \mathcal{H}_∞ optimization as mentioned in Approach 1. For $w_3 \neq 0$, attenuation of exogenous input w_3 on the fault estimation error e_f is achieved by minimizing γ_3 such that:

$$\frac{\|e_f\|_2}{\|w_3\|_2} \leq \gamma_3. \quad (4.5)$$

Remark 4.2.1

Comparing to **Approach 1**, **Approach 2** relaxes the number of elements in non-decoupled UI vector used for \mathcal{H}_∞ optimization.

Details of the observer design for each approach are presented in subsections 4.3.1 and 4.3.2.

4.3 Observer design

In order to design the UI observers, the following conditions are considered for their existence:

$$(C.1) \quad \text{rank} \begin{bmatrix} E & D_{w1} \\ C & 0 \end{bmatrix} = n_x + n_{w1}. \quad (4.6)$$

$$(C.2) \quad \text{rank} \begin{bmatrix} (pE - A) & -B & D_{w1} \\ 0 & pI & 0 \\ C & 0 & 0 \end{bmatrix} = n_x + n_{w1}, \forall \mathcal{R}(p) \geq 0. \quad (4.7)$$

It is noted that the condition (C.1) corresponds to not only the impulse-free condition of the singular system but also the UI-decoupling condition for decoupled UI w_1 . Meanwhile, the condition (C.2) is the condition for R-detectability. Since these conditions concern only the parameter of possibly-decoupled UI w_1 , i.e. D_{w1} , they are less restrictive than those of [Darouach, Zasadzinski, and Hayar 1996; Koenig 2005] for all UIs in w , i.e. D_w .

Then, two methods of observer design are developed with the satisfaction of conditions (C.1) and (C.2).

4.3.1 Approach 1: Global \mathcal{H}_∞ attenuation

In this approach, the impact of both non-decoupled UIs w_2 and w_3 on fault estimation will be attenuated by \mathcal{H}_∞ synthesis. Details on the observer design are given below.

The full-order functional UI observer has the structure (as illustrated in Fig. 4.1):

$$\begin{cases} \dot{z} = Fz + Gu + Ly \\ \hat{x}_a = z + Ny \\ \hat{f} = C_{af}\hat{x}_a \end{cases}, \quad (4.8)$$

where $\hat{x}_a = [\hat{x}^T \quad \hat{f}^T \quad \hat{f}^{(1)T} \quad \dots \quad \hat{f}^{(n-1)T} \quad \hat{f}^{(n)T}]^T$ is the estimated state of x_a in (4.3); \hat{f} is the estimated fault; and $C_{af} = [0_{n_u \times n_x} \quad I_{n_u} \quad 0_{n_u, n_{x_a} - n_x - n_u}]$.

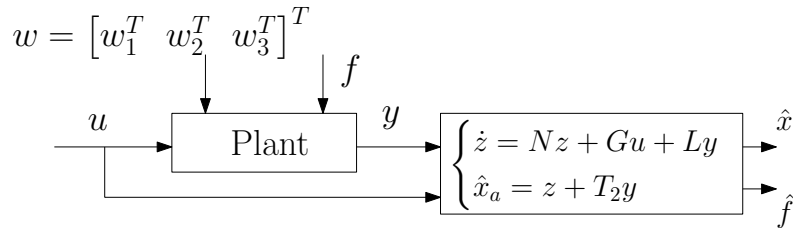


Figure 4.1: General scheme of UI observer

Choose $e = x_a - \hat{x}_a$ as the estimation error and suppose that there exists T such that

$$TE_a + NC_a = I, \quad (4.9)$$

we obtain:

$$e = x_a - z - Ny = TE_a x_a - z. \quad (4.10)$$

Then, its dynamics is presented as:

$$\dot{e} = TE_a \dot{x}_a - \dot{z} \quad (4.11)$$

$$\begin{aligned} &= Fe + (TA_a - FTE_a - LC_a)x_a \\ &+ (TB_a - G)u + TD_{w1a}w_1 + TD_{w23a}w_{23}, \end{aligned} \quad (4.12)$$

where $w_{23} = [w_2^T \ w_3^T]^T \in \mathbb{R}^{n_{w23}}$, $n_{w23} = n_{w2} + n_{w3}$ and $D_{w23a} = [D_{w2a} \ D_{w3a}]$.

In order for e to be stabilized and decoupled from the UI w_1 , the following conditions have to be satisfied:

$$F \text{ is Hurwitz, i.e. } \mathcal{R}(\text{eig}(F)) < 0, \quad (4.13)$$

$$TA_a - FTE_a - LC_a = 0, \quad (4.14)$$

$$G = TB_a, \quad (4.15)$$

$$TD_{w1a} = 0. \quad (4.16)$$

From (4.14), by replacing $TE_a = I - NC_a$ and choosing $K = L - FN$, it follows that:

$$TA_a - KC_a - F = 0. \quad (4.17)$$

By combining the three conditions which are $TE_a + NC_a = I$, (4.16) and (4.17), we obtain:

$$[T \ N \ K \ F] \Theta = \Omega, \quad (4.18)$$

where $\Omega = [I_{n_{x_a}} \ 0_{n_{x_a} \times (n_{x_a} + n_{w1})}]$ and $\Theta = \begin{bmatrix} E_a & A_a & D_{w1a} \\ C_a & 0 & 0 \\ 0 & -C_a & 0 \\ 0 & -I_{n_{x_a}} & 0 \end{bmatrix}$.

The solution of (4.18) exists if and only if $\text{rank} \begin{bmatrix} \Theta \\ \Omega \end{bmatrix} = \text{rank}(\Theta)$, which means that Θ is a full-column rank matrix [Koenig 2005], i.e. $\text{rank}(\Theta) = 2n_{x_a} + n_{w1}$

$$\Leftrightarrow \text{rank} \begin{bmatrix} E_a & D_{w1a} \\ C_a & 0 \end{bmatrix} = n_{x_a} + n_{w1}. \quad (4.19)$$

By replacing the definitions of E_a , C_a , and D_{w1a} with matrices of original system (4.1), a new condition which is equivalent to condition (C.1) is obtained.

Under condition (C.1), the generalized solution of (4.18) is given as:

$$[T \ N \ K \ F] = \Omega \Theta^\dagger - Z \Theta^\perp, \quad (4.20)$$

where $\Theta^\perp = (I - \Theta\Theta^\dagger)$ and Z is a designed matrix, which will be synthesized later in Theorem 4.3.1.

From (4.12), (4.17) and (4.20), the influence of w_{23} on estimation error $e_f = f - \hat{f}$ is expressed as:

$$\begin{cases} \dot{e} = (TA_a - KC_a)e + TD_{w_{23a}}w_{23} \\ e_f = C_{af}e \end{cases} \quad (4.21)$$

In other words,

$$\begin{cases} \dot{e} = (\Omega\Theta^\dagger\phi_1 - Z\Theta^\perp\phi_1)e + (\Omega\Theta^\dagger\phi_2 - Z\Theta^\perp\phi_2)w_{23} \\ e_f = C_{af}e \end{cases} \quad (4.22)$$

where $\phi_1 = \begin{bmatrix} A_a \\ 0_{n_y \times n_{x_a}} \\ -C_a \\ 0_{n_{x_a} \times n_{x_a}} \end{bmatrix}$ and $\phi_2 = \begin{bmatrix} D_{w_{23a}} \\ 0_{(2n_y+n_{x_a}) \times n_{w_{23}}} \end{bmatrix}$.

The above error dynamics can be stabilized thanks to the detectability of the pair $(\Omega\Theta^\dagger\phi_1, \Theta^\perp\phi_1)$ given as the condition below:

$$\text{rank} \begin{bmatrix} pI - \Omega\Theta^\dagger\phi_1 \\ \Theta^\perp\phi_1 \end{bmatrix} = n_{x_a} \quad \forall \mathcal{R}(p) \geq 0, \quad (4.23)$$

which is equivalent to condition (C.2).

Proof: The proof is presented in Appendix B.1. ■

Then, the gain Z , which satisfies the design objectives of Approach 1 such that $\frac{\|e_f\|_2}{\|w_{23}\|_2} \leq \gamma_{23}$, can be computed from the following Theorem.

Theorem 4.3.1

Under conditions (C.1) and (C.2), if there exist a symmetric positive-definite matrix P and a matrix Q which minimize γ_{23} in (4.4) and satisfy that:

$$\begin{bmatrix} \Gamma & P\Omega\Theta^\dagger\phi_2 + Q\Theta^\perp\phi_2 & C_{af}^T \\ (*) & -\gamma_{23}^2 I & 0 \\ (*) & (*) & -I \end{bmatrix} < 0, \quad (4.24)$$

with

$$\Gamma = \mathcal{H}\{P\Omega\Theta^\dagger\phi_1 + Q\Theta^\perp\phi_1\}, \quad (4.25)$$

$$\phi_1 = \begin{bmatrix} A_a^T & 0_{n_y \times n_{x_a}}^T & -C_a^T & 0_{n_{x_a} \times n_{x_a}}^T \end{bmatrix}^T, \quad (4.26)$$

$$\phi_2 = \begin{bmatrix} D_{w_{23a}}^T & 0_{(2n_y+n_{x_a}) \times n_{w_{23}}}^T \end{bmatrix}^T, \quad (4.27)$$

the estimation error in (4.22) satisfies the objectives in **Approach 1** with the gain $Z = -QP^{-1}$.

Remark 4.3.1

If $E = I$ and the columns of Z corresponding to parametric matrices T and N in (4.20) are null, the result in [Gao, Liu, and Chen 2016] is re-obtained. According to [Gao, Liu, and Chen 2016], the parameters T and N are only the basic results of generalized solution, i.e. without the tuning of the arbitrary matrix, thus limiting the freedom of the observer design comparing to that in Theorem 4.3.1.

Proof: The sufficient condition for the stability of (4.22) and attenuation objective (4.4) is that:

$$\dot{V} + e_f^T e_f - \gamma_{23}^2 w_{23}^T w_{23} < 0. \quad (4.28)$$

By choosing the Lyapunov function $V = e^T P e$ and $Q = -PZ$, it follows that:

$$\begin{bmatrix} e^T & w_{23}^T \end{bmatrix} \begin{bmatrix} \Gamma + C_{af}^T C_{af} & P\Omega\Theta^\dagger\phi_2 + Q\Theta^\perp\phi_2 \\ (*) & -\gamma_{23}^2 I \end{bmatrix} \begin{bmatrix} e \\ w_{23} \end{bmatrix} < 0. \quad (4.29)$$

The above inequality holds $\forall [e^T \ w_{23}^T]^T \neq 0$ if:

$$\begin{bmatrix} \Gamma + C_{af}^T C_{af} & P\Omega\Theta^\dagger\phi_2 + Q\Theta^\perp\phi_2 \\ (*) & -\gamma_{23}^2 I \end{bmatrix} < 0. \quad (4.30)$$

Applying the Schur complement to the above LMI, the condition (4.24) is obtained, which completes the proof. ■

Then, the parameters $[T \ N \ K \ F]$ are calculated by replacing values of Z in (4.20), then $L = K + FN$ and $G = TB_a$. That completes the design process for the **Approach 1**.

4.3.2 Approach 2: Combination of the frequency-shaping filter and \mathcal{H}_∞ attenuation

Unlike **Approach 1** where non-decoupled UIs w_2 and w_3 are attenuated together by \mathcal{H}_∞ synthesis, **Approach 2** tackled them separately: w_2 by frequency-shaping filter, while w_3 by \mathcal{H}_∞ synthesis. Details on the observer design are given as below.

Since the bandwidth on non-decoupled UI w_2 is known, the usage of frequency-shaping filter, which is also proposed in Section 3.3.1 of Chapter 3, can be applied as an alternative to \mathcal{H}_∞ synthesis, thus increasing the efficiency of \mathcal{H}_∞ optimization on w_3 . Herein, the filter Q applied to output y in Fig. 4.2 will characterize the UI attenuation for the known bandwidth $[\underline{f}_{w_2}, \overline{f}_{w_2}]$ of UI w_2 . As a result, the signal \bar{y} of the stable filter Q is now considered as a new measurement that is not perturbed by UI w_2 .

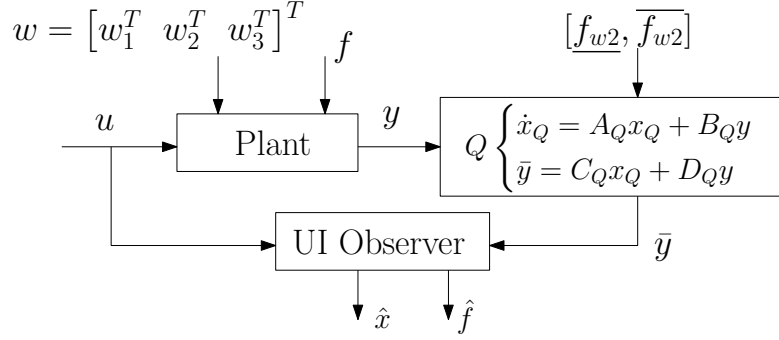


Figure 4.2: Frequency-shaping filter implementation for UI observer

The stable filter Q can be expressed as:

$$Q : \begin{cases} \dot{x}_Q = A_Q x_Q + B_Q y \\ \bar{y} = C_Q x_Q + D_Q y \end{cases} \quad (4.31)$$

where A_Q is Hurwitz.

The integration of filter Q in (4.3) yields an augmented system:

$$\begin{cases} \bar{E}_a \dot{\bar{x}}_a = \bar{A}_a \bar{x}_a + \bar{B}_a u + \bar{D}_{wa} w \\ \bar{y} = \bar{C}_a \bar{x}_a \end{cases} \quad (4.32)$$

In which, $\bar{x}_a = \begin{bmatrix} x_a \\ x_Q \end{bmatrix} \in \mathbb{R}^{n_{\bar{x}_a}}$, $\bar{E}_a = \begin{bmatrix} E_a & 0 \\ 0 & I \end{bmatrix}$, $\bar{A}_a = \begin{bmatrix} A_a & 0 \\ B_Q C_a & A_Q \end{bmatrix}$, $\bar{B}_a = \begin{bmatrix} B_a \\ 0 \end{bmatrix}$, $\bar{D}_{wa} = \begin{bmatrix} D_{wa} \\ 0 \end{bmatrix}$, $\bar{C}_a = \begin{bmatrix} D_Q C_a & C_Q \end{bmatrix}$.

The observer design for the above system (4.32) has the same structure as the conventional UI observer to decouple w_1 while integrating implicitly the frequency-shaping effect for non-decoupled UI w_2 into its dynamics:

$$\begin{cases} \dot{z} = \bar{F} z + \bar{G} u + \bar{L} \bar{y} \\ \hat{\bar{x}}_a = z + \bar{N} \bar{y} \\ \hat{f} = \bar{C}_{af} \hat{\bar{x}}_a \end{cases} \quad (4.33)$$

where $\hat{\bar{x}}_a$ is the estimated state of \bar{x}_a and $\bar{C}_{af} = [0_{n_u \times n_x} \quad I_{n_u} \quad 0_{n_u, n_{\bar{x}_a} - n_x - n_u}]$.

As Q is a stable filter, the conditions for observer existence (C.1) and (C.2) are also those for augmented system (4.32). Like **Approach 1**, **Approach 2** also obtains the following results:

$$[\bar{T} \quad \bar{N} \quad \bar{K} \quad \bar{F}] = \bar{\Omega} \bar{\Theta}^\dagger - \bar{Z} \bar{\Theta}^\perp, \quad (4.34)$$

$$\bar{L} = \bar{K} + \bar{F} \bar{N}, \quad (4.35)$$

$$\bar{G} = \bar{T} \bar{B}_a, \quad (4.36)$$

where $\bar{\Theta} = \begin{bmatrix} \bar{E}_a & \bar{A}_a & \bar{D}_{w1a} \\ \bar{C}_a & 0 & 0 \\ 0 & -\bar{C}_a & 0 \\ 0 & -I_{n_{\bar{x}_a}} & 0 \end{bmatrix}$ and $\bar{\Omega} = [I_{n_{\bar{x}_a}} \ 0 \ 0]$. The gain \bar{Z} is later computed from Theorem 4.3.2.

Due to the implementation of the output filter, the attenuation of UI w_2 is implicitly incorporated in the dynamics of estimation error. Thus, by neglecting w_2 , we obtain:

$$\begin{cases} \dot{\bar{e}} = (\bar{\Omega}\bar{\Theta}^\dagger\bar{\phi}_1 - \bar{Z}\bar{\Theta}^\perp\bar{\phi}_1)\bar{e} + (\bar{\Omega}\bar{\Theta}^\dagger\bar{\phi}_2 - \bar{Z}\bar{\Theta}^\perp\bar{\phi}_2)w_3 \\ e_f = C_{af}\bar{e} \end{cases} \quad (4.37)$$

where $\bar{e} = \bar{x}_a - \hat{x}_a$, $\bar{\phi}_1 = \begin{bmatrix} \bar{A}_a^T & 0_{n_y \times n_{\bar{x}_a}} & -\bar{C}_a^T & 0_{n_{\bar{x}_a} \times n_{\bar{x}_a}} \end{bmatrix}^T$ and $\bar{\phi}_2 = \begin{bmatrix} \bar{D}_{w3a}^T & 0_{(2n_y + n_{\bar{x}_a}) \times n_{w3}} \end{bmatrix}^T$. Then, the gain \bar{Z} has to ensure that w_3 is attenuated by \mathcal{H}_∞ optimization, i.e. $\frac{\|e_f\|_2}{\|w_3\|_2} \leq \gamma_3$. Such objective is achieved by Theorem 4.3.2.

Theorem 4.3.2

Under conditions (C.1) and (C.2), if there exist a symmetric positive-definite matrix \bar{P} and a matrix \bar{Q} which minimize γ_3 in (4.5) and satisfy that:

$$\begin{bmatrix} \bar{\Gamma} & \bar{P}\bar{\Omega}\bar{\Theta}^\dagger\bar{\phi}_2 + \bar{Q}\bar{\Theta}^\perp\bar{\phi}_2 & \bar{C}_{af}^T \\ (*) & -\gamma_3^2 I & 0 \\ (*) & (*) & -I \end{bmatrix} < 0, \quad (4.38)$$

with

$$\bar{\Gamma} = \mathcal{H}\{\bar{P}\bar{\Omega}\bar{\Theta}^\dagger\bar{\phi}_1 + \bar{Q}\bar{\Theta}^\perp\bar{\phi}_1\}, \quad (4.39)$$

$$\bar{\phi}_1 = \begin{bmatrix} \bar{A}_a^T & 0_{n_y \times n_{\bar{x}_a}} & -\bar{C}_a^T & 0_{n_{\bar{x}_a} \times n_{\bar{x}_a}} \end{bmatrix}^T, \quad (4.40)$$

$$\bar{\phi}_2 = \begin{bmatrix} \bar{D}_{w3a}^T & 0_{(2n_y + n_{\bar{x}_a}) \times n_{w3}} \end{bmatrix}^T, \quad (4.41)$$

the estimation error in (4.37) satisfies the objectives in **Approach 2** with the gains $\bar{Z} = -\bar{Q}\bar{P}^{-1}$.

Proof: This theorem is similar to Theorem 4.3.1, so the proof is omitted. ■

Then, the parameters $[\bar{T} \ \bar{N} \ \bar{K} \ \bar{F}]$ are calculated by replacing values of \bar{Z} in (4.34), then $\bar{L} = \bar{K} + \bar{F}\bar{N}$ and $\bar{G} = \bar{T}\bar{B}_a$. That completes the design process for the **Approach 2**. Discussion on Approaches 1 and 2 will be presented in the next section.

4.3.3 Discussions on Frequency-shaping filter and \mathcal{H}_∞ synthesis

Although both \mathcal{H}_∞ synthesis (**Approach 1**) and frequency-shaping filter (**Approach 2**) are able to attenuate the impact of non-decoupled UI w_2 , **Approach 2** gives more advantages

than **Approach 1** for the UI attenuation in a specified bandwidth.

In **Approach 1**, the \mathcal{H}_∞ performance can also be adapted to a specific bandwidth $[\underline{f}_{w_2}, \overline{f}_{w_2}]$ of w_2 by generating a fictive UI \bar{w}_2 through a weighting function F_w , which is strictly stable and causal [Koenig, Marx, and Varrier 2016].

The weighting function F_w can be displayed as:

$$F_w : \begin{cases} \dot{x}_w = A_w x_w + B_w \bar{w}_2 \\ w_2 = C_w x_w + D_w \bar{w}_2 \end{cases} . \quad (4.42)$$

The process is summarized in Fig. 4.3:

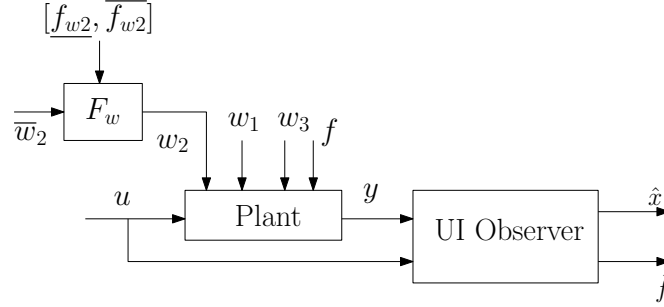


Figure 4.3: Weighting function implementation in \mathcal{H}_∞ synthesis.

As a result, the system can be rewritten as:

$$\begin{cases} \dot{x}_F = A_F x_F + B_F u + D_F \bar{w} \\ y = C_F x_F \end{cases} , \quad (4.43)$$

where $x_F = \begin{bmatrix} x_a \\ x_w \end{bmatrix}$, $A_F = \begin{bmatrix} A_a & D_{w2a} C_w \\ 0 & A_w \end{bmatrix}$, $B_F = \begin{bmatrix} B_a \\ 0 \end{bmatrix}$, $D_F = \begin{bmatrix} D_{w1a} & D_{w2a} D_w & D_{w3a} \\ 0 & B_w & 0 \end{bmatrix}$, and $C_F = \begin{bmatrix} C_a & 0 \end{bmatrix}$.

From (4.4), the objective of observer design for (4.43) is displayed as:

$$\frac{\|e_f\|_2}{\|\bar{w}_{23}\|_2} \leq \gamma_{23}, \quad (4.44)$$

where $\bar{w}_{23} = [\bar{w}_2^T \quad w_3^T]^T$.

In other words,

$$\left\{ \begin{array}{l} \frac{\|e_f\|_2}{\|\bar{w}_2\|_2} \leq \gamma_{23} \\ \frac{\|e_f\|_2}{\|w_3\|_2} \leq \gamma_{23} \end{array} \right\} \Leftrightarrow \left\{ \begin{array}{l} \frac{\|e_f\|_2}{\|w_2\|_2} \leq \gamma_{23} \|F_w\|^{-1} \\ \frac{\|e_f\|_2}{\|w_3\|_2} \leq \gamma_{23} \end{array} \right. \quad (4.45)$$

Consequently, the influence of the non-decoupled w_2 on fault estimation can be shaped by the choice of inversed filter F_w^{-1} .

Although both inverse of weighting function F_w^{-1} in **Approach 2** and frequency-shaping filter Q in **Approach 2** have the same functionality; filter Q only needs to be stable, whereas F_w also requires to be causal. Hence, this difference highlights the benefit of the frequency-shaping filter in **Approach 2**.

In the next section, the numerical example will explain more clearly such difference.

4.4 Numerical Example

In this section, the time-domain comparison between the two above approaches is conducted through a numerical example to illustrate the performance of each method.

4.4.1 Model Example

The following example is modified from the S-LTI system in [Darouach, Zasadzinski, and Hayar 1996]:

$$\begin{cases} E\dot{x} &= Ax + Bu + D_w w + Bf \\ y &= Cx \end{cases}, \quad (4.46)$$

where:

- Distribution Matrices: $E = \begin{bmatrix} 1 & 0 & 0 & 0 \\ 0 & 1 & 0 & 0 \\ 0 & 0 & 1 & 0 \\ 0 & 0 & 0 & 0 \end{bmatrix}$, $A = \begin{bmatrix} -1 & 1 & 0 & 0 \\ -1 & 0 & 0 & 1 \\ 0 & -1 & -1 & 0 \\ 0 & 0 & 0 & 1 \end{bmatrix}$, $B = \begin{bmatrix} 0 \\ 0 \\ 1 \\ 1 \end{bmatrix}$, $D_{w1} = \begin{bmatrix} 0 \\ 0 \\ 1 \\ 1 \end{bmatrix}$, $D_{w2} = \begin{bmatrix} 0 \\ 0.4 \\ 0 \\ 0 \end{bmatrix}$, $D_{w3} = \begin{bmatrix} 0 \\ 0.2 \\ 0.1 \\ 0 \end{bmatrix}$, and $C = \begin{bmatrix} 1 & 0 & 0 & 0 \\ 0 & 0 & -1 & 1 \end{bmatrix}$.

- Frequency bandwidth of UI w_2 : $f_{w2} \in [10, 30]$ (Hz). Since it is a narrow bandwidth, the filter Q is designed as a stable 8th order Butterworth-bandstop, as illustrated in Fig. 4.4. On the other hand, if the inverse of weighting function in \mathcal{H}_∞ synthesis (**Approach 1**), i.e. F_w^{-1} , is chosen as Q , then F_w is not stable, thereby invalidating the causal characteristic in Section 4.3.3. That also proves the advantages of frequency-shaping filter for practical implementation.
- Actuator fault: is supposed to be a 3rd order polynomial (see Fig. 4.5), so $n = 3$ is

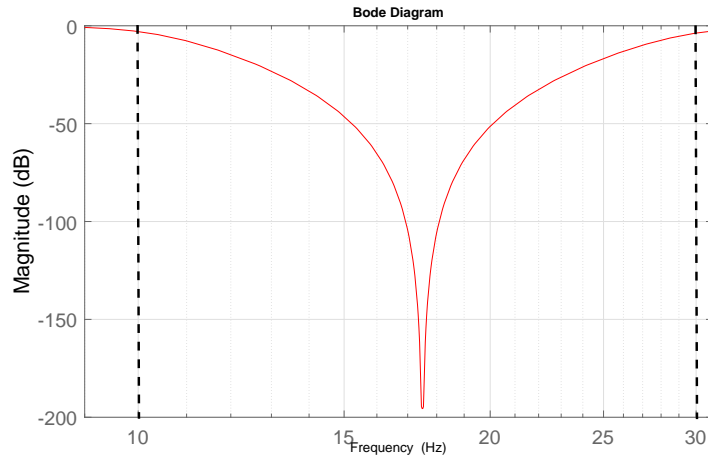


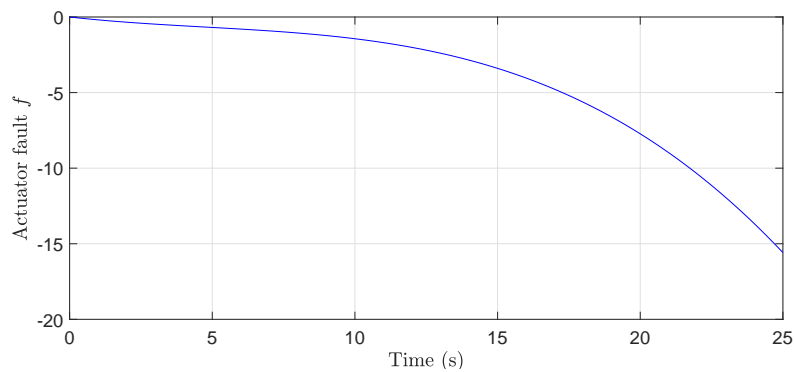
Figure 4.4: Output filter

chosen for observer design.

$$f = \sum_{i=1}^{n=3} \frac{(-0.21)^i}{i!} (t)^i. \quad (4.47)$$

Remark 4.4.1

The order n of the estimated fault \hat{f} chosen for observer synthesis must be equal to or greater than the real order of the fault f .

Figure 4.5: Actuator fault f

4.4.2 Frequency Analysis

In this part, the frequency behaviors of the two approaches in Section 4.3 are compared. by using Yalmip [Lofberg 2004] and Sedumi solver [Sturm 1999], the optimization problem in Theorems 1 and 2 is solved. Thus, the parametric matrices for observer designs in **Approach**

1 and **Approach 2** are synthesized. The attenuation level for UIs in both approaches are presented and compared in the Table 4.1:

Table 4.1: UI attenuation Comparison

	Approach 1	Approach 2
w_2	$\gamma_{23} = -6.990$ (dB)	Characteristics of filter Q
w_3		$\gamma_3 = -13.978$ (dB)

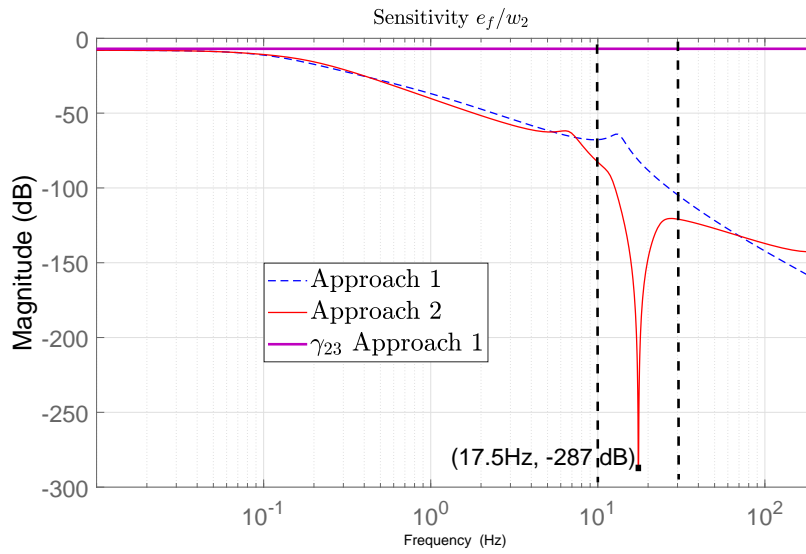
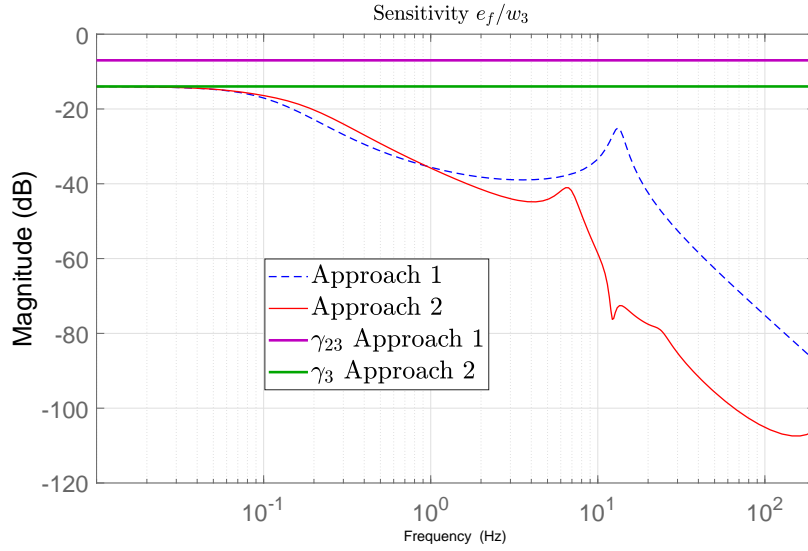


Figure 4.6: Sensitivity $|e_f/w_2|$

In Fig. 4.6, a sudden drop in frequency domain $[10, 30]$ (Hz) highlights the result of filter Q 's implementation as expected. According to Table 4.1, and Figs. 4.6 and 4.7, by relaxing the size of UI vector in \mathcal{H}_∞ synthesis, **Approach 2** gives better attenuation of UI influence on estimation error.

4.4.3 Test Conditions

- Simulation duration: 25 seconds.
- The UIs are defined as:
 - $w_1 = 5\sin(2\pi f_{w1})$ with $f_{w1} = 10$ (Hz);
 - $w_2 = 10\sin(2\pi f_{w2})$ with $f_{w2} = 17.5$ (Hz) to illustrates clearly the difference in both approaches;
 - $w_3 = 15\sin(2\pi f_{w3})$ with $f_{w3} = 35$ (Hz).

Figure 4.7: Sensitivity $|e_f/w_3|$

- Control input: is chosen as a sinusoidal signal:

$$u = 5\sin(2\pi t). \quad (4.48)$$

- Measurement noise is not considered in the output y .
- Initial condition: $x_{(0)} = [0.001 \ 0 \ 0.0020 \ 0]^T$, $x_{Q(0)} = 0$, and $\hat{x}_{(0)} = 0$.

4.4.4 Simulation results

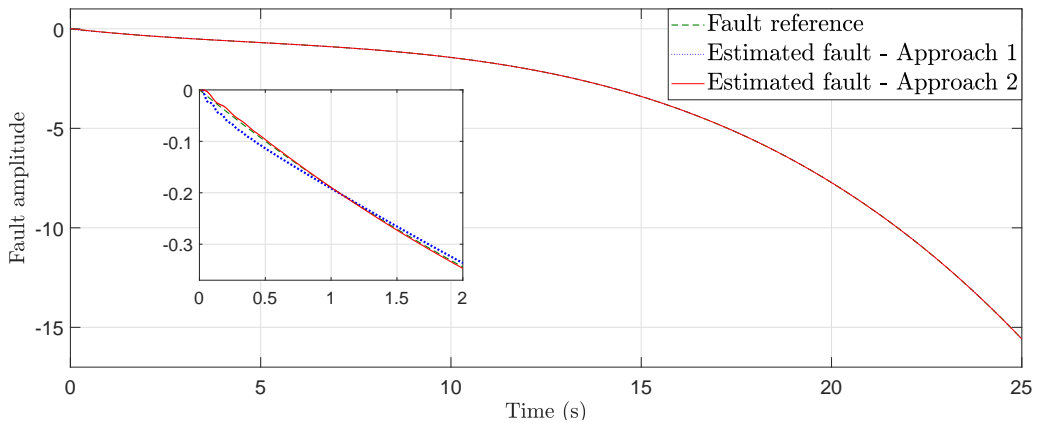
Figure 4.8: Fault estimation under influence of w_1

Fig. 4.8 illustrates the estimation of actuator fault under the existence of UIs, while Figs. 4.9-4.11 demonstrate the estimation error. As observed, all fault estimations are converging

to fault reference after about 10 seconds, i.e. the estimation error is towards 0. However, **Approach 1**, i.e. global \mathcal{H}_∞ attenuation method, is more likely to be affected by UIs w_2 and w_3 than **Approach 2** due to its poor frequency behavior as discussed in subsection 4.2.

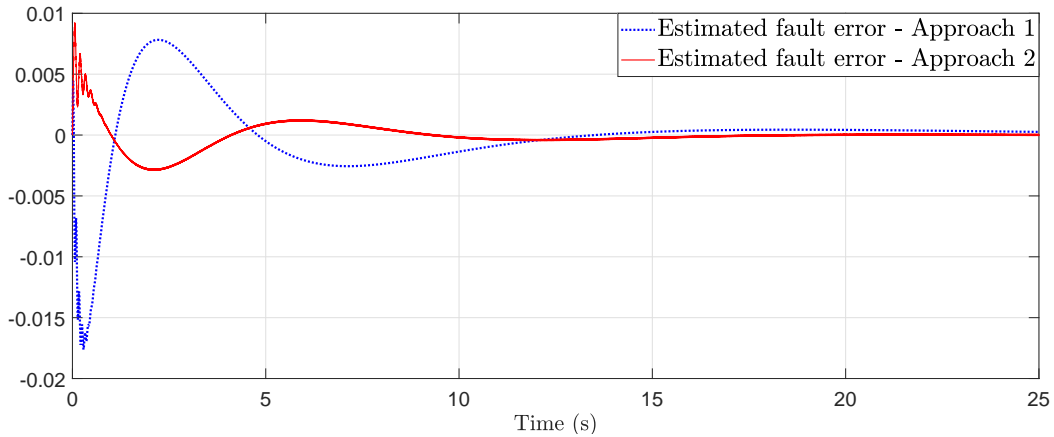


Figure 4.9: Estimation error under influence of w_1

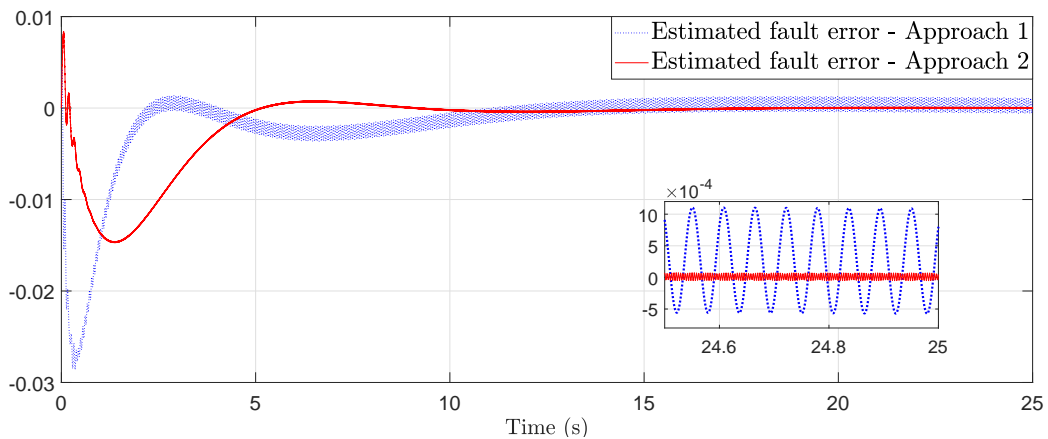


Figure 4.10: Estimation error under influence of w_1 and w_2

To evaluate the accuracy of estimation, the root-mean-square value (RMS) of estimation errors is calculated in Table 4.2. Results show that when there is only w_1 , the decoupling between the UI w_1 and fault estimation error e_f works correctly as designed in both cases. However, the difference starts to appear in the solutions coping with non-decoupled UIs, which proves the better performance of **Approach 2** in relaxing the amount of non-decoupled UIs implemented in \mathcal{H}_∞ synthesis by treating separately UIs w_2 and w_3 .

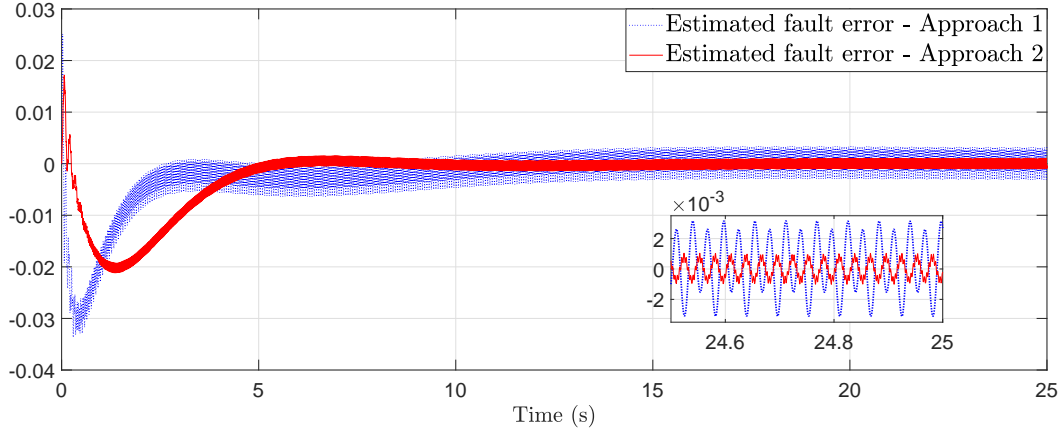
Figure 4.11: Fault error under influence of all UIs (w_1, w_2, w_3)

Table 4.2: RMS of estimation error

Scenarios	Approach 1	Approach 2
w_1	3.881e-4	2.070e-4
$[w_1, w_2]$	7.008e-4	2.045e-4
$[w_1, w_3]$	18.656e-4	5.952e-4
$[w_1, w_2, w_3]$	19.557e-4	5.941e-4

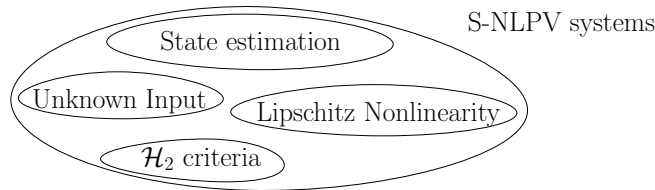
4.5 Conclusion

In this Chapter, based on the UI-decoupling condition and bandwidth of non-decoupled UIs, a generic strategy has been developed to estimate all kinds of actuator faults for the S-LTI system with partially decoupled UIs. The proposed solution handles not only the decoupled UI but also the non-decoupled UIs by two different approaches: the first one considers \mathcal{H}_∞ synthesis, while the other uses output frequency-shaping filter. The numerical comparison in fault estimation between the two solutions has highlighted the advantages of frequency-shaping filter over \mathcal{H}_∞ synthesis in UI attenuation.

On the other hand, the high-order of frequency-shaping filter can exceed the capability of computer in computation, especially when a large order " n " is chosen for the estimated fault. In addition, the measurement noise, which affects the accuracy of estimation in practice, has not been taken into account in observer designs yet.

\mathcal{H}_2 UI Observer for Singular Nonlinear Parameter-Varying System

Abstract: The main contribution of Chapter 5 is a generic design of Unknown Input (UI) observer based on \mathcal{H}_2 criteria for a general class of Singular Nonlinear Parameter-varying system (S-NLPV). Thanks to the strict LMI solution and its generic full-order form, the observer not only relaxes the existing parametrically dependent constraint of UI decoupling but also ensures the stability of estimation dynamics under the Lipschitz condition on nonlinearity. Finally, a numerical example is conducted to illustrate the advantages and drawbacks of the proposed design.



Contents

5.1 Introduction	134
5.1.1 State of the art	134
5.1.2 Chapter Contributions	136
5.2 Problem formulation	136
5.2.1 Case (a): $T_a = T$ and $N_a = N$ are parameter-independent matrices and $TD_{1(\rho)} = 0$	138
5.2.2 Case (b): $T_b = T_{(\rho)}$ and $N_b = N_{(\rho)}$ such that $T_{(\rho)}D_{1(\rho)} = 0$	139
5.2.3 Case (c) - Proposed method: $T_c = T_{(Z)}$ and $N_c = N_{(Z)}$ such that $T_{(Z)}D_{1(\rho)} \rightarrow 0$	140
5.3 Main Results - Observer design of Case (c)	142
5.4 Analytical Existence Condition for observer design	145
5.4.1 Impulse-free condition	146
5.4.2 R-detectability condition	146
5.5 Observer Implementation	146
5.5.1 Finite reformulation for Cost objective in Theorem 5.3.1	147
5.5.2 Algorithm for the grid-based solution	147
5.6 Illustration Example	148

5.6.1	Model Parameters	148
5.6.2	Frequency Analysis	150
5.6.3	Time-domain Simulation	151
5.7	Conclusion	153

5.1 Introduction

5.1.1 State of the art

Due to the existence of Unknown Input (UI) in the system process, the UI observer has been widely developed to take out the influence of UI while ensuring the capability of state estimation. Its application to the Singular Linear Parameter-varying (S-LPV) is especially important in both the research community and industry since a large class of nonlinear systems can be simply modeled under a linear structure with parameter-dependent distribution matrix, such as S-LPV model for an anaerobic bioreactor [López-Estrada et al. 2015b]. The design for this kind of observer can be split into two groups:

In the first one, UI is estimated based on certain assumptions on disturbance or the system output; thus, its impact is easily compensated in error dynamics. Notably, in [Aguilera-González et al. 2012], given slowly time-varying dynamics, the UI is rewritten as an augmented state and is estimated along with the system state by the Polytopic LPV Proportional-Integral (PI) observer. The same principle can also be applied to polynomial UIs with the implementation of the Proportional Multi-Integral observer, as proposed in [Koenig 2005] and [Zhang, Zhang, and Wang 2015]. In [Ichalal and Mammar 2015], a LPV UI observer with a special structure is derived from the output's derivatives, which are not always available. Although the above designs have justified their effectiveness in theoretical circumstances, their required conditions, such as slowly time-varying UI or high-order derivatives of output, are sometimes not practical for implementation.

In the second group, the structurally algebraic condition is used to eliminate the UI impact on state estimation error. First introduced in [Darouach, Zasadzinski, and Xu 1994], the constraint is, in fact, a multiplication of a designed matrix T in the observer and the system matrix D_1 corresponding to UI such that $TD_1 = 0$ (more details are discussed in Section 5.2). Thus, to satisfy this requirement, an UI PI observer is developed in [Hamdi et al. 2012], using the pseudo-inverse solution of algebraic condition to estimate the slow-varying fault. The same UI-decoupling method is presented in [Lopez-Estrada et al. 2014] to promote a polytopic observer for the uncertainty of the Time-Varying Parameter (TVP). Meanwhile, in [Rodrigues, Theilliol, and Sauter 2005], the algebraic condition for a polytopic UI observer is relaxed thanks to the approximation of D_1 based on Frobenius norm. Nevertheless, the above works are primarily focused on finding a matrix T such that $TD_1 = 0$, and only hold if the distribution matrix D_1 of UI is independent of TVP. Hence, many researchers have

intensively studied to provide an effective solution to the parameter-dependent case of $D_{1(\rho)}$. For instance, [Rodrigues et al. 2014] has incorporated the equality of UI-decoupling $TD_{1(\rho)} = 0$ for all TVPs into the polytopic adaptive observer. However, this new condition can lead to an unfeasible LMI solution. In [Ichalal et al. 2015; Marx et al. 2019], instead of using the common unique T for all values of $D_{1(\rho)}$, a polytopic LPV observer is proposed to calculate the parameter-dependent of T , i.e. $T_{(\rho)}$ and $T_{(\rho)}D_{1(\rho)} = 0$. Although the designed $T_{(\rho)}$ helps adapt the observer dynamics to the changes in UI matrix $D_{1(\rho)}$, the existence of its derivative in the dynamics of estimation error makes the design complicated with more assumptions required, such as the bounded derivatives of TVP. Consequently, there is a need for a simpler solution satisfying the algebraic condition for UI decoupling.

Briefly, it is clear that much additional work is needed before a complete solution for UI observer, especially for the case of $D_{1(\rho)}$ in the second group, can be reached. Hence, the Chapter will focus on the relaxation of UI-decoupling constraint in UI observer. In fact, there are two possibly applied solutions to this problem: \mathcal{H}_∞ and \mathcal{H}_2 approaches. However, \mathcal{H}_∞ method is focused on the transfer function between UI w and estimation error e through the the minimization of attenuation level γ_∞ , i.e. $\sup_{\rho \in \mathcal{P}_\rho, \|w\|_2 \neq 0, w \in \mathcal{L}_2} \frac{\|e\|_2}{\|w\|_2} \leq \gamma_\infty$, whereas the approach of \mathcal{H}_2 criteria tackles directly the term $T_{(\rho)}D_{1(\rho)}$ in the UI-decoupling condition $T_{(\rho)}D_{1(\rho)} = 0$. Therefore, concerning the UI observer, \mathcal{H}_2 -criteria solution is chosen to develop in this Chapter, where the term $T_{(\rho)}D_{1(\rho)}$ can be minimized through its induced 2-norm to obtain a zero approximation. Details are given in Section 5.2.3. On the other hand, the \mathcal{H}_∞ observer design will be presented in the Chapter 6.

In addition to UI, nonlinearity also poses a huge challenge to the stability of estimation error. In specific, the nonlinear behavior of the original system cannot be accurately demonstrated due to the nonlinear representation of time-varying parameters. Consequently, the development of nonlinear parameter varying (NLPV) systems, which can integrate the nonlinear parts into the classical non-singular LPV system, is of great importance, as well as its observer design. Notably, in [Boukroune, Aitouche, and Cocquempot 2015], a polytopic observer has been introduced for the NLPV model of diesel engines with once-differentiable nonlinearity. Meanwhile, in [Us Saqib et al. 2017] a \mathcal{H}_∞ output-feedback controller is suggested for the NLPV model. However, its major drawback is that the constraints in LMI optimization to handle Lipschitz condition can lead to an unfeasible solution. The issue is then solved in the study of [Abdullah and Qasem 2019] for a LPV functional observer whose solution is based on a special structure of parameter-dependent Lyapunov function. In [Pham, Sename, and Dugard 2019], the \mathcal{H}_∞ polytopic Luenberger-based observer has been presented for the NLPV model of the suspension system to estimate non-linear damper force under the influence of road disturbance. Unfortunately, all of the above works are only applicable to the non-singular system. Therefore, this Chapter will provide a new class of S-NLPV system which unifies the framework of both S-LPV and NLPV systems.

5.1.2 Chapter Contributions

The lack of studies tackling the nonlinear problem and the idea of designing a simpler UI observer for a wider class than S-LPV system have motivated the following contributions in this Chapter for the LPV framework:

- A new general class of singular NLPV system considering Lipschitz nonlinearity (S-NLPV) is introduced, which unifies all the so far existing kinds of LPV systems;
- A generic concept of \mathcal{H}_2 full-order UI observer design is developed for the S-NLPV system regardless of its LPV representation. In which, the parameter-dependent condition for UI-decoupling is relaxed by the minimization of \mathcal{H}_2 criteria while the stability of estimation error under the Lipschitz constraint is ensured thanks to a strict LMI solution. Also, the existence conditions for observer are analytically verified thanks to grid-based approach.

A numerical example will be illustrated to prove the performance of the observer design in the S-NLPV system.

The Chapter is organized as follows. Firstly, the representation of the S-NLPV system is presented in Section 5.2. Also, the UI observer is discussed through three cases (a)-(c), where Cases (a)-(b) present the existing problems and Case (c) introduces the methodology of the proposed design. Next, Section 5.3 demonstrates in detail the design process of the proposed UI observer, which decouples the estimation error from UI thanks to \mathcal{H}_2 criteria. Discussions on the existence conditions of the proposed observer are summarized in Section 5.4. Then, the implementation algorithm is examined in Section 5.5. Later, Section 5.6 illustrates a numerical example with the frequency analysis. Finally, the conclusion is provided in Section 5.7.

5.2 Problem formulation

Consider the following class of S-NLPV:

$$\begin{cases} E\dot{x} &= A_{(\rho)}x + B_{(\rho)}u + B_{\phi(\rho)}\phi(x, u) + D_{1(\rho)}w \\ y &= C_yx \end{cases} \quad (5.1)$$

In which,

- $x \in \mathbb{R}^{n_x}$ is the state vector; $y \in \mathbb{R}^{n_y}$ is the measurement output vector; $u \in \mathbb{R}^{n_u}$ is the input vector; and $w \in \mathbb{R}^{n_d}$ is the UI vector such that $\|w\|_2 \leq \bar{w}$.
- Matrices E and C_y are constant, while other distribution matrices are parameter-varying with appropriate dimensions.

- Time-varying measurable parameter ρ takes values in the parameter space \mathcal{P}_ρ :

$$\mathcal{P}_\rho = \{\rho = [\rho_1(t) \ \rho_2(t) \ \dots \ \rho_m(t)]^T \mid \underline{\rho}_i \leq \rho_i(t) \leq \bar{\rho}_i, \forall i = 1 : m, t \geq 0\}. \quad (5.2)$$

Remark 5.2.1

If the output y is perturbed by the UI w , i.e. $y = C_y x + D_2 w$, and $\text{rank } C_y > \text{rank } D_2$, the structure of system (5.1) can always be obtained by applying the output decomposition in Section 1.5.3.2. This structure is still correct even if the output depends on the time-varying parameter ρ , i.e. $y = C_{y(\rho)} x + D_{2(\rho)} w$ with the implementation of the output filter in Section 1.5.3.1.

Remark 5.2.2

If the input u exists in the output $y = C_y x + Du$, the calculation for a new output $y^* = y - Du = Cx$ is required in order to obtain the same formulation of (5.1).

The following assumptions are made in this Chapter:

- (A.1) Nonlinear term $\phi(x, u)$ with bounded u (due to saturation in practice) is a Lipschitz function that satisfies:

$$\|\tilde{\phi}\| = \|\phi(x, u) - \phi(\hat{x}, u)\| \leq \gamma \|x - \hat{x}\| \quad (5.3)$$

for all $x, \hat{x} \in \mathbb{R}^{n_x}$, where γ is a known Lipschitz constant and \hat{x} is the estimated of the state x .

- (A.2) S-NLPV system (5.1) is impulse-free and R-detectable $\forall \rho$, which is later analytically verified by the conditions discussed in Sections 5.4.1-5.4.2.

Under Assumptions (A.1)-(A.2), the UI NLPV observer, which is based on the generic form of full-order observer widely used in UI observer design, is proposed:

$$\begin{cases} \dot{\xi} &= F_{(\rho)} \xi + J_{(\rho)} u + L_{(\rho)} y + T_i B_{\phi(\rho)} \phi(\hat{x}, u) \\ \dot{\hat{x}} &= \xi + N_i y \end{cases}. \quad (5.4)$$

In which, the matrices $F_{(\rho)}$, $J_{(\rho)}$, $L_{(\rho)}$, T_i and N_i are computed such that:

- State estimation errors $e = x - \hat{x}$ converge towards 0 or at least in a bounded ball in the presence of w ;
- Matrices T_i and N_i have to ensure the constraint:

$$T_i E + N_i C_y = I, \quad (5.5)$$

where $i = \{a, b, c\}$ is the index of study cases. In which, Cases (a) and (b) determine the existing problems of UI observers, while Case (c) introduces the methodology of the proposed solution. Details are given in the following sections.

5.2.1 Case (a): $T_a = T$ and $N_a = N$ are parameter-independent matrices and $TD_{1(\rho)} = 0$

The state estimation error can be expressed as:

$$e = x - (\xi + Ny) = (I - NC_y)x - \xi = TE x - \xi, \quad (5.6)$$

Hence, from (5.1), (5.4) and (5.6), the error dynamics becomes:

$$\dot{e} = TE\dot{x} - \dot{\xi} \quad (5.7)$$

$$= TA_{(\rho)}x - F_{(\rho)}\xi - L_{(\rho)}y + (J_{(\rho)} - TB_{(\rho)})u + TB_{\phi(\rho)}\tilde{\phi} + TD_{1(\rho)}w \quad (5.8)$$

As $\xi = TE x - e$ and $y = C_y x$, it follows that:

$$\dot{e} = F_{(\rho)}e + TB_{\phi(\rho)}\tilde{\phi} + (J_{(\rho)} - TB_{(\rho)})u + (TA_{(\rho)} - F_{(\rho)}TE - L_{(\rho)}C_y)x + TD_{1(\rho)}w. \quad (5.9)$$

Then, from (5.5) and by defining the following algebraic constraints:

$$J_{(\rho)} - TB_{(\rho)} = 0, \quad (5.10)$$

$$TA_{(\rho)} - F_{(\rho)}TE - L_{(\rho)}C_y = 0, \quad (5.11)$$

$$K_{(\rho)} = -F_{(\rho)}N + L_{(\rho)}, \quad (5.12)$$

Also, since $TE + NC_y = I$, we obtain:

$$TA_{(\rho)} - F_{(\rho)}(I - NC_y) - L_{(\rho)}C_y = 0, \quad (5.13)$$

$$TA_{(\rho)} - F_{(\rho)} + (F_{(\rho)}N - L_{(\rho)})C_y = 0, \quad (5.14)$$

$$F_{(\rho)} = TA_{(\rho)} - K_{(\rho)}C_y. \quad (5.15)$$

Thus, the dynamics (5.9) can be rewritten as:

$$\dot{e} = F_{(\rho)}e + TB_{\phi(\rho)}\tilde{\phi} + TD_{1(\rho)}w. \quad (5.16)$$

Thanks to the condition $TD_{1(\rho)} = 0$, the estimation error e is perfectly decoupled from the impact of UI w , so the relation (5.16) becomes:

$$\dot{e} = F_{(\rho)}e + TB_{\phi(\rho)}\tilde{\phi}. \quad (5.17)$$

To design the matrices $F_{(\rho)}$, $J_{(\rho)}$, $L_{(\rho)}$, T and N , the following equality, derived from relations (5.5), (5.15) and $TD_{1(\rho)} = 0$, must have a feasible solution:

$$\underbrace{\begin{bmatrix} T & N & F_{(\rho)} & K_{(\rho)} \end{bmatrix}}_{\theta_{a(\rho)}} \underbrace{\begin{bmatrix} E & A_{(\rho)} & D_{1(\rho)} \\ C_y & 0 & 0 \\ 0 & -I & 0 \end{bmatrix}}_{\psi_a} = \underbrace{\begin{bmatrix} I & 0 & 0 \end{bmatrix}}_{\psi_a}, \quad (5.18)$$

The existence condition for the solution of (5.18) is that $\text{rank} \begin{bmatrix} \theta_{a(\rho)} \\ \psi_a \end{bmatrix} = \theta_{a(\rho)} \forall \rho$, or $\theta_{a(\rho)}$ is a matrix of full-column rank, i.e. $\text{rank} \theta_{a(\rho)} = 2n_x + n_w, \forall \rho$. This constraint is equivalent to the UI-decoupling condition (C.0):

$$(C.0) \quad \text{rank} \begin{bmatrix} E & D_{1(\rho)} \\ C_y & 0 \end{bmatrix} = n_x + n_w, \forall \rho \quad (5.19)$$

which is not always attainable. Additionally, suppose that the above condition is satisfied, its general solution is presented as:

$$[T \quad N \quad F_{(\rho)} \quad K_{(\rho)}] = \psi_a \theta_{a(\rho)}^\dagger + \bar{Z}_{(\rho)} (I - \theta_{a(\rho)} \theta_{a(\rho)}^\dagger), \quad (5.20)$$

where $\bar{Z}_{(\rho)}$ is a parameter-dependent arbitrary matrix. However, finding $\bar{Z}_{(\rho)}$ to ensure that matrices T and N are constant $\forall \rho$ is difficult.

Consequently, the solution for constant matrices T and N faces a tough challenge of handling directly parameter-dependent UI-decoupling condition. Thus, the approach for parameter-dependent $T_{(\rho)}$ and $N_{(\rho)}$ is developed in the next section - Case (b).

5.2.2 Case (b): $T_b = T_{(\rho)}$ and $N_b = N_{(\rho)}$ such that $T_{(\rho)} D_{1(\rho)} = 0$

In this approach, a parameter-dependent solution for both matrices $T_{(\rho)}$ and $N_{(\rho)}$ is assumed in order to avoid the problems of a constant solution mentioned in Case (a). However, this kind of representation makes the observer design more complicated with the existence of $\dot{T}_{(\rho)}$, i.e. derivative of $T_{(\rho)}$, in estimation dynamics. In specific, the estimation error $e = x - \hat{x}$ must be rewritten as:

$$e = T_{(\rho)} E x - \xi \quad (5.21)$$

$$\implies \dot{e} = T_{(\rho)} E \dot{x} + \dot{T}_{(\rho)} E x - \dot{\xi} \quad (5.22)$$

$$= \{T_{(\rho)} A_{(\rho)} x + \dot{T}_{(\rho)} E x - F_{(\rho)} \xi - L_{(\rho)} y\} \\ + (J_{(\rho)} - T_{(\rho)} B_{(\rho)}) u + T_{(\rho)} B_{\phi(\rho)} \tilde{\phi} + T_{(\rho)} D_{1(\rho)} w \quad (5.23)$$

$$\implies \dot{e} = F_{(\rho)} e + T B_{\phi(\rho)} \tilde{\phi} + (J_{(\rho)} - T B_{(\rho)}) u \\ + (T_{(\rho)} A_{(\rho)} + \dot{T}_{(\rho)} E - F_{(\rho)} T_{(\rho)} E - L_{(\rho)} C_y) x + T_{(\rho)} D_{1(\rho)} w. \quad (5.24)$$

To eliminate the impact of state x , input u and disturbance w , the following conditions are to be satisfied:

$$J_{(\rho)} - T B_{(\rho)} = 0, \quad (5.25)$$

$$T_{(\rho)} A_{(\rho)} + \dot{T}_{(\rho)} E - F_{(\rho)} T_{(\rho)} E - L_{(\rho)} C_y = 0, \quad (5.26)$$

$$T_{(\rho)} D_{1(\rho)} = 0. \quad (5.27)$$

Additionally, concerning the constraint $K_{(\rho)} = -F_{(\rho)} N + L_{(\rho)}$, the relation (5.26) can be rewritten as:

$$F_{(\rho)} = T A_{(\rho)} - K_{(\rho)} C_y + \dot{T}_{(\rho)} E. \quad (5.28)$$

Unlike Case (a) where $\dot{T} = 0$, Case (b) requires the following equality to find the matrices $T_{(\rho)}$ and $N_{(\rho)}$:

$$[T_{(\rho)} \quad N_{(\rho)}] \underbrace{\begin{bmatrix} E & D_{1(\rho)} \\ C_y & 0 \end{bmatrix}}_{\theta_{b(\rho)}} = \underbrace{[I \quad 0]}_{\psi_b}, \quad (5.29)$$

Under the condition (C.0), $\text{rank} \begin{bmatrix} \theta_{b(\rho)} \\ \psi_b \end{bmatrix} = \theta_{b(\rho)} \forall \rho$; thus, general solution for $T_{(\rho)}$ and $N_{(\rho)}$ is expressed as below:

$$[T_{(\rho)} \quad N_{(\rho)}] = \psi_b \theta_{b(\rho)}^\dagger + \bar{Z}_{(\rho)} (I - \theta_{b(\rho)} \theta_{b(\rho)}^\dagger), \quad (5.30)$$

However, although the usage of $T_{(\rho)}$ and $N_{(\rho)}$ can ensure the decoupling for parameter-dependent UI matrix $D_{1(\rho)} \forall \rho$, their calculation is difficult, especially in case where $D_{1(\rho)}$ has the complicated structure and high dimension. Moreover, due to the incorporation of $\dot{T}_{(\rho)}$ in (5.24) and (5.28), the solutions to these functions demand highly exclusive assumptions and system reformulation. A notable case is illustrated in [Marx et al. 2019] where $E = I$, $\bar{Z}_{(\rho)} = 0$ and $\phi(x, u) = 0$.

In brief, the above problems in two Cases (a) and (b) have necessitated the development of an UI observer that ensures not only the simple time-invariant formulation of matrices T and N in Section 5.2.1 to bypass the derivatives $\dot{T}_{(\rho)}$ in Section 5.2.2 but also the UI decoupling condition $\forall \rho$. As a result, the methodology of the proposed method will be discussed in Case (c).

5.2.3 Case (c) - Proposed method: $T_c = T_{(Z)}$ and $N_c = N_{(Z)}$ such that $T_{(Z)} D_{1(\rho)} \rightarrow 0$.

In this case, the matrices $T_{(Z)}$ and $N_{(Z)}$ are represented by a time-invariant matrix Z , which is later defined in Section 5.3. Accordingly, not only is the impact of the derivative $\dot{T}_{(Z)}$ on estimation error eliminated, but the freedom/flexibility in the observer design is also ensured with the help of Z .

Thanks to the time-invariant characteristics, the dynamics of estimation error can be derived similarly to that in Case (a):

$$\dot{e} = F_{(\rho)} e + T B_{\phi(\rho)} \tilde{\phi} + T_{(Z)} D_{1(\rho)} w, \quad (5.31)$$

where

$$J_{(\rho)} = T_{(Z)} B_{(\rho)}, \quad (5.32)$$

$$K_{(\rho)} = -F_{(\rho)} N_{(Z)} + L_{(\rho)}, \quad (5.33)$$

$$F_{(\rho)} = T_{(Z)} A_{(\rho)} - K_{(\rho)} C_y. \quad (5.34)$$

Based on \mathcal{H}_2 optimization or Minimization of Maximal Eigenvalue, the proposed method does not aim for a perfect UI-decoupling in the classical UI observer design of Cases (a) and (b), but instead seek an approximation of the UI-decoupling constraint, i.e. the term $T_{(Z)}D_{1(\rho)}$ has to be as small as possible towards 0 :

$$T_{(Z)}D_{1(\rho)} \rightarrow 0, \quad (5.35)$$

which is achieved by the minimization of:

$$(O.1) \quad \min_{T_{(Z)}, N_{(Z)}, K_{(\rho)}} \|T_{(Z)}D_{1(\rho)}\|_2^2, \quad (5.36)$$

where $\|X\|_2$ is the induced 2-norm of matrix $X = TD_{1(\rho)}$. Indeed, since $\|X\|_2 = \bar{\sigma}(X)$ the largest singular value of X , the equality constraint of UI decoupling is now approximately satisfied thanks to the optimization in the new objective (O.1).

Under Assumptions (A.1)-(A.2), the proposed observer (5.4) for system (5.1) is rewritten as:

$$\begin{cases} \dot{\xi} &= F_{(\rho)}\xi + J_{(\rho)}u + L_{(\rho)}y + T_{(Z)}B_{\phi(\rho)}\phi(\hat{x}, u) \\ \hat{x} &= \xi + N_{(Z)}y \end{cases}, \quad (5.37)$$

whose objectives are now defined as:

(O.1) Finding a time-invariant matrix Z such that:

$$\min_{T_{(Z)}, N_{(Z)}, K_{(\rho)}} \|T_{(Z)}D_{1(\rho)}\|_2^2. \quad (5.38)$$

(O.2) When UI $w = 0$, the dynamics of estimation error e , reduced from (5.31), i.e.

$$\dot{e} = F_{(\rho)}e + T_{(Z)}B_{\phi(\rho)}\tilde{\phi}, \quad (5.39)$$

is exponentially stable under the Lipschitz constraint.

The relation between S-NLPV system (5.1) and its observer (5.37) is illustrated in Fig. 5.1.

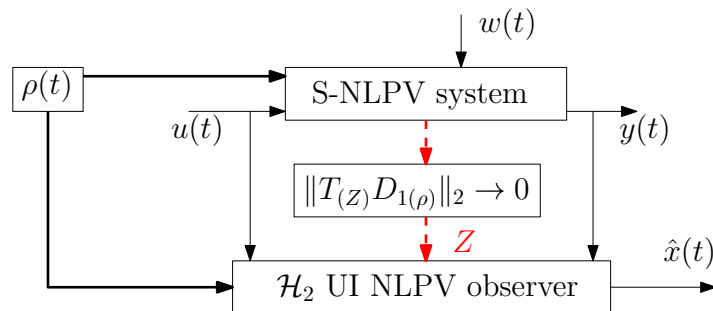


Figure 5.1: Implementation scheme of \mathcal{H}_2 UI NLPV observer

In the next section, details on how to define the matrix Z and to design the observer (5.37) satisfying the objectives (O.1)-(O.2) are demonstrated. In fact, this generic design for UI observer is also the main contribution of this Chapter.

5.3 Main Results - Observer design of Case (c)

In this section, the UI NLPV observer based on the methodology in Case (c) - Section 5.2.3 is developed as follows.

As easily observed, the matrices T and N , as well as the matrix $K_{(\rho)}$, play important roles in the optimization for UI-decoupling problem (O.1). To simplify the design process, the relation between matrices T and N is rewritten as:

$$\begin{bmatrix} T_{(Z)} & N_{(Z)} \end{bmatrix} \begin{bmatrix} E \\ C_y \end{bmatrix} = I. \quad (5.40)$$

If $\text{rank} \begin{bmatrix} E \\ C_y \end{bmatrix} = n_x$, which is also the impulse-free condition, the general solution of (5.40) is given by:

$$\begin{bmatrix} T_{(Z)} & N_{(Z)} \end{bmatrix} = \begin{bmatrix} E \\ C_y \end{bmatrix}^\dagger - Z \left(I - \begin{bmatrix} E \\ C_y \end{bmatrix} \begin{bmatrix} E \\ C_y \end{bmatrix}^\dagger \right), \quad (5.41)$$

where Z is a constant matrix which is later synthesized in Theorem 5.3.1. Thus, the matrices T and N can be calculated by:

$$\begin{cases} T_{(Z)} = T_1 - ZT_2, \\ N_{(Z)} = N_1 - ZN_2, \end{cases} \quad (5.42)$$

where: $T_1 = \begin{bmatrix} E \\ C_y \end{bmatrix}^\dagger \delta_T$, $T_2 = \left(I - \begin{bmatrix} E \\ C_y \end{bmatrix} \begin{bmatrix} E \\ C_y \end{bmatrix}^\dagger \right) \delta_T$, $N_1 = \begin{bmatrix} E \\ C_y \end{bmatrix}^\dagger \delta_N$, $N_2 = \left(I - \begin{bmatrix} E \\ C_y \end{bmatrix} \begin{bmatrix} E \\ C_y \end{bmatrix}^\dagger \right) \delta_N$, $\delta_T = \begin{bmatrix} I \\ 0 \end{bmatrix}$, and $\delta_N = \begin{bmatrix} 0 \\ I \end{bmatrix}$.

Remark 5.3.1

In some studies such as [Hamdi et al. 2012; Rodrigues et al. 2014], the matrix $Z = 0$ is chosen for $T_{(Z)}$ and $N_{(Z)}$ since the beginning of observer design process, consequently $T_{(Z)} = T_1$ and $N_{(Z)} = N_1$. However, this selection leads to non-optimal solutions of Objective (O.1) as it fixes the values of $T_{(Z)}D_{1(\rho)}$.

In addition, it also yields that:

$$\begin{aligned} F_{(\rho)} &= T_1 A_{(\rho)} - ZT_2 A_{(\rho)} - K_{(\rho)} C_y, \\ &= T_1 A_{(\rho^j)} - [Z \quad K_{(\rho^j)}] \begin{bmatrix} T_2 A_{(\rho^j)} \\ C_y \end{bmatrix}, \end{aligned} \quad (5.43)$$

$$B_{e(\rho)} = T_{(Z)} B_{\phi(\rho)} = T_1 B_{\phi(\rho)} - ZT_2 B_{\phi(\rho)} \quad (5.44)$$

Since the matrices $T_{(Z)}$ and $N_{(Z)}$ are now represented by the matrix Z , the aim of the proposed observer design is to find the pair $(Z, K_{(\rho)})$, whose solutions are presented in the following Theorem, such that the objectives (O.1) and (O.2) are accomplished.

Theorem 5.3.1

Under Assumptions (A.1)-(A.2), the design objectives (O.1)-(O.2) are achieved if there exist symmetric positive definite matrices $P \geq I_{n_x}$, matrix Y_1 , matrix $Y_{2(\rho)}$, and positive scalar ϵ such that:

$$\begin{aligned} \min_{Y_1, Y_{2(\rho)}} J(\rho) &= \text{Tr}(\Omega_{13(\rho)}^T \Omega_{13(\rho)}), \\ \text{s.t. } \begin{bmatrix} \Omega_{11(\rho)} + \eta & \Omega_{12(\rho)} \\ (*) & -\epsilon I \end{bmatrix} &< 0, \end{aligned} \quad (5.45)$$

where

$$\Omega_{11(\rho)} = \mathcal{H}\{PT_1A(\rho) + Y_1T_2A(\rho) + Y_{2(\rho)}C_y\}, \quad (5.46)$$

$$\Omega_{12(\rho)} = PT_1B_{\phi(\rho)} + Y_1T_2B_{\phi(\rho)}, \quad (5.47)$$

$$\Omega_{13(\rho)} = PT_1D_{1(\rho)} + Y_1T_2D_{1(\rho)}, \quad (5.48)$$

$$\eta = \epsilon(\gamma I)^T(\gamma I), \quad (5.49)$$

then the matrices Z and $K(\rho)$ are calculated by: $Z = -P^{-1}Y_1$, $K(\rho) = -P^{-1}Y_{2(\rho)}$. Also, the estimation error is exponentially stable, i.e.

$$\|e\|_2 \leq \sqrt{\underline{\beta}^{-1}V_{(e(0))}} \exp(-\frac{1}{2}\delta\bar{\beta}^{-1}t), \quad (5.50)$$

where $V_{e(t)} = e(t)^T P e(t)$ is Lyapunov function, $\underline{\beta} = \underline{\sigma}(P)$, $\bar{\beta} = \bar{\sigma}(P)$, and δ is a positive scalar.

Proof: The proof is decomposed into 2 parts corresponding to two design objectives (O.1)-(O.2) mentioned in Section 5.2.3:

Firstly, to satisfy the objective (O.2), a LMI condition for the stability of estimation error (5.39) must be found by choosing the Lyapunov function:

$$V = e^T P e, \quad (5.51)$$

with $P > 0$ and $\dot{V} < 0$.

Remark 5.3.2

Since the matrix P in Lyapunov function is chosen to be independent of time-varying parameter ρ , finding the constant matrix $Y_1 = -PZ$ ensures that the matrix Z , as well as the matrices T and N , does not depend on ρ .

From the Lyapunov function, it follows that:

$$\dot{V} = \mathcal{H}\{e^T P \dot{e}\} \quad (5.52)$$

$$= \mathcal{H}\{e^T P F(\rho)e + e^T P B_{e(\rho)}\tilde{\phi}\} \quad (5.53)$$

Using Eq. (5.39), we obtain:

$$\dot{V} = \Upsilon^T \begin{bmatrix} \Omega_{11(\rho)} & \Omega_{12(\rho)} \\ (*) & 0 \end{bmatrix} \Upsilon = \Upsilon^T \Omega(\rho) \Upsilon < 0, \quad (5.54)$$

where $\Upsilon = [e^T \quad \tilde{\phi}^T]^T$.

Also, the Lipschitz condition (5.3) yields the constraint:

$$\|\tilde{\phi}\| \leq \gamma \|e\| \Rightarrow (\tilde{\phi})^T(\tilde{\phi}) - e^T(\gamma I)^T(\gamma I)e \leq 0, \quad (5.55)$$

which is equivalent to:

$$J_\epsilon = \epsilon((\tilde{\phi})^T(\tilde{\phi}) - e^T(\gamma I)^T(\gamma I)e) \leq 0, \quad (5.56)$$

for a small scalar $\epsilon > 0$.

Since $J_\epsilon \leq 0$, the derivative of Lyapunov function \dot{V} can be majorized by the following inequality:

$$\dot{V} \leq \dot{V} - J_\epsilon \quad (5.57)$$

Hence $\dot{V} < 0$ if:

$$\dot{V} - J_\epsilon < 0, \quad (5.58)$$

$$\Leftrightarrow \Upsilon^T \Omega_{(\rho)} \Upsilon - \epsilon(\tilde{\phi})^T(\tilde{\phi}) + \epsilon e^T(\gamma I)^T(\gamma I)e < 0, \quad (5.59)$$

$$\Leftrightarrow \Upsilon^T \begin{bmatrix} \Omega_{11(\rho)} + \eta & \Omega_{12(\rho)} \\ (*) & -\epsilon I \end{bmatrix} \Upsilon < 0, \quad (5.60)$$

which is equivalent to the following LMI $\forall \Upsilon \neq 0$:

$$\mathcal{X}_{(\rho)} = \begin{bmatrix} \Omega_{11(\rho)} + \eta & \Omega_{12(\rho)} \\ (*) & -\epsilon I \end{bmatrix} < 0. \quad (5.61)$$

Since $\mathcal{X}_{(\rho)} < 0$, there always exists a scalar $\delta > 0$ such that $\forall \rho$:

$$\mathcal{X}_{(\rho)} < -\delta I \quad (5.62)$$

It follows that:

$$-\dot{V} \geq \Upsilon^T(-\mathcal{X}_{(\rho)})\Upsilon > \Upsilon^T \delta I \Upsilon, \quad (5.63)$$

$$\Rightarrow -\dot{V} > e^T \delta e + \underbrace{\tilde{\phi}^T \delta \tilde{\phi}}_{\geq 0} > \delta \|e\|_2^2. \quad (5.64)$$

Meanwhile, $V = e^T P e \leq \bar{\beta} \|e\|_2^2 \Rightarrow \|e\|_2^2 \geq \bar{\beta}^{-1} V$, it yields that:

$$-\dot{V} > \delta \|e\|_2^2 \geq \delta \bar{\beta}^{-1} V, \quad (5.65)$$

$$\Rightarrow \dot{V}_{(e(t))} < -\delta \bar{\beta}^{-1} V_{(e(t))}, \quad (5.66)$$

$$\Rightarrow V_{(e(t))} < \exp(-\delta \bar{\beta}^{-1} t) V_{(e(0))}, \quad (5.67)$$

Since $\underline{\beta} \|e(t)\|_2^2 \leq V_{(e(t))}$, the boundary of estimation error (5.50) is deduced. That completes the requirement in synthesis for objective (O.2).

Secondly, there is a need to reformulate the objective (O.1) so that it can be optimized by matrices P , Y_1 and $Y_{2(\rho)}$ which are implied from the above LMI solution. Moreover, directly solving the minimization (O.1) is not easy in practice (programming in Matlab), so one of the methods is to minimize the boundness of $\|X\|_2$ (with $X = T_{(Z)} D_{1(\rho)}$) by the Frobenius norm $\|X\|_F$, which is more easily expressed. In specific,

$$\|X\|_2 \leq \|X\|_F = \sqrt{\text{Tr}(X^T X)} \quad (5.68)$$

Consequently, the objective (O.1) is bounded by the following optimization:

$$\min_{T_{(Z)}, N_{(Z)}, K_{(\rho)}} Tr((T_{(Z)}D_{1(\rho)})^T(T_{(Z)}D_{1(\rho)})). \quad (5.69)$$

To integrate the LMI solution in the above optimization, the condition $P \geq I_{n_x}$ is restrictively required, such that

$$P^T P \geq I_{n_x} \quad (5.70)$$

Consequently,

$$(T_{(Z)}D_{1(\rho)})^T I_{n_x} (T_{(Z)}D_{1(\rho)}) \leq (T_{(Z)}D_{1(\rho)})^T P^T P (T_{(Z)}D_{1(\rho)}). \quad (5.71)$$

In other words, with $T_{(Z)} = T_1 - ZT_2$,

$$Tr((T_{(Z)}D_{1(\rho)})^T(T_{(Z)}D_{1(\rho)})) \leq \underbrace{Tr((\Omega_{13(\rho)}^T \Omega_{13(\rho)})}_{J_{(\rho)}}). \quad (5.72)$$

Therefore, under the constraint $P \geq I_{n_x}$, the objective (O.1) is bounded by the objective:

$$\min_{P, Y_1, Y_{2(\rho)}} J_{(\rho)} = Tr((\Omega_{13(\rho)}^T \Omega_{13(\rho)}). \quad (5.73)$$

Combining the two above parts, the proof of Theorem 5.3.1 is completed. ■

After obtaining the matrices Z and $K_{(\rho)}$ from Theorem 5.3.1, the matrices T and N , matrix $J_{(\rho)}$ are then calculated by (5.42) and (5.32), while Eqs. (5.34) and (5.33) respectively implies the matrices $F_{(\rho)}$ and $L_{(\rho)}$.

In Theorem 5.3.1, since the matrix $Y_{2(\rho)}$ depends on the values of parameter-varying vector ρ , an effective solution to tackle the LMI (5.45) is required. Thus, the gridding-based approach (see Section 1.3.2) is proposed, which is applicable to any representation of NLPV system (5.1). Details on implementation algorithms will be given in Section 5.5. Meanwhile, the existence conditions of the proposed observer can be analytically verified by this approach in Section 5.4.

5.4 Analytical Existence Condition for observer design

In grid-based approach, the parameter space is divided in the form of a grid that is defined by the number of gridding points $n_g^{\rho^i}$. At each time-frozen point ρ^j ($j = 1 : N_g$, $N_g = n_g^{\rho^1} \times n_g^{\rho^2} \times \dots \times n_g^{\rho^m}$), i.e. the coordinates in the grid, the (singular) LPV system (under Lipschitz condition) is considered as (singular) linear time-invariant (LTI) system [Apkarian, Gahinet, and Becker 1995]. Therefore, the existence conditions for the observer design can be analytically derived from Assumption (A.2) for each point ρ^j in the grid. Details are given in Sections 5.4.1 and 5.4.2.

Remark 5.4.1

¹ If the polytopic representation is possibly available for the S-NLPV system (5.1), all the

results mentioned later in Sections 5.4.1-5.4.2 and 5.5 can be implemented for each corner of the polytope.

5.4.1 Impulse-free condition

As mentioned in (5.40), the requirement for the existence of $T_{(Z)}$ and $N_{(Z)}$ is the impulse-free condition (C.1), which is independent of time-varying parameter ρ :

$$(C.1) \quad \text{rank} \begin{bmatrix} E \\ C_y \end{bmatrix} = n_x. \quad (5.74)$$

5.4.2 R-detectability condition

The feasibility of Theorem 5.3.1 implies that $F_{(\rho^j)}$ is Hurwitz for each time-frozen ρ^j . In other words, there exists a matrix gain $[Z \ K_{(\rho^j)}]$ such that $F_{(\rho^j)}$ is stable if and only if the pair $(T_1 A_{(\rho^j)}, \begin{bmatrix} T_2 A_{(\rho^j)} \\ C_y \end{bmatrix})$ is R-detectable since $F_{(\rho^j)} = T_1 A_{(\rho^j)} - [Z \ K_{(\rho^j)}] \begin{bmatrix} T_2 A_{(\rho^j)} \\ C_y \end{bmatrix}$.

Also, the R-detectability condition of $(T_1 A_{(\rho^j)}, \begin{bmatrix} T_2 A_{(\rho^j)} \\ C_y \end{bmatrix})$ is equivalent to the condition (C.2):

$$(C.2) \quad \text{rank} \begin{bmatrix} pE - A_{(\rho^j)} \\ C_y \end{bmatrix} = n_x, \forall j = 1 : N_g, \mathcal{R}(p) \geq 0. \quad (5.75)$$

Proof: The proof is presented in Appendix B.2. ■

It should be noted that the condition (C.2) is only an analytically necessary condition implied for the R-detectability of the S-NLPV system at each time-frozen point ρ^j in the context of the grid-based approach.

5.5 Observer Implementation

In order to apply the grid-based solution to Theorem 5.3.1, besides rewriting the infinite LMI (5.45) as a set of finite LMIs, the infinite cost criteria $J_{(\rho)}$ also needs to be reformulated as a finite one, which is the combination of costs at each time-frozen point ρ^j . Details for this reformulation will be presented in Section 5.5.1. Then, the implementation algorithms are demonstrated in Section 5.5.2

5.5.1 Finite reformulation for Cost objective in Theorem 5.3.1

Regarding Theorem 5.3.1, the cost $J_{(\rho)}$ is expressed by:

$$J_{(\rho)} = \text{Tr}(\Omega_{13(\rho)}^T \Omega_{13(\rho)}), \quad (5.76)$$

where $\Omega_{13(\rho)} = PT_1D_{1(\rho)} + Y_1T_2D_{1(\rho)}$. Hence, the cost for each time-frozen point ρ^j is implied:

$$J_{(\rho^j)} = \text{Tr}(\Omega_{13(\rho^j)}^T \Omega_{13(\rho^j)}), \forall j = 1 : N_g, \quad (5.77)$$

where $\Omega_{13(\rho^j)} = PT_1D_{1(\rho^j)} + Y_1T_2D_{1(\rho^j)}$.

Since $\|TD_{1(\rho^j)}\|_2 \leq J_{(\rho^j)}$, the minimization of $J_{(\rho^j)}$ will also minimize the largest singular of $TD_{1(\rho)}$ at each time-frozen points. Thus, the following cost J_{total} is chosen to obtain the smallest $J_{(\rho^j)}$ as possible:

$$J_{total} = \sum_{j=1}^{N_g} \lambda_j J_{(\rho^j)}. \quad (5.78)$$

In which, $\lambda_j \forall j = 1 : N_g$ is the weighting coefficient indicating the importance of each $J_{(\rho^j)}$ such that $\sum_{j=1}^{N_g} \lambda_j = 1$. By minimizing J_{total} , the value of $J_{(\rho^j)}$ will also be optimized according to coefficients λ_j . When $\lambda_j = \frac{1}{N_g}$, the minimization for $J_{(\rho^j)}$ at each point ρ^j is handled equally. Therefore, this finite cost J_{total} will be considered as an approximation for the initial cost $J_{(\rho)}$ in grid-based solution.

5.5.2 Algorithm for the grid-based solution

The algorithms for the implementation of the proposed method is summarized into two steps:

Step 1: Offline Synthesis

- Define the gridding points for TVP vector ρ ; accordingly, a total of N_g time-frozen points ρ^j ($j = 1 : N_g$) is to be obtained.
- Conduct the gridding-based synthesis: for $j = 1 : N_g$
 - Verify the impulse-free and R-detectability conditions (C.1) and (C.2). If the conditions are satisfied, continue to the next step; otherwise, stop the algorithm.
 - Define the distribution matrices $A_{(\rho^j)}$, $B_{\phi(\rho^j)}$, and $D_{1(\rho^j)}$ corresponding to ρ^j , as well as the matrices C_y , T_1 , T_2 and Lipschitz constant γ .
 - Declare the matrices P , Y_1 and Y_{2k} that define the basis function of $Y_{2(\rho)}$, for example 2^{nd} -order polynomial $Y_{2(\rho)} = Y_{20} + (\rho)Y_{21} + (\rho)^2Y_{22} = \sum_{k=0}^2 \rho^k Y_{2k}$.

- Define the set of LMIs and the cost objective J_{total} which represent Theorem 5.3.1, i.e.

$$\begin{aligned} \min_{Y_1, Y_2(\rho^j)} J_{total} &= \sum_{j=1}^{N_g} \frac{1}{N_g} Tr(\Omega_{13(\rho^j)}^T \Omega_{13(\rho^j)}), \\ s. t. \quad &\begin{bmatrix} \Omega_{11(\rho^j)} + \eta & \Omega_{12(\rho^j)} \\ (*) & -\epsilon I \end{bmatrix} < 0, \end{aligned} \quad (5.79)$$

where $\Omega_{11(\rho^j)} = \mathcal{H}\{PT_1A_{(\rho^j)} + Y_1T_2A_{(\rho^j)} + Y_2(\rho^j)C_y\}$, $\Omega_{12(\rho^j)} = PT_1B_{\phi(\rho^j)} + Y_1T_2B_{\phi(\rho^j)}$, $\Omega_{13(\rho^j)} = PT_1D_{1(\rho^j)} + Y_1T_2D_{1(\rho^j)}$, $\eta = \epsilon(\gamma I)^T(\gamma I)$.

- Compute the constant matrices $P > I_{n_x}$, Y_1 , and element matrix Y_{2k} such that all the above LMIs are satisfied.
- Calculate the time-invariant matrices: $Z = -P^{-1}Y_1$, $T_{(Z)} = T_1 - ZT_2$, and $N_{(Z)} = N_1 - ZN_2$.

Step 2: Online Implementation

- For instant t , update the value of TVP vector $\rho(t)$.
- Compute the matrix $Y_{2(\rho(t))}$ defined by $\rho(t)$ and the known matrices Y_{2k} .
- Calculate the time-varying parameter-dependent observer matrices:

$$K_{(\rho(t))} = -P^{-1}Y_{2(\rho(t))}, \quad (5.80)$$

$$J_{(\rho(t))} = T_{(Z)}B_{(\rho)}, \quad (5.81)$$

$$F_{(\rho(t))} = T_{(Z)}A_{(\rho)} - K_{(\rho)}C_y, \quad (5.82)$$

$$L_{(\rho(t))} = K_{(\rho)} + F_{(\rho)}N_{(Z)}. \quad (5.83)$$

That completes the algorithms for the NLPV \mathcal{H}_2 UI observer design.

5.6 Illustration Example

In order to highlight the performance of the proposed UI observer, a numerical example is demonstrated as below.

5.6.1 Model Parameters

Consider the system:

$$\begin{cases} E\dot{x} &= A_{(\rho)}x + Bu + B_{\phi} \sin(Gx)u + D_{1(\rho)}w, \\ y &= C_yx \end{cases}, \quad (5.84)$$

- Varying-parameter ρ is defined as: $\rho = 0.25\sin(8t) + 0.75$, so $0.5 \leq \rho \leq 1$.
- System parameters are chosen as follows:

$$E = \begin{bmatrix} 1 & 0 & 0 \\ 0 & 1 & 0 \\ 0 & 0 & 0 \end{bmatrix}, A_{(\rho)} = \begin{bmatrix} -5 + \rho & 1 & 1 \\ 0 & -5 & 0 \\ 0.5 & 0 & -1 \end{bmatrix}, B = \begin{bmatrix} 0 \\ 0.2 \\ 0.5 \end{bmatrix}, B_\phi = \begin{bmatrix} 0 \\ 0.2 \\ 0 \end{bmatrix}, C_y = [1 \quad 1 \quad -0.05],$$

$$D_{1(\rho)} = \begin{bmatrix} 0.5\rho \\ 0.1\rho \\ 0 \end{bmatrix}, \text{ and } G = [0 \quad 0 \quad 1].$$

- Control input u is bounded in the region $|u| \leq u_0 = 5$, which leads to the Lipschitz condition:

$$\|\phi(x, u) - \phi(\hat{x}, u)\| \leq u_0 G \|x - \hat{x}\|, \quad (5.85)$$

where $\phi(x, u) = \sin(Gx)u$ and $\gamma = u_0 G$.

- Time-domain simulation: 10 seconds.
- UI vector is defined as:

$$w = \sin(4\pi t), \quad (5.86)$$

so its \mathcal{L}_2 is bounded by $\bar{w} = 1$.

- Control input: $u = u_0 \sin(8\pi t)$.
- Measurement noise is not considered in the output.
- Initial condition: $x_1(0) = x_2(0) = 0$, so (5.84) $\implies x_3(0) = 0.5x_1(0) + 0.5u(0) = 0$; and $\hat{x}(0) = [-0.2 \quad 0.1 \quad -2]^T$.

Since the perfect UI-decoupling condition (C.0) cannot be satisfied, the methodologies discussed in Cases (a) and (b) of Section 5.2 are not applicable to this simulation example. Meanwhile, the proposed method in Case (c) is regarded as a workable alternative because only the fulfillment of basic requirements for the singular system, i.e. impulse-free condition (C.1) and the R-detectability (C.2), is demanded.

To solve Theorem 5.3.1, the gridding-based methodology is applied, in which: $n_g^\rho = N_g = 20$ points (the number of TVPs $m = 1$); $\lambda_j = \frac{1}{N_g}$; and 2^{nd} -order basis function that is proposed by [Abbas et al. 2014], i.e.

$$Y_{2(\rho)} = Y_{20} + \rho Y_{21} + \rho^2 Y_{22} = \sum_{k=0}^2 \rho^k Y_{2k}, \quad (5.87)$$

Also, the above choices define a set of N_g LMIs corresponding to the inequality (5.45) at each time-frozen points ρ^j . With the implementation of Yalmip toolbox [Lofberg 2004], sdpt3 solver [Toh, Todd, and Tütüncü 1999] and the above approach, Theorem1 can be tackled simply by finding constant matrices $P > 0$, Y_1 and Y_{2k} ($k = 0 : 2$).

5.6.2 Frequency Analysis

In this section, the performance of proposed observer design is evaluated in frequency domain. The sensitivity ρ^j in the following Bode diagrams represents the frequency response at each time-frozen value ρ^j ($j = 1 : N_g, N_g = 20$) of varying parameter ρ . Without loss of generality, only the sensitivities ρ^1 , ρ^{10} , and ρ^{20} are illustrated to evaluate the whole varying range.

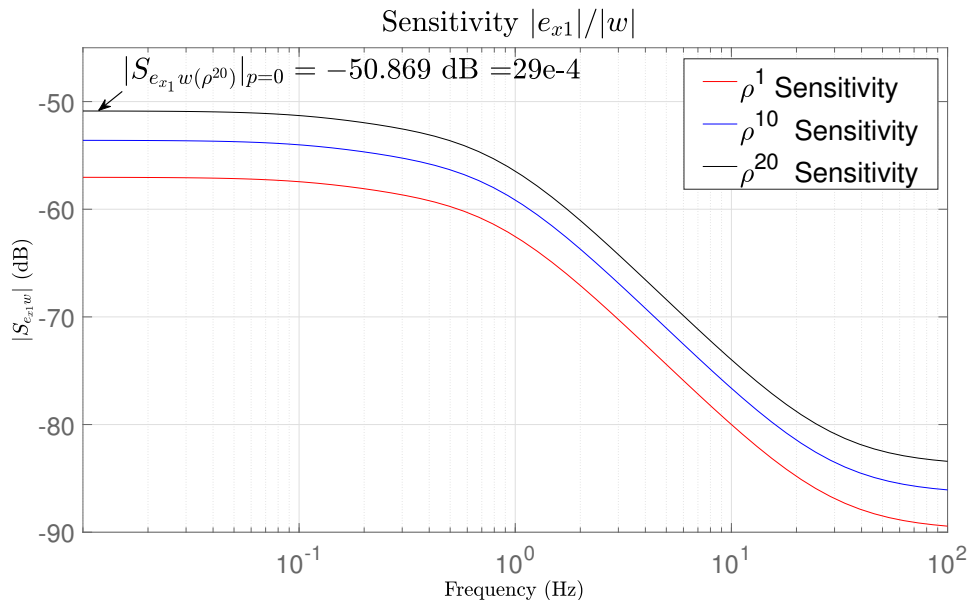


Figure 5.2: Sensitivity function $|S_{e_{x1}w}| = |e_{x1}/w|$

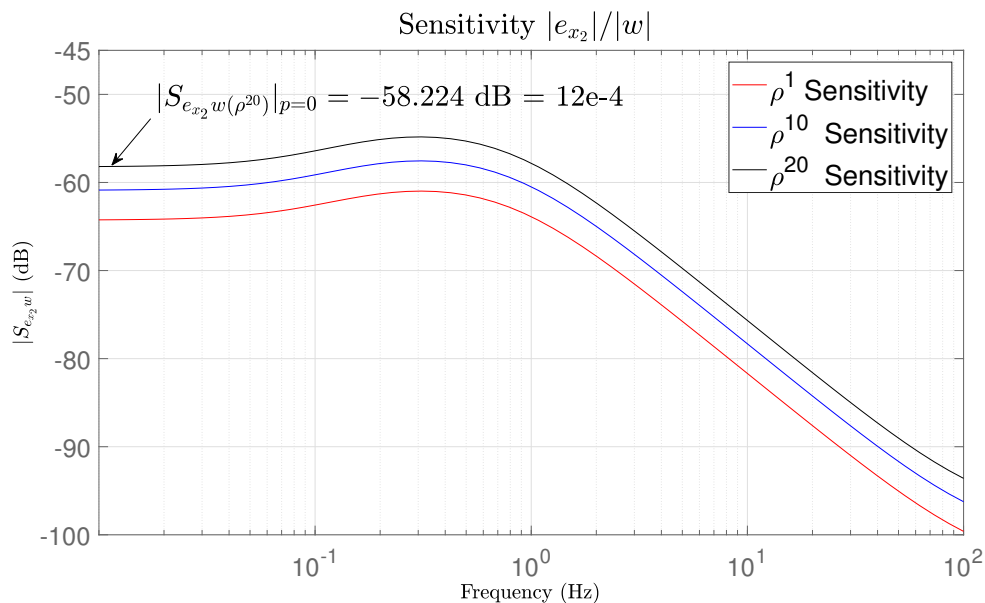


Figure 5.3: Sensitivity function $|S_{e_{x2}w}| = |e_{x2}/w|$

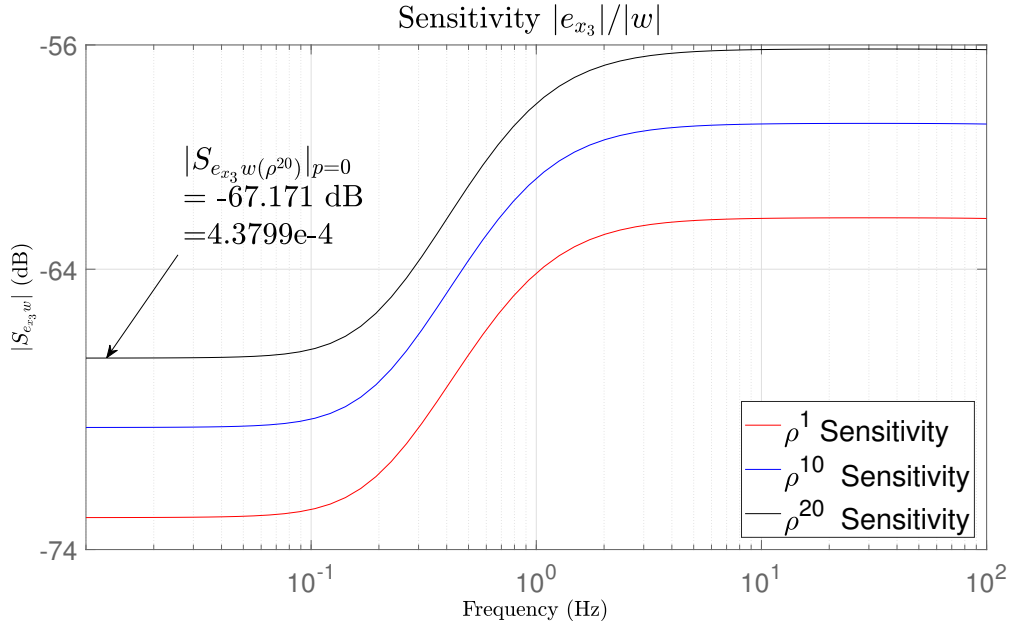


Figure 5.4: Sensitivity function $|S_{e_{x_3}w}| = |e_{x_3}/w|$

From (5.31), for each time-frozen point ρ^j , the sensitivity functions are analytically rewritten as:

$$S_{e_{x_i}w(\rho^j)} = \left. \frac{e_{xi}(p)}{w(p)} \right|_{\rho^j} = C_i(pI - F(\rho^j))^{-1}T_{(Z)}D_{1(\rho^j)}, \quad (5.88)$$

where $e_{xi} = C_i e$ ($i = 1, 2, 3$), $C_1 = [1 \ 0 \ 0]$, $C_2 = [0 \ 1 \ 0]$, and $C_3 = [0 \ 0 \ 1]$.

As observed in Figs. 5.2–5.4, all sensitivities of the proposed method demonstrate great attenuation (< -50 dB) of UI impact. Hence, the proposed method ensures the UI-decoupling effect on state estimation for the whole range of the analyzed frequency.

5.6.3 Time-domain Simulation

Although the initial condition $\hat{x}(0)$ is far from the real $x(0)$, Figs. 5.5–5.7 show that all the state estimation signals \hat{x}_1 , \hat{x}_2 , and \hat{x}_3 have followed well the real state x_1 , x_2 and x_3 . The estimation error is then evaluated by the root-mean-square (RMS) values to verify the accuracy of estimation when the error stabilization is established ($t \geq 2(s)$). With all acceptable RMS values that express $e \rightarrow 0$, Table 5.1 strengthens the performance of the proposed method in UI attenuation without the need to satisfy the perfect UI-decoupling condition.

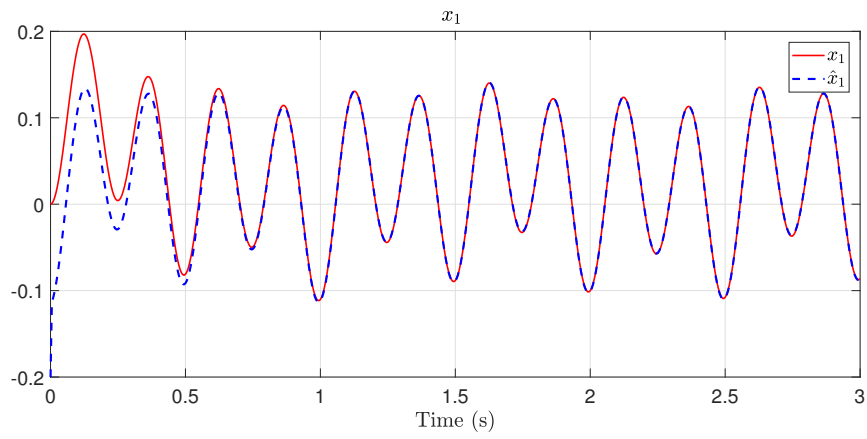
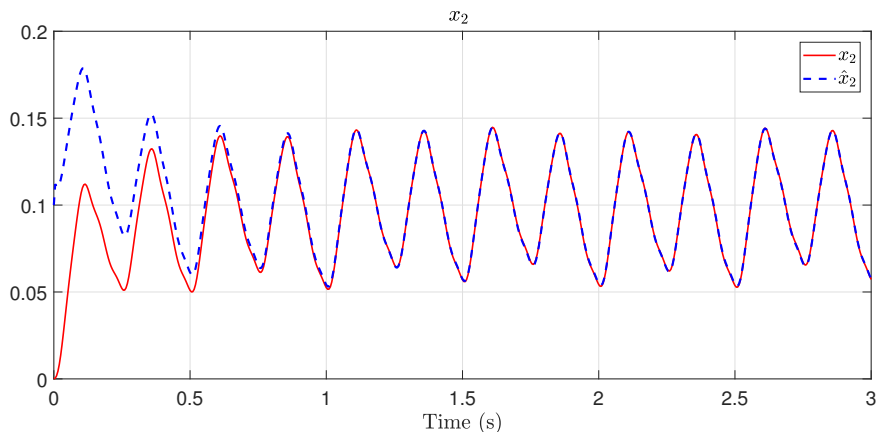
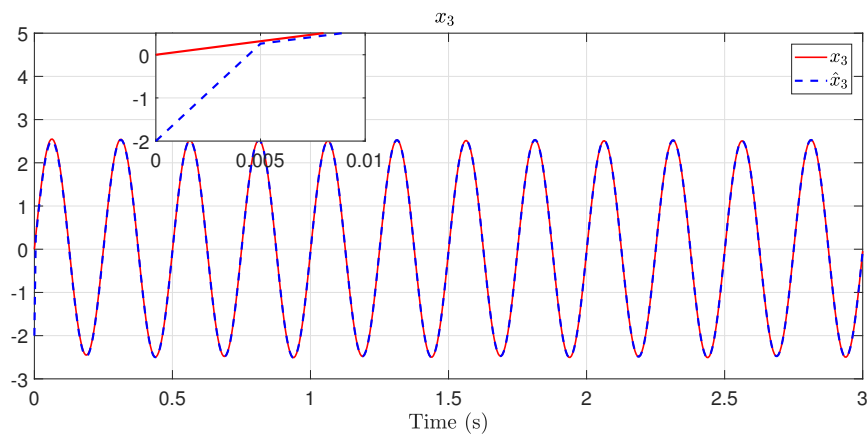
Figure 5.5: x_1 estimationFigure 5.6: x_2 estimationFigure 5.7: x_3 estimation

Table 5.1: RMS Evaluation of estimation error

	e_{x_1}	e_{x_2}	e_{x_3}
RMS	$4.7312e-4$	$4.0726e-4$	$7.6155e-4$

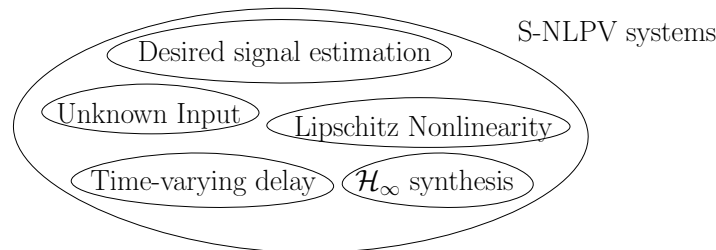
5.7 Conclusion

In this Chapter, a generic design for UI observer has been developed for a new class of general S-NLPV system, which unifies all the so far existing kinds of LPV systems. Based on the \mathcal{H}_2 criteria, this proposed observer design relaxes the parameter-dependent UI-decoupling condition while ensuring the stability of estimation error under Lipschitz condition. Moreover, the specific parameter-dependent forms of the matrices $T_{(Z)}$ and $N_{(Z)}$ are able to facilitate the design process and observer implementation without additional assumptions such as those on $\dot{\rho}$ in [Marx et al. 2019]. Furthermore, the numerical simulation is conducted to highlight the capability of the proposed observer design in decoupling with UI.

However, the proposed design also has certain drawbacks. Firstly, the nonlinearity in S-NLPV system is limited for only Lipschitz condition. Secondly, the output measurement must be independent of TVP, which is a constraint in sensor installation and observer implementation. Finally, the measurement noise, which affects the accuracy of estimation in practice, is has not been taken into account in observer designs yet. Thus, these drawbacks that should be overcome in future work.

\mathcal{H}_∞ Observer Design for Singular Time-delay Nonlinear Parameter-Varying System

Abstract: The main contribution of Chapter 6 consists of the generic conception of \mathcal{H}_∞ NLPV observer design for a general class of singular time-delay Nonlinear Parameter-varying (SD-NLPV) systems. Under the the presence of UIs and Lipschitz condition on nonlinearity, the proposed design is based on the generic form of full-order observer and is applicable to S-NLPV system with/without time-varying delay in state/input. In specific, the impact of UIs is attenuated by \mathcal{H}_∞ -norm synthesis, while the parameter-(in)dependent stability and delay-independent stability of estimation errors are ensured thanks to LMI optimization. Finally, the numerical example illustrated to highlight the proposed design for SD-NLPV systems.



Contents

6.1 Introduction	156
6.1.1 Related works	156
6.1.2 Chapter Contributions	157
6.2 Problem formulation	158
6.2.1 SD-NLPV representation	158
6.2.2 Design objectives for time-delay NLPV \mathcal{H}_∞ observer	159
6.3 Main results	161
6.3.1 \mathcal{H}_∞ full-order NLPV Observer design with exact memory (known $h(t)$)	161
6.3.2 \mathcal{H}_∞ full-order NLPV Observer design for S-NLPV systems	168
6.4 General Discussion	170
6.4.1 Analytical Existence Condition for \mathcal{H}_∞ observer designs	170
6.4.2 Implementation Algorithm	171

6.5	Numerical Examples	173
6.5.1	Model Parameters	173
6.5.2	Frequency Analysis	174
6.5.3	Simulation result	176
6.6	Conclusion	177

6.1 Introduction

6.1.1 Related works

Since the UI-decoupling condition for UI observers cannot always be satisfied, many studies have been conducted to develop a comprehensive solution in LPV frameworks. Besides the approach of \mathcal{H}_2 criteria developed in Chapter 5, the \mathcal{H}_∞ synthesis has also been widely developed to bypass this condition and will be discussed in this Chapter. In which, the impact of UI w on estimation error e is attenuated through the minimization of attenuation level γ_∞ , i.e. $\sup_{\rho \in \mathcal{P}_\rho} \sup_{\|w\|_2 \neq 0, w \in \mathcal{L}_2} \frac{\|e\|_2}{\|w\|_2} \leq \gamma_\infty$. This method is still workable when the desired signal e_z , which is a combination of e , is applied instead of e . Thanks to its convenience and flexible integration in observer stability, the usage of \mathcal{H}_∞ observers is applicable to not only S-LPV systems but also Time-delay LPV systems, which is able to model the propagation/transportation phenomena and state-input-output interactions between interconnected dynamics [Briat 2015]. Notable works on the topic are briefly summarized as below:

- **Singular approach:** Based on the full-order design [Darouach, Zasadzinski, and Hayar 1996] and \mathcal{H}_∞ observer [Marx, Koenig, and Georges 2003] for S-LTI systems, [Habib et al. 2010] introduced a new \mathcal{H}_∞ observer design to detect faults in S-LPV systems. Similarly, a \mathcal{H}_∞ proportional derivative observer was developed by [Shi and Patton 2015b] for fault estimation. Unfortunately, its singular structure is not pragmatic enough for implementation. Meanwhile, concerning the impact of inexact time-varying parameters, [López-Estrada et al. 2015a] has proposed a \mathcal{H}_∞ -based observer which can overcome the robust problem in the S-LPV system. Nonetheless, all of the above works focus only on the polytopic approach of S-LPV systems.
- **Time-delay approach:** Based on the successful incorporation of \mathcal{H}_∞ synthesis into delay-independent stability analysis [Wu and Grigoriadis 2001], Briat and al have extensively studied this method for delay-dependent controllers and observers. Regarding delay knowledge, observer/controller designs are divided into three groups [Briat, Sename, and Lafay 2010]: exact-memory (known delay), memoryless (unknown delay), and memory-resilient (uncertain delay). Herein, the exact-memory approach is the most widely applied, based on which a \mathcal{H}_∞ -LPV Luenberger observer is introduced in [Briat, Sename, and Lafay 2007], while its reduced-order form is presented in [Briat, Sename, and Lafay 2011].

Recently, singular delayed LPV system (SD-LPV) is introduced to unify these two approaches, thus generating a comprehensive method of observer design for state-fault estimation. Regarding its stability and observation, [Li and Zhang 2012] and [Li and Zhang 2013] have conducted studies on delay-(in)dependent admissibility and \mathcal{H}_∞ filtering. Unfortunately, their delay-dependent solutions can generate bilinear matrix inequalities (BMIs) for control and observer design. Meanwhile, in [Hassanabadi, Shafiee, and Puig 2016] a \mathcal{H}_∞ observer design for SD-LPV systems with multiple delays is introduced. Then, concerning uncertain time-varying parameters, [Hassanabadi, Shafiee, and Puig 2018] develop the robust \mathcal{H}_∞ time-delay observer with exact memory for sensor fault estimation. Nonetheless, the conservative stability of delay-independent observer and the strict polytopic representation of the initial system can limit the implementation of their works.

6.1.2 Chapter Contributions

To overcome the limitation of the polytopic approach in SD-LPV systems and the nonlinear phenomenon of S-NLPV system in Chapter 5, this Chapter makes the following contributions for LPV framework:

- A class of general S-NLPV with time-varying delay and Lipschitz nonlinearity (SD-NLPV), which unifies all the so far existing LPV systems;
- A generic design of \mathcal{H}_∞ NLPV observers that is applicable to SD-NLPV systems, as well as S-NLPV systems, regardless of their LPV representation. This proposed solution is based on the generic form of full-order observer which integrates the state-input delays and Lipschitz nonlinearity. Also, the parameter-(in)dependent stability and delay-independent stability for SD-NLPV systems are ensured, even under the influence of UI, by solving LMI optimization.

In addition, a numerical example is illustrated to emphasize the performance of \mathcal{H}_∞ observer design in the proposed SD-LPV system.

The Chapter is organized as follows. Firstly, the problem formulation for generic \mathcal{H}_∞ observers in the SD-NLPV system is presented in Section 6.2. Next, Section 6.3 demonstrates the design process of the exact-memory \mathcal{H}_∞ NLPV observer. Also, some corollaries for S-NLPV systems are implied. In Section 6.4, the existence conditions of the proposed observers and some remarks on time-delay observer are discussed. Then, Section 6.5 illustrates a numerical example along with the frequency analysis to highlight the time-delay proposed observer. Finally, the conclusion is provided in Section 6.6.

6.2 Problem formulation

This Section introduces the general class of SD-NLPV systems with time-varying delay $h(t)$. Also, the observer formulation and its design objectives are presented.

6.2.1 SD-NLPV representation

Consider the following class of SD-NLPV systems:

$$\begin{cases} E\dot{x}(t) &= A_{(\rho)}x(t) + A_{d(\rho)}x(t - h(t)) + B_{(\rho)}u(t) + B_{d(\rho)}u(t - h(t)) \\ &\quad + \Phi(x(t), x(t - h(t)), u(t), u(t - h(t)), h(t), \rho(t)) + D_{1(\rho)}w(t), \\ y(t) &= C_yx(t), \\ z(t) &= C_zx(t), \\ x(\lambda) &= \varpi_x(\lambda), \lambda \in [-\bar{h}, 0] \\ u(\lambda) &= \varpi_u(\lambda), \lambda \in [-\bar{h}, 0] \end{cases} \quad (6.1)$$

where

- $x \in \mathbb{R}^{n_x}$ is the state vector; $y \in \mathbb{R}^{n_y}$ is the measurement output vector; $u \in \mathbb{R}^{n_u}$ is the input vector; $w \in \mathbb{R}^{n_d}$ is the UI vector with bounded energy; $z \in \mathbb{R}^{n_z}$ is the vector of the desired signals, which can be state x or a combination of x , to be estimated.
- $\varpi_x(t)$ ($\varpi_u(t)$) is the functional initial condition for state x (input u).
- Matrices E and C_y are constant, while other distribution matrices are parameter-varying with appropriate dimensions.
- Measurable TVP ρ takes values in parameter space \mathcal{P}_ρ :

$$\mathcal{P}_\rho = \{\rho = [\rho_1(t) \ \rho_2(t) \ \dots \ \rho_m(t)]^T \mid \underline{\rho}_i \leq \rho_i(t) \leq \bar{\rho}_i, \forall i = 1 : m, t \geq 0\}. \quad (6.2)$$

Remark 6.2.1

The structure of system (6.1) can always be obtained even if the output depends on the time-varying parameter ρ , i.e. $y = C_{y(\rho)}x + D_{2(\rho)}w$ with the implementation of the output filter in Section 1.5.3.1.

The following assumptions are considered in this Chapter:

(A.1) Time-varying delay $h(t)$ is known and belongs to the set \mathcal{H}_d :

$$\mathcal{H}_d = \{h : \mathbb{R}_{\geq 0} \rightarrow [0, \bar{h}], \dot{h}(t) \leq \mu < 1, t \geq 0\}, \quad (6.3)$$

where \bar{h} is a finite constant presenting the maximum of delay.

(A.2) Parameter variations are bounded. In other words, $|\dot{\rho}_i| \leq \vartheta_i$ where ϑ_i is non-negative constant boundness [Wu et al. 1996].

(A.3) $\Phi(x(t), x(t-h(t)), u(t), u(t-h(t)), h(t), \rho(t))$ is the non-linear dynamics, which can be decomposed as:

$$\begin{aligned} \Phi(x(t), x(t-h(t)), u(t), u(t-h(t)), h(t), \rho(t)) = \\ B_{\phi(\rho)}\phi(x(t), u(t)) + B_{\phi_d(\rho)}\phi_d(x(t-h(t)), u(t-h(t))), \end{aligned} \quad (6.4)$$

In which, $\phi(x(t), u(t))$ and $\phi_d(x(t-h(t)), u(t-h(t)), h(t))$ are Lipschitz functions with bounded input u (due to saturation in practice) satisfying:

1. $\|\tilde{\phi}(t)\| = \|\phi(x(t), u(t)) - \phi(\hat{x}(t), u(t))\| \leq \gamma\|x(t) - \hat{x}(t)\|$,
2. $\|\tilde{\phi}_d(t-h(t))\| = \|\phi_d(x(t-h(t)), u(t-h(t))) - \phi_d(\hat{x}(t-h(t)), u(t-h(t)))\| \leq \gamma_d\|x(t-h(t)) - \hat{x}(t-h(t))\|$,

for all $x(t), \hat{x}(t), x(t-h(t)), \hat{x}(t-h(t)) \in \mathbb{R}^{n_x}$, where γ and γ_d are known Lipschitz constants. Meanwhile, $\hat{x}(t)$ and $\hat{x}(t-h(t))$ is the estimated of the state $x(t)$ and its delayed state $x(t-h(t))$, respectively.

(A.4) SD-NLPV system (6.1) is impulse-free and R-detectable $\forall \rho$ when $h(t) = 0$, which is later analytically verified by the conditions discussed in Section 6.4.1.

6.2.2 Design objectives for time-delay NLPV \mathcal{H}_∞ observer

Under Assumptions (A.1)-(A.4), this Chapter is focused on the design of a time-delay NLPV observer with exact memory, i.e. known $h(t)$, which has the generic full-order form:

$$\begin{cases} \dot{\xi}(t) &= F_{(\rho)}\xi(t) + F_{d(\rho)}\xi(t-h(t)) + J_{(\rho)}u(t) + J_{d(\rho)}u(t-h(t)) + L_{(\rho)}y(t) + L_{d(\rho)}y(t-h(t)) \\ &\quad + TB_{\phi(\rho)}\phi(\hat{x}(t), u(t)) + TB_{\phi_d(\rho)}\phi_d(\hat{x}(t-h(t)), u(t-h(t))) \\ \hat{x}(t) &= \xi(t) + Ny(t), \\ \hat{z}(t) &= C_z\hat{x}(t), \\ \xi(t) &= \varpi_\xi(t), t \in [-\bar{h}, 0] \end{cases}, \quad (6.5)$$

such that the following objectives are satisfied:

(O.1) When $w(t) = 0$, the estimation error, defined later in (6.32), is asymptotically stable.

(O.2) When $w(t) \neq 0$, the impact of UI $w(t)$ on the desired estimation error $e_z(t) = z(t) - \hat{z}(t)$ is attenuated such that:

$$\sup_{\rho \in \mathcal{P}, \|w(t)\|_2 \neq 0, w(t) \in \mathcal{L}_2} \frac{\|e_z(t)\|_2}{\|w(t)\|_2} \leq \gamma_\infty, \quad (6.6)$$

where

- $\hat{z}(t)$ is the estimated of $z(t)$, which is useful to design the state-feedback controller ($C_z = I_{n_x}$), as well as the output-feedback controller or fault estimation ($C_z \neq I_{n_x}$);
- $\hat{x}(t)$ is the estimated state of $x(t)$, $\varpi_\xi(t)$ is the functional initial condition for observer
- The constant matrix T satisfies that:

$$TE + NC_y = I, \quad (6.7)$$

while the observer matrices $F_{(\rho)}$, $J_{(\rho)}$, T , $L_{(\rho)}$, and N are later synthesized in Section 6.3.1.

Remark 6.2.2

In case the input u has a different time-delay signal $h_u(t) \neq h(t)$, i.e. $u(t - h_u(t))$, the observer design process is still correct since the elements corresponding to $u(t - h_u(t))$ in the dynamics of estimation errors are eliminated by the choice of observer matrices.

Remark 6.2.3

The observer design with the existence of w in the measurement output y is always possible. In fact, the additional UI \dot{w} will be generated along with w during the design process, i.e. the impact of new UI vector $w^* = [w^T \ \dot{w}^T]^T$ is needed to be attenuated. Consequently, certain negative results on the \mathcal{H}_∞ optimization are expected, especially if w is a high-frequency signal. For such reasons, the system reformulations in Remark 6.2.1 is proposed to avoid this issue if necessary.

Remark 6.2.4

The full-order form of observer (6.5) is chosen instead of the singular Luenberger observer since the stability conditions for estimation error, whose dynamics is described by singular system, contain a LME (Linear Matrix Equality), i.e. $E^T P_{(\rho)} = P_{(\rho)}^T E$, and thus cause the numerical problem.

The relation between SD-NLPV system (6.1) and its observer (6.5) is illustrated in Fig. 6.1. Meanwhile, details on the design process of the observer are presented in the next section.

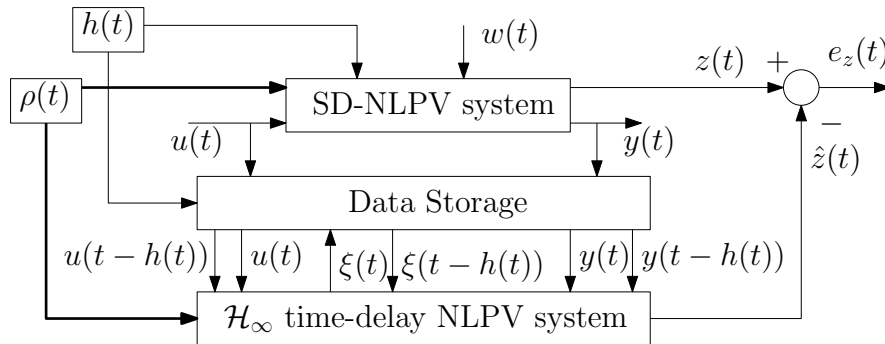


Figure 6.1: Implementation scheme of \mathcal{H}_∞ time-delay observer

6.3 Main results

In this Section, the time-delay NLPV observer, whose solution is given in Section 6.3.1, is developed to estimate the desired signal $z(t)$ in SD-NLPV system (6.1). Also, some corollaries implied from time-delay NLPV observer will be presented for S-NLPV systems in Section 6.3.2.

6.3.1 \mathcal{H}_∞ full-order NLPV Observer design with exact memory (known $h(t)$)

In this section, the generic design of \mathcal{H}_∞ time-delay full-order NLPV observer with exact memory for SD-NLPV system will be introduced.

Firstly, the estimation error $e(t) = x(t) - \hat{x}(t)$ can be expressed as:

$$e(t) = x(t) - \hat{x}(t) \quad (6.8)$$

$$= (I - NC_y)x(t) - \xi(t) \quad (6.9)$$

$$= TE x(t) - \xi(t) \quad (6.10)$$

Thus, its dynamics is displayed as:

$$\dot{e}(t) = TE\dot{x}(t) - \dot{\xi}(t) \quad (6.11)$$

$$\begin{aligned} &= \{TA_{(\rho)}x(t) + TA_{d(\rho)}\xi(t - h(t)) - F_{(\rho)}\xi(t) - F_{d(\rho)}\xi(t - h(t)) - L_{(\rho)}y(t) \\ &\quad - L_{d(\rho)}y(t - h(t))\} + (J_{(\rho)} - TB_{(\rho)})u(t) + (J_{d(\rho)} - TB_{d(\rho)})u(t - h(t)) \\ &\quad + TB_{\phi(\rho)}\tilde{\phi}(t) + TB_{\phi d(\rho)}\tilde{\phi}_d(t - h(t)) + TD_{1(\rho)}w(t) \end{aligned} \quad (6.12)$$

As $\xi(t) = TE x(t) - e(t)$, $\xi(t - h(t)) = TE x(t - h(t)) - e(t - h(t))$, $y(t) = C_y x(t)$, and $y(t - h(t)) = C_y x(t - h(t))$, it follows that:

$$\begin{aligned} \dot{e}(t) &= F_{(\rho)}e(t) + F_{d(\rho)}e(t - h(t)) + TB_{\phi(\rho)}\tilde{\phi}(t) + TB_{\phi d(\rho)}\tilde{\phi}_d(t - h(t)) \\ &\quad + (J_{(\rho)} - TB_{(\rho)})u(t) + (J_{d(\rho)} - TB_{d(\rho)})u(t - h(t)) + TD_{1(\rho)}w(t) \\ &\quad + (TA_{(\rho)} - F_{(\rho)}TE - L_{(\rho)}C_y)x(t) + (TA_{d(\rho)} - F_{d(\rho)}TE - L_{d(\rho)}C_y)x(t) \end{aligned} \quad (6.13)$$

Consider the following conditions:

$$J_{(\rho)} - TB_{(\rho)} = 0, \quad (6.14)$$

$$J_{d(\rho)} - TB_{d(\rho)} = 0, \quad (6.15)$$

$$TA_{(\rho)} - F_{(\rho)}TE - L_{(\rho)}C_y = 0, \quad (6.16)$$

$$TA_{d(\rho)} - F_{d(\rho)}TE - L_{d(\rho)}C_y = 0, \quad (6.17)$$

$$K_{(\rho)} = -F_{(\rho)}N + L_{(\rho)}, \quad (6.18)$$

$$K_{d(\rho)} = -F_{d(\rho)}N + L_{d(\rho)}, \quad (6.19)$$

the error dynamics (6.13) is rewritten as:

$$\dot{e}(t) = F_{(\rho)}e(t) + F_{d(\rho)}e(t - h(t)) + TB_{\phi(\rho)}\tilde{\phi}(t) + TB_{\phi d(\rho)}\tilde{\phi}_d(t - h(t)) + TD_{1(\rho)}w(t). \quad (6.20)$$

From $TE + NC_y = I$ and Eqs. (6.16)-(6.17), it follows that:

$$F_{(\rho)} = TA_{(\rho)} - K_{(\rho)}C_y, \quad (6.21)$$

$$F_{d(\rho)} = TA_{d(\rho)} - K_{d(\rho)}C_y, \quad (6.22)$$

Similar to the proposed design in Case (c) - Section 5.2.3, the relation (6.7) is rewritten to avoid the dependence of matrices T and N on the time-varying parameter ρ :

$$[T \quad N] \begin{bmatrix} E \\ C_y \end{bmatrix} = I. \quad (6.23)$$

If $\text{rank} \begin{bmatrix} E \\ C_y \end{bmatrix} = n_x$, which is also the impulse-free condition, then the general solution for Eq.(6.23) is given by:

$$[T_{(Z)} \quad N_{(Z)}] = \begin{bmatrix} E \\ C_y \end{bmatrix}^\dagger - Z \left(I - \begin{bmatrix} E \\ C_y \end{bmatrix} \begin{bmatrix} E \\ C_y \end{bmatrix}^\dagger \right), \quad (6.24)$$

where Z is a designed matrix which will be computed later in Theorem 6.3.1.

Thus, the matrices $T_{(Z)}$ and $N_{(Z)}$ can be now rewritten as functions of Z :

$$T_{(Z)} = T_1 - ZT_2, \quad (6.25)$$

$$N_{(Z)} = N_1 - ZN_2, \quad (6.26)$$

where $T_1 = \begin{bmatrix} E \\ C_y \end{bmatrix}^\dagger \delta_T$, $T_2 = \left(I - \begin{bmatrix} E \\ C_y \end{bmatrix} \begin{bmatrix} E \\ C_y \end{bmatrix}^\dagger \right) \delta_T$, $\delta_T = \begin{bmatrix} I \\ 0 \end{bmatrix}$, $N_1 = \begin{bmatrix} E \\ C_y \end{bmatrix}^\dagger \delta_N$, $N_2 = \left(I - \begin{bmatrix} E \\ C_y \end{bmatrix} \begin{bmatrix} E \\ C_y \end{bmatrix}^\dagger \right) \delta_N$, and $\delta_N = \begin{bmatrix} 0 \\ I \end{bmatrix}$.

It follows that:

$$F_{(\rho)} = T_{(Z)}A_{(\rho)} - K_{(\rho)}C_y = T_1A_{(\rho)} - ZT_2A_{(\rho)} - K_{(\rho)}C_y, \quad (6.27)$$

$$F_{d(\rho)} = T_{(Z)}A_{d(\rho)} - K_{d(\rho)}C_y = T_1A_{d(\rho)} - ZT_2A_{d(\rho)} - K_{d(\rho)}C_y, \quad (6.28)$$

$$T_{(Z)}B_{\phi(\rho)} = T_1B_{\phi(\rho)} - ZT_2B_{\phi(\rho)}, \quad (6.29)$$

$$T_{(Z)}B_{\phi d(\rho)} = T_1B_{\phi d(\rho)} - ZT_2B_{\phi d(\rho)}, \quad (6.30)$$

$$T_{(Z)}D_{1(\rho)} = T_1D_{1(\rho)} - ZT_2D_{1(\rho)}. \quad (6.31)$$

From Eq. (6.20), it yields that:

$$\dot{e}(t) = F_{(\rho)}e(t) + F_{d(\rho)}e(t - h(t)) + B_{e(\rho)}\tilde{\phi}(t) + B_{de(\rho)}\tilde{\phi}_d(t - h(t)) + W_{(\rho)}w(t), \quad (6.32)$$

where

$$F_{(\rho)} = T_1 A_{(\rho)} - Z T_2 A_{(\rho)} - K_{(\rho)} C_y, \quad (6.33)$$

$$F_{d(\rho)} = T_1 A_{d(\rho)} - Z T_2 A_{d(\rho)} - K_{d(\rho)} C_y, \quad (6.34)$$

$$B_{e(\rho)} = T_1 B_{\phi(\rho)} - Z T_2 B_{\phi(\rho)}, \quad (6.35)$$

$$B_{de(\rho)} = T_1 B_{\phi d(\rho)} - Z T_2 B_{\phi d(\rho)}, \quad (6.36)$$

$$W_{(\rho)} = T_1 D_{1(\rho)} - Z T_2 D_{1(\rho)}. \quad (6.37)$$

Since the matrices $F_{(\rho)}$ and $F_{d(\rho)}$ are defined by the matrices Z , $K_{(\rho)}$, and $K_{d(\rho)}$, the objectives (O.1)-(O.2) are achieved by finding the triple $(Z, K_{(\rho)}, K_{d(\rho)})$, whose solutions are given in Theorem 6.3.1.

Theorem 6.3.1 (Delay-dependent Stability)

Under Assumptions (A.1)-(A.4), the objectives (O.1)-(O.2) are achieved if there exist a matrix X ; symmetric positive definite matrices $P_{(\rho)}$, Q , and R ; matrices Y_1 , $Y_{2(\rho)}$ and $Y_{2d(\rho)}$; positive scalars ϵ and ϵ_d which minimize γ_∞ and satisfy that:

$$\begin{bmatrix} -X - X^T & XF_{(\rho)} + P_{(\rho)} & XF_{d(\rho)} & XB_{e(\rho)} & XB_{de(\rho)} & XW_{(\rho)} & X & \bar{h}R \\ (*) & \Xi_{11(\rho)} & R & 0 & 0 & 0 & 0 & 0 \\ (*) & (*) & \Xi_{22(\rho)} & 0 & 0 & 0 & 0 & 0 \\ (*) & (*) & (*) & -\epsilon I & 0 & 0 & 0 & 0 \\ (*) & (*) & (*) & (*) & -\epsilon_d I & 0 & 0 & 0 \\ (*) & (*) & (*) & (*) & (*) & -\gamma_\infty^2 I & 0 & 0 \\ (*) & (*) & (*) & (*) & (*) & (*) & -P_{(\rho)} & -\bar{h}R \\ (*) & (*) & (*) & (*) & (*) & (*) & (*) & -R \end{bmatrix} < 0, \quad (6.38)$$

where

$$XF_{(\rho)} = XT_1 A_{(\rho)} + Y_1 T_2 A_{(\rho)} + Y_{2(\rho)} C_y, \quad (6.39)$$

$$XF_{d(\rho)} = XT_1 A_{d(\rho)} + Y_1 T_2 A_{d(\rho)} + Y_{2d(\rho)} C_y, \quad (6.40)$$

$$XB_{e(\rho)} = XT_1 B_{\phi(\rho)} + Y_1 T_2 B_{\phi(\rho)}, \quad (6.41)$$

$$XB_{de(\rho)} = XT_1 B_{\phi d(\rho)} + Y_1 T_2 B_{\phi d(\rho)}, \quad (6.42)$$

$$XW_{(\rho)} = XT_1 D_{1(\rho)} + Y_1 T_2 D_{1(\rho)}, \quad (6.43)$$

$$\Xi_{11(\rho)} = \sum_i^m \pm \vartheta_i \frac{\partial P_{(\rho)}}{\partial \rho_i} - P_{(\rho)} + Q - R + C_z^T C_z + \eta, \quad (6.44)$$

$$\Xi_{22(\rho)} = -(1 - \mu)Q - R + \eta_d, \quad (6.45)$$

$$\eta = \epsilon(\gamma I)^T (\gamma I), \quad (6.46)$$

$$\eta_d = \epsilon_d(\gamma_d I)^T (\gamma_d I), \quad (6.47)$$

then $[Z \quad K_{(\rho)} \quad K_{d(\rho)}] = -X^{-1} Y_{(\rho)} = -X^{-1} [Y_1 \quad Y_{2(\rho)} \quad Y_{2d(\rho)}]$.

Remark 6.3.1

The notion $\sum_i^m \pm(\cdot)$ expresses all combinations of $+(\cdot)$ and $-(\cdot)$ that are included in the inequality (6.38). Consequently, the inequality (6.38) actually represents 2^m different inequalities that correspond to the 2^m different combinations in the summation.

Proof: The following Lyapunov-Krasovskii functional for delay-dependent stability is chosen as: [Briat 2015]

$$V_{(\rho)} = e^T(t)P_{(\rho)}e(t) + \int_{t-h(t)}^t e(\theta)Qe(\theta)d\theta + \bar{h} \int_{-\bar{h}}^0 \int_{t+\theta}^t \dot{e}^T(s)R\dot{e}(s) ds d\theta. \quad (6.48)$$

The constraint $J_\infty < 0$ holds if

$$J_\infty = \dot{V}_{(\rho)} + z(t)^T z(t) - \gamma_\infty^2 w^T(t)w(t) < 0. \quad (6.49)$$

The Lipschitz conditions yield the following conditions:

$$\begin{aligned} & \bullet \|\tilde{\phi}(t)\| \leq \gamma \|e(t)\|, \\ \implies J &= (\tilde{\phi}(t))^T (\tilde{\phi}(t)) - e^T(t)(\gamma I)^T (\gamma I)e(t) \leq 0, \end{aligned} \quad (6.50)$$

$$\begin{aligned} & \bullet \|\tilde{\phi}_d(t-h(t))\| \leq \gamma_d \|e(t-h(t))\|, \\ \implies J_d &= (\tilde{\phi}_d(t-h(t)))^T (\tilde{\phi}_d(t-h(t))) - e^T(t-h(t))(\gamma_d I)^T (\gamma_d I)e(t-h(t)) \leq 0 \end{aligned} \quad (6.51)$$

Since $J \leq 0$ and $J_d \leq 0$, J_∞ can be majorized by:

$$J_\infty \leq J_\infty - \epsilon J - \epsilon_d J_d \quad (6.52)$$

where ϵ and ϵ_d are positive scalars.

The constraint $J_\infty < 0$ holds if:

$$J_\infty - \epsilon J - \epsilon_d J_d < 0, \quad (6.53)$$

Eq. (6.48) follows that:

$$\begin{aligned} \dot{V}_{(\rho)} &= e^T(t) \frac{\partial P_{(\rho)}}{\partial t} e(t) + \mathcal{H}\{e^T(t)P_{(\rho)}\dot{e}(t)\} + e^T(t)Qe(t) - (1-\dot{h})e^T(t-h(t))Qe(t-h(t)) \\ &\quad + \bar{h}^2 \dot{e}^T(t)R\dot{e}(t) - \bar{h} \int_{t-h(t)}^t \dot{e}^T(s)R\dot{e}(s) ds, \end{aligned} \quad (6.54)$$

$$\begin{aligned} &= e^T(t) \frac{\partial P_{(\rho)}}{\partial t} e(t) + \mathcal{H}\{e^T(t)P_{(\rho)}F_{(\rho)}e(t) + e^T(t)P_{(\rho)}F_{d(\rho)}e(t-h(t)) \\ &\quad + e^T(t)P_{(\rho)}B_{e(\rho)}\tilde{\phi}(t) + e^T(t)P_{(\rho)}B_{de(\rho)}\tilde{\phi}_d(t-h(t)) \\ &\quad + e^T(t)P_{(\rho)}W_{(\rho)}w(t)\} + e^T(t)Qe(t) - (1-\dot{h})e^T(t-h(t))Qe(t-h(t)) \\ &\quad + \bar{h}^2 \Upsilon \begin{bmatrix} F_{(\rho)}^T \\ F_{d(\rho)}^T \\ B_{e(\rho)}^T \\ B_{de(\rho)}^T \\ W_{(\rho)}^T \end{bmatrix} R \begin{bmatrix} F_{(\rho)} & F_{d(\rho)} & B_{e(\rho)} & B_{de(\rho)} & W_{(\rho)} \end{bmatrix} \Upsilon - \bar{h} \int_{t-h(t)}^t \dot{e}^T(s)R\dot{e}(s) ds. \end{aligned} \quad (6.55)$$

On the other hand, using the Jensen's inequality, we obtain:

$$-\bar{h} \int_{t-h(t)}^t \dot{e}^T(s) R \dot{e}(s) ds \leq \int_{t-h(t)}^t \dot{e}^T(s) ds R \int_{t-h(t)}^t \dot{e}(s) ds, \quad (6.56)$$

$$\implies -\bar{h} \int_{t-h(t)}^t \dot{e}^T(s) R \dot{e}(s) ds = (e(t) - e(t-h(t)))^T R (e(t) - e(t-h(t))) \quad (6.57)$$

Combined with $\dot{h} \leq \mu$, (6.57) yields that:

$$J_\infty - \epsilon J - \epsilon_d J_d \leq \Upsilon^T \Xi \Upsilon, \quad (6.58)$$

where

$$\Xi_{(\rho)} = \begin{bmatrix} \Omega_{11(\rho)} & \Omega_{12(\rho)} & \Omega_{13(\rho)} & \Omega_{14(\rho)} & \Omega_{15(\rho)} \\ (*) & \Xi_{22(\rho)} & 0 & 0 & 0 \\ (*) & (*) & -\epsilon I & 0 & 0 \\ (*) & (*) & (*) & -\epsilon_d I & 0 \\ (*) & (*) & (*) & (*) & -\gamma_\infty^2 I \end{bmatrix} + \bar{h} \begin{bmatrix} F_{(\rho)}^T \\ F_{d(\rho)}^T \\ B_{e(\rho)}^T \\ B_{de(\rho)}^T \\ W_{(\rho)}^T \end{bmatrix} R R^{-1} \bar{h} R \begin{bmatrix} F_{(\rho)}^T \\ F_{d(\rho)}^T \\ B_{e(\rho)}^T \\ B_{de(\rho)}^T \\ W_{(\rho)}^T \end{bmatrix}^T, \quad (6.59)$$

$$\Omega_{11(\rho)} = \mathcal{H}\{P_{(\rho)} F_{(\rho)}\} + P_{(\rho)} + \Xi'_{11(\rho)}, \quad (6.60)$$

$$\Xi'_{11(\rho)} = \sum_{i=1}^m \dot{\rho}_i \frac{\partial P_{(\rho)}}{\partial \rho_i} - P_{(\rho)} + Q - R + C_z^T C_z + \eta, \quad (6.61)$$

$$\Xi_{22(\rho)} = -(1-\mu)Q - R + \eta_d, \quad (6.62)$$

$$\Omega_{12(\rho)} = P_{(\rho)} F_{d(\rho)} + R, \quad (6.63)$$

$$\Omega_{13(\rho)} = P_{(\rho)} B_{e(\rho)}, \quad (6.64)$$

$$\Omega_{14(\rho)} = P_{(\rho)} B_{de(\rho)}, \quad (6.65)$$

$$\Omega_{15(\rho)} = P_{(\rho)} W_{(\rho)}. \quad (6.66)$$

Eq. (6.53) holds $\forall \Upsilon \neq 0$ if:

$$\Xi_{(\rho)} < 0. \quad (6.67)$$

Applying the Schur's complement to the above inequality, we obtain:

$$\begin{bmatrix} \Omega_{11(\rho)} & \Omega_{12(\rho)} & \Omega_{13(\rho)} & \Omega_{14(\rho)} & \Omega_{15(\rho)} & \bar{h} F_{(\rho)}^T R \\ (*) & \Xi_{22(\rho)} & 0 & 0 & 0 & \bar{h} F_{d(\rho)}^T R \\ (*) & (*) & -\epsilon I & 0 & 0 & \bar{h} B_{e(\rho)}^T R \\ (*) & (*) & (*) & -\epsilon_d I & 0 & \bar{h} B_{de(\rho)}^T R \\ (*) & (*) & (*) & (*) & -\gamma_\infty^2 I & \bar{h} W_{(\rho)}^T R \\ (*) & (*) & (*) & (*) & (*) & -R \end{bmatrix} < 0. \quad (6.68)$$

Due to the cross multiplications such as $P_{(\rho)} F_{(\rho)} = P_{(\rho)} \Gamma_1 \delta_F + P_{(\rho)} Z_{(\rho)} \Gamma_2 \delta_F$ and $R F_{(\rho)} = R \Gamma_1 \delta_F + R Z_{(\rho)} \Gamma_2 \delta_F$, the inequality (6.68) cannot be linearized by variable transformation (BMI problem). Consequently, the LMI (6.38) is proposed and then proved to be the sufficient solution for (6.68) thanks to the implementation of projection lemma.

Suppose LMI (6.38) is achieved, it can be displayed as:

$$\Omega_{(\rho)} + U_{(\rho)}^T X^T V + V^T X U_{(\rho)} < 0, \quad (6.69)$$

where

$$\Omega_{(\rho)} = \begin{bmatrix} 0 & P_{(\rho)} & 0 & 0 & 0 & 0 & 0 & \bar{h}R \\ (*) & \Xi'_{11(\rho)} & R & 0 & 0 & 0 & 0 & 0 \\ (*) & (*) & \Xi_{22(\rho)} & 0 & 0 & 0 & 0 & 0 \\ (*) & (*) & (*) & -\epsilon I & 0 & 0 & 0 & 0 \\ (*) & (*) & (*) & (*) & -\epsilon_d I & 0 & 0 & 0 \\ (*) & (*) & (*) & (*) & (*) & -\gamma_\infty^2 I & 0 & 0 \\ (*) & (*) & (*) & (*) & (*) & (*) & -P_{(\rho)} & -\bar{h}R \\ (*) & (*) & (*) & (*) & (*) & (*) & (*) & -R \end{bmatrix}, \quad (6.70)$$

$$U_{(\rho)} = [-I \quad F_{(\rho)} \quad F_{d(\rho)} \quad F_{d(\rho)} \quad B_{e(\rho)} \quad B_{de(\rho)} \quad I \quad 0], \quad (6.71)$$

$$V = [I \quad 0 \quad 0 \quad 0 \quad 0 \quad 0 \quad 0 \quad 0]. \quad (6.72)$$

Consequently, the bases of the null-space of $U_{(\rho)}$ and V are respectively defined as:

$$U_{\perp(\rho)} = \begin{bmatrix} F_{(\rho)} & F_{(\rho)} & F_{d(\rho)} & B_{e(\rho)} & B_{de(\rho)} & I & 0 \\ I & 0 & 0 & 0 & 0 & 0 & 0 \\ 0 & I & 0 & 0 & 0 & 0 & 0 \\ 0 & 0 & I & 0 & 0 & 0 & 0 \\ 0 & 0 & 0 & I & 0 & 0 & 0 \\ 0 & 0 & 0 & 0 & I & 0 & 0 \\ 0 & 0 & 0 & 0 & 0 & I & 0 \\ 0 & 0 & 0 & 0 & 0 & 0 & I \end{bmatrix}, \quad (6.73)$$

$$V_{\perp} = \begin{bmatrix} 0 & 0 & 0 & 0 & 0 & 0 & 0 \\ I & 0 & 0 & 0 & 0 & 0 & 0 \\ 0 & I & 0 & 0 & 0 & 0 & 0 \\ 0 & 0 & I & 0 & 0 & 0 & 0 \\ 0 & 0 & 0 & I & 0 & 0 & 0 \\ 0 & 0 & 0 & 0 & I & 0 & 0 \\ 0 & 0 & 0 & 0 & 0 & I & 0 \\ 0 & 0 & 0 & 0 & 0 & 0 & I \end{bmatrix}. \quad (6.74)$$

The implementation of Projection lemma (in Section 1.5.1.3) on (6.69) yields that:

$$\Omega_{1(\rho)} = U_{\perp(\rho)}^T \Omega_{(\rho)} U_{\perp(\rho)}$$

$$= \begin{bmatrix} \mathcal{H}\{P_{(\rho)} F_{(\rho)}\} + \Xi'_{11(\rho)} & \Omega_{12(\rho)} & \Omega_{13(\rho)} & \Omega_{14(\rho)} & \Omega_{15(\rho)} & P_{(\rho)} & \bar{h}F_{(\rho)}^T R \\ (*) & \Xi_{22(\rho)} & 0 & 0 & 0 & 0 & \bar{h}F_{d(\rho)}^T R \\ (*) & (*) & -\epsilon & 0 & 0 & 0 & \bar{h}B_{e(\rho)}^T R \\ (*) & (*) & (*) & -\epsilon_d & 0 & 0 & \bar{h}B_{de(\rho)}^T R \\ (*) & (*) & (*) & (*) & -\gamma_\infty^2 I & 0 & \bar{h}W_{(\rho)}^T R \\ (*) & (*) & (*) & (*) & (*) & -P_{(\rho)} & 0 \\ (*) & (*) & (*) & (*) & (*) & (*) & -R \end{bmatrix} < 0, \quad (6.75)$$

$$\Omega_{2(\rho)} = V_{\perp}^T \Omega_{(\rho)} V_{\perp} = \begin{bmatrix} \Xi'_{11(\rho)} & R & 0 & 0 & 0 & 0 & 0 \\ (*) & \Xi_{22(\rho)} & 0 & 0 & 0 & 0 & 0 \\ (*) & (*) & -\epsilon & 0 & 0 & 0 & 0 \\ (*) & (*) & (*) & -\epsilon_d & 0 & 0 & 0 \\ (*) & (*) & (*) & (*) & -\gamma_\infty^2 I & 0 & 0 \\ (*) & (*) & (*) & (*) & (*) & -P_{(\rho)} & -\bar{h}R \\ (*) & (*) & (*) & (*) & (*) & (*) & -R \end{bmatrix} < 0. \quad (6.76)$$

To avoid the existence of derivative $\dot{\rho}(t)$, under the Assumption (A.1), the term $\Xi'_{11(\rho)}$ can be rewritten as follows : [Wu 1995]

$$\Xi_{11(\rho)} = \sum_i^m \pm \vartheta_i \frac{\partial P(\rho)}{\partial \rho_i} - P(\rho) + Q - R + C_z^T C_z + \eta. \quad (6.77)$$

In which, the notion $\sum_i^m \pm(\cdot)$ expresses all combinations of $+(\cdot)$ and $-(\cdot)$ that are included in the inequality (6.38). Consequently, the inequality (6.38) actually represents 2^m different inequalities that correspond to the 2^m different combinations in the summation.

Apply the Schur's complement to Ω_1 , the inequality (6.68) is obtained, which completes the proof. ■

Remark 6.3.2

It is worth noting that the LMI (6.38) is the sufficient condition for delay-dependent stability and UI attenuation objectives. However, it imposes the additive constraint $\Omega_{2(\rho)}$ to the the solution space, which may make the proposed solution conservative. For example, $\Omega_{2(\rho)} < 0$ leads to restrictive conditions such as $\Xi'_{11(\rho)} < 0$ for (1, 1) element and $-P(\rho) + \bar{h}^2 R < 0$ for the right-bottom block (derived from Schur's complement).

Remark 6.3.3

In Theorem 6.3.1, since the time-invariant designed matrix X is the decision matrix to compute Z for the time-invariant matrices $T_{(Z)}$ and $N_{(Z)}$, the parameter-dependent matrix $P(\rho)$ has been chosen for the Lyapunov-Krasovskii function (6.48) to ensure both delay-dependent and parameter-dependent stability.

With the gains Z , $K(\rho)$, and $K_{d(\rho)}$, the observer matrices can be calculated by: $J(\rho) = T_{(Z)}B(\rho)$, $J_{d(\rho)} = T_{(Z)}B_{d(\rho)}$, $K(\rho) = -F(\rho)N_{(Z)} + L(\rho)$, $K_{d(\rho)} = -F_{d(\rho)}N_{(Z)} + L_{d(\rho)}$, $F(\rho) = T_{(Z)}A(\rho) - K(\rho)C_y$, and $F_{d(\rho)} = T_{(Z)}A_{d(\rho)} - K_{d(\rho)}C_y$. That completes the design process for time-delay NLPV observer (6.5).

On the other hand, it should be noted that the time-varying parameter $\rho(t)$ and time-varying delay $h(t)$ are considered independent in Theorem 6.3.1. However, in some studies such as [Wu and Grigoriadis 2001], $h(t)$ becomes a function of $\rho(t)$, i.e. $h(t) = h(\rho(t))$; thus, modifications to LMI solutions are required.

Since $h(t) = h(\rho(t))$, its derivatives can be expressed as:

$$\dot{h}(\rho(t)) = \sum_{i=1}^p \dot{\rho}_i \frac{\partial h(\rho)}{\partial \rho_i} \quad (6.78)$$

and be bounded by:

$$\dot{h}(\rho(t)) \leq \sup_{\rho \in U_\rho, \|\dot{\rho}\| \leq \vartheta} \left\{ \sum_{i=1}^p \dot{\rho}_i \frac{\partial h(\rho)}{\partial \rho_i} \right\} \quad (6.79)$$

Consequently, Theorem 6.3.1 must be modified with the following element:

$$\Xi_{22(\rho)} = -\left(1 - \sum_{i=1}^p \pm \vartheta_i \frac{\partial h(\rho)}{\partial \rho_i}\right)Q - R + \eta_d. \quad (6.80)$$

In the next section, the corollaries concerning the S-NLPV systems in Chapter 5 are implied from time-delay NLPV observer.

6.3.2 \mathcal{H}_∞ full-order NLPV Observer design for S-NLPV systems

In this section, the generic design of \mathcal{H}_∞ observer for S-NLPV system will be implied based on that of SD-NLPV in Section 6.3.1. Also, two design approaches corresponding to parameter-(in)dependent stability are introduced along with Corollaries of Theorem 6.3.1.

Consider the following class of S-NLPV systems:

$$\begin{cases} E\dot{x} &= A_{(\rho)}x + B_{(\rho)}u + B_{\phi(\rho)}\phi(x, u) + D_{1(\rho)}w, \\ y &= C_y x, \\ z &= C_z x. \end{cases} \quad (6.81)$$

Under Assumptions (A.2)-(A.4), the \mathcal{H}_∞ full-order NLPV observer that has the generic form:

$$\begin{cases} \dot{\xi} &= F_{(\rho)}\xi + J_{(\rho)}u + L_{(\rho)}y + TB_{\phi(\rho)}\phi(\hat{x}, u) \\ \hat{x} &= \xi + Ny \\ \hat{z} &= C_z \hat{x} \end{cases}, \quad (6.82)$$

which is directly deduced from SD-NLPV observer (6.5) with exact memory.

As a result, the following dynamics of observer is obtained:

$$\dot{e} = F_{(\rho)}e + T_{(Z)}B_{\phi(\rho)}\tilde{\phi} + T_{(Z)}D_{1(\rho)}w, \quad (6.83)$$

where

$$J_{(\rho)} = T_{(Z)}B_{(\rho)}, \quad (6.84)$$

$$K_{(\rho)} = -F_{(\rho)}N_{(Z)} + L_{(\rho)}, \quad (6.85)$$

$$F_{(\rho)} = T_{(Z)}A_{(\rho)} - K_{(\rho)}C_y. \quad (6.86)$$

$$T_{(Z)} = T_1 - ZT_2, \quad (6.87)$$

$$N_{(Z)} = N_1 - ZN_2, \quad (6.88)$$

In Case (c) of Chapter 5 for S-NLPV systems, the time-invariant matrices $T_{(Z)}$ and $N_{(Z)}$ are also be expressed by Z . However, this matrix Z must be optimized for \mathcal{H}_2 UI-decoupling condition, thus requiring matrix P in Lyapunov function be also a constant. On the other hand, the value of Z in \mathcal{H}_∞ observers of this Chapter is not restricted to any constraint like UI-decoupling condition. Therefore, two approaches are suggested for this issue:

- **Approach 1:** Z is not chosen but designed to ensure the stability of estimation error; thus, the constant P must be chosen for Lyapunov function to ensure the time-invariant matrices $T_{(Z)}$ and $N_{(Z)}$. Therefore, estimation error is quadratically stable.
- **Approach 2:** Z is chosen at the beginning of design process, for instance $Z = 0$ in [Hamdi et al. 2012; Rodrigues et al. 2014] is a common choice. Therefore, $T_{(Z)}$ and $N_{(Z)}$ are always time-invariant matrices. Accordingly, the parameter-dependent $P_{(\rho)}$ is applied to ensure the parameter-dependent stability of estimation error.

Consequently, the following corollaries corresponding to each approach are obtained:

Corollary 6.3.1 (Parameter-independent/Quadratic Stability)

Under the Assumptions (A.2)-(A.4), the design objectives (O.1)-(O.2) are achieved if there exist a symmetric positive definite matrix P , matrices Y_1 and $Y_{2(\rho)}$, a positive scalar ϵ which minimize γ_∞ and satisfy that:

$$\begin{bmatrix} \Omega_{11(\rho)} & \Omega_{12(\rho)} & \Omega_{13(\rho)} \\ (*) & -\epsilon I & 0 \\ (*) & (*) & -\gamma_\infty^2 I \end{bmatrix} < 0. \quad (6.89)$$

where

$$\Omega_{11(\rho)} = \mathcal{H}\{PT_1A_{(\rho)} + Y_1T_2A_{(\rho)} + Y_{2(\rho)}C_y\} + C_z^T C_z + \eta, \quad (6.90)$$

$$\Omega_{12(\rho)} = PT_1B_{\phi(\rho)} + Y_1T_2B_{\phi(\rho)}, \quad (6.91)$$

$$\Omega_{13(\rho)} = PT_1D_{1(\rho)} + Y_1T_2D_{1(\rho)}, \quad (6.92)$$

$$\eta = \epsilon(\gamma I)^T(\gamma I), \quad (6.93)$$

then the matrices Z and $K_{(\rho)}$ are calculated by: $Z = -P^{-1}Y_1$ and $K_{(\rho)} = -P^{-1}Y_{2(\rho)}$.

Using Z , matrices T and N are computed by (6.87)-(6.88). Meanwhile, the matrices $F_{(\rho)}$, $J_{(\rho)}$, $L_{(\rho)}$ are respectively implied from Eqs. (6.86), (6.84), and (6.85).

Corollary 6.3.2 (Parameter-dependent Stability)

Under the Assumptions (A.3)-(A.4) and the choice of $Z = 0$, the design objectives (O.1)-(O.2) are achieved if there exist a symmetric positive definite matrix $P_{(\rho)}$, a matrix $Y_{2(\rho)}$, a positive scalar ϵ which minimize γ_∞ and satisfy that:

$$\begin{bmatrix} \Omega_{11(\rho)} & \Omega_{12(\rho)} & \Omega_{13(\rho)} \\ (*) & -\epsilon I & 0 \\ (*) & (*) & -\gamma_\infty^2 I \end{bmatrix} < 0. \quad (6.94)$$

$$\text{where } \Omega_{11(\rho)} = \sum_i^m \pm \vartheta_i \frac{\partial P_{(\rho)}}{\partial \rho_i} + \mathcal{H}\{P_{(\rho)}T_1A_{(\rho)} + Y_{2(\rho)}C_y\} + C_z^T C_z + \eta, \quad (6.95)$$

$$\Omega_{12(\rho)} = P_{(\rho)}T_1B_{\phi(\rho)}, \quad (6.96)$$

$$\Omega_{13(\rho)} = P_{(\rho)}T_1D_{1(\rho)}, \quad (6.97)$$

$$\eta = \epsilon(\gamma I)^T(\gamma I), \quad (6.98)$$

then the matrix $K_{(\rho)}$ is calculated by: $K_{(\rho)} = -P_{(\rho)}^{-1}Y_{2(\rho)}$. Then, Eq. (6.86) implies the matrix $F_{(\rho)}$, while the matrices $J_{(\rho)}$ and $L_{(\rho)}$ are calculated from Eqs. (6.84) and (6.85).

Proof: By considering $Q = 0$ and $R = 0$ in Lyapunov-Krasovskii functional (6.48) and time-delay distribution matrices be null, eq. (6.68) implies that:

$$\begin{bmatrix} \Omega_{11(\rho)} & \Omega_{12(\rho)} & \Omega_{13(\rho)} \\ (*) & -\epsilon & 0 \\ (*) & (*) & -\gamma_\infty^2 I \end{bmatrix} < 0. \quad (6.99)$$

where

$$\Omega_{11(\rho)} = \sum_i^m \pm \vartheta_i \frac{\partial P_{(\rho)}}{\partial \rho_i} + \mathcal{H}\{P_{(\rho)}T_1A_{(\rho)} - P_{(\rho)}ZT_2A_{(\rho)} - P_{(\rho)}K_{2(\rho)}C_y\} + C_z^T C_z + \eta, \quad (6.100)$$

$$\Omega_{12(\rho)} = P_{(\rho)}T_1B_{\phi(\rho)} + -P_{(\rho)}ZT_2B_{\phi(\rho)}, \quad (6.101)$$

$$\Omega_{13(\rho)} = P_{(\rho)}T_1D_{1(\rho)} - P_{(\rho)}ZT_2D_{1(\rho)}, \quad (6.102)$$

$$\eta = \epsilon(\gamma I)^T(\gamma I). \quad (6.103)$$

Then, based on the choice of Z and the corresponding value of $P_{(\rho)}$ in Lyapunov function, Corollaries 6.3.1-6.3.2 are re-obtained. That completes the proof. \blacksquare

In brief, the generic design of \mathcal{H}_∞ observers is introduced for both SD-NLPV and S-NLPV systems in this section. Next part will present discussions on existence of \mathcal{H}_∞ time-delay NLPV observer and its implementation algorithms.

6.4 General Discussion

With the existence of $P_{(\rho)}$, $Y_{2(\rho)}$, and $Y_{2d(\rho)}$, the gridding approach in Section 1.3.2 is applied regardless of NLPV representation to solve effectively Theorem 6.3.1, as well as the Corollaries 6.3.1-6.3.2. As a result, analytical results for existence conditions of SD-NLPV systems will be introduced in Section 6.4.1, thus enabling the implementation of algorithms in Section 6.4.2.

6.4.1 Analytical Existence Condition for \mathcal{H}_∞ observer designs

In the gridding-based approach, the (singular time-delay) LPV system (under Lipschitz condition) is considered as (singular) linear time-invariant (LTI) time-delay system at each time-frozen gridding point ρ^j ($j = 1 : N_g$, $N_g = n_g^{\rho_1} \times n_g^{\rho_2} \times \dots \times n_g^{\rho_p}$) [Apkarian, Gahinet, and Becker 1995]. Therefore, the existence conditions for the observer design can be analytically derived for each point ρ^j in the grid as follows.

6.4.1.1 Impulse-free Condition

As observed in (6.23), the requirement for the existence of T and N is the impulse-free condition, which is independent of the time-varying parameter ρ :

$$(C.1) \quad \text{rank} \begin{bmatrix} E \\ C_y \end{bmatrix} = n_x. \quad (6.104)$$

6.4.1.2 R-detectability condition when $h(t) = 0$

The feasibility of Theorem 6.3.1 implies that for each time-frozen ρ^j (at $h(t) = 0$) there exists a matrix gain $[Z \ K_{(\rho^j)}]$ such that $F_{(\rho^j)}$ is stable. That is explained by the relation:

$$F_{(\rho^j)} = T_1 A_{(\rho^j)} - Z T_2 A_{(\rho^j)} - K_{(\rho^j)} C_y = T_1 A_{(\rho^j)} - [Z \ K_{(\rho^j)}] \begin{bmatrix} T_2 A_{(\rho^j)} \\ C_y \end{bmatrix}. \quad (6.105)$$

In other words, the pair $(T_1 A_{(\rho^j)}, \begin{bmatrix} T_2 A_{(\rho^j)} \\ C_y \end{bmatrix})$ must be R-detectable. This R-detectability condition is equivalent to:

$$(C.2) \quad \text{rank} \begin{bmatrix} pE - A_{(\rho^j)} \\ C_y \end{bmatrix} = n_x, \forall j = 1 : N, \mathcal{R}(p) \geq 0, \quad (6.106)$$

which has been proven in the Appendix B.2.

The satisfaction of analytical conditions allows the implementation of the grid-based algorithms in the next section.

6.4.2 Implementation Algorithm

Based on the grid-based methodology, the algorithms for the implementation of the time-delay NLPV proposed observer (6.5) consist of two steps:

Step 1: Offline Synthesis

- Define the gridding points for TVP vector ρ (consists of m elements ρ_i); accordingly, a total of N_g time-frozen points ρ^j ($j = 1 : N_g$) is to be obtained.
- Conduct the gridding-based synthesis: for $j = 1 : N_g$
 - Verify the impulse-free and R-detectability conditions (C.1) and (C.2). If the conditions are satisfied, continue to the next step; otherwise, stop the algorithm.
 - Define the distribution matrices dependent on ρ^j , as well as the time-invariant matrices C_y and Lipschitz constants γ and γ_d .

- Declare the matrices P_k , Y_{2k} , and Y_{2kd} that define the basis functions of $P_{(\rho)}$ and $Y_{(\rho)}$. For example 2^{nd} -order polynomial ($k = 0 : 2$) for $m = 1$:

$$P_{(\rho)} = P_0 + (\rho)P_1 + (\rho)^2P_2 \implies \frac{\partial P_{(\rho)}}{\partial \rho} = P'_{(\rho)} = P_1 + 2(\rho)P_2, \quad (6.107)$$

$$Y_{2(\rho)} = Y_{20} + (\rho)Y_{21} + (\rho)^2Y_{22}, \quad (6.108)$$

$$Y_{2d(\rho)} = Y_{20d} + (\rho)Y_{21d} + (\rho)^2Y_{22d}, \quad (6.109)$$

- Define the set of LMIs which represent Theorem 6.3.1, i.e.

$$\begin{bmatrix} -X - X^T & XF_{(\rho^j)} + P_{(\rho^j)} & XF_{d(\rho^j)} & XB_{e(\rho^j)} & XB_{de(\rho^j)} & XW_{(\rho^j)} & X & \bar{h}R \\ (*) & \Xi_{11(\rho^j)} & R & 0 & 0 & 0 & 0 & 0 \\ (*) & (*) & \Xi_{22(\rho^j)} & 0 & 0 & 0 & 0 & 0 \\ (*) & (*) & (*) & -\epsilon I & 0 & 0 & 0 & 0 \\ (*) & (*) & (*) & (*) & -\epsilon_d I & 0 & 0 & 0 \\ (*) & (*) & (*) & (*) & (*) & -\gamma_\infty^2 I & 0 & 0 \\ (*) & (*) & (*) & (*) & (*) & (*) & -P_{(\rho^j)} & -\bar{h}R \\ (*) & (*) & (*) & (*) & (*) & (*) & (*) & -R \end{bmatrix} < 0, \quad (6.110)$$

where

$$XF_{(\rho^j)} = XT_1A_{(\rho^j)} + Y_1T_2A_{(\rho^j)} + Y_{2(\rho^j)}C_y, \quad (6.111)$$

$$XF_{d(\rho^j)} = XT_1A_{d(\rho^j)} + Y_1T_2A_{d(\rho^j)} + Y_{2d(\rho^j)}C_y, \quad (6.112)$$

$$XB_{e(\rho^j)} = XT_1B_{\phi(\rho^j)} + Y_1T_2B_{\phi(\rho^j)}, \quad (6.113)$$

$$XB_{de(\rho^j)} = XT_1B_{\phi d(\rho^j)} + Y_1T_2B_{\phi d(\rho^j)}, \quad (6.114)$$

$$XW_{(\rho^j)} = XT_1D_{1(\rho^j)} + Y_1T_2D_{1(\rho^j)}, \quad (6.115)$$

$$\Xi_{11(\rho^j)} = \sum_i^m \pm \vartheta_i P'_{(\rho^j, i)} - P_{(\rho^j)} + Q - R + C_z^T C_z + \eta, \quad (6.116)$$

$$\Xi_{22(\rho^j)} = -(1 - \mu)Q - R + \eta_d, \quad (6.117)$$

$$\eta = \epsilon(\gamma I)^T(\gamma I), \quad (6.118)$$

$$\eta_d = \epsilon_d(\gamma_d I)^T(\gamma_d I), \quad (6.119)$$

- Compute the constant matrices P_k , Y_{2k} and Y_{2kd} , which are used to define $P_{(\rho)}$, $Y_{2(\rho)}$, and $Y_{2d(\rho)}$, such that $P_{(\rho^j)} > 0$ and all the above LMIs are satisfied.
- Calculate the time-invariant matrices: $Z = -X^{-1}Y_1$, $T_{(Z)} = T_1 - ZT_2$, and $N_{(Z)} = N_1 - ZN_2$.

Step 2: Online Implementation

- For instant t , update the values of TVP vector $\rho(t)$ and time-varying delay $h(t)$.

- Compute the matrices $P_{(\rho(t))}$, $Y_{2(\rho(t))}$ and $Y_{2d(\rho(t))}$ defined by $\rho(t)$ and the known matrices P_k , Y_{2k} , and Y_{2kd} .
- Calculate the parameter-varying observer matrices:

$$K_{(\rho(t))} = -X^{-1}Y_{2(\rho(t))}, \quad K_{d(\rho(t))} = -X^{-1}Y_{2d(\rho(t))}, \quad (6.120)$$

$$J_{(\rho(t))} = T_{(Z)}B_{(\rho(t))}, \quad J_{d(\rho(t))} = T_{(Z)}B_{d(\rho(t))}, \quad (6.121)$$

$$F_{(\rho(t))} = T_{(Z)}A_{(\rho(t))} - K_{(\rho(t))}C_y, \quad F_{d(\rho(t))} = T_{(Z)}A_{d(\rho(t))} - K_{d(\rho(t))}C_y, \quad (6.122)$$

$$L_{(\rho(t))} = K_{(\rho(t))} + F_{(\rho(t))}N, \quad L_{d(\rho(t))} = K_{d(\rho(t))} + F_{d(\rho(t))}N. \quad (6.123)$$

That completes the algorithms for the proposed time-delay observer.

6.5 Numerical Examples

In this section, a numerical example is demonstrated to justify the proposed \mathcal{H}_∞ observer design with exact memory for SD-NLPV system.

6.5.1 Model Parameters

Consider the SD-NLPV system:

$$\begin{cases} E\dot{x}(t) &= A_{(\rho)}x(t) + A_{d(\rho)}x(t - h(t)) + Bu(t) + B_d u(t - h(t)) \\ &+ B_\phi \sin(Gx(t))u(t) + B_{\phi d} \tanh(G_d x(t - h(t)))u(t - h(t)) + D_{1(\rho)}w, \\ y &= C_y x, \\ z &= C_z x, \end{cases}$$

where

- System parameters, which satisfy the analytical conditions (C.1) and (C.2), are chosen as follows:

$$E = \begin{bmatrix} 1 & 0 & 0 \\ 0 & 1 & 0 \\ 0 & 0 & 0 \end{bmatrix}, \quad A_{(\rho)} = \begin{bmatrix} -5 + \rho & 1 & 1 \\ 0 & -5 & 0 \\ 0.5 & 0 & -1 \end{bmatrix}, \quad A_{d(\rho)} = \begin{bmatrix} -1 & 0 & 0 \\ 1 & -2 + \rho & 0 \\ 0 & 0 & 0 \end{bmatrix}, \quad B = \begin{bmatrix} 0 \\ 0.2 \\ 0.5 \end{bmatrix},$$

$$B_d = \begin{bmatrix} 0 \\ 0.1 \\ 0 \end{bmatrix}, \quad B_\phi = \begin{bmatrix} 0 \\ 0.5 \\ 0 \end{bmatrix}, \quad B_{\phi d} = \begin{bmatrix} 0.1 \\ 0.1 \\ 0 \end{bmatrix}, \quad D_{1(\rho)} = \begin{bmatrix} 0.5\rho \\ 0.1\rho \\ 0 \end{bmatrix}, \quad C_y = \begin{bmatrix} 1 & 1 & -0.5 \\ 0 & 2 & -1 \end{bmatrix}, \quad G =$$

$$\begin{bmatrix} 0 & 0 & 1 \end{bmatrix}, \quad \text{and } G_d = \begin{bmatrix} 0 & 1 & 0 \end{bmatrix}.$$

- Delay $h(t) \leq \bar{h} = 2$ (s) and $\dot{h} \leq \mu = 0.7$ is expressed by:

$$h(t) = \frac{\bar{h}}{3} \sin\left(\frac{3\mu}{\bar{h}}t\right) + \frac{2\bar{h}}{3} \quad (6.124)$$

- Time-varying parameter $\rho = 0.25\sin(8t) + 0.75$ with $\dot{\rho} \leq 2$.
- Control input $u(t)$ is bounded in the region $|u(t)| \leq u_0 = 3$, thereby leading to the Lipschitz condition:

$$\|\phi(x(t), u(t)) - \phi(\hat{x}(t), u(t))\| \leq u_0 G \|x(t) - \hat{x}(t)\|, \quad (6.125)$$

$$\begin{aligned} & \|\phi(x(t-h(t)), u(t-h(t))) - \phi(\hat{x}(t-h(t)), u(t-h(t)))\| \\ & \leq u_0 G_d \|x(t-h(t)) - \hat{x}(t-h(t))\|, \end{aligned} \quad (6.126)$$

where $\phi(x(t), u(t)) = \sin(Kx(t))u(t)$, $\phi(x(t-h(t)), u(t-h(t))) = \tanh(K_d x(t-h(t)))u(t-h(t))$, $\gamma = u_0 G$ and $\gamma_d = u_0 G_d$.

The following parameters are chosen for the grid-based methodology: $N_g = 30$ points ($m = 1$, one time-varying parameter ρ) and 2^{nd} -order basis functions as suggested by [Abbas et al. 2014] for $P_{(\rho)}$, $Y_{2(\rho)}$, $Y_{2d(\rho)}$, i.e.

$$P_{(\rho)} = P_0 + \rho P_1 + \rho^2 P_2, \quad (6.127)$$

$$Y_{2(\rho)} = Y_{20} + \rho Y_{21} + \rho^2 Y_{22}, \quad (6.128)$$

$$Y_{2d(\rho)} = Y_{d20} + \rho Y_{d21} + \rho^2 Y_{d22}. \quad (6.129)$$

Then Theorem 6.3.1 is solved by finding constant matrices P_k , Y_{2k} , and Y_{d2k} ($k = 0 : 2$) such that $P_{(\rho)} > 0$ and LMI (6.38) are satisfied. The optimal attenuation indicators are obtained as: $\gamma_\infty = 0.0017$ (or -55.2284 dB) with the scalars $\epsilon = 6.2943$, and $\epsilon_d = 0.7140$.

6.5.2 Frequency Analysis

The sensitivity ρ^j in the following Bode diagrams represents the frequency response at each time-frozen value ρ^j ($j = 1 : 30$) of varying parameter ρ . Without loss of generality, $h(t) = \bar{h}$ is chosen and only the sensitivities ρ^1 , ρ^{10} , and ρ^{20} are presented to evaluate the whole varying range.

From (6.32), the sensitivity function can be analytically rewritten as:

$$S_{e_z w(t)(\rho^j)} = C_z (pI - F_{(\rho^j)} - e^{-p\bar{h}} F_{d(\rho^j)})^{-1} W_{1(\rho^j)}, \quad (6.130)$$

$$S_{e_z \tilde{\phi}(t)(\rho^j)} = C_z (pI - F_{(\rho^j)} - e^{-p\bar{h}} F_{d(\rho^j)})^{-1} B_{e(\rho^j)} \quad (6.131)$$

$$S_{e_z \tilde{\phi}(t-h(t))(\rho^j)} = C_z (pI - F_{(\rho^j)} - e^{-p\bar{h}} F_{d(\rho^j)})^{-1} B_{de(\rho^j)}. \quad (6.132)$$

Fig. 6.2 points out that all the sensitivities of UI $w(t)$ to the estimation error e_z have been attenuated by the \mathcal{H}_∞ -norm (induced \mathcal{L}_2 norm). In specific, their magnitudes are less than -140 (dB) ($< \gamma_\infty$). Meanwhile, the differences in the estimation of nonlinearity that satisfies the Lipschitz constraints exert a strong influence on estimation in the low frequency zone (peak around -40 dB < 1 Hz), but their impacts are drastically attenuated when the frequency of nonlinearity increases, as illustrated in Figs. 6.3-6.4.

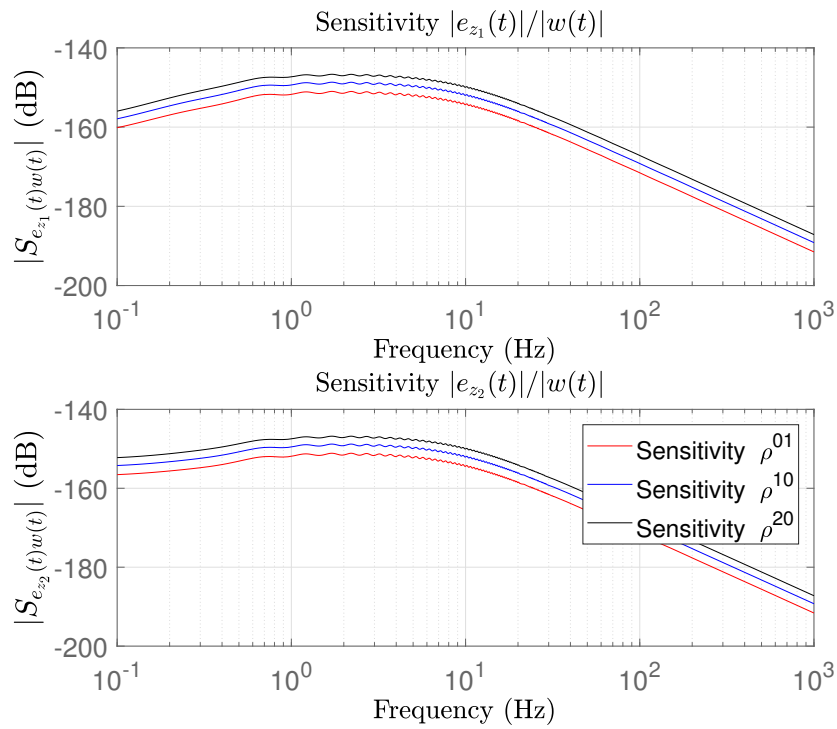


Figure 6.2: Sensitivity function $e_z(t)/w(t)$

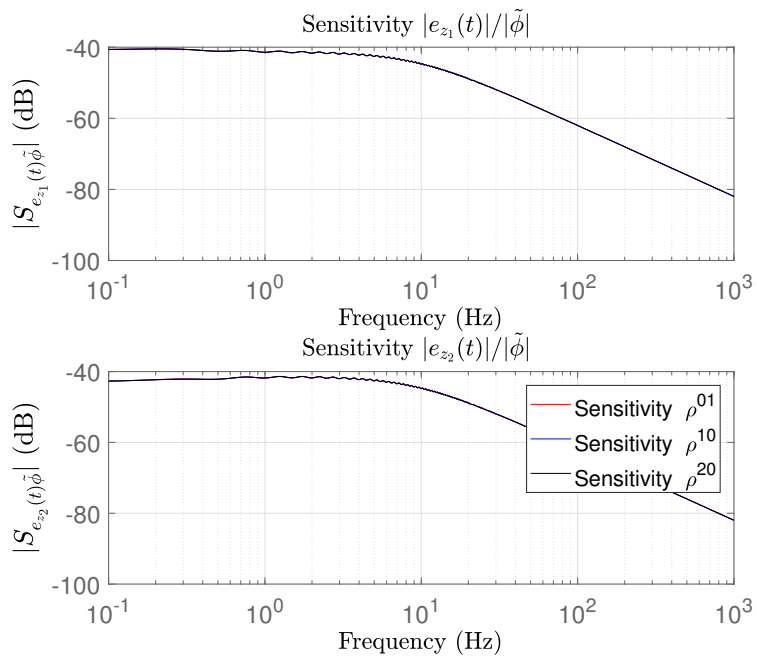
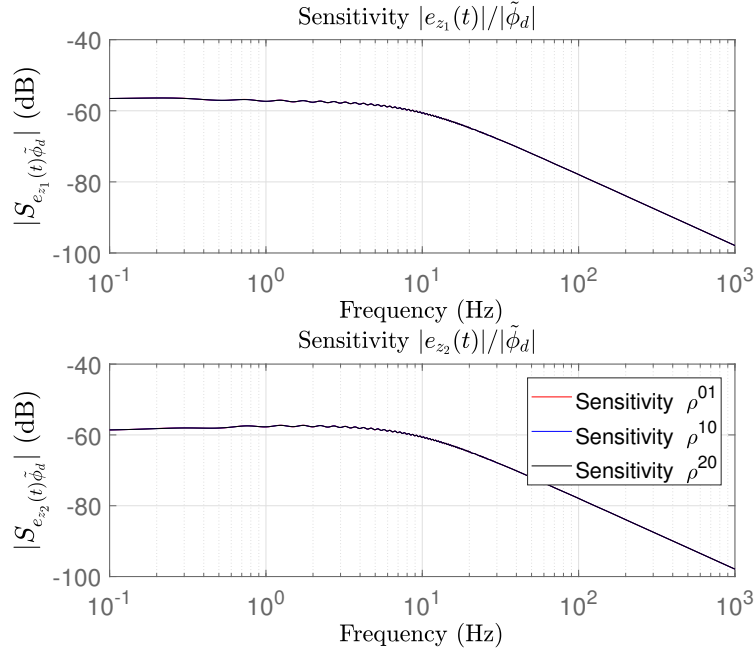


Figure 6.3: Sensitivity function $e_z(t)/\tilde{\phi}(t)$

Figure 6.4: Sensitivity function $e_z(t)/\tilde{\phi}_d(t-h(t))$

6.5.3 Simulation result

The time-domain simulation is realized with the following conditions:

- Simulation time: 4 (s).
- The UI is chosen as a sinusoidal signal:

$$w(t) = 2 \sin(2\pi t). \quad (6.133)$$

- The control input u is chosen as:

$$u(t) = u_0 \sin(10\pi t). \quad (6.134)$$

- Initial conditions: $\forall \lambda \in [-\bar{h}, 0] : \varpi_x(\lambda) = 0, \varpi_u(\lambda) = 0$, and $\varpi_\xi(\lambda) = [0.1 \quad 0.01 \quad -1]^T$.

As observed in Figs. 6.5-6.6, the estimated signals \hat{z}_1 and \hat{z}_2 have converge to their respective z_1 and z_2 after 2 seconds. Moreover, the small RMS values of estimation errors, which are computed in Table 6.1 when the estimation is accomplished, have highlighted the effectiveness of \mathcal{H}_∞ Time-delay NLPV observer with exact memory in UI attenuation and estimation of the desired signals z_1 and z_2 .

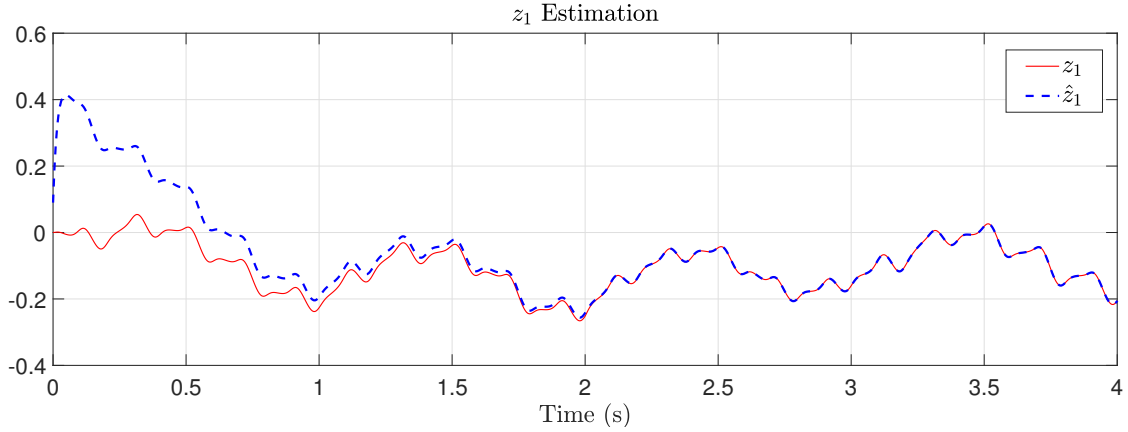
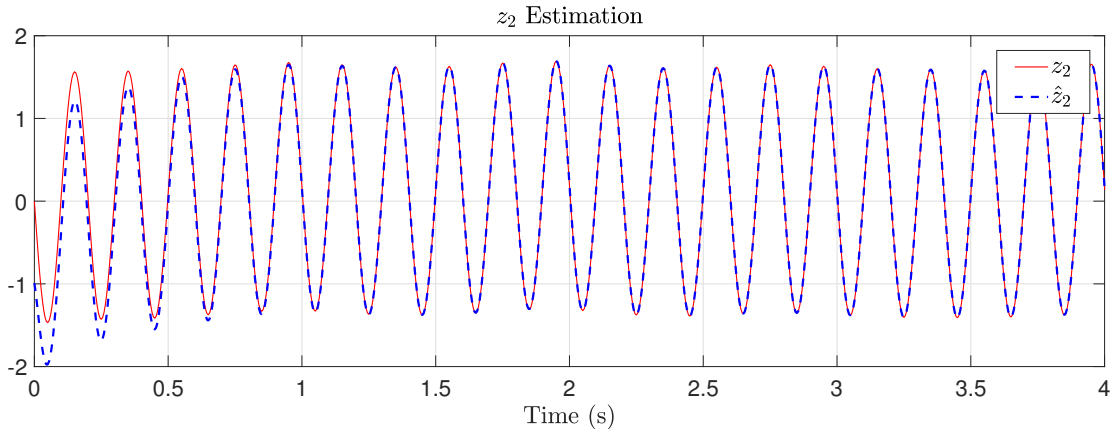
Figure 6.5: z_1 estimationFigure 6.6: z_2 estimation

Table 6.1: RMS Evaluation of estimation error

	e_{z_1}	e_{z_2}
RMS	$0.0724e-3$	$0.2349e-3$

6.6 Conclusion

In this Chapter, an extension of the S-NLPV system with Lipschitz nonlinearity and time-delay phenomenon is introduced, which promotes the implementation of the LPV framework in modeling the nonlinear system. Then, a diversity of \mathcal{H}_∞ observer designs with parameter-(in)dependent stability and delay-(in)dependent stability are proposed to attenuate the UI impact on estimation error. Moreover, their capability is further justified by numerical simulations under the existence of Lipschitz nonlinearity and time-varying delay.

On the other hand, besides the drawbacks mentioned in Chapter 5 for S-NLPV systems,

the proposed designs also have two additional limitations that should be overcome in future work. Firstly, the uncertainty, such as inexact time-varying parameters between system and its observer, has not been taken into account in the robustness and stability of \mathcal{H}_∞ observer designs. Secondly, the problem of fault and state estimation has not yet been investigated.

Conclusions and Perspectives

General Conclusions

The Thesis has considered many observer designs for (non-)singular LPV (S-LPV) systems, as well as their local time-frozen S-LTI models. Hereunder are the problems tackled during the design process:

- First, the problem of parametric uncertainty is the cause for instability of observer design in FDD and the closed-loop dynamics in FTC. Also, their available formulation such as polytopic can exceed the number of LMIs or generate a complicated solution for robust observer design.
- Second, due to the simultaneous existence of disturbances (uncertainty, UI, stochastic noise), the multi-objective problem poses challenges in finding an optimal solution for disturbance attenuation. In addition, the existing methods are applicable to only one or two kinds of disturbances at the same time.
- Third, studies on nonlinearity of scheduling parameter ρ have not been addressed for the S-LPV systems.
- Fourth, the UI-decoupling problem has always generated restrictive constraints in UI Observers. However, its solutions for partially decoupled UIs (LTI system) or parameter-varying UI-decoupling condition (LPV system) are only applicable to non-singular systems. Also, those methods cannot take advantage of UI bandwidth or must require many assumptions and system reformulations.

To resolve such above issues, five chapters have been developed in this Thesis with the contributions summarized as below. In specific, the first and second problems have been respectively addressed in Chapters 2 and 3. Then, Chapter 4 tackles the four one concerning partially decoupled UIs in S-LTI systems, while Chapters 5-6 developed the NLPV solutions for both third and four issues.

- **Chapter 2** proposes a robust observer-controller co-design for FDD in uncertain LPV systems with drift faults. In which, the uncertainty terms are rewritten by a generalized formulation to avoid exceeding the number of LMIs in the polytopic one, then are handled in stability analysis by majorization lemma to prevent the inconveniences of parameter-dependent null-space due to the usage of projection lemma. Moreover, since the proposed observer for FDD is synthesized through a closed-loop with a state-feedback controller, both observer and controller gains can be robustly obtained by solving a LMI

optimization. Meanwhile, the designed observer can be independently applied for the FDD process while the robust co-design is the foundation for active FTC developed later in Chapter 3. Finally, the application of the proposed co-design to sensor fault estimation is presented for suspension platform INOVE, thus emphasizing the importance of robust synthesis in observer-based designs and the FDD process.

- **Chapter 3** introduces a generic strategy of designing polytopic observer-based fault compensators for degradation estimation and accommodation in uncertain stochastic LPV system. In essence, these robust-stochastic integrated designs are built based on the robust co-design for FDD in Chapter 2, along with the fault accommodation of the FTC process. Meanwhile, the degradation is modeled by a special expression of polynomial fault and then estimated together with system state in an augmented system. Based on the matching condition of UI frequency, the design strategy is divided into two groups. For matched UI, a novel methodology of output frequency-shaping filter is introduced to alternate the \mathcal{H}_∞ synthesis, thus avoiding the multi-objective problem in attenuating both impacts of noise and UI. For unmatched UI, an extension for the classical $\mathcal{H}_\infty / \mathcal{H}_2$ synthesis is developed. Since the solutions for both groups are based on closed-loop dynamics, observer-controller gains ensure the robust stability of the system against the simultaneous presence of uncertainties, UIs, and stochastic noise. Furthermore, by rewriting the actuator saturation as a LPV problem, the results for the anti-windup controller are obtained. Finally, a numerical example has been conducted to illustrate the proposed designs and thus highlight the benefits of the frequency-shaping filter in disturbance attenuation.
- **Chapter 4** develops a generic approach for actuator fault estimation in S-LTI systems perturbed by the partially decoupled UIs. In which, the actuator fault is expressed in a general form (including abrupt/incipient faults, and even degradation). Meanwhile, partially decoupled UIs are divided into decoupled and non-decoupled UI, thus relaxing UI-decoupling condition since only a few columns of UI matrices are needed to satisfy the UI-decoupling constraint. Based on the conventional UI observer, the generic solution decouples the fault estimation with decoupled UIs, while the non-decoupled UIs are handled by either \mathcal{H}_∞ synthesis or frequency-shaping filter, depending on UI bandwidth. Furthermore, the proposed approach is applicable to not only S-LTI systems but also the LTI systems. Finally, a numerical example is presented to emphasize the advantages of the frequency-shaping filter, which only needs to be stable but not necessarily causal, over \mathcal{H}_∞ synthesis in UI attenuation for a specified bandwidth.
- **Chapter 5** and **Chapter 6** provide the generic conception of NLPV observer designs which relax/bypass the parameter-dependent UI-decoupling condition. In which, the proposed designs are built based on the generic full-order observer and are applicable to the general class of S-NLPV system which not only unifies all the so far existing LPV systems but also takes into account the Lipschitz nonlinearity and time-delay phenomena. In specific, to tackle the UI-decoupling condition, two solutions are proposed: \mathcal{H}_2 - criteria (Chapter 5) and \mathcal{H}_∞ synthesis (Chapter 6). In which, \mathcal{H}_2 approach handles directly the condition by minimizing its induced 2-norm without requiring additional assumptions on time-varying parameters and system reformulations. Meanwhile, the

\mathcal{H}_∞ observers attenuate the impact of UI on estimation error by minimizing the attenuation level γ_∞ . Also, their conditions of R-detectability and impulse-free are analytically verified thanks to the grid-based method, which can be applied regardless of LPV system representation. Finally, the numerical examples have highlighted the performance of the proposed designs.

Based on the above remarks, the developed observers in this Thesis have successfully overcome the mentioned problems. However, they also have certain drawbacks, which are the motivation for future work presented in the next section.

Perspectives

Despite the effective performance of the proposed designs, there still exist problems in experimental validation and design assumptions that need to be relaxed or lifted up if possible. Hereunder are the suggestions for the short-term and long-term development, classified based on the complexity of issues and availability of references.

Short-term Development

- **Degradation Estimation**

In Chapter 3, only numerical examples are used to demonstrate the capability of the proposed observer-based controller in degradation estimation and accommodation. In the future, it is necessary to verify the method with a real platform where its actuator is stretched out to its degradation point. In fact, the author is planning to cooperate with the laboratory CRAN in Nancy for the experimental test.

- **Inexact measurement/estimation of time-varying parameter ρ**

As mentioned in Chapter 3, since the UI frequency, which acts as a time-varying parameter in integrated designs, is estimated/identified, there exists the uncertainty in the dynamics of the frequency-shaping filter. Thus, a study about its impact on the performance of the closed-loop system should be carried out. In addition, the observer designs in Chapters 5-6 for S-NLPV systems should also consider the uncertainty of time-varying parameter ρ and the Lipschitz condition on nonlinearity, as in the robust research of [López-Estrada et al. 2015a].

- **Stochastic Measurement in Full-order observers**

In Chapters 4-6, the full-order observers are only applicable to the deterministic UI w . Moreover, the stochastic noise in measurement can intervene in the dynamics of estimation error, thus affecting the general quality and accuracy of estimation. Therefore, a full-order observer integrating Kalman filtering should be considered in the future as in [Darouach et al. 1995] for S-LTI systems.

- **Fault estimation problem in S-NLPV systems**

Although the observer designs developed in Chapters 5-6 are able to estimate the state in both S-NLPV and SD-NLPV systems, their application to fault estimation has not been studied yet. One possible solution is to rewrite the faults as augmented states of the S-NLPV system, similar to [Shi and Patton 2015a] in S-LPV systems.

- **Nonlinearity in S-NLPV systems**

In this Thesis, the Lipschitz constraint is assumed in order to tackle non-linearity in the S-NLPV system. However, its Lipschitz constant γ must be fixed, i.e. maximal bound of nonlinearity, which means the LMI solution is actually not giving the optimal value. Consequently, the study on the parameter-varying $\gamma(\rho)$ and its impact on stability synthesis should be conducted to obtain better values of observer gains. One notable study on this topic is [Yang, Rotondo, and Puig 2019] where the quadratic stability with parameter-dependent Lipschitz constraint is studied for controller synthesis.

Furthermore, since the Lipschitz condition is not always attainable in practice, solutions for a more general property of nonlinearity, such as Hölder condition [Kress, Mazya, and Kozlov 1989], are needed in future work.

Long-term Development

- **Parameter-dependent stability for stochastic integrated design**

To incorporate the stochastic problem in the integrated design, a constant matrix \mathcal{X} has been used in Theorem 3.3.1 of Chapter 3, thus ensuring the parameter-independent stability (quadratic stability) of the closed-loop synthesis. Since \mathcal{X} is conservative, it is necessary to find a parameter-dependent $\mathcal{X}(\rho)$ in order to widen the feasible region of the LMI solution. Unfortunately, until now, there has been only the research concerning the usage constant \mathcal{X} for stochastic noise, such as [Wu et al. 1996] and [Tuan, Apkarian, and Nguyen 2001].

- **Integrated design for S-NLPV systems**

In Chapters 2 and 3, the integrated design of classical LPV systems has been discussed. However, due to the non-linearity in the S-NLPV system, the linear observer-based controller with fault compensation is no more applicable. Consequently, there is a need for a new integrated design that is based on non-linear fault accommodation, namely the combination of sliding mode control [Tanelli et al. 2016] and fault compensation. In addition, a robust co-design for FDD and an integrated design for FTC can be deduced for uncertain S-NLPV systems.

- **Parameter-dependent singular matrix $E(\rho)$ for the family of S-LPV systems**

To the best of the author's knowledge, the usage of constant E is the most applied study case for S-LPV systems in order to take advantage of the analysis and observer designs in S-LTI systems. Meanwhile, the case where $E(\rho(t))$ depends on the time-varying parameter $\rho(t)$ has not been broadly studied yet due to difficulties in the analysis of parameter-dependent regularity, impulse-free condition, and stability.

On the other hand, in Singular Linear Time-Varying (S-LTV) systems, the observability [Hernández et al. 2019] and impulse analysis [Yan and Duan 2006] have been conducted for $E(t)$. However, the implementation of these works to LPV systems should be carefully examined since the LPV systems are considered as a generalization of the general class of LTV Systems [Briat 2008]. Also, $E_{(\rho(t))}$ of S-LPV systems depends on real-time measured $\rho(t)$ instead of being prior known like $E(t)$ of S-LTV systems. Therefore, $E_{(\rho(t))}$ is an interesting topic for further study in widening the modeling and application of S-LPV systems.

- **Extension results for Multi-agent systems**

Although the \mathcal{H}_∞ observer developed in this Thesis is applied to time-delay S-NPV systems, it can be modified for multi-agent systems. In fact, multi-agent systems [Dorri, Kanhere, and Jurdak 2018] share many common characteristics with SD-NPLV systems, also having communication delays and requiring algebraic constraints in input-output relation as S-NLPV systems do. [Chadli, Davoodi, and Meskin 2016] and [Chen et al. 2016] are two typical papers on \mathcal{H}_∞ observer for multi-agent LPV systems. However, these works have not yet considered the propagation delays in state/input/output.

Suspension/Quarter-car LPV Modeling

This appendix is devoted to the LPV modeling of quarter-car dynamics or semi-active vehicle suspension. It serves as the foundation for the experimental tests of platform INOVE in Chapter 2 and the motivation for the development of S-NLPV systems in Chapters 5-6.

As mentioned in [Savaresi et al. 2010], a suspension system can be modeled by a mass-spring-damper system as described in Fig. A.1.

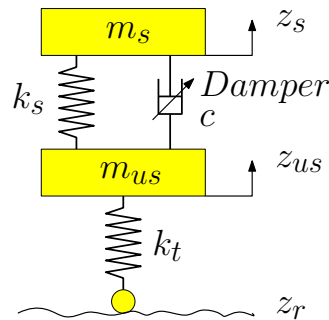


Figure A.1: The quarter-car scheme

In which:

- The sprung mass m_s represents a quarter of the chassis body and z_s is the vertical displacement around the equilibrium point of m_s ;
- The sprung mass m_{us} represents the vehicle wheel/tire of the vehicle and z_{us} is the vertical displacement around the equilibrium point of m_{us} ;
- The semi-active suspension is composed of a spring with the stiffness coefficient k_s and a controllable damper with the damping coefficient c , in which $c_{min} \leq c \leq c_{max}$;
- The tire is modeled by a spring with the stiffness coefficient k_t ;
- The road profile z_r is considered as an unknown input d for the suspension.

The suspension dynamics is defined by the followings: [Savaresi et al. 2010]

$$\begin{cases} m_s \ddot{z}_s &= -k_s(z_s - z_{us}) - F_d \\ m_{us} \ddot{z}_{us} &= k_s(z_s - z_{us}) + F_d - k_t(z_{us} - z_r) \end{cases} \quad (\text{A.0.1})$$

where F_d is the controlled damper force.

Depending on the model of damper, the suspension models are given as follows:

A.1 Linear Model of Damper

The linear damper force is expressed as: [Savaresi et al. 2010]

$$F_d = c \cdot \dot{z}_{def} \quad (\text{A.1.1})$$

The damper force F_d can also be rewritten as:

$$F_d = (c_0 + u) \dot{z}_{def} = c_0 \dot{z}_{def} + u \dot{z}_{def}. \quad (\text{A.1.2})$$

In which, u is the additive damping coefficient or system control input and c_0 is the nominal value of the damper.

By choosing deflection speed \dot{z}_{def} as the time-varying parameter ρ [Do et al. 2011], the LPV suspension system is demonstrated by:

$$\dot{x} = Ax + B_{(\rho)}u + E_w w, \quad (\text{A.1.3})$$

where: $x = [z_{def} \quad \dot{z}_s \quad z_{us} \quad \dot{z}_{us}]^T$ is the system state; $w = z_r$ is the unknown input; $A = \begin{bmatrix} 0 & 1 & 0 & -1 \\ -\frac{k_s}{m_s} & -\frac{c_0}{m_s} & 0 & \frac{c_0}{m_s} \\ 0 & 0 & 0 & 1 \\ \frac{k_s}{m_{us}} & \frac{c_0}{m_{us}} & -\frac{kt}{m_{us}} & -\frac{c_0}{m_{us}} \end{bmatrix}$; $B_{(\rho)} = \begin{bmatrix} 0 \\ -\frac{\rho}{m_s} \\ 0 \\ \frac{\rho}{m_{us}} \end{bmatrix}$; and $E_w = \begin{bmatrix} 0 \\ 0 \\ 0 \\ \frac{kt}{m_{us}} \end{bmatrix}$.

In Part I of this dissertation, the experimental results on fault estimation and fault-tolerant control will be primarily concerned with the linear model of the damper.

A.2 Nonlinear Model of Damper

According to [Pham, Sename, and Dugard 2019], the nonlinear damper force F_d can be displayed as:

$$\begin{cases} F_d &= k_0(z_s - z_{us}) + c_0(\dot{z}_s - \dot{z}_{us}) + F_{ER} \\ \dot{F}_{ER} &= -\frac{1}{\tau} F_{ER} + \frac{F_c}{\tau} u \underbrace{\tanh(k_1(z_s - z_{us}) + c_1(\dot{z}_s - \dot{z}_{us}))}_{\phi(Kx)}. \end{cases} \quad (\text{A.2.1})$$

In which, $k_0, c_0, k_1, c_1, F_c, \tau$, and $K = [k_1 \ c_1 \ 0 \ -c_1 \ 0]$ are known parameters of the damper; system state $x = [z_s - z_{us} \ \dot{z}_s \ z_{us} - z_r \ \dot{z}_{us} \ F_{ER}]^T$; and u is the controlled pwm signal generating the voltage ($F_c/\tau u$) as the input of the damper.

If the time-varying parameter $\rho = \phi(Kx)$ is chosen, a quasi-LPV model is to be obtained. However, $\rho(t)$ can not be directly measured but must be implied from the full states of the system, which can only be partly estimated or fully estimated. Consequently, the non-linearity of the initial physical dynamics is not always expressed correctly and the quality of controller/observer designs for the LPV system is adversely affected.

On the other hand, since $-1 \leq \tanh(\cdot) = \phi(\cdot) \leq 1$, the Lipschitz condition is obtained: $\|\phi(Kx) - \phi(K\hat{x})\| \leq 1 \cdot \|Kx - K\hat{x}\| = K\|x - \hat{x}\|$. Hence, the LPV model with Lipschitz nonlinearity is rewritten as:

$$\dot{x} = Ax + B_{\phi(\rho)}\phi(Kx) + E_w w, \quad (\text{A.2.2})$$

where $\rho = u$ is the scheduling parameter; $w = \dot{z}_r$ is the unknown input; $B_{(\rho)} = \begin{bmatrix} 0 \\ 0 \\ 0 \\ 0 \\ -\frac{F_c}{\tau}\rho \end{bmatrix}$;

$$E_w = \begin{bmatrix} 0 \\ 0 \\ -1 \\ 0 \\ 0 \end{bmatrix}; \text{ and } A = \begin{bmatrix} 0 & 1 & 0 & -1 & 0 \\ -\frac{k_s+k_0}{m_s} & -\frac{c_0}{m_s} & 0 & \frac{c_0}{m_s} & -\frac{1}{m_s} \\ 0 & 0 & 0 & 1 & 0 \\ \frac{k_s+k_0}{m_{us}} & \frac{c_0}{m_{us}} & -\frac{kt}{m_{us}} & -\frac{c_0}{m_{us}} & -\frac{1}{m_{us}} \\ 0 & 0 & 0 & 0 & -\frac{1}{\tau} \end{bmatrix}.$$

The existence of Lipschitz nonlinearity in system dynamics motivates the development of observation methods applicable to not only the classical LPV system in Section A.1 but also the nonlinear parameter-varying system (NLPV) in Section A.2. More details regarding the non-singular NLPV model can be found in the works of [Boukroune, Aitouche, and Cocquempot 2015; Us Saqib et al. 2017; Abdullah and Qasem 2019; Pham 2020]. In this thesis, the solutions to the singular NLPV system will be focused and presented as main results in Part II.

R-detectability of singular systems

Contents

B.1 R-detectability condition for UI observer in S-LTI systems	189
B.2 R-detectability condition for UI observer in S-NLPV systems	191

This appendix presents the proofs concerning the R-detectability condition of the S-LTI system in Chapter 4 and that of S(D)-NLPV system in Chapters 5-6.

B.1 R-detectability condition for UI observer in S-LTI systems

In this section, the proof that the condition (C.2) for S-LTI systems in Chapter 4 is equivalent to the R-detectability of the pair $(\Omega\Theta^\dagger\phi_1, \Theta^\perp\phi_1)$ is introduced. Thus, the two following issues will be examined.

(a) Condition (C.2) is equivalent to:

$$\text{rank} \begin{bmatrix} pI_{n_{x_a}} & \Omega \\ \phi_1 & \Theta \end{bmatrix} - 2n_{x_a} = n_{x_a} + n_{w_1}, \forall \mathcal{R}(p) \geq 0. \quad (\text{B.1.1})$$

(b) The relation (B.1.1) is proved to be equivalent to:

$$\text{rank} \begin{bmatrix} pI - \Omega\Theta^\dagger\phi_1 \\ \Theta^\perp\phi_1 \end{bmatrix} = n_{x_a} \quad \forall \mathcal{R}(p) \geq 0, \quad (\text{B.1.2})$$

which is also the detectability of the pair $(\Omega\Theta^\dagger\phi_1, \Theta^\perp\phi_1)$.

Accordingly, the proof is divided into 2 parts:

Proof (a):

Define $X_1 = \begin{bmatrix} -I_{n_{x_a}} & 0 & 0 & 0 & 0 \\ pI_{n_{x_a}} & I_{n_{x_a}} & 0 & 0 & 0 \\ 0 & 0 & 0 & I_{n_{x_a}} & 0 \\ 0 & 0 & 0 & 0 & -I_{n_{w_1}} \end{bmatrix}$ which is a non-singular matrix, then (B.1.1)

is equivalent to:

$$\text{rank} \begin{bmatrix} pI_{n_{x_a}} & \Omega \\ \phi_1 & \Theta \end{bmatrix} X_1 - 2n_{x_a} = n_{x_a} + n_{w_1}, \forall \mathcal{R}(p) \geq 0, \quad (\text{B.1.3})$$

$$\text{where } \Omega = \begin{bmatrix} I_{n_{x_a}} & 0_{n_{x_a} \times (n_{x_a} + n_{w_1})} \end{bmatrix}, \Theta = \begin{bmatrix} E_a & A_a & D_{w_1 a} \\ C_a & 0 & 0 \\ 0 & -C_a & 0 \\ 0 & -I_{n_{x_a}} & 0 \end{bmatrix}, \text{ and } \phi_1 = \begin{bmatrix} A_a \\ 0_{n_y \times n_{x_a}} \\ -C_a \\ 0_{n_{x_a} \times n_{x_a}} \end{bmatrix}$$

$$(\text{B.1.3}) \Leftrightarrow \text{rank} \begin{bmatrix} pE_a - A_a & D_{w_1 a} \\ C_a & 0 \end{bmatrix} = n_{x_a} + n_{w_1}, \forall \mathcal{R}(p) \geq 0. \quad (\text{B.1.4})$$

$$\Leftrightarrow \text{rank} \begin{bmatrix} (pE - A) & -B & 0 & \dots & 0 & 0 & D_{w_1} \\ 0 & pI & -I & \dots & 0 & 0 & 0 \\ 0 & 0 & pI & \dots & 0 & 0 & 0 \\ \dots & \dots & \dots & \dots & \dots & \dots & \dots \\ 0 & 0 & 0 & \dots & pI & -I & 0 \\ 0 & 0 & 0 & \dots & 0 & pI & 0 \\ C & 0 & 0 & \dots & 0 & 0 & 0 \end{bmatrix} = n_x + (n+1)n_u + n_{w_1}, \forall \mathcal{R}(p) \geq 0,$$

which is equivalent to (C.2):

$$(\text{C.2}) \quad \text{rank} \begin{bmatrix} (pE - A) & -B & D_{w_1} \\ 0 & pI & 0 \\ C & 0 & 0 \end{bmatrix} = n_x + n_{w_1}, \forall \mathcal{R}(p) \geq 0. \quad (\text{B.1.5})$$

Proof (b):

Define the full-column rank matrix X_2 and the non-singular matrix X_3 :

$$X_2 = \begin{bmatrix} I_{n_{x_a}} & -\Omega\Theta^\dagger \\ 0 & \Theta^\perp \\ 0 & \Theta\Theta^\dagger \end{bmatrix}, \quad X_3 = \begin{bmatrix} I_{n_{x_a}} & 0 \\ -\Theta^\dagger\phi_1 & I_{2n_{x_a} + n_{w_1}} \end{bmatrix} \quad (\text{B.1.6})$$

As $\Theta\Theta^\dagger\Theta = \Theta$, $\Theta^\dagger\Theta\Theta^\dagger = \Theta^\dagger$, and $\text{rank} \begin{bmatrix} \Theta \\ \Omega \end{bmatrix} = \text{rank} \Theta$, we obtain (B.1.1)

$$\Leftrightarrow \text{rank} X_2 \begin{bmatrix} pI_{n_{x_a}} & \Omega \\ \phi_1 & \Theta \end{bmatrix} X_3 - 2n_{x_a} = n_{x_a} + n_{w_1}, \forall \mathcal{R}(p) \geq 0 \quad (\text{B.1.7})$$

$$\Leftrightarrow \text{rank} \Theta + \text{rank} \begin{bmatrix} pI - \Omega\Theta^\dagger\phi_1 \\ \Theta^\perp\phi_1 \end{bmatrix} - 2n_{x_a} = n_{x_a} + n_{w_1}, \forall \mathcal{R}(p) \geq 0 \quad (\text{B.1.8})$$

Since (C.1), i.e. $\text{rank} \begin{bmatrix} E & D_{w_1} \\ C & 0 \end{bmatrix} = n_x + n_{w_1}$, implies $\text{rank} \Theta = 2n_{x_a} + n_{w_1}$, (B.1.1) \Leftrightarrow (B.1.2).

Combining the result of two parts (a) and (b), the proof for detectability is completed.

B.2 R-detectability condition for UI observer in S-NLPV systems

This section provides the proof that the condition (C.2) for S(D)-NLPV system in Chapters 5 and 6 is equivalent to the detectability of the pair $(T_1 A_{(\rho^j)}, \begin{bmatrix} T_2 A_{(\rho^j)} \\ C_y \end{bmatrix})$. Thus, the two following issues will be examined.

(a) The condition (C.2) is equivalent to :

$$\text{rank} \begin{bmatrix} pI - T_{(Z)} A_{(\rho^j)} \\ C_y \end{bmatrix} = n_x, \forall j = 1 : N_g, \mathcal{R}(p) \geq 0. \quad (\text{B.2.1})$$

(b) The condition (B.2.1) is equivalent to the R-detectability of the pair $(T_1 A_{(\rho^j)}, \begin{bmatrix} T_2 A_{(\rho^j)} \\ C_y \end{bmatrix})$.

Accordingly, the proof is divided into 2 parts:

Proof (a):

The condition (C.2) is expressed by:

$$\text{rank} \begin{bmatrix} pE - A_{(\rho^j)} \\ C_y \end{bmatrix} = n_x, \forall j = 1 : N_g, \mathcal{R}(p) \geq 0, \quad (\text{B.2.2})$$

which is equivalent to:

$$\text{rank} \begin{bmatrix} pE - A_{(\rho^j)} \\ pC_y \\ C_y \end{bmatrix} = n_x, \forall j = 1 : N_g, \mathcal{R}(p) \geq 0. \quad (\text{B.2.3})$$

By defining the matrix $X_1 = \begin{bmatrix} T_{(Z)} & N_{(Z)} & 0 \\ 0 & I_{n_y} & -pI_{n_y} \\ 0 & 0 & I_{n_y} \end{bmatrix}$, the above condition is equivalent to:

$$\text{rank}(X_1 \begin{bmatrix} pE - A_{(\rho^j)} \\ pC_y \\ C_y \end{bmatrix}) = n_x, \forall j = 1 : N_g, \mathcal{R}(p) \geq 0. \quad (\text{B.2.4})$$

$$\Leftrightarrow \text{rank} \begin{bmatrix} pT_{(Z)}E - T_{(Z)}A_{(\rho^j)} + pN_{(Z)}C_y \\ 0 \\ C_y \end{bmatrix} = n_x, \quad (\text{B.2.5})$$

$$\forall j = 1 : N_g, \mathcal{R}(p) \geq 0.$$

As $T_{(Z)}E + N_{(Z)}C_y = I$, it follows that:

$$\text{rank} \begin{bmatrix} pI - T_{(Z)}A_{(\rho^j)} \\ C_y \end{bmatrix} = n_x, \forall j = 1 : N_g, \mathcal{R}(p) \geq 0.$$

Proof (b):

The R-detectability of the pair $(T_1 A_{(\rho^j)}, \begin{bmatrix} T_2 A_{(\rho^j)} \\ C_y \end{bmatrix})$ is explicitly written as:

$$\text{rank} \begin{bmatrix} pI_{n_x} - T_1 A_{(\rho^j)} \\ T_2 A_{(\rho^j)} \\ C_y \end{bmatrix} = n_x, \forall j = 1 : N_g, \mathcal{R}(p) \geq 0. \quad (\text{B.2.6})$$

By defining the full-row rank matrix $X_2 = \begin{bmatrix} I & Z & 0 \\ 0 & 0 & I \end{bmatrix}$, the above condition is equivalent to:

$$\text{rank}(X_2 \begin{bmatrix} pI_{n_x} - T_1 A_{(\rho^j)} \\ T_2 A_{(\rho^j)} \\ C_y \end{bmatrix}) = n_x, \forall j = 1 : N_g, \mathcal{R}(p) \geq 0, \quad (\text{B.2.7})$$

$$\Leftrightarrow \text{rank} \begin{bmatrix} pI_{n_x} - T_1 A_{(\rho^j)} + Z T_2 A_{(\rho^j)} \\ C_y \end{bmatrix} = n_x, \forall j = 1 : N_g, \mathcal{R}(p) \geq 0, \quad (\text{B.2.8})$$

$$\Leftrightarrow \text{rank} \begin{bmatrix} pI_{n_x} - T_{(Z)} A_{(\rho^j)} \\ C_y \end{bmatrix} = n_x, \forall j = 1 : N_g, \mathcal{R}(p) \geq 0, \quad (\text{B.2.9})$$

By combining the parts (a) and (b), the proof is completed.

Bibliography

- Abbas, Hossam Seddik et al. (2014). “LPV state-feedback control of a control moment gyroscope.” In: *Control Engineering Practice* 24, pp. 129–137 (cit. on pp. 26, 57, 149, 174).
- Abdallah, Chaouki et al. (1993). “Delayed positive feedback can stabilize oscillatory systems.” In: *1993 American Control Conference*. IEEE, pp. 3106–3107 (cit. on p. 22).
- Abdallah, Chaouki T et al. (2011). “Stability and Stabilization of Systems with Time Delay: Limitations and Opportunities.” In: *IEEE Transactions on Control Systems Technology* 31.1, p. 38 (cit. on p. 22).
- Abdullah, Ali and Omar Qasem (2019). “Full-order and reduced-order observers for linear parameter-varying systems with one-sided Lipschitz nonlinearities and disturbances using parameter-dependent Lyapunov function.” In: *Journal of the Franklin Institute* 356.10, pp. 5541–5572 (cit. on pp. 135, 187).
- Abou Jaoude, Abdo (2015). “Analytic and linear prognostic model for a vehicle suspension system subject to fatigue.” In: *Systems Science & Control Engineering* 3.1, pp. 81–98 (cit. on pp. 70, 75).
- Aguilera-González, A et al. (2012). “Sensor Fault and Unknown Input Estimation Based on Proportional Integral Observer Applied to LPV Descriptor Systems.” In: *IFAC Proceedings Volumes* 45.20, pp. 1059–1064 (cit. on p. 134).
- Alwi, Halim, Christopher Edwards, and Chee Pin Tan (2011). *Fault detection and fault-tolerant control using sliding modes*. Springer Science & Business Media (cit. on p. 40).
- Apkarian, Pierre and Richard J Adams (2000). “Advanced gain-scheduling techniques for uncertain systems.” In: *Advances in linear matrix inequality methods in control*. SIAM, pp. 209–228 (cit. on pp. 26, 57).
- Apkarian, Pierre and Pascal Gahinet (1995). *A convex characterization of gain-scheduled \mathcal{H}_∞ controllers*. Citeseer (cit. on pp. 29, 33, 76).
- Apkarian, Pierre, Pascal Gahinet, and Greg Becker (1995). “Self-scheduled \mathcal{H}_∞ control of linear parameter-varying systems: a design example.” In: *Automatica* 31.9, pp. 1251–1261 (cit. on pp. 25, 33, 34, 145, 170).
- Åström, Karl J and Björn Wittenmark (2013). *Computer-controlled systems: theory and design*. Courier Corporation (cit. on p. 96).
- Barmish, B Ross (1985). “Necessary and sufficient conditions for quadratic stabilizability of an uncertain system.” In: *Journal of Optimization theory and applications* 46.4, pp. 399–408 (cit. on p. 20).
- Bernstein, Dennis S and Anthony N Michel (1995). “A chronological bibliography on saturating actuators.” In: *International Journal of Robust and Nonlinear Control* 5.5, pp. 375–380 (cit. on p. 96).
- Bezzaoucha, Souad et al. (2011). “On the unknown input observer design: a decoupling class approach.” In: *2011 9th IEEE International Conference on Control and Automation (ICCA)*. IEEE, pp. 602–607 (cit. on p. 116).
- Biannic, JM (1996). *Robust control of parameter varying systems: aerospace applications*. PhD Thesis, Université Paul Sabatier (ONERA) (cit. on pp. 24, 76).

- Boulkroune, Boulaid, Abdel Aitouche, and Vincent Cocquempot (2015). “Observer design for nonlinear parameter-varying systems: Application to diesel engines.” In: *International Journal of Adaptive Control and Signal Processing* 29.2, pp. 143–157 (cit. on pp. 135, 187).
- Boyd, Stephen et al. (1994). *Linear matrix inequalities in system and control theory*. SIAM (cit. on pp. 30, 31, 71, 86, 88, 90).
- Briat, Corentin (2008). *Robust control and observation of LPV time-delay systems*. PhD Thesis, Université Grenoble Alpes (cit. on pp. 8, 21, 22, 183).
- (2015). “Introduction to LPV Time-Delay Systems.” In: *Linear Parameter-Varying and Time-Delay Systems*. Springer, pp. 245–264 (cit. on pp. 19, 22, 156, 164).
- Briat, Corentin, Olivier Sename, and J-F Lafay (2007). “Full order LPV/ \mathcal{H}_∞ observers for LPV time-delay systems.” In: *IFAC Proceedings Volumes* 40.20, pp. 148–153 (cit. on p. 156).
- (2011). “Design of LPVobservers for LPVtime-delay systems: an algebraic approach.” In: *International Journal of Control* 84.9, pp. 1533–1542 (cit. on p. 156).
- Briat, Corentin, Olivier Sename, and Jean-François Lafay (2010). “Memory-resilient gain-scheduled state-feedback control of uncertain LTI/LPV systems with time-varying delays.” In: *Systems & Control Letters* 59.8, pp. 451–459 (cit. on p. 156).
- Bruzelius, FH (2004). *Linear parameter-varying systems: An approach to gain scheduling*. PhD Thesis, University of Technology of Goteborg (cit. on p. 24).
- Chadli, Mohammed, Mohammadreza Davoodi, and Nader Meskin (2016). “Distributed state estimation, fault detection and isolation filter design for heterogeneous multi-agent linear parameter-varying systems.” In: *IET Control Theory & Applications* 11.2, pp. 254–262 (cit. on pp. 8, 183).
- Chen, Jianliang et al. (2016). “Observer-based consensus control against actuator faults for linear parameter-varying multiagent systems.” In: *IEEE Transactions on Systems, Man, and Cybernetics: Systems* 47.7, pp. 1336–1347 (cit. on pp. 8, 183).
- Chen, Jie and Ron J Patton (2012). *Robust model-based fault diagnosis for dynamic systems*. Vol. 3. Springer Science & Business Media (cit. on pp. 1, 9).
- Chen, Jie, Ron J Patton, and Hong-Yue Zhang (1996). “Design of unknown input observers and robust fault detection filters.” In: *International Journal of control* 63.1, pp. 85–105 (cit. on pp. 80, 116).
- Dai, Liyi (1989). *Singular control systems*. Vol. 118. Springer (cit. on pp. 17, 27, 116).
- Darouach, M and M Boutayeb (1995). “Design of observers for descriptor systems.” In: *IEEE transactions on Automatic Control* 40.7, pp. 1323–1327 (cit. on p. 116).
- Darouach, Mohamed, Latifa Boutat-Baddas, and Mohamed Zerrougui (2011). “ \mathcal{H}_∞ observers design for a class of nonlinear singular systems.” In: *Automatica* 47.11, pp. 2517–2525 (cit. on p. 46).
- Darouach, Mohamed, Michel Zasadzinski, and Mohamed Hayar (1996). “Reduced-order observer design for descriptor systems with unknown inputs.” In: *IEEE Transactions on Automatic Control* 41.7, pp. 1068–1072 (cit. on pp. 116, 120, 127, 156).
- Darouach, Mohamed, Michel Zasadzinski, and Shi Jie Xu (1994). “Full-order observers for linear systems with unknown inputs.” In: *IEEE Transactions on Automatic Control* 39.3, pp. 606–609 (cit. on pp. 3, 11, 134).

- Darouach, Mohamed et al. (1995). “Kalman filtering with unknown inputs via optimal state estimation of singular systems.” In: *International journal of systems science* 26.10, pp. 2015–2028 (cit. on pp. 7, 181).
- Ding, Steven X (2008). *Model-based fault diagnosis techniques: design schemes, algorithms, and tools*. Springer Science & Business Media (cit. on pp. 1, 9, 118).
- Do, Anh Lam et al. (2011). “Control design for LPV systems with input saturation and state constraints: an application to a semi-active suspension.” In: *Decision and Control and European Control Conference (CDC-ECC), 2011 50th IEEE Conference on*. IEEE, pp. 3416–3421 (cit. on pp. 53, 186).
- Do, Manh-Hung, Damien Koenig, and Didier Theilliol (2018a). “An Integrated Design for Robust Actuator Fault Accommodation Based on \mathcal{H}_∞ Proportional-Integral Observer.” In: *2018 IEEE Conference on Decision and Control (CDC)*. IEEE, pp. 6346–6352 (cit. on p. xix).
- (2018b). “Robust \mathcal{H}_∞ proportional integral observer design for actuator fault estimation.” In: *2018 16th International Mini Conference on Vehicle System Dynamics, Identification and Anomalies (VSDIA), Budapest, Hungary*. Budapest, Hungary (cit. on p. xix).
- (2018c). “Robust \mathcal{H}_∞ proportional-integral observer for fault diagnosis: Application to vehicle suspension.” In: *In 2018 10th IFAC Symposium on Fault Detection, Supervision and Safety for Technical Processes (SAFEPROCESS)*. Vol. 51. 24. IFAC-PapersOnLine, pp. 536–543 (cit. on pp. xx, 44).
- (2019). “Robust \mathcal{H}_2 observer design for actuator degradation: Application to suspension system.” In: *2019 4th Conference on Control and Fault Tolerant Systems (SysTol)*. IEEE. hal-02173099 (cit. on p. xix).
- (2020a). “Fault estimation methods in descriptor system with partially decoupled disturbances.” In: *2020 21st IFAC World Congress*. IFAC-PapersOnLine (cit. on p. xix).
- (2020b). “ \mathcal{H}_∞ observer design for Singular Nonlinear Parameter-varying System.” In: *2020 IEEE Conference on Decision and Control (CDC)*. IEEE. hal-02793187 (cit. on p. xix).
- (2020c). “Robust \mathcal{H}_∞ proportional-integral observer-based controller for uncertain LPV system.” In: *Journal Of The Franklin Institute-Engineering And Applied Mathematics* 357.4, pp. 2099–2130 (cit. on p. xix).
- Do, Manh-Hung et al. (2020). “Frequency-shaping observer-based controller design for actuator.” In: *2020 28th Mediterranean Conference on Control and Automation (MED)*. IEEE. hal-02901558 (cit. on p. xix).
- Dorri, Ali, Salil S Kanhere, and Raja Jurdak (2018). “Multi-agent systems: A survey.” In: *Ieee Access* 6, pp. 28573–28593 (cit. on pp. 8, 183).
- Fleps-Dezasse, Michael et al. (2018). “LPVfeedforward control of semi-active suspensions for improved roll stability.” In: *Control Engineering Practice* 78, pp. 1–11 (cit. on p. 96).
- Gahinet, Pascal and Pierre Apkarian (1994). “A linear matrix inequality approach to \mathcal{H}_∞ control.” In: *International Journal of Robust and Nonlinear Control* 4.4, pp. 421–448 (cit. on pp. 31, 32).
- Gahinet, Pascal, Pierre Apkarian, and Mahmoud Chilali (1996). “Affine parameter-dependent Lyapunov functions and real parametric uncertainty.” In: *IEEE Transactions on Automatic Control* 41.3, pp. 436–442 (cit. on pp. 46, 71).

- Gao, Zhiwei, Xiaoxu Liu, and Michael ZQ Chen (2016). “Unknown input observer-based robust fault estimation for systems corrupted by partially decoupled disturbances.” In: *IEEE Transactions on Industrial Electronics* 63.4, pp. 2537–2547 (cit. on pp. 3, 4, 11, 116–119, 123).
- Giurgiutiu, Victor (2007). *Structural health monitoring: with piezoelectric wafer active sensors*. Elsevier (cit. on p. 73).
- Gouaisbaut, Frédéric and Dimitri Peaucelle (2006). “Delay-dependent robust stability of time delay systems.” In: *IFAC Proceedings Volumes* 39.9, pp. 453–458 (cit. on p. 22).
- Grenaille, Sylvain, David Henry, and Ali Zolghadri (2008). “A method for designing fault diagnosis filters for LPV polytopic systems.” In: *Journal of Control Science and Engineering* 2008 (cit. on p. 71).
- Habib, Hamdi et al. (2010). “Robust \mathcal{H}_∞ fault diagnosis for multi-model descriptor systems: A multi-objective approach.” In: *18th Mediterranean Conference on Control and Automation, MED’10*. IEEE, pp. 833–838 (cit. on p. 156).
- Hamdi, Habib et al. (2012). “Fault detection and isolation in linear parameter-varying descriptor systems via proportional integral observer.” In: *International journal of adaptive control and signal processing* 26.3, pp. 224–240 (cit. on pp. 29, 40, 42, 134, 142, 169).
- Hassanabadi, Amir Hossein, Masoud Shafiee, and Vicenc Puig (2015). “State and fault estimation in singular delayed LPV systems.” In: *Electrical Engineering (ICEE), 2015 23rd Iranian Conference on*. IEEE, pp. 1030–1035 (cit. on p. 40).
- Hassanabadi, Amir Hossein, Masoud Shafiee, and Vicenc Puig (2016). “Robust fault detection of singular LPV systems with multiple time-varying delays.” In: *International Journal of Applied Mathematics and Computer Science* 26.1, 45–61. 10.1515/amcs-2016-0004 (cit. on p. 157).
- Hassanabadi, Amir Hossein, Masoud Shafiee, and Vicenc Puig (2017). “Actuator fault diagnosis of singular delayed LPV systems with inexact measured parameters via PI unknown input observer.” In: *IET Control Theory & Applications* 11.12, pp. 1894–1903 (cit. on pp. 1, 9, 40, 71).
- Hassanabadi, Amir Hossein, Masoud Shafiee, and Vicenc Puig (2018). “Sensor fault diagnosis of singular delayed LPV systems with inexact parameters: an uncertain system approach.” In: *International Journal of Systems Science* 49.1, pp. 179–195. 10.1080/00207721.2017.1390700 (cit. on p. 157).
- Henry, David (2012). “Structured fault detection filters for LPV systems modeled in an LFR manner.” In: *International Journal of Adaptive Control and Signal Processing* 26.3, pp. 190–207 (cit. on p. 71).
- Henry, David et al. (2015). “ $\mathcal{H}_\infty/\mathcal{H}_-$ LPV solutions for fault detection of aircraft actuator faults: Bridging the gap between theory and practice.” In: *International Journal of Robust and Nonlinear Control* 25.5, pp. 649–672 (cit. on p. 71).
- Hernández, Debbie et al. (2019). “On the strong observability in linear time-varying singular systems.” In: *Automatica* 101, pp. 60–65 (cit. on pp. 8, 183).
- Hoffmann, Christian and Herbert Werner (2015). “A survey of linear parameter-varying control applications validated by experiments or high-fidelity simulations.” In: *IEEE Transactions on Control Systems Technology* 23.2, pp. 416–433 (cit. on pp. 23, 26).

- Ichalal, Dalil and Saïd Mammar (2015). “On unknown input observers for LPV systems.” In: *IEEE Transactions on Industrial Electronics* 62.9, pp. 5870–5880 (cit. on p. 134).
- Ichalal, Dalil et al. (2015). “Unknown input observer for LPV systems with parameter varying output equation.” In: *IFAC-PapersOnLine* 48.21, pp. 1030–1035 (cit. on p. 135).
- Isermann, Rolf (2006). *Fault-diagnosis systems: an introduction from fault detection to fault tolerance*. Springer Science & Business Media (cit. on p. 40).
- ISO, Standard (1995). “8608, Mechanical vibration—Road Surfaces Profiles—Reporting of measured data.” In: *International Organization for Standardization, Switzerland* (cit. on p. 54).
- Jabbari, Faryar and RW Benson (1992). “Observers for stabilization of systems with matched uncertainty.” In: *Dynamics and Control* 2.3, pp. 303–323 (cit. on pp. 1, 9, 40).
- Jensen, Johan Ludwig William Valdemar et al. (1906). “Sur les fonctions convexes et les inégalités entre les valeurs moyennes.” In: *Acta mathematica* 30, pp. 175–193 (cit. on p. 31).
- Jiang, Jin and Xiang Yu (2012). “Fault-tolerant control systems: A comparative study between active and passive approaches.” In: *Annual Reviews in control* 36.1, pp. 60–72 (cit. on pp. 1, 9).
- Kalman, Rudolph Emil (1960). “A new approach to linear filtering and prediction problems.” In: *Journal of basic Engineering* 82.1, pp. 35–45 (cit. on p. 71).
- Kamen, E, P Khargonekar, and A Tannenbaum (1985). “Stabilization of time-delay systems using finite-dimensional compensators.” In: *IEEE Transactions on Automatic Control* 30.1, pp. 75–78 (cit. on p. 22).
- Kammler, David W (2007). *A first course in Fourier analysis*. Cambridge University Press (cit. on p. 79).
- Kheloufi, Houria et al. (2013). “On LMI conditions to design observer-based controllers for linear systems with parameter uncertainties.” In: *Automatica* 49.12, pp. 3700–3704 (cit. on pp. 46, 49, 57, 72, 87).
- Khosrowjerdi, Mohammad Javed, R Nikoukhah, and N Safari-Shad (2004). “A mixed $\mathcal{H}_2/\mathcal{H}_\infty$ approach to simultaneous fault detection and control.” In: *Automatica* 40.2, pp. 261–267 (cit. on pp. 3, 10, 71).
- Kim, Nam-Ho, Dawn An, and Joo-Ho Choi (2017). “Prognostics and health management of engineering systems.” In: *Switzerland: Springer International Publishing* (cit. on p. 70).
- Koenig, Damien (2005). “Unknown input proportional multiple-integral observer design for linear descriptor systems: application to state and fault estimation.” In: *IEEE Transactions on Automatic Control* 50.2, pp. 212–217 (cit. on pp. 9, 70, 74, 82, 116, 120, 121, 134).
- Koenig, Damien, Benoît Marx, and Sébastien Varrier (2016). “Filtering and fault estimation of descriptor switched systems.” In: *Automatica* 63, pp. 116–121 (cit. on p. 126).
- Kothamasu, Ranganath, Samuel H Huang, and William H VerDuin (2006). “System health monitoring and prognostics—a review of current paradigms and practices.” In: *The International Journal of Advanced Manufacturing Technology* 28.9-10, pp. 1012–1024 (cit. on p. 70).
- Kress, Rainer, V Maz’ya, and V Kozlov (1989). *Linear integral equations*. Vol. 82. Springer (cit. on pp. 7, 182).
- Lan, Jianglin and Ron J Patton (2016). “A new strategy for integration of fault estimation within fault-tolerant control.” In: *Automatica* 69, pp. 48–59 (cit. on pp. 2, 10, 50, 72).

- Levine, William S (2010). *The control handbook: Control system fundamentals*. CRC press (cit. on pp. 79, 80).
- Lewis, Frank L, Draguna Vrabie, and Vassilis L Syrmos (2012). *Optimal control*. John Wiley & Sons (cit. on pp. 71, 85, 86).
- Li, Fanbiao and Xian Zhang (2012). “A delay-dependent bounded real lemma for singular LPV systems with time-variant delay.” In: *International Journal of Robust and Nonlinear Control* 22.5, pp. 559–574 (cit. on p. 157).
- (2013). “Delay-range-dependent robust \mathcal{H}_∞ filtering for singular LPV systems with time variant delay.” In: *International Journal of Innovative Computing, Information and Control* 9.1, pp. 339–353 (cit. on p. 157).
- Lien, Chang-Hua (2004). “Robust observer-based control of systems with state perturbations via LMI approach.” In: *IEEE Transactions on Automatic Control* 49.8, pp. 1365–1370 (cit. on pp. 46, 87).
- Liu, Yang, Zidong Wang, and Donghua Zhou (2018). “State estimation and fault reconstruction with integral measurements under partially decoupled disturbances.” In: *IET Control Theory & Applications* 12.10, pp. 1520–1526 (cit. on p. 116).
- Lofberg, Johan (2004). “YALMIP: A toolbox for modeling and optimization in MATLAB.” In: *Computer Aided Control Systems Design, 2004 IEEE International Symposium on*. IEEE, pp. 284–289 (cit. on pp. 23, 59, 104, 128, 149).
- López-Estrada, Francisco-Ronay (2014). *Model-based fault diagnosis observer design for descriptor LPV system with unmeasurable gain scheduling*. PhD Thesis, CRAN - Centre de Recherche en Automatique de Nancy, Université de Lorraine. NNT:2014LORR0162. tel-01751059v2 (cit. on p. 29).
- Lopez-Estrada, Francisco-Ronay et al. (2014). “Fault diagnosis based on robust observer for descriptor-LPV systems with unmeasurable scheduling functions.” In: *IFAC Proceedings Volumes* 47.3, pp. 1079–1084 (cit. on p. 134).
- López-Estrada, Francisco-Ronay et al. (2015a). “Robust \mathcal{H}_- / \mathcal{H}_∞ fault detection observer design for descriptor-LPV systems with unmeasurable gain scheduling functions.” In: *International Journal of Control* 88.11, pp. 2380–2391 (cit. on pp. 6, 156, 181).
- López-Estrada, Francisco-Ronay et al. (2015b). “Robust sensor fault estimation for descriptor-LPV systems with unmeasurable gain scheduling functions: Application to an anaerobic bioreactor.” In: *International Journal of Applied Mathematics and Computer Science* 25.2, pp. 233–244 (cit. on pp. 3, 11, 134).
- Lu, Wei-Min and John C Doyle (1993). *\mathcal{H}_∞ Control of Nonlinear Systems: A Class of Controllers*. Tech. rep. CALIFORNIA INST OF TECH PASADENA CONTROL and DYNAMICAL SYSTEMS (cit. on p. 20).
- Luo, Jianhui et al. (2008). “Model-based prognostic techniques applied to a suspension system.” In: *IEEE Transactions on Systems, Man, and Cybernetics-Part A: Systems and Humans* 38.5, pp. 1156–1168 (cit. on pp. 70, 73, 75).
- Marx, B, D Koenig, and D Georges (2003). “Robust fault diagnosis for linear descriptor systems using proportional integral observers.” In: *Decision and Control, 2003. Proceedings. 42nd IEEE Conference on*. Vol. 1. IEEE, pp. 457–462 (cit. on pp. 40, 42, 156).
- Marx, Benoît et al. (2019). “Unknown input observer for LPV systems.” In: *Automatica* 100, pp. 67–74 (cit. on pp. 4, 11, 71, 135, 140, 153).

- Mendoza, Jorge Aurelio Brizuela et al. (2016). “State and actuator fault estimation observer design integrated in a riderless bicycle stabilization system.” In: *ISA Transactions* 61, pp. 199–210 (cit. on pp. 56, 63).
- Nguyen, Manh Quan (2016). *LPV approaches for modelling and control of vehicle dynamics: application to a small car pilot plant with ER dampers*. PhD Thesis, Université Grenoble Alpes (cit. on p. 51).
- Olgac, Nejat and Rifat Sipahi (2002). “An exact method for the stability analysis of time-delayed linear time-invariant (LTI) systems.” In: *IEEE Transactions on Automatic Control* 47.5, pp. 793–797 (cit. on p. 22).
- Pham, Thanh-Phong (2020). “LPV observer and Fault-tolerant control of vehicle dynamics: application to an automotive semi-active suspension system.” PhD thesis. Université Grenoble Alpes (cit. on p. 187).
- Pham, Thanh-Phong, Olivier Sename, and Luc Dugard (2019). “Real-time Damper Force Estimation of Vehicle Electrorheological Suspension: A NonLinear Parameter Varying Approach.” In: *IFAC-PapersOnLine* 52.28, pp. 94–99 (cit. on pp. 135, 186).
- Pham, Thanh-Phong, Olivier Sename, Luc Dugard, et al. (2019). “LPV force observer design and experimental validation from a dynamical semi-active ER damper model.” In: *IFAC-PapersOnLine* 52.17, pp. 60–65 (cit. on pp. 3, 11).
- Poussot-Vassal, Charles et al. (2008). “A new semi-active suspension control strategy through LPV technique.” In: *Control Engineering Practice* 16.12, pp. 1519–1534 (cit. on pp. 24, 76).
- Rodrigues, Mickaël, Didier Theilliol, and Dominique Sauter (2005). “Design of a robust polytopic unknown input observer for FDI: Application for systems described by a multi-model representation.” In: *Proceedings of the 44th IEEE Conference on Decision and Control*. IEEE, pp. 6268–6273 (cit. on p. 134).
- Rodrigues, Mickael et al. (2014). “Observer-based fault tolerant control design for a class of LPV descriptor systems.” In: *Journal of the Franklin Institute* 351.6, 3104–3125. hal-00959769. 10.1016/j.jfranklin.2014.02.016 (cit. on pp. 2, 10, 72, 135, 142, 169).
- Rodrigues, Mickael et al. (2015). “Actuator fault estimation based adaptive polytopic observer for a class of LPV descriptor systems.” In: *International Journal of Robust and Nonlinear Control* 25.5, pp. 673–688 (cit. on p. 71).
- Savaresi, Sergio M et al. (2010). *Semi-active suspension control design for vehicles*. Elsevier, pp. 60–68 (cit. on pp. 53, 185, 186).
- Scherer, C, Pascal Gahinet, and M Chilali (1996). “ \mathcal{H}_∞ design with pole placement constraints: An LMI approach.” In: *IEEE Transactions on Automatic Control* 41.3, pp. 358–367 (cit. on p. 66).
- Scherer, Carsten, Pascal Gahinet, and Mahmoud Chilali (1997). “Multiobjective output-feedback control via LMI optimization.” In: *IEEE Transactions on Automatic Control* 42.7, pp. 896–911 (cit. on p. 46).
- Scherer, Carsten and Siep Weiland (2001). “Linear matrix inequalities in control.” In: (cit. on pp. 32, 71).
- Sename, Olivier, Peter Gaspar, and József Bokor (2013). *Robust control and linear parameter varying approaches: Application to vehicle dynamics*. Berlin, Germany: Springer-Verlag (cit. on pp. 1, 9).

- Shi, Fengming and Ron J Patton (2015a). “Fault estimation and active fault tolerant control for linear parameter varying descriptor systems.” In: *International Journal of Robust and Nonlinear Control* 25.5, pp. 689–706 (cit. on pp. 7, 82, 182).
- (2015b). “Fault estimation and active fault tolerant control for linear parameter varying descriptor systems.” In: *International Journal of Robust and Nonlinear Control* 25.5, pp. 689–706 (cit. on p. 156).
- Sobczyk, K and J Trebicki (2000). “Stochastic dynamics with fatigue-induced stiffness degradation.” In: *Probabilistic Engineering Mechanics* 15.1, pp. 91–99 (cit. on p. 70).
- Sturm, Jos F (1999). “Using SeDuMi 1.02, a MATLAB toolbox for optimization over symmetric cones.” In: *Optimization methods and software* 11.1-4, pp. 625–653 (cit. on p. 128).
- Suciu, CV and Kazuhiko Yaguchi (2009). “Endurance tests on a colloidal damper destined to vehicle suspension.” In: *Experimental mechanics* 49.3, p. 383 (cit. on pp. 73, 74).
- Tan, K, KM Grigoriadis, and F Wu (2003). “ \mathcal{H}_∞ and \mathcal{L}_2 -to- \mathcal{L}_∞ gain control of linear parameter-varying systems with parameter-varying delays.” In: *IEEE Proceedings-Control Theory and Applications* 150.5, pp. 509–517 (cit. on pp. 19, 22).
- Tanelli, Mara et al. (2016). “Sliding mode control for LPV systems.” In: *2016 American Control Conference (ACC)*. IEEE, pp. 3686–3691 (cit. on pp. 8, 182).
- Toh, Kim-Chuan, Michael J Todd, and Reha H Tütüncü (1999). “SDPT3 – a MATLAB software package for semidefinite programming, version 1.3.” In: *Optimization methods and software* 11.1-4, pp. 545–581 (cit. on pp. 23, 59, 104, 149).
- Tuan, Hoang Duong, Pierre Apkarian, and Truong Q Nguyen (2001). “Robust and reduced-order filtering: new LMI-based characterizations and methods.” In: *IEEE Transactions on Signal Processing* 49.12, pp. 2975–2984 (cit. on pp. 7, 86, 182).
- Tudón-Martínez, Juan C et al. (2015). “Adaptive road profile estimation in semiactive car suspensions.” In: *IEEE Transactions on Control Systems Technology* 23.6, pp. 2293–2305 (cit. on pp. 51, 54).
- Us Saqib, Najam et al. (2017). “Static antiwindup design for nonlinear parameter varying systems with application to DC motor speed control under nonlinearities and load variations.” In: *IEEE Transactions on Control Systems Technology* 26.3, pp. 1091–1098 (cit. on pp. 3, 11, 135, 187).
- Wang, Ye, Vicenç Puig, and Gabriela Cembrano (2018). “Set-membership approach and Kalman observer based on zonotopes for discrete-time descriptor systems.” In: *Automatica* 93, pp. 435–443 (cit. on p. 71).
- Wang, Youyi, Lihua Xie, and Carlos E de Souza (1992). “Robust control of a class of uncertain nonlinear systems.” In: *Systems & Control Letters* 19.2, pp. 139–149 (cit. on p. 30).
- Wojciechowski, B (1978). “Analysis and synthesis of proportional-integral observers for single-input-single-output time-invariant continuous systems.” In: *Gliwice, Poland* (cit. on p. 40).
- Wu, Fen (1995). *Control of linear parameter varying systems*. PhD Thesis, University of California, Berkeley (cit. on pp. 20, 21, 26, 29, 31–33, 45, 57, 66, 86, 167).
- (2001). “A generalized LPV system analysis and control synthesis framework.” In: *International Journal of Control* 74.7, pp. 745–759 (cit. on pp. 1, 9).
- Wu, Fen and Karolos M Grigoriadis (2001). “LPV systems with parameter-varying time delays: analysis and control.” In: *Automatica* 37.2, pp. 221–229 (cit. on pp. 22, 156, 167).

- Wu, Fen, Karolos M Grigoriadis, and Andy Packard (2000). “Anti-windup controller design using linear parameter-varying control methods.” In: *International Journal of Control* 73.12, pp. 1104–1114 (cit. on p. 96).
- Wu, Fen and Andy Packard (1995). “Optimal LQG performance of linear uncertain systems using state-feedback.” In: *Proceedings of 1995 American Control Conference-ACC’95*. Vol. 6. IEEE, pp. 4435–4439 (cit. on pp. 71, 86).
- Wu, Fen et al. (1996). “Induced \mathcal{L}_2 -norm control for LPV systems with bounded parameter variation rates.” In: *International Journal of Robust and Nonlinear Control* 6.9-10, pp. 983–998 (cit. on pp. 7, 42, 45, 49, 159, 182).
- Xu, Feng et al. (2016). “A novel design of unknown input observers using set-theoretic methods for robust fault detection.” In: *2016 American Control Conference (ACC)*. IEEE, pp. 5957–5961 (cit. on pp. 3, 11, 116).
- Xu, Shengyuan and James Lam (2007). “On equivalence and efficiency of certain stability criteria for time-delay systems.” In: *IEEE Transactions on Automatic Control* 52.1, pp. 95–101 (cit. on p. 22).
- Yamamoto, Kazusa et al. (2015). “Driver torque estimation in Electric Power Steering system using an $\mathcal{H}_\infty/\mathcal{H}_2$ Proportional Integral observer.” In: *Decision and Control (CDC), 2015 IEEE 54th Annual Conference on*. IEEE, pp. 843–848 (cit. on p. 71).
- Yamamoto, Kazusa et al. (2019). “Design and experimentation of an LPV extended state feedback control on Electric Power Steering systems.” In: *Control Engineering Practice* 90, pp. 123–132 (cit. on p. 72).
- Yan, Zhibin and Guangren Duan (2006). “Impulse analysis of linear time-varying singular systems.” In: *IEEE transactions on automatic control* 51.12, pp. 1975–1979 (cit. on pp. 8, 183).
- Yang, Ruicong, Damiano Rotondo, and Vicenç Puig (2019). “D-stable Controller Design for Lipschitz NLPVSystem.” In: *IFAC-PapersOnLine* 52.28, pp. 88–93 (cit. on pp. 7, 182).
- Yao, Xingyan and Michael Pecht (2018). “Performance Degradation of Hydraulic Vehicle Dampers.” In: *2018 Prognostics and System Health Management Conference (PHM-Chongqing)*. IEEE, pp. 364–368 (cit. on pp. 73, 75).
- Zhang, Guoguang, Hui Zhang, and Junmin Wang (2015). “Robust fault estimation for time-varying and high-order faults in vehicle electric steering systems.” In: *Decision and Control (CDC), 2015 IEEE 54th Annual Conference on*. IEEE, pp. 1539–1544 (cit. on pp. 40, 70, 134).
- Zhang, Youmin and Jin Jiang (2007). “Issues on integration of fault diagnosis and reconfigurable control in active fault-tolerant control systems.” In: *Fault Detection, Supervision and Safety of Technical Processes 2006*. Elsevier, pp. 1437–1448 (cit. on pp. 1, 9).
- Zill, Dennis, Warren S Wright, and Michael R Cullen (2011). *Advanced engineering mathematics*. Jones & Bartlett Learning (cit. on p. 73).
- Zin, Alessandro et al. (2008). “Robust LPV- \mathcal{H}_∞ control for active suspensions with performance adaptation in view of global chassis control.” In: *Vehicle System Dynamics* 46.10, pp. 889–912 (cit. on p. 53).

Synthèse robuste d'observateurs pour systèmes singuliers linéaires à paramètres variants

Résumé — Cette thèse s'inscrit dans le cadre de l'étude de l'estimation d'état et des défauts des systèmes dynamiques Linéaires à Paramètres Variants (LPV). La thèse s'attache à considérer deux classes de systèmes: d'une part les systèmes réguliers et les systèmes singuliers. Les estimateurs proposés sont synthétisés pour être robustes aux incertitudes paramétriques, aux perturbations présentes sur l'équation d'état et de sortie, aux bruits de mesures, aux non-linéarités Lipschitziennes et aux retards. Les contributions majeures de ces travaux de recherche sont respectivement: la conception simultanée d'un régulateur et d'un observateur pour un système LPV incertain avec l'atténuation des perturbations par modelage fréquentielle des sorties, la conception d'observateurs pour l'estimation des défaillances/dégradations avec découplage partiel des entrées inconnues, la synthèse \mathcal{H}_∞ et \mathcal{H}_2 d'observateurs réguliers pour les systèmes singuliers avec entrée Lipschitzienne, et la synthèse \mathcal{H}_∞ d'un observateur régulier pour un système LPV à retards. La qualité des estimations est validée avec des données de terrain (plateforme INOVE) et des exemples numériques.

Mots clés : Estimation d'états et de défauts, Systèmes LPV singuliers, Systèmes LPV à retards, synthèse régulateur/observateur, Non-linéarité Lipschitzienne, Synthèses \mathcal{H}_∞ / \mathcal{H}_2 .

Robust observer designs for singular linear parameter-varying systems

Abstract — This Thesis is focused on the study of state and fault estimation in Linear Parameter-Varying (LPV) systems. The Thesis considers two classes of systems: non-singular and singular systems. In specific, the proposed observers are synthesized to be robust against parametric uncertainties, input and output disturbances, measurement noise, Lipschitz nonlinearities, and time delays. The major contributions of this research are respectively: an integrated observer-controller design for uncertain LPV systems with a new methodology of disturbance attenuation called output frequency-shaping filter; the design and the development of unknown input (UI) observers for fault estimation under the existence of partially decoupled UIs; the synthesis of \mathcal{H}_∞ and \mathcal{H}_2 observers for the singular system with Lipschitz nonlinearity; and a \mathcal{H}_∞ observer design for time-delay LPV system. Finally, the performance of the proposed methods is justified by laboratory experiments with INOVE platform and numerical examples.

Keywords: State and Fault estimation, Singular LPV systems, Time-delay LPV systems, Observer and controller design, Lipschitz nonlinearity, \mathcal{H}_∞ / \mathcal{H}_2 synthesis.
